

Investigating the biology of nuclear IGF-1R in prostate cancer

Submission for the degree of Doctor of Philosophy

(DPhil)

Department of Oncology

Jack Viron Mills

St Edmund Hall, Oxford

Trinity 2021



Table of Contents

I List of Figures ..... **vi**
II List of Tables ..... **ix**
III List of Abbreviations ..... **xi**
IV List of Contributors ..... **xvii**
V Acknowledgements ..... **xix**
VI Abstract ..... **xx**

1 Chapter I: Introduction **1**
1.1 Prostate Cancer 1

1.2 The IGF-axis 6
1.2.1 IGF receptors 6
1.2.2 IGF ligands 8
1.2.3 IGF binding proteins 9
1.2.4 IGF-1R and INSR hybrids 10

1.3 IGF-1R signalling pathways 11
1.3.1 PI3K-Akt signalling 12
1.3.2 MAPK signalling 18

1.4 IGF signalling in cancer 21
1.4.1 Alteration of IGF-axis components in cancer 21
1.4.2 Role in cancer progression 23
1.4.3 IGF-axis signalling in prostate cancer 24
1.4.4 IGF-axis signalling as a treatment target 25

1.5 RTKs in the nucleus 31
1.5.1 ErbB receptor family 32
1.5.2 Endocytosis-dependent nuclear RTKs 35
1.5.3 Protease dependent nuclear RTKs 37
1.5.4 Insulin receptor 39

1.6 Nuclear IGF-1R 41
1.6.1 Translocation mechanism 41
1.6.2 Interaction of nuclear IGF-1R with regulatory regions of chromatin 44
1.6.3 Nuclear IGF-1R interacting proteins 47

1.6.4 Clinical relevance of nuclear IGF-1R 51

1.7 Hypothesis and Aims 53

2 Chapter II: Materials and Methods 56

2.1 Cell Lines 56

2.2 Fresh Frozen Prostate Tissue 56

2.3 Western Blotting 57

2.4 Irradiation Treatments 58

2.5 Cell Fractionation 59

2.6 Chromatin Fractionation 60

2.7 Cell Surface Protein Biotinylation and Isolation 60

2.8 Co-Immunoprecipitation (Co-IP) 62

2.9 Immunofluorescence Staining (IF) 63

2.10 Immunohistochemistry (IHC) 64

2.10.1 Staining Protocol 64

2.10.2 IGF-1R scoring 66

2.11 Chromatin immunoprecipitation (ChIP) 66

2.11.1 ChIP from adherent cells 66

2.11.2 ChIP from fresh frozen TURP tissue 69

2.11.3 ChIP from fresh frozen biopsy tissue 69

2.12 Real time quantitative Polymerase Chain Reaction (qPCR) 70

2.12.1 Primer Design 70

2.12.2 qPCR 71

2.13 Generation of luciferase reporter plasmids 72

2.13.1 Genomic DNA Extraction 72

2.13.2 Amplification and purification of IGF-1R DNA binding regions 72

2.13.3 Digestion, ligation, and transformation of IGF-1R DNA binding regions into pNLCol2 reporter plasmid 74

2.14 Transfection of luciferase reporter plasmids 79
2.14.1 Transient transfections 79
2.14.2 Generation of stable cell lines 79

2.15 Luciferase Assays 80
2.15.1 Testing of transiently transfected cells 80
2.15.2 Testing of stable reporter cell lines 81

2.16 Mass Spectrometric Analysis of Interactome 81
2.16.1 Preparation of samples 81
2.16.2 Silver staining and Western blot analysis of co-IPs 82
2.16.3 On-bead digest and processing of samples 83
2.16.4 Mass Spectrometry Analysis 84

2.17 ChIP-sequencing Analysis 87

2.18 Statistical Analysis 87

3 Chapter III: Detection of IGF-1Rα-subunit in the nucleus 88
3.1 Introduction 88

3.2 Results 88
3.2.1 Testing for the presence of cell surface originating IGF-1Rα and β and their interaction in the nucleus 88
3.2.2 Immunofluorescence detection of nuclear IGF-1Rα- and β-subunits 94
3.2.3 Detection of recruitment of IGF-1Rα to known IGF-1R chromatin binding regions 100

3.3 Conclusion 102

4 Chapter IV: Assessment of assays for use in high throughput screening for inhibitors of nuclear IGF-1R 107
4.1 Introduction 107

4.2 Results 108
4.2.1 Immunofluorescence based screening platform 108
4.2.2 Luciferase reporter assay-based screening platform 115

4.3 Conclusion 133

5 Chapter V: Recruitment of IGF-1R to chromatin binding sites *in vivo* 137

5.1 Introduction 137

5.2 Results 138

5.2.1 Testing for IGF-1R ChIP from TURP tissue samples 138

5.2.2 Validation of IGF-1R ChIP from biopsy tissues from radical prostatectomies 144

5.2.3 IGF-1R IHC staining of parallel RP tissue sections 150

5.2.4 Analysis of *in vivo* IGF-1R ChIP-seq data 157

5.3 Discussion 175

6 Chapter VI: Investigating the nuclear interactome of IGF-1R 181

6.1 Introduction 181

6.2 Results 182

6.2.1 Immunoprecipitation of nuclear IGF-1R 182

6.2.2 Mass Spectrometry analysis of nuclear IGF-1R interactome 185

6.2.3 Validation of DNA-PKcs interaction 188

6.3 Discussion 196

7 Chapter VII: Conclusion and Future Directions 201

8 Appendices 208

8.1 List of IGF-1R ChIP-seq hits identified both *in vitro* and *in vivo* 208

8.2 List of *in vivo* IGF-1R ChIP-seq hits coincident with *in vivo* AR binding sites 214

8.3 List of nuclear IGF-1R interactome hits identified by mass spectrometry 222

8.4 Antibody List 245

9 Bibliography 246

I List of Figures

Figure 1.1 Structure of IGF-1R and IGF-2R 8

Figure 1.2 IGF-1R signalling pathways 20

Figure 1.3 Translocation mechanisms of RTKs 40

Figure 3.1 IGF-1Rα- and β-subunits are present in the nucleus of DU145 and 22Rv1 cells 91

Figure 3.2 Nuclear IGF-1Rα- and β-subunits originate from the cell surface and interact in the nucleus 92

Figure 3.3 Antibodies for IGF-1Rα- and β-subunits give specific immunofluorescent staining 96

Figure 3.4 Changes in levels of nuclear IGF-1Rα- and β-subunits are detectable by immunofluorescence 99

Figure 3.5 Recruitment of IGF-1Rα is detectable at IGF-1Rβ DNA binding sites 101

Figure 3.6 Model of potential nuclear translocation mechanism of IGF-1R in its holoreceptor form 105

Figure 4.1 Reduction in nuclear IGF-1R in response to inhibitors is detectable by immunofluorescence 109

Figure 4.2 Visualisation of IGF-1R staining in 96-well plate 110

Figure 4.3 Changes in nuclear IGF-1R are not detected by immunofluorescence in a 96-well plate format 111

Figure 4.4 Immunofluorescent staining of His-tagged IGF-1R 113

Figure 4.5 Immunofluorescent staining of His-tagged IGF-1R with NTA-Atto 488 114

Figure 4.6 *JUN* promoter is IGF-1 responsive 117

Figure 4.7 Recruitment of IGF-1R to IGF-1R chromatin binding sites is IGF-1 dependent 119

Figure 4.8 Cloning of IGF-1R binding regions for potential luciferase reporters 122
Figure 4.9 Colony PCR amplification of Chromosome 17 intergenic region..... 122
Figure 4.10 Luciferase assay testing IGF-1 responsiveness of nuclear IGF-1R reporters 124
Figure 4.11 Transiently transfected Chromosome 17 intergenic region reporter is IGF-1 responsive..... 125
Figure 4.12 Chromosome 17 intergenic region reporter showed no luciferase expression in stable clones 127
Figure 4.13 UCSC Genome Browser image of IGF-1R binding site in Chromosome 17 intergenic region..... 129
Figure 4.14 Cloning and colony PCR amplification of Chromosome 17 Peak region for luciferase reporter..... 130
Figure 4.15 Chromosome 17 Peak region luciferase reporter did not show IGF-1 responsiveness..... 132
Figure 5.1 Agarose gel showing DNA fragment sizes of homogenised TURP tissue..... 139
Figure 5.2 ChIP-qPCR validation of recruitment of RNAPolII and IGF-1Rβ at the *JUN* and *FAM21A* promoter regions in TURP tissue samples..... 142
Figure 5.3 Agarose gels showing DNA fragment size pre- and post-sonication 145
Figure 5.4 Western blot validation and ChIP-qPCR from benign tissue biopsy..... 147
Figure 5.5 ChIP-qPCR quantification of IGF-1Rβ ChIP from malignant tissue biopsies 149
Figure 5.6 IHC staining of IGF-1R in FFPE sections of RPs from which biopsies were analysed by ChIP-seq 155
Figure 5.7 Peak calling by MACS2 and LanceOtron in IGF-1R ChIP-seq *in vitro* data.. 159
Figure 5.8 UCSC Genome Browser images showing IGF-1R binding peaks identified in MACS2 and LanceOtron..... 160

Figure 5.9 Overlap of peaks identified by MACS2 parameters and LanceOtron from IGF-1R ChIP-seq *in vivo* 163
Figure 5.10 Overlap of peaks identified by indicated peak calling software from IGF-1R ChIP-seq *in vitro* and *in vivo* 164
Figure 5.11 Distance from TSS of ChIP-seq peaks identified *in vivo* 165
Figure 5.12 Distance of IGF-1R peaks from TSS of consensus genes 166
Figure 5.13 Distance of IGF-1R peaks from TSS of specific consensus genes identified in multiple tissue samples 170
Figure 5.14 PANTHER classification of protein class and biological pathways of identified consensus genes 171
Figure 5.15 UCSC genome browser image of binding peaks identified at TPTE TSS 173
Figure 6.1 Testing nuclear IGF-1R IP for suitability for mass spectrometry analysis 184
Figure 6.2 Distribution of the number of protein hits detected in WT and IGF-1R null IPs by mass spectrometry 186
Figure 6.3 IGF-1Rβ-subunit interacts with DNA-PKcs in the nucleus of 22Rv1 cells 190
Figure 6.4 DNA-PKcs shows differential phosphorylation following IR in WT vs IGF-1R null 22Rv1 clones 191
Figure 6.5 IGF-1R interacts with phosphorylated DNA-PKcs in 22Rv1 cells 193
Figure 6.6 IGF-1R and DNA-PKcs interaction is independent of IR 194
Figure 6.7 DNA-PKcs recruitment to chromatin is reduced in IGF-1R null cells 195

II List of Tables

Table 2.1 ChIP-qPCR primers 71

Table 2.2 PCR primers for cloning genomic DNA 78

Table 2.3 Mascot Data Search Parameters 86

Table 3.1 List of the IGF-1Rα IF primary antibodies used and the various dilutions at which they were tested 96

Table 4.1 Cloned IGF-1R binding sites for testing as luciferase reporters 121

Table 4.2 Successfully cloned IGF-1R binding sites 123

Table 5.1 List of fresh frozen human prostate tissue samples collected for ChIP 139

Table 5.2 ChIP-qPCR Ct values from benign biopsy sample 145

Table 5.3 Concentration of ChIP DNA samples from DU145 and benign biopsy samples 145

Table 5.4 Table summarising the RP biopsy samples tested by ChIP-qPCR and sent for sequencing 150

Table 5.5 IHC scoring of IGF-1R in FFPE tissue sections 156

Table 5.6 Clinical data for cases from which biopsies were obtained 156

Table 5.7 Number of enrichment peaks identified by MACS2 from *in vivo* ChIP-seq data 162

Table 5.8 Number of enrichment peaks identified by LanceOtron from *in vivo* ChIP-seq data 163

Table 5.9 Genes containing IGF-1R peak proximal to their TSS in 4 or more tissue ChIP-seq samples 169

Table 5.10 IGF-1R binding peaks identified proximal to gene TSS *in vitro* and in all *in vivo* samples 172

Table 5.11 Peak Co-ordinates of IGF-1R binding site identified both *in vitro* and *in vivo* in an intergenic region of chromosome 17 174

Table 6.1 Table of potential nuclear IGF-1R interactome proteins 187

III List of Abbreviations

4EBP1	Eukaryotic translation initiation factor 4E-binding protein 1
ACN	Acetonitrile
ADT	Androgen deprivation therapy
ALS	Acid labile subunit
AML	Acute myeloid leukaemia
APP	Amyloid precursor protein
AR	Androgen receptor
AR-V7	Androgen receptor variant 7
ARE	Androgen response element
Bad	B cell leukaemia 2 antagonist of cell death
BafA1	Bafilomycin A1
BCA	Bicinchoninic Acid
Bcl	B cell lymphoma
BSA	Bovine serum albumin
CDK	Cyclin dependent kinase
Chr17PK	IGF-1R binding peak region of chromosome 17
COP1	Coat protein complex 1
CREB	cAMP response element binding protein
CRM1	Chromosomal region maintenance 1
CRPC	Castrate resistant prostate cancer
CSF1R	Colony stimulating factor-1 receptor
DAPI	4′,6-diamidino-2-phenylindole
DHT	Dihydrotestosterone

DISC	Death inducing signalling complex
DMSO	Dimethyl sulfoxide
DNA-PK	DNA-dependent protein kinase
DNA-PKcs	DNA-dependent protein kinase catalytic subunit
DSB	Double strand break
DTT	Dithiothreitol
ECL	Enhanced chemiluminescence
ECM	Extracellular matrix
EEA-1	Early endosome antigen-1
EGFR	Epidermal growth factor receptor
eIF4B	Eukaryotic initiation factor 4B
EMSA	Electrophoretic mobility shift assay
EMT	Epithelial to mesenchymal transition
ER	Estrogen receptor
ERK	Extracellular signal related kinase
eRMS	Embryonal rhabdomyosarcoma
ES	Ewing sarcoma
ETS	E26 transformation-specific
FAK	Focal adhesion kinase
FBS	Foetal bovine serum
FDR	False discovery rate
FGF	Fibroblast growth factor
FGFR	Fibroblast growth factor receptor
FLT3	Fms-like tyrosine kinase 3
FOXO	Forkhead box O

GH	Growth hormone
GR	Glucocorticoid receptor
Grb2	Growth factor receptor-bound protein 2
GSK-3β	Glycogen synthase kinase-3 beta
HCC	Hepatocellular carcinoma
HCF-1	Host cell factor-1
HR	Homologous recombination
ICD	Intracellular domain
IGF-1/2	Insulin like growth factor-1/-2
IGF-1R	insulin-like growth factor-1 receptor
IGF-2R	Insulin-like growth factor-2 receptor
IGFBP	Insulin-like growth factor binding protein
iNOS	Inducible nitric oxide synthase
INSR	Insulin receptor
IntChr17	Intergenic region of chromosome 17
IP	Immunoprecipitation
IR	Irradiation
IR-1/-2	Internal repeat domain-1/-2
IRS-1/2/3/4	Insulin receptor substrate-1/2/3/4
JNK	c-Jun-amino-terminal kinase
LC-MS/MS	Liquid chromatography tandem mass spectrometry
LHRH	Luteinising hormone-releasing hormone
LRP	Lipoprotein-related protein
mAbs	Monoclonal antibodies
MAPK	Ras-Raf-Mitogen-activated protein kinase

mCRPC	Metastatic castrate resistant prostate cancer
Mdm2	Mouse double minute 2 homolog
MEK-1	MAPK and extracellular signal related kinase (ERK) kinase 1
MMP	Matrix metalloproteinase
mTOR	Mammalian target of rapamycin
mTORC1	Mammalian target of rapamycin complex 1
NHEJ	Non-homologous end joining
NLS	Nuclear localisation sequence
NPC	Nuclear pore complex
NSCLC	Non-small cell lung cancer
OCHRe	Oxford Centre for Histopathology Research
OS	Overall survival
PAPP-A	Pregnancy-associated plasma protein A
PBS	Phosphate buffered saline
PCNA	Proliferating cell nuclear antigen
PCR	Polymerase chain reaction
PDGFR	Platelet derived growth factor receptor
PDK1	Phosphoinositide-dependent kinase 1
PFS	Progression free survival
PH	Pleckstrin homology domain
PI3K	Phosphoinositide-3-kinase
PIA	Proliferative inflammatory atrophy
PIN	Prostatic intraepithelial neoplasia
PIP2	Phosphatidylinositol 4,5-biphosphate
PIP3	Phosphatidylinositol 3,4,5-triphosphate

PLA	Proximity ligation assay
PSA	Prostate specific antigen
PTB	Phosphotyrosine binding domain
PTEN	Phosphastase and tensin homologue
RanBP2	Ran binding protein 2
RanGAP1	Ran GTPase-activating protein
Raptor	Regulatory-associated protein of mTOR
RCC	Renal cell carcinoma
RLU	Relative luminescence units
RNAPolII	RNA-polymerase II
RP	Radical prostatectomy
RSK	40S ribosomal protein S6 kinase
RT	Room temperature
RTK	Receptor tyrosine kinase
S6K	Ribosomal protein S6 kinase 1
SAE	SUMO-activating enzyme
SDS-PAGE	Sodium dodecyl sulphate-polyacrylamide gel electrophoresis
SENP	Sentrin-specific protease
SH2	Src homology 2
Shc	Src homology and collagen domain protein
SIM	SUMO-interaction motif
STAT5	Signal transducer and activator of transcription 5
STS	Soft tissue sarcoma
SUMO	Small ubiquitin-like modifier protein
TBS	Tris-HCl buffered saline

TCF	T-cell factor
TGFα	Transforming growth factor alpha
TKI	Tyrosine kinase inhibitor
TMPRSS2	Transmembrane protease, serine 2
TNBC	Triple negative breast cancer
TRAIL	Tumour necrosis factor-related apoptosis-inducing ligand
TSC1/TSC2	Tuberous sclerosis proteins-1 and -2
TSM	Triple-SUMO-site-mutated
TSS	Transcription start site
TURP	Transurethral resection of the prostate
VEGF	Vascular endothelial growth factor
WCE	Whole cell extract
WT	Wild type

IV List of Contributors

I declare that this thesis describes my own research work except for the following experiments, which were performed with the help of others:

Dr Eliot Osher Macaulay Lab	Generation of DU145 IGF-1R CRISPR null cells, experiments described here using this IGF-1R null cell line were performed by me (Figure **3.3**, Figure **4.4**, Figure **4.5**). *JUN* promoter reporter stable clone was generated by Dr Osher, initial IGF-responsiveness luciferase reporter assay tests were performed by both Dr Osher and me (Figure **4.6**).
Dr Guillaume Rieunier Macaulay Lab	Irradiation treatment of cells. Experimental procedure following irradiation was performed by me (Figure **6.6**).
Dr Avigail Taylor Macaulay Lab	Analysis of *in vitro* and *in vivo* ChIP-seq data using MACS2 and LanceOtron (Section 5.2.4), and generation of related figures (Figure 5.7 - Figure 5.13)
Dr Iolanda Vendrell MRC Oxford Institute for Radiation Oncology, Uni. of Oxford	Liquid Chromatography and tandem mass spectrometry (LC-MS/MS) and subsequent initial analysis (Outlined in Sections 2.16.4 and 6.2.2)
Prof Clare Verrill Nuffield Dept of Surgical Sciences, Uni. of Oxford	IHC tissue histology identification and IGF-1R scoring (Table 5.5)
Dr Simon Engledow Oxford Genomics Centre, Wellcome Centre for Human Genetics	Sequencing of tissue IGF-1R ChIP samples (Section 5.2.2)
Matthew Ellis Macaulay Lab	Generation of 22Rv1 IGF-1R null CRISPR knockout cells, experiments described here using this IGF-1R null cell line were performed by me (Figure **6.1**, Figure **6.4**, Figure **6.5**, Figure **6.7**). Phospho-proteomics validation of differential DNA-PKcs phosphorylation (Figure **6.4**). Chromatin extraction experiments were performed jointly (Figure **6.7**).
Jinseon (Selena) Kim Macaulay Lab	Assistance with immunohistochemistry staining (Figure 5.6)

Portions of the data and figures shown in "Chapter III: Detection of IGF-1Rα-subunit in the nucleus" have previously been published in (Mills *et al.*, 2021), and this is acknowledged in the relevant figure legends. These figures and the relevant material in the

text have been generated and written by me and are reproduced here with permission from publication co-authors.

V Acknowledgements

This thesis is dedicated to many:

To my supervisors, Dr Valentine Macaulay and Prof Ian Mills, for their advice, support and encouragement throughout my DPhil studies. Despite everything, Val's support was both unwavering and inspiring.

To my parents, grandparents and the whole of my family. Without their love and support, I never would have made it this far and would not be the person I am today. I owe you all a huge debt of gratitude.

To Laura, who has been there for me through everything and who I couldn't have done this without.

To the Macaulay Lab past and present, for all the help and advice, as well as the lab lunches, team teas and pub trips that have helped make my time here so enjoyable.

To the Cov Boys, who I can always rely on and who still make me laugh more than ever.

To the welcoming community of Teddy Hall that helped make my time outside of the lab so fun and made Oxford feel like home.

To the housemates of Klub Kingston, who helped keep me sane not just through this DPhil, but through multiple COVID-19 lockdowns, and in whom I hope I can say I have made lifelong friends.

Mostly, this thesis is dedicated to Nan and Venita, who I miss more than I can say. Although you didn't get to see me make it this far, this was for you.

VI Abstract

Insulin-like growth factor 1 receptor (IGF-1R) is a transmembrane receptor tyrosine kinase comprised of two extracellular α- and two transmembrane β-subunits in a heterotetrameric structure. IGF-axis signalling is implicated in cancer progression, metastasis and resistance to treatment including radiotherapy. Recent work by our lab and others has shown the presence and activity of IGF-1R in the nucleus of a range of cancer cell types, interacting with nuclear proteins and undergoing recruitment to chromatin at gene promoters. Nuclear IGF-1R has been detected in malignant but rarely in benign epithelia, and higher levels of nuclear IGF-1R have been shown to be associated with adverse clinical outcomes. Responses in specific subsets of patients have also suggested nuclear IGF-1R may be a potential biomarker for tumours that may be more responsive to anti-IGF-1R targeted treatment. Therefore, nuclear IGF-1R may be a tumour selective property of the IGF-axis that could act as a novel target for treatment. This thesis aimed to further investigate the biological role of nuclear IGF-1R including screening of potential novel inhibitors specific for nuclear IGF-1R, identification of IGF-1R chromatin binding sites *in vivo*, and identification of novel nuclear interacting proteins to further elucidate the role of nuclear IGF-1R in cancer progression and as a treatment target.

The first aim of this work was to investigate the role of the extracellular α-subunit of IGF-1R in the nucleus, as previous work focussed on the β-subunit only. IGF-1Rα-subunit was detected in the nucleus of two prostate cancer cell lines, DU145 and 22Rv1, by co-immunoprecipitation, immunofluorescence microscopy and chromatin immunoprecipitation (ChIP). These experiments showed for the first time that IGF-1Rα- and β-subunits interacted in the nucleus, levels of nuclear IGF-1Rα-subunit were IGF-responsive, and IGF-1Rα-subunit was recruited to chromatin at β-subunit binding sites

identified previously by our group. These data suggest that α-subunit contributes to the function of nuclear IGF-1R.

The second objective, based on potential tumour selective properties of nuclear IGF-1R, aimed to develop a screening platform for small molecule inhibitors of nuclear IGF-1R. Despite multiple attempts to optimise scaled-down immunofluorescence and generate stable IGF-responsive luciferase reporters incorporating IGF-1R DNA binding sites, this screen could not be undertaken. However, these luciferase reporter plasmids can be used in future investigation of the transcriptional function of nuclear IGF-1R.

The third aim was to assess the clinical relevance of recruitment of IGF-1R to chromatin *in vivo*. To assess this, ChIP for IGF-1R was performed from fresh frozen tissue samples obtained from patients undergoing radical prostatectomy. Sequencing analysis detected genome wide recruitment of IGF-1R to chromatin *in vivo* for the first time. IGF-1R peaks were shown to cluster proximal to gene transcription start sites (TSS) and 38% of these peaks were coincident with H3K4me1, a histone mark for active enhancer regions. This suggests IGF-1R is recruited to regulatory DNA regions at these sites, and therefore may play a role in influencing gene expression. Further work is now needed to determine whether there is a link between IGF-1R recruitment and gene expression at the transcriptional and/or epigenetic level and therefore the contribution of IGF-1R recruitment to chromatin to cancer growth and progression *in vivo*.

The final aim was to investigate the nuclear interactome of IGF-1R using 22Rv1 clones expressing WT IGF-1R or IGF-1R null, generated by another student and shown to be radiosensitive. Proteins co-precipitating with IGF-1Rβ in 22Rv1 WT cells were analysed by mass spectrometry. Protein hits were ranked by peptide numbers detected in WT vs IGF-1R null cells, and the top hit was the catalytic subunit of DNA-dependent protein kinase (DNA-PKcs), required for DNA repair by non-homologous end-joining (NHEJ).

Co-precipitation validated the interaction of nuclear IGF-1R with DNA-PKcs and with phospho-S2056 DNA-PKcs, an auto-phosphorylation that occurs upon recruitment to chromatin. Consistent with a requirement for IGF-1R, irradiation-induced DNA-PKcs chromatin recruitment and S2056 phosphorylation were reduced in IGF-1R null cells. Further work is needed to investigate whether direct interaction with nuclear IGF-1R and/or downstream IGF-1R signalling contribute to DNA-PKcs function and radioresistance.

In summary, this work has shown a biological role in prostate cancer for the IGF-1Rα-subunit in the nucleus. For the first time, this work detected recruitment of IGF-1R to chromatin binding sites *in vivo* in malignant prostate cancer tissue at sites proximal to gene TSS and in some cases coincident with histone marker for active enhancer regions. Further *in vitro* work also showed an interaction between nuclear IGF-1R and DNA-PKcs that may play an important role in DNA-PKcs recruitment to chromatin. These factors may have significance for the biological role of nuclear IGF-1R in cancer progression and may contribute to the clinical relevance of nuclear IGF-1R in prostate cancer.

1 Chapter I: Introduction

1.1 Prostate Cancer

Cancer is the name given to a collection of related diseases that involve development of abnormal cell growth that can invade and spread to surrounding tissues. The hallmarks of cancer are defined as self-sufficient growth signals, insensitivity to anti-growth signals, evasion of apoptosis, limitless cell replication, sustained angiogenesis, tissue invasion and metastasis and more recently include deregulated cell metabolism and evasion of immune destruction. These traits are acquired as normal cells evolve towards becoming tumorigenic and potentially malignant and develop via enabling characteristics such as genomic instability and mutation, and tumour promoting inflammation. (Hanahan and Weinberg, 2000, 2011). Prostate cancer is the most common cancer in men worldwide, with 1 in 8 men estimated to be diagnosed in their lifetime and more than 11 500 men a year dying from prostate cancer in the UK (*https://prostatecanceruk.org/prostate-information/about-prostate-cancer*, 2021). Prostate cancer is usually diagnosed by digital rectal examination, or by elevated levels of prostate specific antigen (PSA), a protein produced by both normal epithelial prostate cells and prostate cancer cells but often elevated in the presence of prostate cancer. However, accuracy of diagnosis using PSA is variable (Etzioni *et al.*, 2002; Draisma *et al.*, 2003; Carter *et al.*, 2006). Malignant transformation of the prostate begins with proliferative inflammatory atrophy (PIA) triggering abnormal growth within the prostate epithelia know as prostatic intraepithelial neoplasia (PIN). This leads to the development of localised prostate cancer, which can develop into an advanced adenocarcinoma and eventually metastatic prostate cancer, which generally spreads first to the lymph nodes and can then spread on to the liver, lungs and bones (Shen and Abate-Shen, 2010). The Gleason grading system uses the histological patterns of prostate

carcinomas to assign a Gleason score, which can be used to assess prostate cancer aggressiveness and differentiation, with a higher score denoting more advanced or more poorly differentiated tissue (Gleason and Mellinger, 1974; Epstein *et al.*, 2016). While early stage, localised prostate cancer shows good long-term survival, with over 95% of men surviving for 5 years or more post diagnosis, metastatic prostate cancer mostly cannot be cured and 5 year survival rates drop to approximately 50% in the UK (*https://www.cancerresearchuk.org/about-cancer/prostate-cancer/survival*, 2021).

The main signalling pathway involved in prostate development is via the androgen receptor (AR), a nuclear hormone receptor. Synthesised by the testis, testosterone is the most abundant androgen, and it is converted into dihydrotestosterone (DHT), its active metabolite, by 5α-reductase. DHT binds to and activates AR, triggering its translocation from the cytoplasm to the nucleus where it forms a homodimer and acts as a transcription factor protein. AR binds to specific DNA motifs known as androgen response elements (AREs) and activates genes involved in growth, proliferation and differentiation in the prostate (Eder *et al.*, 2001; Sharma *et al.*, 2013; Davey and Grossmann, 2016). One of these known target genes includes insulin-like growth factor 1 receptor (IGF-1R) (Pandini *et al.*, 2005).

A majority of primary and metastatic prostate cancers have been shown to contain genomic alterations in the androgen signalling pathway, and an early critical step present in prostate cancers is the fusion of E26 transformation-specific (ETS) family transcription factor genes with androgen-responsive promoters, most commonly transmembrane protease, serine 2 (TMPRSS2). Fusion of the 5′ untranslated region of TMPRSS2 with the 3’ untranslated region of ERG, an ETS transcription family member, results in expression of TMPRSS2:ERG, an androgen-responsive oncoprotein present in roughly 50% of all localised prostate cancers (Tomlins *et al.*, 2005, 2009). These types of gene fusions bind to

downstream AREs and have been shown to be associated with development of PIN in combination with phosphoinositide-3-kinase (PI3K) pathway activation (King *et al.*, 2009), prostate cancer development in the presence of phosphatase and tensin homologue (PTEN) inactivation (Carver *et al.*, 2009; Steurer *et al.*, 2014) and cancer progression and invasion (Tomlins *et al.*, 2008; Mitchell and Neal, 2015).

Early work has shown the reliance of prostate cancer on AR signalling (Huggins and Hodges, 1941), and since then the primary treatment for prostate cancer has involved androgen deprivation therapy (ADT) involving either surgical or, more commonly, chemical castration. This involves treatment with gonadotropin-releasing hormone agonists, also called luteinising hormone-releasing hormone (LHRH), which reduce testosterone levels and therefore AR activation. Although most patients respond well to ADT it is not curative and clinical progression occurs after a median of 1-2 years, leading to castrate resistant prostate cancer (CRPC) which can become metastatic (mCRPC). Even after ADT the majority of CRPCs are still androgen dependent due to maintained AR signalling from AR splice variants, activating mutations or overexpression. AR-variant 7 (AR-V7) is the most abundant of the AR mRNA splice variants and encodes for a truncated AR protein that lacks the ligand binding domain and shows constitutive activation in the absence of androgens (Dehm *et al.*, 2008; Sharp, De Bono and Plymate, 2019). Following ADT, the major treatment for CRPC was docetaxel, a chemotherapeutic agent which disrupts mitosis by inhibition of microtubule depolymerisation. However, docetaxel treatment showed only modest increase in median survival and was often followed by palliative care (Petrylak *et al.*, 2004; Tannock *et al.*, 2004; Sumanasuriya and De Bono, 2018). More recently, anti-AR targeted treatments have been developed and have shown good responses due to the AR dependence of CRPC and are often administered as co-treatments alongside ADT. These include enzalutamide and

apalutamide, nonsteroidal antiandrogens which are antagonists of AR (Tran *et al.*, 2009; Clegg *et al.*, 2012), and abiraterone, an inhibitor of androgen production via inhibition of the CYP17A1 enzyme which catalyses production of testosterone precursors (Barrie *et al.*, 1994; Yin and Hu, 2014). Treatment with enzalutamide showed progression free survival (PFS) of 12 months in 65% of mCRPC patients treated with enzalutamide vs 14% treated with placebo control (Beer *et al.*, 2014), and an extra 5-month median survival vs placebo control treated CRPC patients (Scher *et al.*, 2012). Similarly, in mCRPC patients, abiraterone treatment showed an extra 4-month overall survival (OS) vs placebo control treated groups (De Bono *et al.*, 2011) and apalutamide showed an extra 24-month median metastasis free survival time vs control treated groups (Smith *et al.*, 2018). Despite these advances, both CRPC and anti-androgen drug resistant prostate cancer still arises, likely due to development of sustained androgen signalling via androgen independent mechanisms. Androgen signalling can be sustained by AR splice variants, such as the previously mentioned AR-V7, which do not require ligand activation and therefore are not affected by testosterone inhibition, and by development of fusion proteins such as TMPRSS2:ERG (Cai *et al.*, 2009; Mitchell and Neal, 2015; Wang *et al.*, 2018; Zhang *et al.*, 2020). Compensation for AR inhibition can also occur in prostate cancer, with upregulation of the glucocorticoid receptor (GR) seen following enzalutamide treatment. GR target genes overlap with over 50% of AR target genes, so upregulation of GR activity sustains androgen related signalling independent of androgen ligands, leading to enzalutamide resistance (Arora *et al.*, 2013; J. Li *et al.*, 2017). The transcription factor GATA2 also plays a large role in maintenance of androgen related signalling in CRPC. GATA2 binds to AREs in response to androgen stimulation and enables the binding of AR to *PSA* and *TMPRSS2* enhancer regions (Böhm *et al.*, 2009; Wu *et al.*, 2014). GATA2 has been linked to resistance to chemotherapy and cancer progression via regulation of critical

cancer related genes including *IGF2*. GATA2 binds to the promoter of *IGF2* regulating its expression. *IGF2* shows increased expression with cancer progression and in androgen-independent tumours which are resistant to anti-androgen treatment (Vidal *et al.*, 2015; Rodriguez-Bravo *et al.*, 2017). Increased IGF-2 protein levels result in activation of IGF-1R and insulin receptor (INSR) by IGF-2, due to the homology of the IGF-1, IGF-2, and insulin ligands. This triggers activation of both the PI3K and the Ras-Raf-Mitogen-activated protein kinase (MAPK) pathways which activate a range of downstream targets involved in cell growth, proliferation and cell survival, thereby contributing to cancer growth (Adams *et al.*, 2000; Baserga, Peruzzi and Reiss, 2003; Livingstone, 2013). This implicates the IGF-1R signalling pathway in prostate cancer progression and is discussed in further detail in Section 1.4. IGF-2 mediated activation of the MAPK signalling pathway also leads to downstream activation of GATA2, demonstrating a positive feedback loop of GATA2 activation, helping to further sustain androgen related signalling in an androgen-independent manner, and therefore resistance to ADT and anti-androgen targeted therapies (Towatari *et al.*, 1995; Carceles-Cordon *et al.*, 2020). However, recent trials involving co-treatment of ADT or docetaxel with monoclonal antibody inhibitors of IGF-1R did not show statistically significant differences to treatment without IGF-1R inhibition, potentially due to compensatory signalling by INSR (De Bono *et al.*, 2014; Yu *et al.*, 2015).

A wide variety of other compensatory signalling or genetic alterations are also seen in development of treatment resistance, including functional loss of *PTEN* alongside further changes to the PI3K and MAPK signalling pathways, *MYC* oncogene overexpression and defects in the cell cycle and DNA repair mechanisms (Shen and Abate-Shen, 2010; Mitchell and Neal, 2015; Wang *et al.*, 2018; Carceles-Cordon *et al.*, 2020). This demonstrates the need to further investigate and understand the pathways involved in these

resistance mechanisms, allowing for development of targeted co-treatments to counteract current drug resistance and further improve treatment of advanced prostate cancers.

1.2 The IGF-axis

IGF-1R is a transmembrane receptor tyrosine kinase (RTK), a heterotetrameric receptor made up of two extracellular α- and two transmembrane β-subunits, that plays an important role in normal cell growth and differentiation and has been shown to play a role in cancer development. The IGF-axis includes the IGF-1R, its corresponding ligands IGF-1 and IGF-2, as well as ligand binding proteins (IGFBPs) and signalling adaptor proteins including insulin receptor substrates 1 to 4 (IRS-1 to IRS-4), and Src homology and collagen domain protein (Shc). IGF-1R shares a large sequence homology with the related INSR and can form IGF-1R – INSR hybrid receptors containing an α- and a β-subunit from both receptors. The following section outlines the components of the IGF-axis and their functions.

1.2.1 IGF receptors

IGF-1R is a ubiquitously expressed, transmembrane, heterotetrameric RTK made up of two extracellular α- and two transmembrane β-subunits linked by disulphide bonds and is the main mediator of IGF related signalling and activity. The *IGF-1R* gene is a single copy gene located on the long arm of chromosome 15, spanning 100 kilobases (kb) of DNA containing 21 exons. On activation of the gene, IGF-1R is expressed as a single precursor molecule 1367 amino acids in length and made up of a 30-residue signal peptide at its N-terminus followed by the α- and β-subunit sequences known as the pre-proreceptor. The N-terminal signal peptide is cleaved during translation to give a 220 kDa proreceptor (Ullrich *et al.*, 1986). The proreceptor is then post translationally glycosylated in the endoplasmic reticulum, and then processed to the Golgi apparatus where it is cleaved at the

Arg-Lys-Arg-Arg sequence present at residues 707-710. This produces the separate α- (~ 140 kDa) and β-subunits (~ 100 kDa), linked by primary disulphide bonds, which then forms the mature receptor in an $\alpha_2\beta_2$-configuration, where two αβ-chains are joined by secondary disulphide bonds. The mature receptor is then trafficked to the cell surface and inserted into the cell membrane with the extracellular α-subunit containing the ligand binding domain, and the intracellular β-subunit containing small extracellular and trans-membrane domains and an intracellular tyrosine kinase domain (Figure **1.1**a) (Ullrich *et al.*, 1986; Le Roith *et al.*, 1995; Adams *et al.*, 2000; Li *et al.*, 2019). IGF-2R is also ubiquitously expressed, but in contrast to IGF-1R it is a type I transmembrane protein as it only has a single transmembrane domain. Full-length IGF-2R is 300 kDa in size and is made up of a large N-terminal extracellular region of 15 homologous domains, a single transmembrane region, and a small C-terminal cytoplasmic tail and appears to function as a homodimer at the plasma membrane. Each of the 15 homologous extracellular domains are made up of approximately 147 amino acid residues and are homologous to the extracellular domain of the mannose-6-phosphate receptor. The IGF-2 ligand binding site is located in domain 11 of the extracellular region, however the receptor does not contain an intracellular tyrosine kinase domain so is not thought to play a role in signalling activation (Figure **1.1**b) (Braulke, 1999; Ghosh, Dahms and Kornfeld, 2003; Brown *et al.*, 2008).

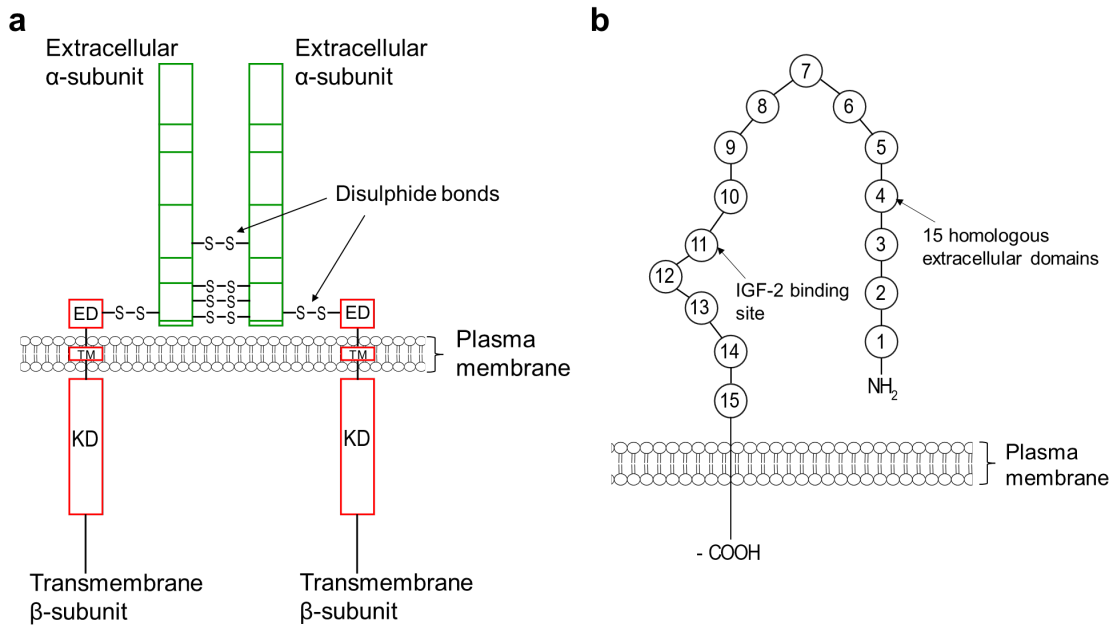


Figure 1.1 Structure of IGF-1R and IGF-2R
a Domain structure of mature IGF-1R at the plasma membrane, showing extracellular α-subunit (green), transmembrane β-subunit (red), extracellular (ED), transmembrane (TM), kinase domains (KD) and disulphide bonds, modified from (Adams *et al.*, 2000). **b** Domain structure of IGF-2R monomer at the plasma membrane, showing the 15 homologous extracellular domains and IGF-2 binding site. IGF-2R does not contain a kinase domain and, although not sure here, is usually active as a homodimer. Modified from (Bergman *et al.*, 2013).

1.2.2 IGF ligands

IGF-1R is activated by the IGF-1 and IGF-2 ligands that are produced by the liver in response to growth hormone (GH) and locally in tissues, exerting both endocrine and paracrine activity (Daughaday and Rotwein, 1989; Le Roith *et al.*, 1991). IGF-1 binds IGF-1R with the highest affinity, followed by IGF-2 which has 5-times lower binding efficiency (De Meyts *et al.*, 1994). Due to its large homology with INSR, approximately 57% sequence identity, IGF-1R also binds insulin ligand, but with roughly 500 – 1000 times lower affinity than IGF-1 (De Meyts *et al.*, 1994). The three ligands share a common 3D structure and, like insulin, the IGFs are made up of a single chain of amino acids. All three have an A and a B chain connected by disulphide bonds, but the IGFs also contain a 12 amino acid long C chain joining the A and B chains. This C chain is present in pro-

insulin but is cleaved during the production of mature insulin ligand (Adams *et al.*, 2000; Laron, 2001).

In normal conditions, IGF-2R functions to clear IGF-2 from the cell surface via receptor mediated endocytosis to attenuate activation of IGF-1R signalling by IGF-2. IGF-2R also transports lysosomal acid hydrolase precursors from the Golgi apparatus to the lysosome but has no intracellular kinase domain so is unlikely to act as a signalling molecule (Braulke, 1999; Ghosh, Dahms and Kornfeld, 2003; Brown *et al.*, 2008).

One molecule of ligand binds to IGF-1R at any one time via the α-CT domain of the extracellular α-subunit. The interaction involves L1 and CR domains of one IGF-1R protomer, and the α-CT and FnIII-1 domains of the other. The α-CT domain from one protomer that is bound to the ligand forms a rigid beam-like structure with the α-CT domain from the other protomer that is unliganded, preventing binding of more than one ligand at a time to the IGF-1R structure. This interaction induces large structural rearrangements of IGF-1R, bringing the two intracellular kinase domains into proximity with each other for receptor activation (Xu *et al.*, 2018; Li *et al.*, 2019). The difference in affinity of IGF-1R and INSR for the IGF and insulin ligands is likely due to minor structural differences between the two receptors. For example, there is a shorter distance between the two FnIII-3 domains in the structure of the INSR ectodomain–insulin complex compared to the IGF-1R-IGF interaction, and while most residues in the ectodomains of the two receptors are conserved, there are some residues found to be key for IGF-1 binding that are not present in the INSR (Xu *et al.*, 2018; Li *et al.*, 2019).

1.2.3 IGF binding proteins

Over 90% of circulating IGF-1 and IGF-2 ligand is bound to one of the 6 homologous IGFBPs, with IGFBP3 accounting for at least 75% of IGF ligand binding. IGFBPs are found in the circulation where they play a role as a circulating transport protein for IGF-1

and IGF-2, forming a ternary complex containing IGF ligand, IGFBP and the acid labile subunit (ALS), regulating the bioavailability and increasing the half-life of the IGF ligand (Hwa, Oh and Rosenfeld, 1999; Firth and Baxter, 2002; Le Roith, 2003). Proteases such as the pregnancy-associated plasma protein-A (PAPP-A) family, can cleave IGFBPs, leading to release of IGFs from the IGF/IGFBP complex and increasing the amount of IGFs available for IGF-1R binding (Lawrence *et al.*, 1999; Oxvig, 2015).

As well as regulating IGF-1R activation by altering availability of IGF ligands, IGFBPs have been shown to play a role in a wide range of other cellular functions via IGF independent mechanisms including cell motility and adhesion, apoptosis and survival, and cell cycle regulation (Rajah, Valentinis and Cohen, 1997; Perks, 1999; Fanayan *et al.*, 2000; Firth and Baxter, 2002). More recently, IGFBP3 has been shown to be detectable in the nucleus and has a characterised nuclear localisation sequence (NLS) that interacts with the nuclear import protein importin-β. Nuclear IGFBP3 is thought to have a role in transcriptional regulation and has been shown to interact with nuclear proteins such as retinoid X receptor-α and some of its dimerization partners, modulating their function (Liu *et al.*, 2000; Schedlich *et al.*, 2007). IGFBP3 has also been shown to form a complex with the epidermal growth factor receptor (EGFR) in response to DNA damage, translocating to the nucleus to interact with DNA-dependent protein kinase catalytic subunit (DNA-PKcs) and promote double strand break (DSB) repair, potentially by non-homologous end joining (NHEJ) (Lin *et al.*, 2014; Baxter, 2015). IGFBP3 has also been shown to be more highly expressed in radiosensitive vs radioresistant cell lines (Zhao *et al.*, 2012; Baxter, 2015).

1.2.4 IGF-1R and INSR hybrids

As previously mentioned, there is a large sequence and structural homology between IGF-1R and INSR. The INSR has a distinct function from IGF-1R and is present in two isoforms, either INSR-A or INSR-B, due to differential splicing of exon 11. This results in

an extra 12 amino acid residues encoded by exon 11 to be present at the carboxyl terminus of the α-subunit in INSR-B. The isoforms also have different functions, with INSR-A involved in prenatal growth and development, and INSR-B, the classical form of the receptor, involved in glucose uptake and metabolic regulation (Lee and Pilch, 1994; Adams *et al.*, 2000; Le Roith, 2003). In tissues that express both IGF-1R and INSR, formation of IGF-1R – INSR hybrid receptors can occur, containing one α- and one β-subunit from each (Federici, Porzio, Zucaro, Fusco, *et al.*, 1997; Federici, Porzio, Zucaro, Giovannone, *et al.*, 1997). Both INSR isoforms can form hybrid receptors with IGF-1R, but depending on the isoform present, the hybrid receptors have different affinities for the IGF and insulin ligands. INSR-A receptor binds IGF-2 with high affinity and may be important in the functional role of IGF-2 in foetal development (Frasca *et al.*, 1999). This potentially explains why IGF-1R/INSR-A hybrid receptors can bind IGF-1, IGF-2, and insulin, exhibiting cell proliferation and migration effects similar to the action of IGF-1R. Hybrid receptors containing the INSR-B isoform in contrast can only bind to IGF-1 ligand, but also exhibit effects similar to that of IGF-1R activation (Pandini *et al.*, 2002).

1.3 IGF-1R signalling pathways

Binding of IGF-1R to its ligand causes a conformational change in the receptor, bringing the two intracellular kinase domains into proximity with each other, causing autophosphorylation of tyrosine residues 1131, 1135 and 1136 resulting in receptor activation (Adams *et al.*, 2000; Li *et al.*, 2019). The autophosphorylation of the tyrosine residues in the receptor kinase domain results in phosphorylation of juxtamembrane tyrosines and carboxyl-terminal serines, forming binding sites for the IRS and Shc adaptor proteins. Recruitment of these adaptor proteins then triggers signalling via the PI3K-Akt pathway and the MAPK pathway (Butler *et al.*, 1998; Adams *et al.*, 2000; Chitnis *et al.*,

2008). Differing phosphorylation of the juxtamembrane tyrosines of IGF-1R may result in differing recruitment of adapter proteins to the receptor (Tartare-Deckert *et al.*, 1995), and the structure of the intracellular juxtamembrane region containing the adaptor protein binding sites mediate the differing signal activation between the closely related IGF-1R and INSR (Cai *et al.*, 2017). The signalling pathways activated by IGF-axis stimulation and their downstream effects are outlined below and illustrated in Figure **1.2**.

1.3.1 PI3K-Akt signalling

There are 4 IRS proteins in mammalian cells, but IRS-1 and IRS-2 are the two most well characterised and are involved in signalling via IGF-1R. When IGF-1R is activated, tyrosine residue 950, located within an NPXY motif in the juxtamembrane region of the cytoplasmic domain, is phosphorylated. This phosphorylated tyrosine is then bound by IRS-1 via its phosphotyrosine binding domain (PTB), which in turn is bound by the PI3K heterodimer (Adams *et al.*, 2000; Le Roith, 2003). This interaction occurs via binding of the PI3K regulatory subunit (p85) to the Src homology 2 (SH2) domain of IRS-1, stimulating the catalytic subunit of PI3K (p110) to convert phosphatidylinositol 4,5-biphosphate (PIP_2) into phosphatidylinositol 3,4,5-triphosphate (PIP_3) by phosphorylation at the inner lipid bilayer of the plasma membrane. The dephosphorylation of PIP_3 to PIP_2 is negatively regulated by PTEN. PIP_3 binds to and recruits various signalling proteins via binding of their pleckstrin homology domains (PH). In this case, PIP_3 binds to phosphoinositide-dependent kinase 1 (PDK1) and AKT via this domain, bringing them into close proximity with each other at the plasma membrane, facilitating PDK1 phosphorylation of AKT at threonine 308 (Currie *et al.*, 1999; Majumder and Sellers, 2005). The phosphorylation of AKT then triggers a wide range of biological responses, including cell survival, cell growth and proliferation and cell motility (Baserga *et al.*, 1997; Chitnis *et al.*, 2008).

1.3.1.1 Cell survival

AKT mediated signalling triggers a response in a wide range of cell survival related effectors, including both pro- and anti-apoptotic proteins and pro-survival gene expression. Activated AKT phosphorylates serine 136 of B cell leukaemia 2 antagonist of cell death (Bad), a pro-apoptotic protein, causing it to form a complex with 14-3-3ζ protein. This prevents Bad from carrying out its normal function of binding and inhibiting the action of antiapoptotic members of the Bcl-2 family, including Bcl-XL and Bcl-2, thus promoting cell survival (Datta *et al.*, 1997; Butler *et al.*, 1998). Activated AKT also phosphorylates serine 196 of caspase 9, in what is thought to be an allosteric inhibition mechanism, preventing caspase 9 activation and therefore preventing activation of the pro-apoptotic caspase cascade (Cardone *et al.*, 1998). Further effects on inhibition of apoptosis are exerted by AKT via regulation of p53 activity, as p53 is involved in activation of pro-apoptotic gene transcription. The BH3-only proteins are proapoptotic members of the Bcl-2 family that bind and inhibit other antiapoptotic members of the Bcl-2 family, such as proteins Bcl-XL and Bcl-2, inhibiting their function. The genes of two of these BH3-only proteins, PUMA and NOXA, are activated by p53 transcription factor activity (Aubrey *et al.*, 2018). Mouse double minute 2 homolog (Mdm2), is an E3 ubiquitin protein ligase that interacts with and ubiquitinates p53, triggering its export from the nucleus to the cytoplasm where it is targeted for degradation (Oliner *et al.*, 1993; Haupt *et al.*, 1997; Michael and Oren, 2003). Activated AKT phosphorylates Mdm2 on serine 186, promoting ubiquitination of p53 by Mdm2, and therefore its degradation (Ogawara *et al.*, 2002). This results in reduced gene expression of genes encoding for pro-apoptotic BH3-only proteins due to lower p53 levels, therefore contributing to cell survival.

Forkhead box O (FOXO) transcription factors are involved in multiple signalling pathways and play critical roles in multiple cellular processes including regulation of apoptosis. For

example, FOXO3a activates expression of the *FasL* gene, encoding for the Fas ligand protein required by the pro-apoptotic death inducing signalling complex (DISC) (Brunet *et al.*, 2004). Also, FOXO3, and potentially FOXO1, activate expression of tumour necrosis factor-related apoptosis-inducing ligand (TRAIL), another pro-apoptotic protein, via interaction with the TRAIL promoter (Modur *et al.*, 2002). Activated AKT exerts transcriptional control over apoptosis related proteins by phosphorylation of serine and threonine sites on these FOXO transcription factors, triggering the binding of 14-3-3 proteins to the FOXOs. The FOXO-14-3-3 protein complex is then exported from the nucleus by chromosomal region maintenance 1 (CRM1) protein and Ran GTPase into the cytoplasm, halting transcription of the FOXO target genes (Burgering and Kops, 2002; Fu and Tindall, 2008). This therefore prevents the expression of the pro-apoptotic proteins transcribed by FOXO target genes, contributing to cell survival.

Phosphorylated AKT also activates NF-κB, a transcription factor which has been shown to be involved in expression of a wide range of antiapoptotic proteins including Bcl-XL and Bcl-2, among others (Van Antwerp *et al.*, 1996; Chen, Edelstein and Gelinas, 2000; Hong *et al.*, 2000; Kreuz *et al.*, 2001).

1.3.1.2 Cell growth and proliferation

The mammalian target of rapamycin complex 1 (mTORC1) is a protein complex involved in control of growth-related gene activation and protein synthesis, made up of regulatory-associated protein of mTOR (Raptor), mammalian lethal with SEC13 protein 8 (MLST8), PRAS40 and DEPTOR (Kim *et al.*, 2002; Yip *et al.*, 2010). The action of the mTORC1 complex is controlled by the TSC1/TSC2 protein complex, a GTPase. mTORC1 is activated by Ras homologue enriched in brain (Rheb)-GTP, a G protein located at the surface of late endosomes and lysosomes. mTORC1 is localised to the surface of these structures via Rag GTPase heterodimers, which are active only in the presence of

sufficient amino acid levels, interacting with the Raptor subunit of mTORC1, allowing the complex to come into proximity and interact with Rheb-GTP (Huang and Manning, 2008; Sancak *et al.*, 2008). Rheb-GTP is hydrolysed by the TSC1/TSC2 complex to form the inactive Rheb-GDP, therefore preventing activation of the mTORC1 complex. Activated AKT can inhibit the action of the TSC1/TSC2 complex by directly phosphorylating serine 939 and threonine 1462 of the TSC2 subunit, disrupting formation of the TSC1/TSC2 heterodimer (Inoki *et al.*, 2002). This therefore prevents hydrolysis of Rheb-GTP meaning the activation of mTORC1 is uninhibited. Phosphorylated AKT can also directly phosphorylate PRAS40, a subunit of mTORC1. This causes PRAS40 to disassociate from the complex, allowing p70 ribosomal protein S6 kinase 1 (S6K) and eukaryotic translation initiation factor 4E-binding protein 1 (4EBP1) substrate uptake by Raptor (Oshiro *et al.*, 2007; Sancak *et al.*, 2007; Wiza, Nascimento and Ouwens, 2012). Activated mTORC1 phosphorylates these S6K and 4EBP1 substrates, triggering their activation. S6K phosphorylates proteins such as S6 ribosomal protein and eukaryotic initiation factor 4B (eIF4B), and phosphorylation of 4EBP1 disrupts its interaction with the cap-dependent translation initiation factor eIF-4E, overall triggering activation of growth-related genes, translation initiation, and protein synthesis (Hay and Sonenberg, 2004; Richter and Sonenberg, 2005; Sonenberg and Hinnebusch, 2009).

AKT mediated signalling also influences cell growth and proliferation via control of cell cycle regulatory proteins (Chang *et al.*, 2003). As previously mentioned, phosphorylated AKT reduces protein levels and therefore action of p53 via activation of Mdm2. One of the targets of p53 is p21, a cyclin dependent kinase (CDK) inhibitor (Xiong *et al.*, 1993). When p21 is activated by p53, it binds to and inhibits CDK2, the kinase required for progression from G_1 to S phase of the cell cycle, causing cell senescence (Wade Harper *et al.*, 1993). Therefore, inhibition of p53 by the activity of AKT causes reduced activation of

p21 and therefore increased progression of the cell cycle from G_1 to S, increasing cell proliferation. p21 has also been shown to regulate proliferating cell nuclear antigen (PCNA) activity, a DNA polymerase co-factor required in S-phase DNA synthesis and DNA damage repair (Waga, Hannon and Beach, 1994; Moldovan, Pfander and Jentsch, 2007). p21 binds to the PIP-box region of PCNA, usually bound by recruited co-factors required for PCNA dependent DNA synthesis, therefore inhibiting PCNA function (Podust *et al.*, 1995). This inhibits S-phase DNA replication and leads to cell senescence, an effect that is abrogated by inhibition of p21 by AKT mediated signalling.

p27 is another CDK inhibitor protein that can regulate CDK2 as well as CDK4 activity, via binding and inhibition of the cyclin E or cyclin D subunits respectively, leading to G_1 arrest (Lacy *et al.*, 2005; Chu, Hengst and Slingerland, 2008). Expression of p27 is controlled by FOXO transcription factors, which are inhibited by AKT mediated signalling as previously mentioned (Medema *et al.*, 2000). Therefore, activation of AKT results in decreased expression of p27, contributing to unchecked progression from G_1 to S phase and cell proliferation. Phosphorylated AKT has also been shown to directly interact and phosphorylate p27 at threonine 157 to exert the same effect (Liang *et al.*, 2002; Shin *et al.*, 2002; Viglietto *et al.*, 2002).

AKT mediated signalling can also control the action of cell cycle regulation by cyclin D via the phosphorylation of glycogen synthase kinase-3 beta (GSK-3β). GSK-3β is a serine/threonine protein kinase that is constitutively active in unstimulated cells. Cyclin D is directly phosphorylated at threonine 286 by GSK-3β, triggering cyclin D to be exported from the nucleus to the cytoplasm and recognised by E1 and E2 ubiquitin-conjugating enzymes for degradation by the ubiquitin-dependent proteolysis pathway (Diehl *et al.*, 1998). This reduces cyclin D protein levels and inhibits their contribution to progression from G_1 to S phase via interaction with CDKs. When AKT is activated, it directly

phosphorylates GSK-3β at serine 9 inhibiting its constitutive activity, this prevents degradation of cyclin D and allows for G_1 to S phase transition (Cross *et al.*, 1995; Van Weeren *et al.*, 1998). Analogous interactions with GSK-3β also occur involving other cell cycle regulation proteins and transcription factors such as cyclin E (Welcker *et al.*, 2003), p27 (Wang *et al.*, 2008), p53 (Charvet and Maurer, 2011), c-Myc (Yada *et al.*, 2004), NF-κB (Hoeflich *et al.*, 2000), and FOXOs (G-Amlak *et al.*, 2002) among others (Mccubrey *et al.*, 2014).

1.3.1.3 Cell motility

Activation of IGF-1R signalling is associated with an increased tendency for cellular invasion and metastasis of cancer cells. Previous work has shown that IGF-1 induced phosphorylation of IRS-1 results in β-catenin phosphorylation. This disrupts the E-cadherin/β-catenin complex, required at the plasma membrane for cellular adherence via the actin cytoskeleton, resulting in cell detachment and contributing to tendency towards cellular metastasis (Playford *et al.*, 2000). IGF-1R also interacts with β1 and β3 integrins via RACK1, a scaffolding protein (Kiely *et al.*, 2005). This integrin interaction mediates a stabilisation of β1 integrin in prostate cancer cells, and formation of a protein complex made up of αv integrin, E-cadherin and IGF-IR in colon and cervical cancer cells, that mediates cell migration (M. R. Shen *et al.*, 2006; Canonici *et al.*, 2008; Soung, Clifford and Chung, 2010; Sayeed *et al.*, 2013; Cox *et al.*, 2015). It has also recently been shown that IGF-1 ligand can directly bind to integrin proteins, forming an integrin-IGF-1-IGF-1R protein complex at the cell surface that may also confer cell migratory effects (Takada, Takada and Fujita, 2017).

Matrix metalloproteases (MMPs) are enzymes involved in degradation of the extra cellular matrix (ECM) during normal physiological processes such as development and wound healing, but also in pathological processes including development of metastasis. AKT

activation via IGF-1R can regulate activity of MMPs (Zhang, Samani and Brodt, 2003) and has specifically been shown to increase the expression and activity of MMP-2 and -9 in DU145 prostate cancer cells, increasing cellular invasion (Saikali *et al.*, 2008). IGF-1R signalling is also thought to drive migration and invasion phenotypes in triple negative breast cancer (TNBC) via a focal adhesion kinase (FAK) pathway mediated mechanism (Taliaferro-Smith *et al.*, 2015), as well as regulating angiogenesis in a wide range of breast cancers via stimulation of vascular endothelial growth factor (VEGF) (Kucab and Dunn, 2003).

1.3.2 MAPK signalling

Activation of IGF-1R also triggers signalling via the MAPK pathway, mediating cell growth, survival, and cellular differentiation. Phosphorylation of the tyrosine kinase domain of IGF-1R triggers recruitment and phosphorylation of the Shc adaptor protein via its PTB domain, which in turn recruits a second adaptor protein called growth factor receptor-bound protein 2 (Grb2). Grb2 then triggers activation of the Ras GTP-binding protein via interaction with Sos, a guanine nucleotide exchange factor, which triggers a phosphorylation signal cascade via Raf, MEK-1 (MAPK and extracellular signal related kinase (ERK) kinase 1) and MEK-2 that activates ERK-1 and ERK-2 via phosphorylation of their threonine and tyrosine residues (Adams *et al.*, 2000; Taniguchi, Emanuelli and Kahn, 2006). Activated ERKs then phosphorylate a wide array of target proteins, including 40S ribosomal protein S6 kinase (RSK) triggering its activation and phosphorylation of ribosomal protein S6, activating it for translation (Taniguchi, Emanuelli and Kahn, 2006). Activated RSK has also been shown to negatively regulate the Ras-MAPK signalling pathway by phosphorylation of Sos (Saha *et al.*, 2012). ERKs also activate a wide range of transcription factors including, c-Myc, c-Fos, c-Jun and cAMP response element binding protein (CREB) among others (Chen *et al.*, 2001), and phosphorylates TSC2, disrupting

the TSC1/TSC2 protein complex involved in inhibition of mTOR signalling (Ma *et al.*, 2005).

Three other subfamilies of MAPKs also exist, including c-Jun-amino-terminal kinase (JNK), p38 kinases, and ERK5 (Chen *et al.*, 2001). JNKs and the p38 kinases are activated in response to stress stimuli such as reactive oxygen species, substrate deprivation and UV radiation, but can also be activated by receptor tyrosine kinase signalling (Ono and Han, 2000; Bode and Dong, 2007). JNKs interact with a wide range of downstream signalling molecules including c-Jun, p53, Elk-1 and STAT-3, among others, contributing to regulation of cell growth and proliferation and cell survival (Bode and Dong, 2007). The p38 kinases activate similar transcription factors to JNKs but are also involved in pro-inflammatory cytokine production and inflammation (Kyriakis and Avruch, 2001; Yang *et al.*, 2014). ERK5 is the most recently discovered MAPK and much less is known about its function. However, it is thought to be activated by a range of growth factors and stress stimuli and play a role in cardiovascular development and vascular integrity, tumour angiogenesis and resistance to apoptosis (Nithianandarajah-Jones *et al.*, 2014).

There also exists some crosstalk between the PI3K/AKT and MAPK signalling pathways. As well as binding Shc to instigate the MAPK pathway signalling, Grb2 can also bind to IRS-1 via its SH2 domain, resulting in activation of the PI3K pathway (Adams *et al.*, 2000). PI3K/AKT activation can also directly phosphorylate and inhibit Raf, preventing activation of the MAPK pathway (Rommel *et al.*, 1999; Reusch *et al.*, 2001), and PDK1 is required for RSK activation along with ERK1/2 (Cargnello and Roux, 2011). As previously mentioned, both AKT and ERK phosphorylate TSC2 resulting in activation of mTOR signalling (Inoki *et al.*, 2002; Ma *et al.*, 2005). This demonstrates some of the overlapping functions of the two pathways and helps to explain the compensatory mechanism of cells when only one of these pathways is inhibited.

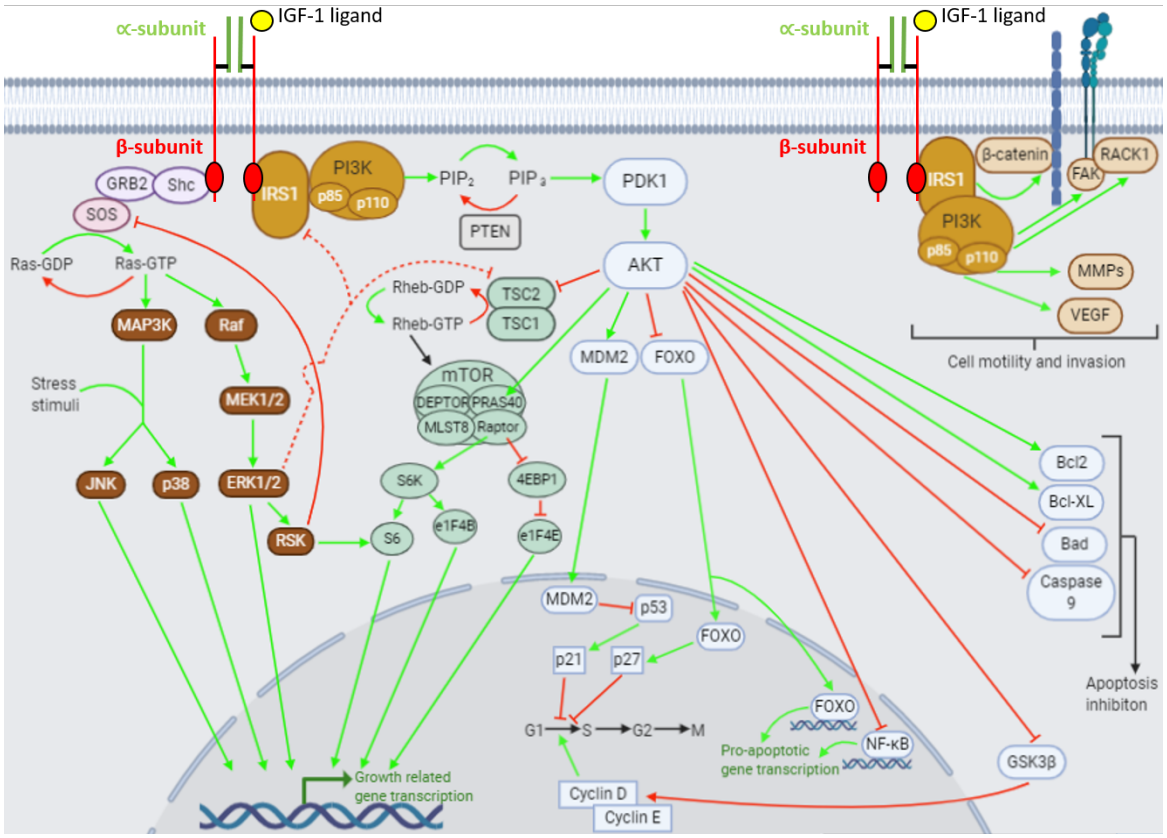


Figure 1.2 IGF-1R signalling pathways

Figure showing the general components involved in signalling from IGF-1R. Upon ligand binding, phosphorylation of the kinase domain of the receptor leads to activation of the PI3K/Akt and the Ras-Raf-MAPK pathways, leading to downstream effects on processes such as cell growth and proliferation, cell motility and cell survival. The green arrows represent activation of subsequent protein, and red lines represent inhibition. Figure was constructed using information from references in the text.

1.4 IGF signalling in cancer

Under normal physiological conditions, IGF-axis signalling is tightly regulated, however the IGF-axis has long been recognised for its contribution to cancer growth and metastasis due to the activation of cell proliferation and survival by IGF signalling (Resnicoff *et al.*, 1995; Baserga, Peruzzi and Reiss, 2003). High levels of circulating IGF-1 ligand have been shown to be associated with increased risk of developing a range of common cancers including breast, colorectal and prostate cancer (Ma *et al.*, 1999; Renehan *et al.*, 2004; Key *et al.*, 2010; Price *et al.*, 2012; Travis *et al.*, 2016). This has also been demonstrated by the almost complete lack of cancer development in patients with Laron dwarfism, who have low levels of serum IGF-1 due to mutation of the GH receptor (Guevara-Aguirre *et al.*, 2011; Steuerman, Shevah and Laron, 2011).

IGF-axis signalling has been implicated in both cancer progression and in treatment resistance, which has led to it becoming a potential target for cancer therapy. The following section outlines the effects of IGF signalling in cancer biology, specific effects in prostate cancer and current IGF targeting treatment methods.

1.4.1 Alteration of IGF-axis components in cancer

Overexpression of IGF-1R is common in cancers, resulting in increased IGF signalling thereby promoting cell growth and proliferation (Hellawell *et al.*, 2002; Law *et al.*, 2008; Cox *et al.*, 2009). Upregulation of IGF-1R is not usually an initial driver of cancer development, but usually occurs following loss of function of tumour suppressor genes or activation of oncogenes. Loss of function of *BRCA1*, *TP53, WT1* or *vHL* tumour suppressor genes which usually negatively regulate IGF-1R expression was shown to cause IGF-1R overexpression in cancers (Werner *et al.*, 1995, 1996; Maor *et al.*, 2000, 2007; Idelman *et al.*, 2003; Yuen *et al.*, 2007). Conversely activation of p53 and c-myb oncogenes also promoted overexpression of IGF-1R (Phillips *et al.*, 1991; Werner *et al.*,

1996; Idelman *et al.*, 2003). Preclinical work has shown overexpression of IGF-1R in lung, breast, prostate, glioma and gastrointestinal cancers and has been found to associate with poor prognosis (Nakajima *et al.*, 2005; Trojan *et al.*, 2007; Pollak, 2012; Heskamp *et al.*, 2015; Sun *et al.*, 2015; Yeo *et al.*, 2015).

Activation of the IGF-axis in cancer is not just reliant on overexpression of IGF-1R, as it is also affected by altered expression or activity of its other components. Loss of function mutation in the *IGF-2R* gene results in reduced anti-proliferative effects due to reduced uptake and degradation of IGF-2 by IGF-2R. This therefore increases the bioavailability of IGF-2 for activation of IGF-1R, thereby contributing to increased proliferative and anti-apoptotic signalling, an effect which has been seen in prostate cancer and melanoma (Hu *et al.*, 2006; Iida *et al.*, 2018). Elevated circulating levels of IGF-2 ligand have been found to associate with increased risk of cancer development, analogous to IGF-1, and loss of imprinting of the *IGF2* gene is clinically associated with colorectal cancer, Wilms tumour and hepatocellular carcinoma (Cui *et al.*, 2003; Breuhahn and Schirmacher, 2008; Riccio *et al.*, 2009; Livingstone, 2013). Contributing to this, more recent work has also shown secretion of IGF-2 ligand by cellular components of the tumour stroma (Lee *et al.*, 2015; Unger *et al.*, 2017).

Reduced expression of IGFBPs has also been detected in cancer, resulting in increased IGF ligand availability for IGF-1R and therefore increased proliferative and cell survival signalling. As previously mentioned, IGFBP3 accounts for the majority of IGF-1 ligand binding and was found to have reduced expression in hepatocellular carcinoma in preclinical studies (Enguita-Germán and Fortes, 2014). IGFBP7 has also been found to act as a tumour suppressor in HCC and overexpression of IGFBP7 resulted in inhibition of tumour growth (Chen *et al.*, 2011). Tumours have been shown to secrete IGFBP proteases, which cleave IGFBPs to release IGF ligands and increase their bioavailability. PSA was

one of the first identified IGFBP proteases and is upregulated in prostate cancer (Cohen *et al.*, 1992). It has been shown to cleave IGFBP5 in prostate cancer bone metastasis, therefore increasing the levels of bioactive IGF ligand (Maeda *et al.*, 2009). MCF-7 breast cancer cells have also been shown to secrete an IGFBP3 protease, and inhibition of proteolysis of IGFBPs has been shown to inhibit growth of PC-3 prostate cancer cell line *in vitro* and inhibit tumour growth in a murine breast cancer model (Angelloz-Nicoud and Binoux, 1995; Salahifar, Baxter and Martin, 1997; Ryan *et al.*, 2009). These effects on IGFBPs result in increased bioavailability of IGF ligand and, combined with overexpression of IGF-1R, contributes to increased IGF-axis-mediated proliferation and cell survival signalling in cancer.

1.4.2 Role in cancer progression

The combination of increased proliferation and cell survival as a result of upregulated IGF-axis signalling in cancer is thought to contribute to development of invasive, metastatic phenotypes (Samani *et al.*, 2007). Early work in IGF-1R null mouse fibroblasts showed that they were unable to undergo transformation and anchorage-independent growth, two factors required for metastasis. Re-introduction of IGF-1R into these cells reversed this phenotype (Sell *et al.*, 1994). Later work in Lewis lung carcinoma found that IGF-I was the major factor promoting the growth of highly metastatic tumour cells in the mouse liver (Brodt *et al.*, 2001; Samani *et al.*, 2004) and similar results were also seen in a colon adenocarcinoma model (Wu *et al.*, 2002). IGF signalling has also been implicated in targeting of metastasis of various cancers to bone, including myeloma, neuroblastoma, breast and prostate cancer, potentially due to the high concentration of IGF ligand produced locally by bone cells (Shariat *et al.*, 2002; Van Golen *et al.*, 2006; Hiraga *et al.*, 2012; Zhang *et al.*, 2013; Rieunier *et al.*, 2019). IGF signalling in cancer contributes to metastasis development by promoting epithelial to mesenchymal transition (EMT) and

anchorage independent growth (H. Li *et al.*, 2017). In prostate and gastric cancer, activation of the MAPK pathway via IGF-1R results in up-regulation of ZEB1 and ZEB2 expression, transcription factors which downregulate E-cadherin and therefore contribute to EMT (Graham *et al.*, 2008; Li *et al.*, 2014, 2015). IGF-1R mediated PI3K and MAPK signalling also results in phosphorylation and inactivation of GSK-3β. GSK-3β has been shown to directly reduce expression of Snail and Slug transcription factors through proteasome-dependent degradation or NF-κB activation, a process which is inhibited by inactivation of GSK-3β via PI3K and MAPK signalling. Slug and Snail play a well characterised role in EMT via suppression of E-cadherin, and therefore IGF-1 signalling contributes to EMT via their increased expression (Zhou *et al.*, 2004; Bachelder *et al.*, 2005; Barrallo-Gimeno and Nieto, 2005; Ding *et al.*, 2005; Kim *et al.*, 2007).

The IGF-axis is also implicated in tumour progression by promoting activity of MMPs, as previously mentioned, which degrade the ECM, a pre-requisite for cellular invasion (Zhang, Samani and Brodt, 2003; Grzmil *et al.*, 2004; Saikali *et al.*, 2008), as well as promoting cell migration and motility (Playford *et al.*, 2000; Soung, Clifford and Chung, 2010; Takada, Takada and Fujita, 2017), and angiogenesis (Kucab and Dunn, 2003).

1.4.3 IGF-axis signalling in prostate cancer

As previously mentioned, high levels of circulating IGF-1 in serum are associated with increased risk of prostate cancer development (Price *et al.*, 2012). In developed prostate cancer, IGF-1R was found to be overexpressed in both primary prostate carcinomas and bone metastasis (Hellawell *et al.*, 2002; Cox *et al.*, 2009; Ma *et al.*, 2012). Expression of the *IGF-1R* gene can be regulated by AR signalling, the main signalling pathway implicated in prostate cancer, as AR has been shown to directly bind to the promoter of *IGF-1R*, upregulating its expression (Pandini *et al.*, 2005; Schayek *et al.*, 2010; Sharma *et al.*, 2013). This upregulation and therefore increased expression of IGF-1R is thought to

contribute to progression of prostate cancer to an androgen independent, or castrate resistant, phenotype. This is due to the increased activation of the PI3K pathway via IGF-1R, which has been shown to be associated with prostate cancer progression via mechanisms discussed above, such as activation of FOXO transcription factors, promoting EMT, and regulation of AR expression (Graff *et al.*, 2000; Wen *et al.*, 2000; H. K. Lin *et al.*, 2001; Manin *et al.*, 2002; Wu *et al.*, 2006; Jiang *et al.*, 2007).

It is also thought that IGF signalling may drive translocation of AR into the nucleus, even in the absence of androgens, creating a positive feedback loop of AR activation and IGF-1R expression and contributing to androgen independence (Wu *et al.*, 2006).

Further work has also shown that IGF-1R expression can be regulated directly by TMPRSS2:ERG (Sharon *et al.*, 2016; Mancarella *et al.*, 2017), one of the most common oncoproteins present in prostate cancer, as previously discussed (Tomlins *et al.*, 2005, 2009). ERG protein positive prostate cancer was shown to have higher protein levels of IGF-1R compared to ERG-negative cancers (Pettersson *et al.*, 2013). This increased IGF-1R expression is likely due to the activity of TMPRSS2:ERG, resulting in increased PI3K pathway activity which may contribute to the increased levels of cancer progression seen in ERG-positive cancer (Pettersson *et al.*, 2013). As previously discussed, IGF-axis activation also contributes to a GATA2 mediated mechanism for prostate cancer progression and development of androgen independence (Towatari *et al.*, 1995; Livingstone, 2013; Rodriguez-Bravo *et al.*, 2017). Overall, these functions demonstrate a significant contribution of IGF-1R mediated signalling in prostate cancer progression.

1.4.4 IGF-axis signalling as a treatment target

1.4.4.1 Role in treatment resistance

Signalling via IGF-1R can contribute to cancer treatment resistance via the general mechanisms just discussed which promote cell proliferation, cell survival, tumorigenesis

and cancer progression. However, the large amount of crosstalk between IGF-1R and other RTKs also results in general compensatory mechanisms and treatment resistance if only individual receptors are targeted in a range of cancer types, most commonly seen with EGFR (Veeken *et al.*, 2009; Wilson *et al.*, 2012; Manstein *et al.*, 2014). Acquired resistance to EGFR inhibition treatments has been seen in various lung cancers due to upregulation of IGF-1R or downregulation of IGFBP3, and therefore increased IGF-1R phosphorylation and maintenance of PI3K signalling (Guix *et al.*, 2008; Browne *et al.*, 2011; Cortot *et al.*, 2013; Suda *et al.*, 2014; Park *et al.*, 2016). Resistance to EGFR inhibition has also been seen in glioblastoma due to continued activation of the PI3K pathway by IGF-1R (Chakravarti, Loeffler and Dyson, 2002; Ma *et al.*, 2016).

Similar increased activation of IGF-1R on gefitinib treatment, an EGFR inhibitor, was also seen in the non-small cell lung cancer (NSCLC)-derived cell line PC9. On treatment with EGFR TKIs, while most cells did not survive, a small population of resistant 'drug tolerant persisters' (DTPs) remained. The cells within these DTP populations were found to have increased IGF-1R signalling and formation of DTP populations was inhibited by co-treatment with both EGFR and IGF-1R tyrosine kinase inhibitors (TKIs) (Sharma *et al.*, 2010).

Similar compensatory based resistance is also seen on single treatment with inhibitors for members of either the PI3K or MAPK signalling pathways (Wilson *et al.*, 2012; Manstein *et al.*, 2014).

Overexpression of IGF-1R has been well characterised to play a role in resistance to radiotherapy treatments, and IGF-1R inhibitor treatment has been shown to induce sensitivity to chemo- and radiotherapy in a wide range of cancers (Lloret *et al.*, 2007; King *et al.*, 2014; Dale *et al.*, 2015; Ramcharan *et al.*, 2015). Sensitivity to radiotherapy following IGF-1R inhibition or depletion in prostate cancer was shown to be due to

delayed DSB repair via inhibition of both NHEJ and homologous recombination (HR), effects which also likely contribute to chemoresistance against DNA damaging agents (Turney *et al.*, 2012; Chitnis *et al.*, 2014). Following on from this, a link between recurrence in prostate cancer patients treated with radiotherapy and increased levels of IGF-1R has been shown (Aleksic *et al.*, 2017).

IGF-1R signalling may also contribute to chemotherapy resistance in colorectal cancer via upregulation of the multidrug-resistance-associated protein-2, an efflux pump which can reduce the intracellular concentration of cytotoxic drugs (Shen *et al.*, 2012). Additionally, chemoresistance in pancreatic cells to paclitaxel treatment was found to be driven by IGF ligands derived from the tumour stroma (Ireland *et al.*, 2016). In prostate cancer, CRPC resistance to docetaxel chemotherapy treatment was shown to be mediated by upregulation of IGF-2 expression by GATA2, resulting in increased signalling via IGF-1R (Vidal *et al.*, 2015).

Signalling via IGF-1R can also contribute to resistance to hormone therapy targeting either estrogen receptor (ER) or AR. Resistance to ER targeted treatment in breast cancer is common and has been found to be mediated at least in part by increased signalling via IGF-1R, stimulating cell growth and proliferation (Wiseman *et al.*, 1993; Belfiore and Frasca, 2008; Iida *et al.*, 2019).

As discussed above, IGF-1R signalling in prostate cancer leads to development of androgen independent phenotypes and more advanced cancers that are resistant to AR-targeted ADT and castration treatments (Carceles-Cordon *et al.*, 2020).

Both the role of IGF-1R signalling in promotion of cancer progression and its contribution to treatment resistance therefore make it an attractive candidate for targeted cancer therapy.

1.4.4.2 IGF targeted therapies

The main IGF-1R targeted therapies involve three strategies including anti-IGF-1R antibodies, small molecule TKIs and ligand neutralising antibodies for IGF-1 and IGF-2. Anti-IGF-1R monoclonal antibodies (mAbs) target the extracellular subunit of IGF-1R, blocking ligand binding and therefore IGF-1R mediated signalling, as well as triggering internalisation and degradation of the receptor (Sachdev *et al.*, 2003). While they do not cross react with INSR, they have been shown to bind to IGF-1R-INSR hybrid receptors, which is likely to contribute to the dose limiting hyperglycaemia seen in some patients, due to the effect on insulin uptake (Sachdev *et al.*, 2006; Pandini *et al.*, 2007). Other mechanisms can compensate for loss of signalling via IGF-1R to counteract the effects of IGF-1R blockade, including increased signalling by INSR (Buck *et al.*, 2010; Forest *et al.*, 2015) and crosstalk from other RTKs such as EGFR (Veeken *et al.*, 2009; Wilson *et al.*, 2012; Manstein *et al.*, 2014). Preclinical work using anti-IGF-1R mAbs showed promising results, inhibiting tumour growth and cell survival in a range of cancer types (Wang *et al.*, 2005; Pandini *et al.*, 2007; Beltran *et al.*, 2009; Kurzrock *et al.*, 2010; Zhang *et al.*, 2014). However, single agent clinical trials with anti-IGF-1R mAbs have shown disappointing results with minimal patient responses, likely due to the compensatory effects mentioned above (Tolcher *et al.*, 2009; Abou-Alfa *et al.*, 2014; Becerra *et al.*, 2014; Gradishar *et al.*, 2016). One exception to this is Ewing sarcoma, which saw roughly a 10% patient response to single agent IGF-1R mAb treatment (Malempati *et al.*, 2012; Anderson *et al.*, 2016; Van Maldegem *et al.*, 2016).

Lack of responses as a single agent treatment has led to more recent trials involving combination treatments of anti-IGF-1R mAbs with other agents such as chemotherapy, hormone therapy or other targeted therapies such as anti-EGFR treatments. Some of these trials have shown positive results, including a phase 2 trial of pancreatic cancer patients

given a combination of standard chemotherapy with the anti-IGF-1R mAb ganitumab that showed an increase in PFS (Kindler *et al.*, 2010), and in NSCLC patients treated with the anti-IGF-1R mAb figitumumab in combination with chemotherapy, which showed higher overall response rates and PFS compared to chemotherapy alone (Karp *et al.*, 2009). However, in general, anti-IGF-1R mAb combination treatment trial results have been disappointing, showing no benefit in wider follow up trials in pancreatic cancer and NSCLC in combination with chemotherapy (Jassem *et al.*, 2010; Fuchs *et al.*, 2015), in breast cancer in combination with anti-estrogen therapy (Robertson *et al.*, 2009) or in NSCLC and colorectal cancer in combination with EGFR targeted treatments (Watkins *et al.*, 2011; Belani, Goss and Blumenschein, 2012), among others (Chen and Sharon, 2013). In prostate cancer, phase 2 trials testing the combination of docetaxel with figitumumab and ADT with cixutumumab, two anti-IGF-1R mAbs, also did not show statistically significant improvements in patient outcomes compared to the standard treatments alone (De Bono *et al.*, 2014; Yu *et al.*, 2015).

Small molecule TKIs have been developed to target IGF-1R signalling, but due to the reduced specificity of small molecules compared to mAbs, and the large amount of sequence homology between the two receptors, they have been found to inhibit INSR as well as IGF-1R (Carboni *et al.*, 2009; Mulvihill *et al.*, 2009; Schwartz *et al.*, 2016). Preclinical data for IGF-1R TKIs was positive, but only a few have undergone clinical trials and results were found to be disappointing. Cross reactivity with INSR resulted in dose limiting side effects such as hyperglycaemia and hyperinsulinemia with ATP-competitive TKIs, including BMS-754807, OSI-906 and XL-228, and a statistically significant improvement in patient outcome was not seen in single agent or combination treatments with these TKIs (Haluska *et al.*, 2011; Fassnacht *et al.*, 2015; Jones *et al.*, 2015; Macaulay *et al.*, 2016; Leighl *et al.*, 2017; Oza *et al.*, 2018). Unlike the three TKIs

mentioned above, AXL1717 and INSM-18 are TKIs that inhibit IGF-1R but not INSR. BMS-754807, OSI-906 and XL-228 are ATP-competitive and therefore interact with the ATP-binding site of the receptors, a region which is identical in IGF-1R and INSR. AXL1717 and INSM-18 are non-ATP competitive so do not bind the identical region of INSR, potentially avoiding the insulin related hyperglycaemia and hyperinsulinemia side effects to treatment. However, clinical trials with these two inhibitors have also had limited success (Youngren *et al.*, 2005; Cortes *et al.*, 2008).

The final major therapeutic strategy in targeting IGF-axis signalling involves development of ligand neutralising mAbs for IGF-1 and IGF-2 that do not bind to insulin. Two of these such antibodies have currently been developed, dusigitumab (MEDI-573) which binds IGF-2 with a slighter higher affinity (Gao *et al.*, 2011), and xentuzumab (BI 836845) which binds IGF-1 with slighter higher affinity (Friedbichler *et al.*, 2014). Targeting the IGF ligands rather than the IGF-1R receptor reduces the cross-reactive effects on insulin regulated activity, helping to avoid hyperglycaemic side effects seen with IGF-1R mAbs and TKIs (Gao *et al.*, 2011; Friedbichler *et al.*, 2014). Both have been tested in clinical trials, with dusigitumab showing good tolerability in a phase 1 study of patients with advanced solid tumours, but minimal single agent activity (Haluska *et al.*, 2014). A further phase 1b/2 trial in hormone receptor positive breast cancer patients in combination with targeted treatment to inhibit estrogen synthesis, showed no benefit versus estrogen inhibition alone (Clinical trial NCT01446159).

Promising preclinical work with xentuzumab showed treatment resulted in growth inhibition in rats and anticancer activity in combination with rapamycin in human tumour xenografts (Friedbichler *et al.*, 2014; Mireuta *et al.*, 2014). Xentuzumab is now being tested in various combination trials including with EGFR targeted treatment in lung cancer (Clinical trial NCT02191891) and with targeted hormone therapy in breast cancer, where

response to treatment was seen in patients with non-visceral metastasis (Crown *et al.*, 2019) and in which trials are still ongoing (Clinical trials NCT02123823 and NCT03659136).

In prostate cancer, the combination of xentuzumab and enzalutamide did not show statistically significant improved outcomes overall versus enzalutamide alone, but there was some evidence of increased PFS in patients with high tumour *IGF1* mRNA (Hussain *et al.*, 2019), and another trial in combination with enzalutamide is still ongoing (Clinical trial NCT02204072).

While overall, trials targeting IGF-axis inhibition have been disappointing, responses seen in Ewing sarcoma patients (Malempati *et al.*, 2012; Anderson *et al.*, 2016; Van Maldegem *et al.*, 2016), breast cancer patients with non-visceral metastasis (Crown *et al.*, 2019), prostate cancer patients with high levels of tumour *IGF1* mRNA (Hussain *et al.*, 2019) and other specific subsets of patients or particular cases within clinical trials (Olmos *et al.*, 2010; Aleksic, Browning, *et al.*, 2016; Sanderson *et al.*, 2017), provide evidence that IGF-targeted treatment can be effective. It is likely that a predictive biomarker for responsiveness to IGF treatment is required, but this has not yet been identified (Simpson *et al.*, 2017; Osher and Macaulay, 2019).

1.5 RTKs in the nucleus

As discussed above, binding of ligand to RTKs triggers a range of cell responses via the activation of signalling cascades. However, ligand binding also triggers endocytosis of the receptor, usually by a clathrin-mediated mechanism in the case of RTKs, followed by translocation to and degradation by the lysosome or recycling back to the plasma membrane (Sorkin and Von Zastrow, 2002; Le Roy and Wrana, 2005a, 2005b). More recently, it has also been shown that, upon activation, RTKs can be internalised and

undergo translocation to the nucleus of cells, where the receptor, either as a whole or as a cleaved fragment, interacts with nuclear proteins and transcription factors or acts as a transcription factor itself. The receptor then directly influences processes such as transcription, DNA repair, and cell growth, complementing known functions of the receptor signalling pathways as well as demonstrating novel functions for the receptor (Massie and Mills, 2006; Carpenter and Liao, 2009, 2013). The monomeric ErbB family of receptors contain the most well characterised examples of both endocytosis dependent and protease dependent mechanisms of internalisation of RTKs. A summary of these processes, the function of nuclear ErbB receptors, and of other analogous monomeric nuclear RTKs, are outlined below and illustrated in Figure **1.3**. Nuclear INSR has also been detected but, unlike the majority of nuclear RTKs, INSR is a heterotetramer with four distinct subunits, rather than a monomeric receptor. The potential mechanism of translocation of INSR and its role in the nucleus is also discussed.

1.5.1 ErbB receptor family

The ErbB family of receptors is a set of RTKs including EGFR (also known as ErbB-1), HER2/neu (ErbB-2), Her 3 (ErbB-3) and Her 4 (ErbB-4). Upon activation by their ligands, including epidermal growth factor (EGF) and transforming growth factor alpha (TGFα) among others, the inactive monomeric receptors form active homodimers or heterodimers with other members of the ErbB family, triggering phosphorylation of their intracellular kinase domains and initiating signalling cascades (Schlessinger, 2002). The ErbB receptors initiate signalling via the PI3K/AKT and MAPK pathways, regulating targets involved in DNA synthesis, cell migration, adhesion, proliferation, and apoptosis, similar to the downstream effects of IGF-1R signalling (Oda *et al.*, 2005). Alongside signalling cascade activation, the ErbB family of receptors also undergo internalisation and translocation to the nucleus.

EGFR (ErbB-1) was the first RTK to be detected in the nucleus of cells following ligand stimulation and was detected in its full-length form (S. Lin *et al.*, 2001). Upon activation, EGFR is thought to undergo either clathrin-dependent or clathrin-independent endocytosis, followed by fusion with the early endosome. During early endosomal sorting EGFR is then targeted to the nucleus due to the presence of an NLS, a sequence conserved among the other ErbB family receptors and located at the intracellular carboxyl terminus of EGFR (Hsu and Hung, 2007). Translocation is thought to occur via retrograde signalling, mediated by coat protein complex 1 (COP1) from the Golgi to the endoplasmic reticulum (Wang *et al.*, 2010). After trafficking to the endoplasmic reticulum, the NLS of EGFR interacts with importin-β (Lo *et al.*, 2006). EGFR and importin-β are then thought to interact with nucleoporins in the nuclear pore complex (NPC) to traffic EGFR across the nuclear membrane and into the nucleus, via a mechanism involving the Sec61 translocon (Liao and Carpenter, 2007; Wang *et al.*, 2012).

Nuclear EGFR has distinct functions from the membrane bound form of the receptor. It can act as a co-transcription factor, alongside E2F1 and signal transducer and activator of transcription 5 (STAT5) regulating genes such as cyclin D (S. Lin *et al.*, 2001), inducible nitric oxide synthase (iNOS) via interaction with STAT3 (Lo *et al.*, 2005), and c-Myc, among others (Brand *et al.*, 2013; Song, Rosen and Corfas, 2013). Nuclear EGFR can also interact with other nuclear proteins, such as PCNA, which it directly phosphorylates at tyrosine 211, increasing its stability and therefore enhancing cell proliferation (Wang *et al.*, 2006). Finally, EGFR can translocate to the nucleus in a ligand independent manner in response to ionizing radiation, interacting with DNA-dependent protein kinase (DNA-PK) to promote repair of radiation-induced DNA DSBs (Dittmann *et al.*, 2005).

ErbB-4 has the most completely understood translocation mechanism and biological function in the nucleus, both within the ErbB family and for RTKs in general. However, it

differs from EGFR in that only a cleaved fragment of the receptor is present in the nucleus. Upon activation by its ligand, ErbB-4 is cleaved to form a 120-kDa ectodomain fragment and an 80-kDa membrane-bound fragment (m80). This cleavage is dependent on a metalloproteinase called ADAM 17 (or tumour necrosis factor-α-converting enzyme (TACE)), thought to cleave the receptor between histidine 651 and serine 652 of the extracellular region (Rio *et al.*, 2000; Cheng *et al.*, 2003). This step is a prerequisite for the cleavage of the m80 fragment by γ-secretase, a complex of at least 4 proteins with a presenilin catalytic protease (Selkoe and Wolfe, 2007; He *et al.*, 2010). γ-secretase cleaves the m80 fragment into a soluble (s80) fragment known as the intracellular domain (ICD) fragment, which is released into the cytosol (Ni *et al.*, 2001; Vidal *et al.*, 2005). The ICD fragment then interacts with transcription factors and adaptor proteins and translocates to the nucleus due to the presence of its NLS, where it exerts a range of physiological effects (see Figure **1.3**). The factors bound by the ICD fragment include STAT5 (Williams *et al.*, 2004; Zscheppang *et al.*, 2011), YAP (Hoeing *et al.*, 2011) and HIF-1α (Paatero *et al.*, 2012) among others, exerting effects over gene expression, development and cellular differentiation (Carpenter and Liao, 2013; Song, Rosen and Corfas, 2013). This γ-secretase dependent cleavage and translocation process is analogous to the same well characterised process involving Notch signalling and amyloid precursor protein (APP) (Tarassishin *et al.*, 2004; Shih and Wang, 2007; Yang *et al.*, 2019).

Much less is known about the nuclear forms of ErbB-2 and ErbB-3, but both have been detected in the nucleus of cells (Offterdinger *et al.*, 2002; Giri *et al.*, 2005). ErbB-2 does not have a ligand binding domain but is thought to be activated by heterodimerisation with another of the ErbB receptor family. The formed heterodimer then undergoes translocation in a mechanism analogous to EGFR, involving internalisation to the early endosome, and importin-β mediated nuclear import (Giri *et al.*, 2005; Wang *et al.*, 2012). Nuclear ErbB-2

has been found to bind to the *COX2* promoter to activate transcription of cyclooxygenase-2 in the inflammatory response (Wang *et al.*, 2004), and is thought to play a role in regulation of transcription of ribosomal RNA genes (Li *et al.*, 2011). The mechanism of how ErbB-3 translocates to the nucleus and its nuclear function remains unclear, but it is thought to contain an NLS and has been detected in its full-length form in the nucleus of prostate cancer cells (Koumakpayi *et al.*, 2006, 2011).

1.5.2 Endocytosis-dependent nuclear RTKs

Fibroblast growth factor receptor (FGFR)-1 and Platelet derived growth factor receptor (PDGFR) are two other monomeric RTKs that have been detected in the nucleus in their full-length, or holoreceptor form. Evidence suggests that they translocate via a mechanism analogous to that of EGFR involving endocytosis of the receptor, fusion with the early endosome and targeting to the nucleus (see Figure **1.3**). This evidence, along with their known nuclear functions, are discussed below. While there may be other RTKs that also translocate to the nucleus as a holoreceptor, including Ron and Met, current data is limited and conflicting (Carpenter and Liao, 2013; Song, Rosen and Corfas, 2013; Huo, Hsu and Hung, 2014; Chen and Hung, 2015).

1.5.2.1 FGFR-1

Fibroblast growth factors (FGFs) bind to FGFRs and activate signalling via the PI3K/AKT pathway and MAPK pathway via activation of both Ras and phospholipase C (PLC)-γ. Signalling from the FGFRs plays a role in cell proliferation, survival, migration, differentiation and an important role in angiogenesis contributing to tumour growth (Yun *et al.*, 2010). Specifically, in angiogenesis, FGF-1 and FGF-2 promote endothelial cell proliferation and the physical organization of endothelial cells into tube-like structures and act as potent promoters of angiogenesis (Javerzat, Auguste and Bikfalvi, 2002; Presta *et al.*, 2005). The FGFR family contains four homologous receptors (FGFR 1-4), but the role

of FGFR-1 in the nucleus is the most well characterised. Full length FGFR-1 has been detected in the nucleus in association with FGF-2 ligand (Maher, 1996; Stachowiak *et al.*, 1996a, 1996b; Myers *et al.*, 2003), and while the mechanism of translocation is unclear, some FGF ligands have been shown to contain an NLS and have previously been detected in the nucleus (Florkiewicz, Baird and Gonzalez, 1991; Joy *et al.*, 1997). FGFR-1 has also been shown to interact with importin-β (Reilly and Maher, 2001). This suggests a potential endocytosis dependent translocation mechanism analogous to EGFR.

Nuclear FGFR-1 has been shown to mediate cAMP-induced differentiation of human neuronal progenitor cells, via interaction with neurofilament-L gene promoter which contributes to activation of CREB to trigger the cAMP signalling pathway (Stachowiak *et al.*, 2003). It is also thought to induce an increase in c-Jun transcription factor contributing to cell proliferation and has been shown to interact with Nurr1 transcription factor, therefore seemingly playing a role as a transcription factor and in transcription control in the nucleus, distinct from signalling pathway activation (Reilly and Maher, 2001; Dunham-Ems *et al.*, 2009; Baron *et al.*, 2012).

1.5.2.2 PDGFR

The PDGFR family contains 5 different receptors, PDGFRα and β, colony stimulating factor-1 receptor (CSF1R), stem cell factor receptor and fms-like tyrosine kinase 3 (FLT3). PDGFRα and β mediate platelet-derived growth factor-induced cell replication, migration, and survival signalling, and have shown to be detectable in the nucleus, although little is known about their nuclear function or translocation mechanism. PDGFRα has been detected in the nucleus of alveolar fibroblasts and plays a role in early embryonic and lung development in a mouse model. Full length, GFP tagged PDGFRα was detected in the nucleus, suggesting it undergoes endocytosis and translocation as a holoreceptor (Hamilton *et al.*, 2003; Chen *et al.*, 2012). More recently, PDGFRβ was detected in the nucleus of

fibroblast cells, among others, and was found to interact with chromatin to trigger chromatin remodelling and control cell proliferation by regulating levels of p21, demonstrating a functional role distinct from canonical signalling pathway activation. PDGFRβ was detected in its full-length form in the nucleus of cells, and translocation was found to be dependent on clathrin-mediated endocytosis, Golgi trafficking and importin-β, demonstrating a translocation mechanism analogous to that of EGFR (Papadopoulos, Lennartsson and Heldin, 2018).

1.5.3 Protease dependent nuclear RTKs

Analogous to ErbB-4, the following receptors do not translocate to the nucleus in their holoreceptor form. Following ligand stimulation, protease dependent cleavage of the receptor generates an ICD fragment which is targeted to the nucleus either alone or in combination with other transcription factors or adaptor proteins (see Figure **1.3**).

1.5.3.1 Vascular endothelial growth factor receptor (VEGFR)

The majority of VEGF signalling occurs through VEGFR-2 and is a major signalling pathway involved in angiogenesis but also plays roles in cell proliferation, migration and survival (Holmes *et al.*, 2007). The signalling role VEGFR-2 plays in angiogenesis makes it particularly important in cancer progression and tumour development (Shibuya, 2011). Ligand stimulation of VEGFR-2 results in activation of MAPKs, but this occurs via PLC-γ, rather than the traditional Ras dependent pathway activated by most other RTKs (Takahashi *et al.*, 2001). Nuclear VEGFR-2 has been detected in endothelial cells following ligand stimulation and dependent on kinase phosphorylation and is thought to play a role in the wound healing response (Constantino Rosa Santos *et al.*, 2007). Interestingly, nuclear VEGFR-2 was also found to interact with Sp-1 transcription factor and bind to the VEGFR-2 promoter, potentially regulating its own gene transcription (Domingues *et al.*, 2011) and has been detected in the nucleus of proliferative tumour and

leukaemia cells (Fox *et al.*, 2004; Blazquez *et al.*, 2006). The translocation mechanism of VEGFR-2 is unclear, but some studies have shown that it undergoes γ-secretase dependent cleavage (Cai *et al.*, 2011; Carpenter and Liao, 2013).

1.5.3.2 Related to receptor tyrosine kinase (Ryk)

The majority of canonical Wnt signalling occurs through the Frizzled receptors and involves the activity of low-density lipoprotein-related proteins (LRP) and the canonical pathway involving β-catenin and T-cell factor (TCF), to mediate cell-to-cell signalling during development, cell proliferation and differentiation (Nusse, 2005). Ryk is a member of the RTK family, and contains an extracellular ligand binding domain, transmembrane domain and C-terminal intracellular domain, however, unlike other RTK family members, this C-terminal domain does not display kinase activity (Katso, Russell and Ganesan, 1999; Halford and Stacker, 2001). Although it doesn't display kinase activity, Ryk has been shown to be cleaved by γ-secretase to generate an ICD fragment which translocates to the nucleus and plays a role in Wnt3-dependent neuronal differentiation when cells are stimulated with Wnt3 ligand (Lyu, Yamamoto and Lu, 2008). As the Ryk ICD fragment does not contain an NLS, it is unclear how it is targeted to the nucleus, but it has been shown to be dependent on stabilisation by Cdc37, a co-chaperone protein involved in the Hsp90 chaperone protein complex (Lyu, Wesselschmidt and Lu, 2009), and Smek1/2, subunits of the protein phosphatase 4 complex (Chang *et al.*, 2017). This demonstrates another role of nuclear RTKs distinct from signalling cascade activation.

Other receptors that have been detected in the nucleus as an ICD fragment include Ephrin-B2, Met and colony-stimulating factor-1 receptor, among others (Carpenter and Liao, 2013; Song, Rosen and Corfas, 2013; Huo, Hsu and Hung, 2014; Chen and Hung, 2015). All of these nuclear RTKs discussed above, regardless of translocation mechanism, show regulatory functions distinct from their canonical signalling pathways.

1.5.4 Insulin receptor

The presence of INSR in the nucleus was initially detected in hepatocytes and has been thought to be a potential mechanism by which INSR potentiates long term transcriptional effects (Goldfine and Smith, 1976; Podlecki *et al.*, 1987). The translocation mechanism of INSR to the nucleus is currently unclear, but the receptor has previously been shown to interact with clathrin-coated pits following ligand stimulation and undergo clathrin-mediated endocytosis to endosomes or lysosomes for recycling to the cell surface or degradation (Carpentier, 1994; Morcavallo *et al.*, 2014). A confirmed NLS sequence has not been identified in the INSR, however internalisation of the receptor was shown to be kinase dependent, and the receptor was shown to interact with importin-α. Both α- and β-subunits of INSR have been detected in the nucleus and shown to interact with RNAPolII (Hancock *et al.*, 2019). This suggests the presence of the mature, full-length holoreceptor in the nucleus and a translocation mechanism analogous to EGFR, dependent on endocytosis of the receptor rather than protease dependent cleavage (see Figure **1.3**). It is also worth noting that, unlike the other RTKs that translocate to the nucleus discussed above, INSR is a heterotetramer with four distinct subunits, rather than a monomeric receptor. (Carpenter and Liao, 2013; Hancock *et al.*, 2019).

Nuclear INSR was detected initially in rat hepatic tumour cells to be recruited to insulin-inducible genes up-regulating their transcription (Nelson, LeBoeuf and Bomsztyk, 2011). More recent work in human hepatocytes found that nuclear INSR interacts with RNAPolII at gene promoters genome wide and induces transcription of genes involved in insulin liver function, including lipid metabolism and protein synthesis, and for genes related to diseases where insulin signalling is dysfunctional such as diabetes (Hancock *et al.*, 2019). The majority of INSR chromatin binding regions were found to be within gene promoter regions (±500 bp from the transcription start site (TSS)), and coincident with RNAPolII

binding peaks as well as overlapping with active transcription markers such as H3K4me3 and H3K27ac. The interaction of INSR and RNAPolII and the recruitment of INSR at chromatin binding regions, altering gene expression, was also found to be ligand dependent (Hancock *et al.*, 2019). Nuclear INSR was also shown to interact with host cell factor-1 (HCF-1) (Hancock *et al.*, 2019), a nuclear protein that acts as a transcriptional co-regulator and is implicated in cell proliferation via regulating transcription of genes involved in cell cycle progression and cell growth (Dejosez *et al.*, 2010; Zargar and Tyagi, 2012; Brandon Parker *et al.*, 2014). These functions therefore display a distinct transcriptional role for nuclear INSR alongside its classical signalling pathways.

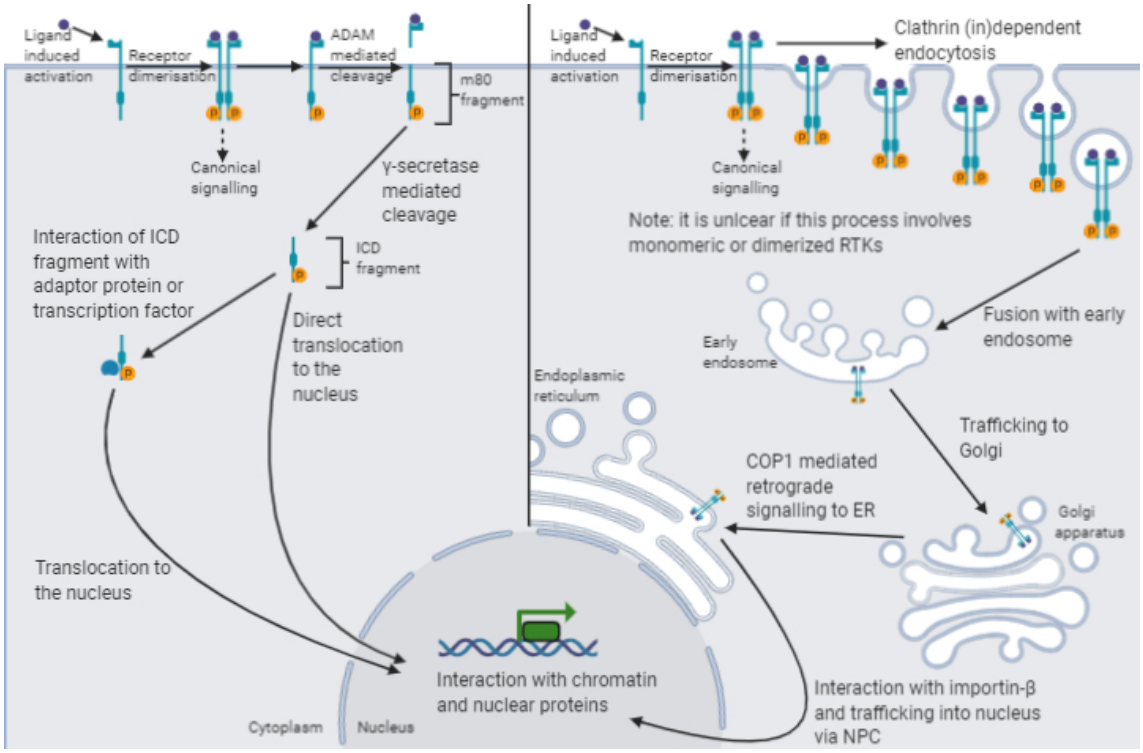


Figure 1.3 Translocation mechanisms of RTKs
Figure showing the broad features of the mechanisms of translocation of RTKs. Upon ligand stimulation, RTKs activate canonical signalling pathways but can also be cleaved or internalised to undergo translocation from the cell membrane to the nucleus. Left: the protease dependent translocation pathway, involving cleavage of the receptor to generate an ICD fragment which then translocates to the nucleus either alone or bound to an adaptor protein or transcription factor. Right: the endocytosis dependent pathway of translocation. The full-length receptor is internalised and targeted to the nucleus via retrograde signalling from the Golgi to the ER, before undergoing importin-β mediated import across the NPC and into the nucleus. Note: it is currently unclear if RTKs undergo endocytosis dependent translocation in their monomeric or homodimeric form. Figure was constructed using information from references in the text.

1.6 Nuclear IGF-1R

Like the previously discussed RTKs, recent work has shown the presence and activity of IGF-1R in the nucleus of cells. The mechanism of translocation of IGF-1R has been partially, but not yet fully elucidated, and studies have shown detection of full length α- and β-subunits of the receptor in the nucleus. Some characteristics and functions of nuclear IGF-1R have been determined, such as interaction with nuclear proteins and transcription factors, and recruitment to regulatory regions of chromatin. Alongside INSR, IGF-1R is also currently one of the only known cell surface receptors that translocates to the nucleus that is not monomeric (Aleksic *et al.*, 2010, 2018; Sehat *et al.*, 2010; Waraky *et al.*, 2017). The potential mechanism of translocation, function, and clinical relevance of nuclear IGF-1R are discussed in detail below. It is worth noting that, unless stated otherwise, detection and validation of the discussed roles of nuclear IGF-1R have been determined via detection of the β-subunit of the receptor.

1.6.1 Translocation mechanism

Previous work has shown that IGF-1 promotes modification of IGF-1R by small ubiquitin-like modifier protein–1 (SUMO-1) targeting it for translocation to the nucleus following activation and internalisation of the receptor (Sehat *et al.*, 2010). SUMO proteins are similar to ubiquitin and are considered members of the ubiquitin-like protein family, performing post-translational modifications of targets to influence protein stability, nuclear-cytosolic transport, and transcriptional regulation (Wang and Dasso, 2009). The SUMO protein is bound and activated by an E1 enzyme such as SUMO-activating enzyme (SAE)-1 or -2, forming a heterodimer. The active heterodimer is then passed to an E2 conjugating enzyme such as Ubc9, which recognises a specific SUMOylation motif on the target protein (Wang and Dasso, 2009). This motif usually consists of a large hydrophobic residue, a lysine, a spacer, and finally an acidic residue in sequential order, referred to as

ΨKxD/E. Ubc9 binds to this motif and a peptide bond is formed between the lysine residue of the ΨKxD/E motif on the target protein, and a diglycine motif on the carboxy terminus of the SUMO tag (Bernier-Villamor *et al.*, 2002; Yunus and Lima, 2006). This process is catalysed by an E3 SUMO ligase, which in the case of SUMO-1 is Ran binding protein 2 (RanBP2) (Wang and Dasso, 2009). RanBP2 is a nuclear pore protein localised to the cytoplasmic face of the pore. Throughout the cell cycle it forms a stable complex with Ran GTPase-activating protein (RanGAP1), which is dependent on SUMO-1 modification of RanGAP1 and involves Ubc9 (Zhu, Zhang and Matunis, 2006). RanBP2 contains two internal repeat domains (IR-1 and IR-2), which are both made up of 50 amino acid residue internal repeats sharing 45% homology and are separated by a 20 amino acid residue spacer region (M) (Pichler *et al.*, 2002). IR-1 and IR-2 can both bind to Ubc9, and RanBP2 has been found to contain a noncovalent SUMO-interaction motif (SIM) directly N terminal of IR-1. Both this SIM region and IR-1 are engaged in the formation of the RanBP2-RanGAP1∗SUMO1-Ubc9 complex (Reverter and Lima, 2005). It is formation of this complex, rather than unbound RanBP2, that is required for E3 ligase activity, and interaction of the IR-2 region of this complex with Ubc9 catalyses SUMOylation of target proteins at the nuclear pore (Werner, Flotho and Melchior, 2012).

The SUMOylation process is reversible, and SUMO proteins can be removed by sentrin-specific proteases (SENP) which hydrolyse the peptide bond between target protein and SUMO tag. There are six different SENPs, (SENP-1, -2, -3, -5, -6, -7), but only SENP-1 and SENP-2, which are localised to the nuclear membrane, have shown deconjugation activity for SUMO-1 (L. Shen *et al.*, 2006; Reverter and Lima, 2006).

In the case of IGF-1R, ligand stimulation triggers clathrin-mediated endocytosis of the receptor into early endosome antigen-1 (EEA-1) positive vesicles (Aleksic *et al.*, 2010; Packham *et al.*, 2014). EEA-1 is important in clathrin-mediated endocytosis and

selectively binds internalized vesicles via phosphatidylinositol 3-phosphate, acting as a tethering molecule required for fusion of early and late endosomes and for endosomal sorting (Dumas *et al.*, 2001; Barysch *et al.*, 2009). Internalised IGF-1R then interacts with $p150^{Glued}$, the largest subunit of the dynactin protein complex (Packham *et al.*, 2014). Dynactin is a cytosolic protein complex required for dynein-dependent transport of vesicles over long distances via microtubules and has been shown to interact with EEA-1 positive vesicles (Deacon *et al.*, 2003; Flores-Rodriguez *et al.*, 2011). $p150^{Glued}$ has also specifically been shown to interact with microtubules (Waterman-Storer, Karki and Holzbaur, 1995). Therefore, the interaction between IGF-1R and $p150^{Glued}$ suggests the internalised receptor undergoes transport to the nucleus via microtubule-dependent dynactin activity. After transport to the nuclear membrane, IGF-1R undergoes tri-SUMOylation of three conserved lysine resides, lysine-1025, -1100 and -1120 in the β-subunit of the receptor. Interestingly theses residues do not lie in the usual ΨKxD/E SUMOylation motif (Sehat *et al.*, 2010). Further work showed that mutation of these three lysine residues significantly decreased nuclear translocation of IGF-1R. The triple-SUMO-site-mutated (TSM) IGF-1R still showed kinase activity comparable to wild type on ligand stimulation, but presence of the receptor in the nucleus was significantly reduced (Lin *et al.*, 2017). The TSM IGF-1R that was detectable in the nucleus was likely due to formation of hybrid receptors by heterodimerisation with INSR which, as discussed previously, can also translocate to the nucleus (Lin *et al.*, 2017; Hancock *et al.*, 2019).

The SUMOylation of IGF-1R was initially shown to be dependent on SUMO-1 and Ubc9 (Sehat *et al.*, 2010), but recent work has also shown the interaction of IGF-1R with RanBP2, which is likely to be acting as an E3 SUMO ligase to catalyse IGF-1R SUMOylation and which promotes the stability of internalised IGF-1R (Packham *et al.*, 2014). The interaction of RanBP2 with the nuclear import protein importin-β has

previously been characterised (Hutten *et al.*, 2008; Hamada *et al.*, 2011) and the interaction of IGF-1R with RanBP2 was shown to be dependent on importin-β. IGF-1R was shown to directly interact with importin-β and mutation of the RanBP2 binding site of importin-β resulted in reduced interaction of IGF-1R and RanBP2 (Packham *et al.*, 2014). This suggests transport of IGF-1R to the nucleus is followed first by interaction with importin-β to align the receptor at the nuclear pore, which then facilitates the interaction with RanBP2. SUMOylation of the receptor by a RanBP2 E3 ligase catalysed mechanism then mediates the translocation of the receptor across the NPC and into the nucleus. This is analogous to the nuclear translocation mechanism of ErbB-2, which has been shown to interact with EEA-1 and involves the importin-β-RanBP2 interaction (see Figure **1.3**) (Giri *et al.*, 2005). However, IGF-1R does not contain an NLS, and therefore it is still unclear how transport of the receptor is directed to the nucleus from the early endosome and may involve interaction of IGF-1R with another NLS-containing protein such as IRS-1 (Prisco *et al.*, 2002; Sehat *et al.*, 2010).

It is also worth noting that both full length α- and β-subunits of IGF-1R have been detected in the nucleus and that inhibition of γ-secretase in prostate cancer cells did not alter the localisation of the receptor, suggesting that the translocation mechanism of the receptor does not involve generation of an ICD fragment or γ-secretase cleavage (Aleksic *et al.*, 2010). Analogous to the INSR, IGF-1R is also an example of a heterotetrameric RTK that translocates to the nucleus in contrast to the majority of other nuclear RTKs that are monomeric (Aleksic *et al.*, 2010; Sehat *et al.*, 2010; Carpenter and Liao, 2013; Hancock *et al.*, 2019).

1.6.2 Interaction of nuclear IGF-1R with regulatory regions of chromatin

As previously discussed, nuclear INSR has recently been shown to be recruited to regulatory regions of chromatin at promoters and enhancers involved in regulation of

insulin related genes (Hancock *et al.*, 2019). This is analogous to the same previously discovered function of nuclear IGF-1R (Aleksic et al., 2018). Initially, ChIP-seq analysis identified 568 different regions within the genome that were statistically significant for enriched binding of IGF-1R in DFB melanoma cell lines. However, the majority of these (80%) were found to be within intergenic regions, and only 7% were found within 20 kb either upstream or downstream of a TSS (Sehat *et al.*, 2010). Other work in immortalised corneal epithelial cells identified the nuclear localisation of full-length IGF-1R-INSR hybrid receptors. ChIP-seq analysis of these hybrid receptors, using either detection for IGF-1R or INSR, found 88 and 86 different regions within the genome that were statistically significant for enriched binding of IGF-1R or INSR respectively. These binding regions were assigned to genes involved in cell differentiation, proliferation, metabolism, cell death and cell-to-cell adhesion, aligning with the known function of IGF and insulin regulated genes (Wu, Zhu and Robertson, 2012).

IGF-1R was also shown to directly interact with Histone H3 of chromatin in the nucleus of DU145 prostate cancer cells (Aleksic *et al.*, 2010), and follow up work found that this interaction involved direct phosphorylation of tyrosine-41 of histone H3 in human cervical carcinoma (HeLa) cells (Warsito *et al.*, 2016). This phosphorylation was found to be IGF-1 dependent and was required for the recruitment and stabilisation of the binding of Brg1 chromatin remodelling protein to Histone H3. Both IGF-1R and Brg1 were found to bind to the promoter and increase the expression of the *SNAI2* oncogene, a gene involved in regulation of cell migration and EMT, and therefore implicated in cancer invasion and metastasis (Barrallo-Gimeno and Nieto, 2005; Warsito *et al.*, 2016).

More recent work in our lab has shown recruitment of IGF-1R to regions of chromatin in DU145 prostate cancer cells and SK-N-MC Ewing sarcoma cells by ChIP-seq, identifying 62 and 66 different regions respectively within the genome that were statistically

significant for enriched binding of IGF-1R. Of these detected regions, 25 were shared between both cell lines and only 2 were shared with those previously identified in melanoma cells (Sehat *et al.*, 2010; Aleksic *et al.*, 2018). While a much lower number of IGF-1R binding regions were detected in comparison to DFB melanoma cells, in contrast to the data in melanoma, most IGF-1R binding regions in DU145 were found to cluster at or near a TSS. Of the 62 IGF-1R binding regions in DU145 cells, 95% were coincident with RNAPolII binding regions, 87% with H3K4me1 and 50% with H3K4me3, markers of active enhancers and promoters respectively. IGF-1R was found to be recruited to promoter regions within the *JUN* and *FAM21A/C* genes coincident with RNAPolII and H3K4me1. This interaction was validated using dsDNA probes in an electrophoretic mobility shift assay (EMSA), and recruitment of IGF-1R to these regions was shown to be IGF-1 responsive by ChIP-qPCR and luciferase reporter assays using a reporter for the *JUN* promoter. Recruitment of RNAPolII to chromatin binding regions coincident with IGF-1R binding regions was also shown to be IGF-1 responsive, and IGF-1R and RNAPolII were shown to directly interact with each other.

The *JUN* and *FAM21A* genes were upregulated in response to IGF-1 treatment, suggesting the increased recruitment of IGF-1R at these promoters induces transcription (Aleksic *et al.*, 2018). Previous work had shown that *JUN* is upregulated by IGF-1 and plays a role in promoting tumour growth (Yang *et al.*, 2011) and is associated with radioresistant prostate cancer (Kajanne *et al.*, 2009), while *FAM21A* is shown to promote chemo-resistance in pancreatic cancer (Deng *et al.*, 2015). In this more recent work, *JUN* and *FAM21A* were also found to be involved in mediation of IGF-induced migration of cells (Aleksic *et al.*, 2018).

The *JUN* gene encodes for the c-Jun transcription factor and is also activated by IGF-1 via the MAPK/ERK signalling pathway, as previously mentioned, and is considered a proto-

oncogene. c-Jun forms a heterodimer with c-Fos forming the AP-1 transcription factor which regulates genes involved in cellular proliferation, differentiation, apoptosis, angiogenesis and invasion and is therefore implicated in cancer growth (Eferl and Wagner, 2003). AP-1 is also a transcription factor for the *JUN* gene, meaning *JUN* is positively autoregulated by its own product (Angel *et al.*, 1988). This likely contributes to the proto-oncogene status of *JUN* and its role in cancer progression. Therefore, IGF-1 responsive activation of *JUN* transcription, and its wider role in gene activation such as *SNAI2*, demonstrates a distinct role for nuclear IGF-1R activity in cancer progression via interactions with chromatin.

1.6.3 Nuclear IGF-1R interacting proteins

As well as interacting with regulatory regions of chromatin, nuclear IGF-1R has also been shown to interact with nuclear proteins. As previously mentioned, IGF-1R interacts with importin-β to align the receptor at the nuclear pore, where SUMOylation of the IGF-1Rβ-subunit is catalysed by the nuclear pore protein RanBP2. Interaction of IGF-1R with these two nuclear pore proteins facilitates translocation of the receptor into the nucleus (Sehat *et al.*, 2010; Packham *et al.*, 2014).

Once inside the nucleus, IGF-1R can directly interact with nuclear proteins to influence their function. The most well characterised of these interactions is the direct phosphorylation of PCNA by IGF-1R (Waraky *et al.*, 2017). PCNA is a nuclear protein that is essential for processing of leading strand synthesis in DNA replication. PCNA interacts with DNA via replication factor C, forming a homotrimeric ring which acts as a DNA clamp and a scaffold for recruitment of replication proteins such as DNA polymerases and ligases, usually at the replication fork (Kelman, 1997; Moldovan, Pfander and Jentsch, 2007; Boehm, Gildenberg and Washington, 2016). PCNA is also involved in coordination of DNA damage repair pathways. PCNA undergoes post-translational

modification via ubiquitination by E2 and E3 ligases and this ubiquitination influences the DNA repair pathway undertaken by the cell. Monoubiquitination of lysine-164 on PCNA is performed by RAD6 (E2) and RAD18 (E3) ligases. This activates the trans-lesion synthesis pathway involving low fidelity DNA polymerases that incorporate damaged DNA bases into their active sites and therefore bypass DNA lesions. Further polyubiquitination of PCNA by UBC13 (E2) and SHPRH/HLTF (E3) ligases, results in activation of the template switching pathway, involving recruitment of the sister strand template and the HR machinery to bypass and repair DNA damage (Moldovan, Pfander and Jentsch, 2007; Andersen, Xu and Xiao, 2008; Boehm, Gildenberg and Washington, 2016). Recently, nuclear IGF-1R was shown to directly interact with and phosphorylate tyrosine-60, -133, and -250 of PCNA (Waraky *et al.*, 2017). The ubiquitination of PCNA was dependent on this phosphorylation and was shown to be dependent on IGF-1 stimulation and translocation of IGF-1R, as cells containing a TSM IGF-1R that cannot translocate to the nucleus showed no phosphorylation or subsequent ubiquitination of PCNA. Recruitment of the required E3 ligases for either mono- or polyubiquitination of PCNA was also found to be IGF-1 responsive. Mutation of any or all of the tyrosine residues of PCNA phosphorylated by IGF-1R, abrogated the IGF-1R:PCNA interaction and the subsequent phosphorylation and ubiquitination of PCNA (Waraky *et al.*, 2017). Following on from this, cells lacking IGF-1R that were exposed to UV radiation showed significantly reduced ubiquitination of PCNA compared to IGF-1R positive cells, and also showed increased replication fork stalling in the absence of the IGF-1R:PCNA interaction (Waraky *et al.*, 2017). Overall, this shows that the co-ordination of DNA damage repair by PCNA in response to external DNA damage is, at least in part, mediated by the phosphorylation of PCNA by nuclear IGF-1R and demonstrates a role for nuclear IGF-1R distinct from its canonical signalling pathway activation.

As previously mentioned, in prostate cancer cells, nuclear IGF-1R is recruited to regulatory regions of chromatin coincident with RNAPolII. Nuclear IGF-1R and RNAPolII were shown to directly interact, and this interaction was dependent on IGF-1. Recruitment of RNAPolII to promoters that also showed IGF-1R binding was increased on treatment with IGF-1 and suppressed on treatment with inhibitors for IGF-1 or IGF-1R. Expression of these genes was upregulated by IGF-1 treatment, an effect abrogated by IGF-1 inhibition. Recruitment of RNAPolII to promoters with no IGF-1R binding were not responsive to IGF-1 treatments (Aleksic *et al.*, 2018). This suggests that the recruitment of RNAPolII to promoters that also show IGF-1R binding is dependent on the IGF-1 induced interaction of RNAPolII with IGF-1R.

As well as this RNAPolII interaction, nuclear IGF-1R can also affect gene expression via direct interaction with transcription factor proteins. Ligand dependent interaction of nuclear IGF-1R with the transcription factors LEF1, GATA2 and NOM1 has been detected in a range of cancer cell lines (Warsito *et al.*, 2012; Aleksic *et al.*, 2018; Solomon-Zemler *et al.*, 2019).

Nuclear IGF-1R was shown to interact with LEF1 transcription factor in human melanoma (DFB), non-small lung carcinoma (H1299) and HeLa cell lines (Warsito *et al.*, 2012). LEF1 is a lymphoid enhancer factor transcription factor involved in activation of genes involved in tumorigenesis and can usually only activate transcription when bound to other factors such as β-catenin (Giese *et al.*, 1995; Tetsu and McCormick, 1999). IGF-1R was shown to interact with LEF1 in the nucleus, promoting recruitment to and activation of LEF1 targeted gene promoters, resulting in increased expression of proteins such as cyclin D1 (Warsito *et al.*, 2012).

GATA2 is a zinc finger transcription factor protein which regulates genes involved in embryonic development and self-renewal and differentiation of stem cells, specifically in

development of hematopoietic and endocrine cells (Tsai *et al.*, 1994). The GATA2 protein contains two zinc finger regions, one at its C-terminus which binds directly to DNA via specific GATA2 binding motifs in the form T/A(GATA)A/G, and one at its N-terminus which binds to nuclear proteins that regulate its function (Orkin, 1992). GATA2 was shown to interact with nuclear IGF-1R in an IGF-1 dependent manner, and the *JUN* promoter region bound by IGF-1R showed a GATA2 binding sequence motif, suggesting that recruitment of IGF-1R to this region could potentially be dependent on the IGF-1R:GATA2 interaction (Aleksic *et al.*, 2018). As previously discussed, GATA2 has been linked to resistance to chemotherapy and cancer progression via regulation of critical cancer related genes, including *IGF2* (Vidal *et al.*, 2015; Rodriguez-Bravo *et al.*, 2017). This suggests there could be broader implications to the nuclear IGF-1R-GATA2 interaction if it contributes to regulation of these cancer related genes.

NOM1 is a transcription factor that is a member of the family of proteins that contain the middle domain of eukaryotic initiation factor 4G (MIF4G) and/or protein-protein interaction module (MA3), and functions in translation, cell growth, proliferation, transformation, and apoptosis. Specifically, NOM1 interacts with eukaryotic initiation factor-4A (eIF4A) family proteins involved in translation initiation, and protein phosphatase-1, a serine/threonine phosphatase required for a wide range of cellular processes including mitogenesis during cell division (Gunawardena *et al.*, 2008; Alexandrov, Colognori and Steitz, 2011). In MCF7 cells, nuclear IGF-1R was shown to directly interact with NOM1 in an IGF-1 dependent manner. Inhibition of IGF-1R nuclear translocation also showed a reduction in nuclear NOM1 levels and silencing of NOM1 resulted in increased protein levels of IGF-1R suggesting cross talk exists between the two proteins (Solomon-Zemler *et al.*, 2019).

Interaction of nuclear IGF-1R with these transcription factors, as well as interaction with RNAPolII, shows that nuclear IGF-1R has a direct role and influence over gene expression and transcription outside of signalling cascade activation, contributing to cell proliferation and therefore cancer growth.

1.6.4 Clinical relevance of nuclear IGF-1R

IGF-1R has been shown to be detectable in the nucleus of a wide array of cancer types including primary and formalin fixed renal cell carcinomas (RCC), prostate cancer and adenocarcinomas of the breast, lung, and ovary and ductal carcinoma in situ. In the case of clear cell RCCs, patients with more intense or more widespread nuclear IGF-1R were found to have shorter OS (Aleksic *et al.*, 2010). Analysis of 137 radical prostatectomies from British men with prostate cancer found that malignant epithelium overexpressed IGF-1R and contained significantly more internalized IGF-1R compared to benign regions. Higher levels of nuclear IGF-1R were also associated with a more advanced tumour stage and there was a borderline association between internalized IGF-1R and higher Gleason grade (Aleksic *et al.*, 2018). A similar association of nuclear IGF-1R with worse prognosis was seen in embryonal rhabdomyosarcoma (eRMS), an aggressive soft tissue sarcoma. The presence of nuclear IGF-1R in eRMS tumour samples was an adverse prognostic factor showing significantly reduced 5-year disease specific survival of 46.9 ± 18.7% versus 84.4 ± 5.9% in those lacking nuclear IGF-1R staining (n=53, p = 0.006) (van Gaal *et al.*, 2013).

Work on acute myeloid leukaemia (AML) found that expression of IGF-1R was upregulated in AML cell lines versus healthy cells and treatment with IGF-1 induced proliferation in AML. In AML, IGF-1R was found to interact with SUMO-1, required for IGF-1R nuclear translocation, and inhibition of Ubc9 reduced this interaction as well as reducing IGF-1 induced cellular proliferation. Similar results were seen in AML cell lines

transfected with IGF-1R containing point mutations at lysine-1025 or -1100 of the β-subunit, two of the three conserved lysine residues that are SUMOylated during IGF-1R translocation. This suggests that the IGF-1 induced proliferation of AML is dependent on the action of nuclear IGF-1R and may explain the issues with clinical trials for AML using anti-IGF-1R therapies (Zhang *et al.*, 2015). Similar effects on cell proliferation were seen in an *igf-1r*-/- murine embryonic fibroblast model transfected with either wildtype or TSM IGF-1R, where TSM IGF-1R cells showed reduced cell cycle progression and reduced proliferation on stimulation with IGF-1 compared to wildtype cells (Lin *et al.*, 2017). This nuclear IGF-1R dependent proliferation may explain why higher levels of nuclear IGF-1R are seen in more advanced cancers.

Increased nuclear IGF-1R levels could also be a potential biomarker for patients that will be more responsive to anti-IGF-1R based therapies. A minority of patients with advanced sarcoma show prolonged PFS following anti-IGF-1R monoclonal antibody treatment therapy. From patients with advanced soft tissue sarcomas (STS), Ewing sarcoma (ES) or osteosarcoma treated with anti-IGF-1R monoclonal antibody treatment therapy, 75% of tumours showed either nuclear or nuclear and cytoplasmic staining for IGF-1R, but only exclusively nuclear staining was significantly associated with a better PFS ($p = 0.01$) and increased OS ($p = 0.007$) following treatment (Asmane *et al.*, 2012).

As previously discussed, IGF-1R signalling plays a role in mediating resistance to a range of cancer treatments and recent studies have now also shown a role for nuclear IGF-1R in treatment resistance. Hepatocellular carcinoma (HCC) Mahlavu cells show resistance to treatment with gefitinib, a TKI of EGFR. On treatment with gefitinib, Mahlavu cells showed an increased phosphorylation of IGF-1R and a dose-dependent increase in levels of nuclear IGF-1R (Bodzin *et al.*, 2012).

Overall, nuclear IGF-1R appears to be a marker for cancer progression and may contribute to treatment resistance.

1.7 Hypothesis and Aims

This introduction has described the important role that IGF-axis signalling plays in cancer growth, proliferation, and progression. In prostate cancer specifically, IGF-axis signalling contributes towards progression to metastatic disease and androgen independence, resulting in resistance to standard chemotherapy and ADT treatments. These more advanced cancers have drastically reduced patient survival rates compared to early, localised prostate cancer (Wu *et al.*, 2006; Wang *et al.*, 2018; Carceles-Cordon *et al.*, 2020). IGF-1R signalling targeted treatments have overall shown disappointing results in clinical trials (Simpson *et al.*, 2017; Osher and Macaulay, 2019), but strong responses in some patient subsets suggest a potential biomarker is needed for patients who may be responsive to anti-IGF-1R treatment (Malempati *et al.*, 2012; Aleksic, Browning, *et al.*, 2016; Anderson *et al.*, 2016; Sanderson *et al.*, 2017; Crown *et al.*, 2019; Hussain *et al.*, 2019).

More recent work has described a second non-canonical function of IGF-1R, involving translocation of the receptor to the nucleus following activation. Nuclear IGF-1R has been found to interact with regulatory regions of chromatin to alter gene expression and interact with nuclear proteins involved in gene transcription and DNA replication (Aleksic *et al.*, 2010, 2018; Sehat *et al.*, 2010; Warsito *et al.*, 2012; Waraky *et al.*, 2017; Solomon-Zemler *et al.*, 2019). In prostate cancer, higher levels of nuclear IGF-1R were seen in malignant compared to benign epithelium and were associated with a more advanced tumour stage (Aleksic *et al.*, 2010, 2018). This suggests nuclear IGF-1R could be a potential biomarker for prostate cancer progression and has previously been suggested as a potential marker for

tumours that may be more responsive to anti-IGF-1R targeted treatment (Asmane *et al.*, 2012). Therefore, it is important to understand the role of nuclear IGF-1R more fully in prostate cancer and, to investigate this, the aims of this project are as follows.

Previous work on nuclear IGF-1R has mostly focussed on detection of the β-subunit of the receptor. Recent work on the INSR showed that it translocated to the nucleus as a complex of its α- and β-subunits (Hancock *et al.*, 2019), and due to the analogous structure and functions of IGF-1R and INSR it is possible similar mechanisms are taking place with IGF-1R. Therefore, the first aim relates to the α-subunit of IGF-1R in the nucleus.

1. Investigate the role of the α-subunit in the nucleus of prostate cancer cells, testing for its presence and interaction with the β-subunit in the nucleus and role in the chromatin interactions of nuclear IGF-1R.

As higher levels of nuclear IGF-1R were found to be associated with worse clinical outcomes as well as rarely being found in benign tissue (Aleksic *et al.*, 2010, 2018), it is possible that nuclear IGF-1R may be a tumour selective property of the IGF-axis that could act as a novel target for treatment. Targeting nuclear IGF-1R may also help to avoid issues of cross reactivity with INSR seen with previous small molecule drugs (Simpson *et al.*, 2017; Osher and Macaulay, 2019). Therefore, we aimed to investigate the possibility of developing inhibitors specific for nuclear IGF-1R.

2. Develop a screening platform that could be used to screen a library of small molecule drugs for potential novel inhibitors of nuclear IGF-1R.

The third aim of this project relates to the chromatin interactions of nuclear IGF-1R. This will build on work seen with the AR, which showed a large number of extra chromatin binding sites for AR in clinical tissue compared to cell lines (Sharma *et al.*, 2013). Only a

small number of regulatory chromatin binding regions have currently been detected for IGF-1R in prostate cancer (Aleksic *et al.*, 2018), therefore this project aims to further investigate the relevance of these interactions *in vivo*.

3. Investigate additional promoter and regulatory regions of chromatin bound by nuclear IGF-1R in prostate cancer clinical tissue.

Nuclear IGF-1R has been shown to directly interact with a small number of other nuclear proteins involved in gene transcription and DNA replication (Warsito *et al.*, 2012; Waraky *et al.*, 2017; Aleksic *et al.*, 2018; Solomon-Zemler *et al.*, 2019). The final aim of this project will build on that previous work to further investigate nuclear IGF-1R function.

4. Identification of novel nuclear IGF-1R interacting proteins and characterisation of the role of novel interactions.

The ultimate aim of this work is to expand the current understanding of the role of nuclear IGF-1R in cancer biology and its contribution to cancer progression. Identification of novel nuclear IGF-1R protein interactions will potentially provide novel treatment targets and validation of these, as well as investigation into novel chromatin interactions, will contribute to more fully understanding nuclear IGF-1R function. Validation of nuclear IGF-1R binding to regulatory regions of chromatin in clinical tissue will also confirm the relevance of these interactions *in vivo*. Overall, the initial hypothesis of this project is that IGF-1R is present as a nuclear complex of its α- and β-subunits where it interacts with proteins involved in gene transcription, DNA replication and repair, and with chromatin regulatory regions *in vivo*.

2 Chapter II: Materials and Methods

2.1 Cell Lines

DU145 prostate cancer cells were obtained from Cancer Research UK Laboratories, Clare Hall, Hertfordshire, UK, and were authenticated using Human Cell Line Authentication Services at Eurofins Scientific. 22Rv1 prostate cancer cells were obtained from the laboratory of Sir Walter Bodmer (Weatherall Institute of Molecular Medicine, University of Oxford, UK). DU145 IGF-1R null CRISPR knockout and 22Rv1 IGF-1R null CRISPR knockout cell lines were generated in our lab by Dr Eliot Osher and Matthew Ellis respectively. IGF-1R knock-out was validated by Sanger sequencing analysis (Source BioScience) of the IGF-1R gene locus and Western blotting. All cell lines were cultured in RPMI-1640 at 37°C in 5% CO_2, supplemented with 10% foetal bovine serum (FBS), 100 units/ml of penicillin and 0.1 mg/ml streptomycin.

2.2 Fresh Frozen Prostate Tissue

Fresh frozen prostate tissue samples were obtained and used under approval from the Research Ethics Committee and the Health Research authority (REC reference 07/H0606/120: The role of insulin-like growth factor (IGF) signaling in tumour biology (South Central – Oxford C REC, valid to Nov 2022, ORB_20/A032 (Oxford Radcliffe Biobank)) from prostate cancer patients at the Churchill Hospital Cancer Centre, Oxford, UK undergoing transurethral resection of the prostate (TURP) or channel-TURP operations, or from biopsies taken from patients undergoing radical prostatectomies (RPs). TURP samples were obtained with the help of Lois Vesty-Edwards (Senior Research Nurse, Surgical Research Team, Nuffield Department of Surgical Sciences (NDS), University of Oxford, UK), Mr Simon Brewster (Consultant Urologist, Prostate Cancer

Lead, Oxford University Hospitals (OUH), UK) and Mr Alastair Lamb (Honorary Consultant Urologist, Churchill Hospital Cancer Centre, Oxford, UK). Biopsy samples were obtained with the help of Miriam O'Hanlon (Biobank Technician, NDS), David Maldonado-Perez (Biobanking Coordinator, NDS) and Richard Colling (Consultant Pathologist, OUH) via the Oxford Radcliffe Biobank (ORB). Fresh samples were stored on ice until they could be snap frozen, and then stored at -80^{o}C until use. Corresponding tissue sample slides for immunohistochemical staining were also obtained with the help of Miriam O'Hanlon and Prof Clare Verrill (Associate Professor in Pathology and Honorary Consultant in Cellular Pathology, NDS) via the Oxford Centre for Histopathology Research (OCHRe). Relevant required clinical data was pseudo anonymised and stored in password protected files.

2.3 Western Blotting

Adherent monolayer cells were treated as per the experimental conditions. Cells were washed twice with ice cold phosphate buffered saline (PBS) and collected by scraping. Cells were pelleted by centrifugation at 500 x g, 5 mins at 4°C, resuspended in IGF-1R lysis buffer (50 mM HEPES, 100 mM NaCl, EDTA pH8 10 mM, sodium pyrophosphate 4 mM, sodium orthovanadate 2 mM, sodium fluoride 10 mM and 1% Triton^{TM} X-100 in Milli-Q water) and then incubated on ice for 30 mins. Samples were then centrifuged at 16000 x g, 5 mins at 4°C and soluble whole cell protein lysate (supernatant) transferred to a pre-chilled Eppendorf tube. Soluble protein was quantified against Bovine Serum Albumin (BSA) standards with a Pierce Bicinchoninic Acid (BCA) assay (ThermoFisher Cat. No. 23225) using a POLARstar Omega plate reader (BMG Labtech). Equal amounts of protein were then prepared with NuPAGE™ LDS Sample Buffer (4X) (ThermoFisher Cat. No, NP0007) and dithiothreitol (DTT, 0.1M), typically, 70 µg of lysate with 7.5 µl

LDS and 2.5 µl of DTT. Samples were then denatured for 5 mins at 95°C and separated by sodium dodecyl sulphate-polyacrylamide gel electrophoresis (SDS-PAGE) on a 7.5% Criterion™ TGX™ Precast Midi Protein Gel (Bio Rad Cat. No. 5671024). Proteins were then transferred to an 8.5 x 13.5 cm, 0.2 µm nitrocellulose membrane using "Mixed Molecular Weight" setting on a Bio-Rad Trans-Blot Turbo Transfer System (Bio-Rad Cat. No. 1704150) and blocked for 1 hr at RT on a rocker in Blocking Solution (5% BSA in PBS-T (0.1% Tween™ 20 (Sigma Aldrich, Cat. No. P1379)). Note: For of DNA-PKcs protein, due to its large molecular weight (450 kDa), Bio-Rad Trans-Blot Turbo Transfer System settings were altered to the "High Molecular Weight" setting.

Blocking Solution was removed, and membranes were incubated with relevant primary antibody at appropriate dilution in fresh Blocking Solution overnight at 4°C. The membrane was then washed three times with PBS-T (0.1% Tween™ 20) for 5 mins at room temperature (RT) on a rocker, followed by incubation for 1 hr at RT on a rocker with relevant horseradish peroxidase (HRP)-conjugated secondary antibody diluted in Blocking Solution. Secondary antibody was removed, and membranes were washed three times with PBS-T for 5 min at RT on a rocker. Proteins were then detected by addition of enhanced chemiluminescence (ECL) reagent (Promega, Cat. No. W1015) and visualisation with either Amersham ECL Hyperfilm (GE Healthcare Cat. No. 28-9068-37) or Bio-Rad Chemidoc MP.

2.4 Irradiation Treatments

All irradiation treatments were carried out by either Dr Guillaume Rieunier (post-doctoral researcher) or Matthew Ellis (DPhil student) from our lab, using a Gamma-Service Medical GmbH GSR D1 (Caesium-137) irradiator at indicated doses for each experiment. Cells were then incubated at 37°C in 5% CO_2 for indicated time points.

2.5 Cell Fractionation

Cells were treated as appropriate for the relevant experimental conditions, before fractionation into nuclear and cytoplasmic fractions using NE-PER™ Nuclear and Cytoplasmic Extraction Reagent kit (ThermoFisher Cat. No. 78833) as per manufacturers protocol with slight alterations. Briefly, cells were seeded into two 15 cm dishes per condition and harvested at approximately 75-80% confluency. Cells were washed twice in ice cold PBS on ice before being scraped and collected into 1.5 ml Eppendorf tubes by centrifugation at 500 x g, 5 mins at 4^{o}C. Cells were resuspended in ice-cold CER I buffer (ThermoFisher Cat. No. 78833) containing protease and phosphatase inhibitors (100 µl per 1 x 15 cm dish of cells), vortexed vigorously for 1 min, and incubated on ice for 15 mins. Ice-cold CER II buffer (ThermoFisher Cat. No. 78833) containing protease and phosphatase inhibitors was then added (5.5 µl CER II per sample) and samples were vortexed for 20 secs before incubating on ice for 3 mins. Samples were vortexed again for 20 secs, and centrifuged at 16000 x g, 5 mins at 4^{o}C. Supernatant (cytoplasmic extract) was then immediately transferred to a pre-chilled Eppendorf tube, and stored at 4^{o}C until use, or -20^{o}C long-term. Remaining insoluble pellet was washed with 20 µl PBS, before being resuspended in ice-cold NER buffer (ThermoFisher Cat. No. 78833) containing protease and phosphatase inhibitors (50 µl NER per sample), vortexed for 20 secs and incubated with shaking at 600 rpm, 1 hr at 4^{o}C. Samples were then centrifuged at 16000 x g, 10 mins at 4^{o}C, and supernatant (nuclear fraction) was transferred to a pre-chilled Eppendorf tube. The protein content of the fractions was quantified by Pierce BCA protein assay (ThermoFisher Cat. No. 23225) and equal amounts of nuclear and cytoplasmic protein were then prepared, alongside equal amount of whole cell extract control, for SDS-PAGE and Western blot analysis as described in Section 2.3.

2.6 Chromatin Fractionation

Chromatin fractionation protocol was adapted from (Britton, Coates and Jackson, 2013; Ochi *et al.*, 2015). Briefly, cells were grown in appropriate culture medium before treatment with 8 Gy IR. After indicated time points post-IR, cells were either processed for whole cell lysis as in Section 2.3 and stored at 4^{o}C until use, or for chromatin fractionation. For chromatin fractionation, cells were washed twice with ice cold PBS on ice before incubation for 3 min, on a rocker at 4^{o}C in cytoskeleton buffer (CSK Buffer: 100 mM NaCl, 300 mM sucrose, 3 mM MgCl2, 0.7% Triton X-100, 10 mM PIPES, pH 7.0, supplemented with 0.3 mg/ml RNase A). CSK buffer was then removed, and cells were washed twice with ice cold PBS on ice before a second incubation with CSK buffer, 3 min on a rocker at 4^{o}C. CSK buffer was removed, cells were washed 3 times with ice cold PBS on ice and remaining chromatin was lysed with SDS lysis buffer (2% SDS, 10% glycerol, 25 mM TCEP#, 62.5 mM Tris-HCl, pH 6.8) at RT before scraping and transfer to 1.5 ml Eppendorf tubes. Samples were briefly vortexed before being boiled for 10 min at 95^{o}C to dissolve samples. Samples were centrifuged at 15 000 rpm, 1 min at RT and supernatants (chromatin) were transferred to fresh 1.5 ml Eppendorf tubes. Protein concentrations were measured using a NanoDrop One (ThermoFisher) and were analysed alongside previously collected whole cell lysates by Western blot as in Section 2.3.

2.7 Cell Surface Protein Biotinylation and Isolation

The reagent kits used in this overall process were Pierce™ Cell Surface Protein Biotinylation and Isolation Kit (ThermoFisher Cat. No. A44390), and NE-PER™ Nuclear and Cytoplasmic Extraction Reagent kit (ThermoFisher Cat. No. 78833). Biotinylated

proteins that were isolated from nuclear extracts were analysed by SDS-PAGE and Western blotting.

DU145 or 22Rv1 cells were cultured in 15 cm dishes until >85% confluency before being serum starved for 24 hrs. Biotinylation of cell surface proteins was performed according to the manufacturer's instructions and involved the following steps: serum starved cells were washed twice with ambient BupH™ PBS (ThermoFisher Cat. No. A44390), before incubation with either BupH™ PBS control or EZ-Link™ Sulfo-NHS-SS-Biotin label dissolved in BupH™ PBS (ThermoFisher Cat. No. A44390) for 10 mins at RT (2 x 15 cm dishes per condition). Cells were then washed twice with ice cold BupH™ Tris-HCl Buffered Saline (TBS) (ThermoFisher Cat. No. A44390) and treated with RPMI-1640 medium supplemented with 10% FBS for 20 mins at 37^{o}C. Cells were washed once with ice cold BupH™ TBS on ice before being scraped and collected into pre-chilled 1.5 ml Eppendorf tubes. Cells were pelleted by centrifugation at 500 x g, 5 mins at 4^{o}C and fractionated as per the NE-PER™ Nuclear and Cytoplasmic Extraction Reagent kit protocol described in Section 2.5. Protein content of the isolated nuclear lysate was quantified by Pierce BCA protein assay (ThermoFisher Cat. No. 23225), and 10% of the lysate was retained and stored at 4^{o}C to be used as input control.

NeutrAvidin™ Agarose columns (ThermoFisher Cat. No. A44390) for biotinylated protein isolation were then prepared as follows. The bottom tip of the provided columns was removed, and the columns placed into a provided collection tube. To each column, 250 µl of the NeutrAvidin™ Agarose slurry (ThermoFisher Cat. No. A44390) was added, and the columns centrifuged at 1000 x g, 1 min at RT. A provided bottom plug was applied to the columns, and equal amounts of either BupH™ PBS control lysate or biotin labelled lysate was added to the appropriate column. Top caps were applied to the columns, before incubation for 30 mins, at RT with end-over-end rotation. Bottom caps were then removed,

and the columns placed into collection tubes and centrifuged at 1000 x g, 1 min at RT. Flowthrough was discarded, and 500 µl of Wash buffer (ThermoFisher Cat. No. A44390) was applied to the column and mixed by inversion. Columns were centrifuged at 1,000 × g, 1 min at RT and wash was discarded. This was repeated 3 times for a total of 4 washes. To elute the retained biotinylated proteins, 225 µl Elution Buffer and 25 µl DTT stock solution (ThermoFisher Cat. No. A44390) were mixed and 100 µl of this stock buffer was added to each column. Columns, with both top and bottom caps attached, were then placed into collection tubes, and incubated for 30 mins at RT with end-over-end rotation. After incubation, columns were placed into 1.5 ml Eppendorf tubes and centrifuged at 1000 x g, for 2 mins at RT to elute proteins. Previously stored nuclear inputs and whole cell extract control were then prepared alongside eluted samples for SDS-PAGE and Western blot analysis as described in Section 2.3.

2.8 Co-Immunoprecipitation (Co-IP)

Firstly, Protein A agarose beads were prepared from lyophilized powder (Merck Millipore Cat. No. P9269). Briefly, 25 mg of powder was weighed out into a screw cap Eppendorf and swelled with 250 µl of cold PBS. Beads were swelled by incubation for 30 mins on ice, and then collected by centrifugation at 16000 x g, 30 secs at 4°C and washed with 3 x 1 ml cold PBS. After final wash, beads were resuspended in original volume of PBS and stored at 4°C until use.

Cells were treated as appropriate (2 x 15 cm dish per condition for whole cell IP, 10 x 15 cm dish per condition for nuclear extract IP), and then washed twice with ice cold PBS before either whole cell lysis in IGF-1R lysis buffer or fractionation using NE-PER™ Nuclear and Cytoplasmic Extraction Reagent kit as described in Sections 2.3 and 2.4 respectively. For each sample, equal amount of protein was prepared (1-1.5 mg) and 10%

of each sample was retained for input control and stored at -20ºC until use. To each sample, 20 µl of Protein A agarose beads and 1 µl of normal rabbit IgG antibody (CST-2729) was added and incubated for 1 hr at 4ºC with end-over-end rotation for preclear step. Beads were centrifuged at 16000 x g, 3 mins at 4ºC and precleared lysates were transferred to a fresh Eppendorf tube. Antibodies were then added as appropriate, either normal rabbit IgG control (CST-2729, 1 µl of a 1:3 dilution with IGF-1R lysis buffer (approx. 0.1 µg)), IGF-1Rα (24-60) (MA5-13817, 20 µl) or IGF-1Rβ (CST-3027, 20 µl) per sample and incubated overnight at 4ºC with end-over-end rotation.

Following overnight incubation, 40 µl of protein A agarose beads were added to each sample and incubated for 2 hrs at 4ºC with end-over-end rotation. Protein A agarose beads were then collected by centrifugation at 3000 x g, 3 mins at 4ºC and washed with 3 x 1 ml ice cold IGF-1R lysis buffer containing protease and phosphatase inhibitors for 5 mins at 4ºC with end-over-end rotation. Inputs were defrosted and prepared alongside Co-IP samples for SDS-PAGE and Western blot analysis as described in Section 2.3.

2.9 Immunofluorescence Staining (IF)

Immunofluorescence staining was performed as per Cell Signalling Technology (CST) general protocol with slight modifications. Briefly, cover slips were washed in 70% ethanol followed by PBS and one coverslip was placed into each well of a 6-well plate. Cells were seeded at 300,000 cells/well onto the cover slips and cultured overnight at 37°C in 5% CO_2. For IGF-1 stimulation experiments, cells were serum starved for 24 hrs and then treated with 10 mM HCl solvent control or IGF-1 (50 nM, 20 mins). For inhibition experiments, after overnight culture, cells were treated with either 0.1% DMSO (control) or BMS-754807 (100 nM, 6 hrs. Sigma Aldrich Cat. No. BM0003), an IGF-1R tyrosine kinase inhibitor. After appropriate treatment, the medium was removed, and cells were

washed in ambient PBS for 3 x 5 mins at RT on a rocker, before fixation with 4% paraformaldehyde (methanol free, Alfa Aesar 43368) in ambient PBS for 20 mins at RT on a rocker. Cells were then washed in PBS for 3 x 5 mins at RT on a rocker, followed by incubation with Blocking Solution (5% BSA and 0.3% Triton^{TM} X-100 in ambient PBS) for 1 hr at RT on a rocker. Blocking Solution was then removed and the required primary antibodies, diluted in Blocking Solution, were added to relevant wells, and incubated overnight at 4^{o}C on a rocker (IGF-1Rα (24-60), (MA5-13817) at 1:250 or IGF-1Rβ (CST 9750) at 1:500).

Antibody solutions were removed, and cells were washed in ambient PBS for 3 x 5 mins, RT on a rocker. The corresponding secondary antibody, diluted in blocking solution, Goat anti-Mouse IgG (H+L) Highly Cross-Adsorbed Secondary Antibody) Alexa Fluor 488 (Invitrogen, Cat. No. A11039) at 1:2000 or Goat anti-Rabbit IgG (H+L) Highly Cross-Adsorbed Secondary Antibody, Alexa Fluor 594 (Invitrogen, Cat. No. A11037) at 1:2000 was then added and incubated for 1 hr at RT on a rocker with protection from light. Cells were then washed in ambient PBS for 3 x 5 mins, RT on a rocker, and cover slips were mounted on to slides using mounting medium containing 4′,6-diamidino-2-phenylindole (DAPI). The slides were stored at 4^{o}C until visualisation on a Zeiss LSM 780 Confocal microscope using x63 magnification. Nuclear IGF-1R was quantified using FIJI (ImageJ) software via quantification of IGF-1R signal within the boundaries of outlined DAPI stained nuclei.

2.10 Immunohistochemistry (IHC)

2.10.1 Staining Protocol

Tissue sample slides for immunohistochemical staining were obtained with the help of Miriam O'Hanlon (Biobank Technician, NDS) and Prof Clare Verrill (Associate Professor

in Pathology and Honorary Consultant in Cellular Pathology, NDS) via OCHRe. Immunohistochemical staining was performed as per (Aleksic, Ross Worrall, *et al.*, 2016) with help from Jinseon (Selena) Kim, Research Assistant in our lab. Briefly, slides were incubated in Citroclear (TCS Bioscience Ltd, UK) for 2 x 8 min followed by 2 min incubation consecutively in 100% then 75% ethanol and finally 2 x 2min in 50% ethanol before being washed 5 x 1 min in distilled water to dewax and rehydrate tissue slides. For antigen retrieval, slides were incubated in a decloaking chamber (DC2002, Biocare Medical, USA) at 125 ^{o}C for 2 min, 85 ^{o}C for 10 min in 50 mM Tris-Cl, 2 mM EDTA pH 9. Cells were then cooled to RT by incubation on ice for 20 min followed by 3 x 5 min washes in PBS at RT on a rocker. Slides were then incubated in 3% H_2O_2 in dH_2O at RT for 10 min to block endogenous peroxidases. Slides were then washed again for 3 x 5 min in PBS before being incubated in blocking solution (5% BSA, 5% goat serum in PBS) for 1 hr at RT on a rocker. Tissue areas were then marked with a PAP pen and slides were incubated in a humidified chamber with antibody for IGF-1Rβ (CST-9750) diluted 1:50 in blocking solution using 100-200 µl of antibody per slide. Slides were then incubated on a level surface in the humidified chamber overnight at 4 ^{o}C.

The following day, primary antibody was removed, and slides were washed 3 x 5 min in PBS at RT on a rocker. Bound antibody was then detected using MP-531-M3R25 Menarini Diagnostics kit (Winnersh-Wokingham, UK). Approximately 1-3 drops of rabbit probe (MP-531-M3R25 Menarini Diagnostics kit) was added to each slide and incubated for 15 min at RT. Slides were then washed 3 x 5 min in PBS at RT on a rocker before being incubated with rabbit HRP polymer (MP-531-M3R25 Menarini Diagnostics kit) for 15 min at RT. Slides were again washed 3 x 5 min in PBS before incubation with DAB substrate (Envision) for 6 min at RT, washed 3 x 2 min in tap water and then counterstained with Mayer's haematoxylin (Vector Laboratories, USA) for 40 sec and then

washed with copious amounts of tap water until water ran clear. Slides were then dehydrated by incubation for 2 x 2 min in 50% ethanol, 2 min in 75% ethanol, 2 min in 100% ethanol and finally 2 min in Xylene. Cover slips were then mounted to slides using DePex reagent (VWR International, UK) and allowed to dry before slides were imaged using an Aperio ScanScope slide scanner.

2.10.2 IGF-1R scoring

Histology of the stained tumour slides were identified by Prof Clare Verrill, along with scoring of IGF-1R staining. Levels of membrane, cytoplasmic and nuclear IGF-1R were assessed as in (Aleksic *et al.*, 2018). Briefly, membrane, cytoplasmic and nuclear IGF-1R were scored for intensity (0, nil; 1, weak; 2, moderate; 3, heavy) and percentage (0%, nil; 1: 1-10%; 2: 11-50%; 3: 51-80%; 4: 81-100%) of tumour stained, generating immunoreactive scores (range 0-12) for membrane, cytoplasmic and nuclear IGF-1R.

2.11 Chromatin immunoprecipitation (ChIP)

2.11.1 ChIP from adherent cells

For ChIP from adherent cells, cells were cultured in full medium or treated with IGF-1 (50 nM, 10 mins) after being serum starved for 24 hrs, as appropriate (5 x 15 cm dish per condition). Samples were then processed using Merck Millipore ChIP kit (Cat. No. 17-295) as per the manufacturers protocol with some modifications. Briefly, cells were washed twice with ice cold PBS, before fixation with 1% formaldehyde (methanol free, Alfa Aesar) in PBS. Cells were scraped and collected into 15 ml falcon tubes by centrifugation at 500 x g, 5 mins at 4^{o}C before being resuspended in 1% formaldehyde in serum free medium and incubated for 10 mins, RT on a rocker. Fixation was quenched by addition of 125 mM glycine in nuclease free water and cells were collected by centrifugation at 500 x g, 5 mins before being washed twice with ice cold PBS containing

protease inhibitor (Roche EDTA-free). Cell pellets were resuspended in 200 µl SDS lysis buffer (Millipore ChIP kit, Cat. No. 17-295), containing protease inhibitor (Roche EDTA-free), and transferred to pre-chilled Eppendorf tubes. Samples were incubated on ice for 30 mins, then snap frozen in dry ice and ethanol and stored overnight at -20ºC.

Samples were thawed on ice and sonicated for 18 cycles on high voltage (30 secs on, 30 secs off) using a Bioruptor® Plus sonicator (Diagenode Cat. No. B01020001). Samples were then centrifuged at 16000 x g, 5 mins at 4ºC, and 5 µl of each sample was separated using electrophoresis on a 1% agarose gel to ensure DNA had been sheared into fragments of 150 – 500 bp. From the remaining supernatant, 200 µl was transferred to a fresh, prechilled Eppendorf tube along with 1.3 ml of cold ChIP dilution buffer (Millipore ChIP kit, Cat. No. 17-295) containing protease inhibitor (Roche EDTA-free). Samples were mixed by inversion and 50 µl was removed for input and stored at -20ºC. To the remaining sample, 50 µl of salmon sperm DNA/Protein A agarose slurry (Millipore ChIP kit, Cat. No. 17-295) was added along with 1 µl of normal rabbit IgG (CST-2729), and samples were pre-cleared by incubation with end-over-end rotation for 1 hr at 4ºC. Supernatants were then collected by centrifugation at 16000 x g, 3 mins at 4ºC, and appropriate antibodies were added, either RNA Polymerase II (CTD repeat YSPTSPS (phospho S2) antibody, Abcam (ab5095), 10 µl), IGF-1Rα (24-60) (MA5-13817, 20 µl) or IGF-1Rβ (CST-3027, 20 µl) before incubation overnight at 4ºC with end-over-end rotation.

Following overnight incubation, 70 µl of salmon sperm DNA/Protein A agarose slurry (Millipore ChIP kit, Cat. No. 17-295) was added, and samples were incubated for 2 hrs at 4ºC with end-over-end rotation. Protein A agarose beads were collected by centrifugation at 3000 x g, 3 mins at 4ºC and supernatant was discarded. Beads were then washed sequentially with 1 ml low salt buffer, 1 ml high salt buffer, 1 ml LiCl wash buffer and 2 x 1 ml TE buffer (Millipore ChIP kit, Cat. No. 17-295). Beads were incubated for 5 mins at

4°C with end-over-end rotation for each wash and supernatant was discarded between washes following centrifugation at 3000 x g, 3 mins at 4°C. After the final wash, samples were eluted with 500 µl ChIP elution buffer (1% SDS + 0.1M $NaHCO_3$. Master mix: 250 µl 20% SDS, 555.5 µl $NaHCO_3$, 4194 µl nuclease free water), and incubated at RT for 30 mins with shaking (400 rpm). After incubation, supernatant was collected by centrifugation at 3000 x g, 3 mins at RT. Previously stored inputs were thawed and made up to 500 µl with 450 µl of elution buffer. To all samples and inputs, 20 µl of 5M NaCl (Millipore ChIP kit, Cat. No. 17-295) was added, and crosslinks were reversed by incubation at 65°C overnight.

To all samples and inputs 10 µl 0.5M EDTA (Millipore ChIP kit, Cat. No. 17-295), 20 µl 1 M Tris (pH 6.5, Millipore ChIP kit, Cat. No. 17-295) and 2 µl of 20 mg/ml Proteinase K (Thermo Fisher EO 0491) were added and incubated for 1 hr at 45°C. DNA was then phenol chloroform extracted as follows: 500 µl of phenol chloroform was added to all samples, mixed by inversion, and the upper phase collected by centrifugation at 16000 x g, 5 mins at 4°C. To the collected supernatant 500 µl of chloroform was added, mixed by inversion, and upper phase collected by centrifugation at 16000 x g, 5 mins at 4°C. To this collected upper phase, 1 ml of ice-cold ethanol (96 - 100%), 50 µl of 3 M sodium acetate (Invitrogen, Cat. No. AM9740) and 2 µl of UltraPure™ glycogen (ThermoFisher Cat. No. 10814010) were added, mixed by inversion, and incubated overnight at -20°C.

Samples were centrifuged at 16000 x g, 45 mins at 4°C. All supernatant was discarded, and DNA pellet was washed with 500 µl of 70% ethanol. Samples were centrifuged at 16000 x g, 10 mins at 4°C and then dried for 5 mins at 60°C on a heat block. Pellets were resuspended in 20 µl of nuclease free water and then stored at -20°C until required for qPCR.

2.11.2 ChIP from fresh frozen TURP tissue

For ChIP from fresh frozen prostate tissue TURP samples, samples were cut into thin sections (approx. 1-2 mm^3) using a scalpel on ice in ice-cold PBS, before fixation in 1% formaldehyde in PBS for 20 mins at RT on a rocker. The fixation reaction was then stopped with 125 mM glycine, and tissue was washed with ice-cold PBS. Tissue was then homogenised and lysed in 500 µl SDS Lysis buffer containing protease inhibitor in Lysing Matrix A ceramic bead tubes (MP biomedical Cat. No. 6910050) using a FastPrep Homogenizer for a total of 3 min homogenisation time (30 secs on, 30 secs off) at 4.5 m/sec speed. Samples were then incubated on ice for 30 mins, before being snap frozen and stored overnight at -20ºC. Samples were then thawed on ice and sonicated using a Bioruptor® Pico sonicator (Diagenode Cat. No. B01060010) (30 secs on, 30 secs off) to generate DNA fragments between 150 – 500 bp in size before being processed using Merck Millipore ChIP kit (Cat. No. 17-295) as described in Section 2.11.1.

2.11.3 ChIP from fresh frozen biopsy tissue

For ChIP from fresh frozen prostate tissue biopsy samples, the protocol from (Singh *et al.*, 2019) was adapted for use. Samples were cut into 30 µm slices at -20ºC using a Leica CM1950 cryostat before fixation in 1% formaldehyde in PBS for 10 mins at RT on a rocker. The fixation reaction was then stopped with 125 mM glycine, and tissue was washed with ice-cold PBS. Tissue was lysed in 500 µl SDS Lysis buffer containing protease inhibitor on ice for 20 mins before homogenisation using a Pellet Pestle homogeniser. Samples were then incubated on ice for a further 30 mins, before being snap frozen and stored overnight at -20ºC. Samples were thawed on ice and sonicated using a Bioruptor® Pico sonicator (Diagenode Cat. No. B01060010) (30 secs on, 30 secs off) to generate DNA fragments between 150 – 500 bp in size. Samples were then centrifuged at 16000 x g, 5 mins at 4ºC and chromatin supernatant was split evenly between ChIP

conditions before being made up to 1.5 ml with cold ChIP dilution buffer (Millipore ChIP kit, Cat. No. 17-295) containing protease inhibitor (Roche EDTA-free). Samples were then further processed for ChIP using Merck Millipore ChIP kit (Cat. No. 17-295) as described in Section 2.11.1.

2.12 Real time quantitative Polymerase Chain Reaction (qPCR)

2.12.1 Primer Design

Primers for qPCR were designed using NCBI Primer BLAST for relevant regions of interest previously identified by ChIP-seq (Aleksic *et al.*, 2018), and DNA sequences of these regions were obtained from hg19 human genome assembly using the UCSC Genome Browser. Primers were designed to have GC content <60%, melting temperatures (T_M) within 2-3^oC of each other, no 3' complementarity and, for qPCR, amplicons of approximately 50 – 250 bp. Primers were obtained from Integrated DNA Technologies (IDT) and are alongside amplicon lengths in
Table **2.1**.

DNA region	Primer sequences	Amplicon length (bp)
JUN promoter region	F 5'-CTCGCCCAAGTTCAACAACC-3'	94
	R 5'-ACGGCGGTAAAGACCAGAAG-3'	
FAM21A promoter region	F 5'-GAGGTCCCCTCTTTCCAGAC-3'	169
	R 5'-GGTTCTACCCTAGGTTGGGG-3'	
Chromosome 17 Intergenic Region	F 5'-GTCATATGATTCCAGGGGGAGC-3'	76
	R 5'-GTGTTACCAGCGTGGCAGAG-3'	
DUSP8 promoter region	F 5'-CGCGAGTGACAGGCCC-3'	83
	R 5'-GGTGACGTCAGGGGCTTTTT-3'	

Table 2.1 ChIP-qPCR primers
Table showing primers used in qPCR validation of IGF-1R ChIP for indicated IGF-1R binding sites previously identified in our lab via ChIP-seq (Aleksic *et al.*, 2018).

2.12.2 qPCR

qPCR was performed using Luna® Universal qPCR Master Mix (New England Biolabs Cat. No. M3003), a 2X reaction mix containing Sybr® Green I dye, Hot Start Taq DNA Polymerase, dNTPs, $MgCl_2$ and universal reference dye. Each PCR reaction was run in triplicate and consisted of 10 µl Master Mix, 1 µl of forward and 1 µl of reverse primers (10 µM stock, 0.5 µM final concentration for both), 1 µl of ChIP DNA as template and 7 µl of nuclease free water. The PCR was run using a 7500 Fast RT-PCR machine, with the following protocol: 20 secs at 95°C, followed by 40 cycles of 3 secs at 95°C and 30 secs at 60°C. A non-template negative control which contained only nuclease free water and no ChIP DNA template was also run for each set of primers to check for contamination.

2.13 Generation of luciferase reporter plasmids

2.13.1 Genomic DNA Extraction

Genomic DNA was extracted from DU145 and 22Rv1 cells using the DNeasy kit (Qiagen Cat. No. 69504) according to the manufacturers protocol with slight alterations. Briefly, cells were collected (max 5 x 10^6 cells) by scraping and pelleted by centrifugation at 300 x g, 5 mins at 4^{o}C. The cell pellet was then resuspended in 200 µl of PBS and 20 µl of 20 mg/ml Proteinase K and mixed briefly by vortexing. Next, 200 µl of Buffer AL (Qiagen Cat. No. 69504) was added and mixed thoroughly by vortexing before incubation for 10 mins at 56^{o}C. Following incubation, 200 µl of ethanol (96-100%) was added to the sample and mixed thoroughly by vortexing. The mixture was then transferred to a DNeasy Spin Column placed into a 2 ml collection tube (Qiagen Cat. No. 69504), and 500 µl of Buffer AW1 (Qiagen Cat. No. 69504) was added and washed through by centrifugation at 6000 x g, 1 min at RT. Flowthrough was discarded, and column placed back into the collection tube before addition of 500 µl of Buffer AW2 (Qiagen Cat. No. 69504), washed through by centrifugation at 20000 x g, 3 mins at RT. Flowthrough was discarded and centrifugation at 20000 x g, 3 mins at RT was repeated to ensure the column was dry. The column was then transferred to a clean Eppendorf tube and 100 µl of ultrapure water was added to the column, incubated for 5 mins at RT before elution of genomic DNA by centrifugation at 20000 x g, 2 mins at RT.

2.13.2 Amplification and purification of IGF-1R DNA binding regions

Primers for relevant IGF-1R binding regions were designed as described in Section 2.12.1 with addition of cutting sites for restriction enzymes XhoI and HindiIII, and for relevant larger amplicon sizes required. Primer sequences are listed in
Table **2.2** alongside annealing temperatures and amplicon sizes. Regions were amplified using Phusion® High-Fidelity PCR Master Mix with HF Buffer (Promega M0531),

containing Phusion DNA Polymerase, dNTPs and reaction buffer containing $MgCl_2$, as per the manufacturers protocol. Briefly, the PCR reaction consisted of 12.5 µl Master Mix, 1.25 µl of forward and 1.25 µl of reverse primers (10 µM stock, 0.5 µM final concentration for both), 100 ng of DNA as template and nuclease free water to make up to 25 µl. The PCR thermocycling reaction was then run on a SimpliAmp Thermal Cycler PCR machine (ThermoFisher), as follows: incubated for 30 secs at 98°C, then 30 cycles of 10 secs at 98°C, 30 secs at relevant annealing temperature (see Table **2.2**) and 72°C for 30 secs per 1 kb amplicon length (see Table **2.2**). Samples were then incubated for 10 mins at 72°C and then infinite hold at 4°C. Amplified DNA (5 µl) was analysed by electrophoresis on a 1% agarose gel, and samples containing amplified DNA at expected amplicon size were column purified using QIAquick PCR Purification Kit (Qiagen Cat. No. 28106) as per manufacturers protocol. Briefly, 5 volumes of Buffer PB (Qiagen Cat. No. 28106) were added to 1 volume of PCR product, mixed thoroughly by pipetting, and applied to a QIAquick spin column placed in a 2 ml collection tube (Qiagen Cat. No. 28106). The column was then centrifuged at 16000 x g, 1 min at RT and flowthrough was discarded. The column was placed back into the collection tube and 750 µl of Buffer PE (Qiagen Cat. No. 28106) was added before centrifugation at 16000 x g, 1 min at RT. Flowthrough was discarded and the centrifugation was repeated at 16000 x g, 1 min at RT to dry the column. The column was transferred to a clean Eppendorf tube and the DNA was eluted by addition of 30 µl of ultrapure water to the column, incubation for 5 mins at RT and then centrifugation at 16000 x g, 2 mins at RT. Concentration of the DNA was analysed using a NanoDrop One (ThermoFisher).

2.13.3 Digestion, ligation, and transformation of IGF-1R DNA binding regions into pNLCol2 reporter plasmid

Purified IGF-1R DNA binding regions amplified by PCR and pNLCol2[luc2-P2A-NlucP/minP/Hygro] reporter backbone (Promega Cat. No. N147A) were digested with XhoI (NEB Cat. No. R0146) and HindiIII-HF (NEB Cat. No. R3104) digestion enzymes as per the manufacturer's protocol. Briefly, the digestion reaction was set up with 1 µg of amplified DNA or pNLCol2 vector as appropriate, 5 µl of 10X CutSmart endonuclease buffer (NEB Cat. No. B7204), 1 µl of Xho1 enzyme, 1 µl of HindiIII-HF enzyme and made up to 50 µl with nuclease free water. The reaction mixture was incubated at 37ºC in a water bath for 30 mins. After this 30 min incubation, 1 µl of Shrimp Alkaline Phosphatase (rSAP, NEB Cat. No. 0371) was added to the pNLCol2 vector digestion and incubated for a further 30 mins at 37ºC to remove 5' or 3' phosphates from ends of DNA. The restriction enzymes and rSAP were then heat inactivated by incubation at 80ºC for 20 mins, and digested DNA and vector were purified by column purification using QIAquick PCR Purification Kit (Qiagen Cat. No. 28106) as described in Section 2.13.2, and concentration of the DNA was analysed using a NanoDrop One (ThermoFisher).

The digested pNLCol2 vector and IGF-1R DNA binding region were then ligated using T4 DNA Ligase (NEB. Cat. No. M0202) as per the manufacturers protocol. Briefly, the ligation reaction was set up on ice with either 1:3, 1:6 or 1:9 molar ratios of vector to insert depending on length of DNA insert, using the NEBioCalculator Programme (*http://nebiocalculator.neb.com/#!/ligation*). The reaction mixture was then set up as follows, in this example for a 1:3 vector to insert ratio: 2 µl of T4 DNA Ligase Buffer (10X) (NEB. Cat. No. M0202), 50 ng of vector DNA of 5945 bp (0.020 pmol), 37.5 ng of insert DNA of 1100 bp (0.060 pmol), 1 µl of T4 DNA Ligase (NEB Cat. No. M0202. Note – this was added to the reaction mixture last), and nuclease free water up to 20 µl. Control ligations

were also set up using vector DNA only with no insert. The reactions were mixed gently by pipetting before being incubated at 4ºC overnight and then heat-inactivated at 70ºC for 10 mins.

For transformation of the plasmid, NEB® Turbo Competent E. coli (High Efficiency) (NEB Cat. No. C2984) were defrosted on ice for 10 mins and then 50 µl of the cells were mixed with 5 µl of ligation mixture by pipetting and incubated on ice for 30 mins. The cells were then heat shocked at 42ºC for 30 secs, 50 µl was added to 950 µl of SOC outgrowth medium (NEB Cat. No. B9020) and incubated at 37ºC for 1 hr with shaking (250 rpm). Relevant LB Agar antibiotic selection plates, in this case ampicillin (final concentration of antibiotic 100 µg/ml), were also warmed to 37ºC and 100 µl of each ligation reaction was spread onto the selection plate. A negative control selection plate was also prepared to which no ligation mixture was added. Plates were incubated overnight at 37ºC, and the following day colonies were tested by colony PCR using primers external to the inserted DNA region (see Table **2.2** - pNL forward and reverse primers). The PCR reaction was set up as described in Section 2.13.2 for cloning of IGF-1R DNA binding sequences with relevant annealing temperature and extension time (see Table **2.2**). The PCR products were then analysed by electrophoresis on a 1% agarose gel, and colonies that contained amplified DNA at expected amplicon size were inoculated into 10 ml of LB Broth culture containing ampicillin (final concentration of antibiotic 100 µg/ml) and grown overnight at 37ºC with shaking (250 rpm).

DMSO stocks of bacterial cultures were prepared (900 µl of bacterial culture with 100 µl of DMSO) and stored at -80ºC. Plasmid constructs were purified from bacterial cultures using QIAprep Spin Miniprep Kit (Qiagen, Cat. No. 27106) as per the manufacturer's instructions. Briefly, bacterial cells were pelleted at 6000 x g, 20 mins at 4ºC, resuspended in 250 µl of Buffer P1 (Qiagen, Cat. No. 27106) and transferred to an Eppendorf tube.

Next, 250 µl of Buffer P2 (Qiagen, Cat. No. 27106) was added and the tube mixed thoroughly by inversion 5 times, followed by 350 µl of Buffer N3 and mixed again by inversion 5 times. The sample was then centrifuged at 16000 x g, 10 mins at RT and the supernatant was transferred to a QIAprep 2.0 spin column placed in a collection tube (Qiagen, Cat. No. 27106). The column was centrifuged at 16000 x g, 1 min at RT and the flowthrough was discarded. Next, the column was washed using 750 µl of Buffer PE (Qiagen, Cat. No. 27106) and centrifuged twice at 16000 x g, 1 min at RT with the flowthrough discarded each time. The column was then transferred to a clean Eppendorf tube, and plasmid DNA was eluted by addition of 30 µl of nuclease free water to the column, incubation for 5 min at RT and centrifugation at 16000 x g, 2 mins at RT. Concentration of purified plasmid DNA was analysed using a NanoDrop One (ThermoFisher), and the DNA sequence was confirmed by Sanger sequencing analysis (Source BioScience, Oxford, UK) using pNL External primers listed in Table **2.2**.

DNA region	Primer sequences	Amplicon length (bp)	Annealing temperature (°C)
JUN promoter region	F 5'-GTTGTTCTCGAGGACGCAGGAAAGGCTTGCA-3'	1375	66
	R 5'-GTTGTTAAGCTTGTTTCGGATCGCCTACACGCT-3'		
Chromosome 17 Intergenic Region	F 5'-GTTGTTCTCGAGAGCTTATGCATGTCTTTCCTGCTT-3'	1078	69
	R 5'-AACAACAAGCTTGTGATGTCGCCCATCATGTGA-3'		
Chromosome 17 Peak Region	F 5'-GTTGTTCTCGAGGGATGGGCGATGTCATGTGA-3'	803	63
	R 5'-AACAACAAGCTTTCACCCATCACATGATTGCC-3'		
Laptm5 intergenic region	F 5'-GTTGTTCTCGAGGCGGTTTGAAGCAGTGAGTC-3'	614	66
	R 5'-AACAACAAGCTTTTCCCCTTCTGGCCTGAGTA -3'		
ARG2 promoter region	F 5'-GTTGTTCTCGAGTTTAATAACCAGCGCTCCCGT -3'	896	66
	R 5'-AACAACAAGCTTCGCTGTCTCCAGGTTCTAGG -3'		

DNA region cont.	Primer sequences cont.	Amplicon length (bp) cont.	Annealing temperature (°C) cont.
FAM21A promoter region	F 5'-GTTGTTCTCGAGGATGATGCCCAGGCAGATCA-3'	895	67
	R 5'-AACAACAAGCTTCTAAACGGGGCGTGTGTTCC -3'		
FAM21C promoter region	F 5'-GTTGTTCTCGAGGATGATGCCCAGGCAGATCA-3'	910	67
	R 5'-AACAACAAGCTTGGCATTCTCGGGGGCTAAAC-3'		
LOC79999 intergenic region	F 5'-GTTGTTCTCGAGGGCATCGGAACTAGCGAAAG-3'	444	64
	R 5'-AACAACAAGCTTCCCCGAGAAAACCCAAGAGC-3'		
pNL External primers	F 5'-GGCCTAACTGGCCGGTACCT-3'	Variable	66
	R 5'-GGCATCTTCCATGGTGGCTTTA-3'		

Table 2.2 PCR primers for cloning genomic DNA

The list of primers used to clone luciferase reporter regions alongside their amplicon length and required annealing temperature. The primers incorporated cutting sites for XhoI (CTCGAG) and HindiIII (AAGCTT) (underlined). pNL external primers were those used for sequencing, and amplicon length was variable, depending on the length of the inserted region.

2.14 Transfection of luciferase reporter plasmids

2.14.1 Transient transfections

DU145 cells were transfected with reporter constructs using Lipofectamine 3000™ (Invitrogen Cat. No. L3000008) as per manufacturer's protocol. Briefly, for cells in a 96-well plate, cells were plated to be 70-90% confluent at the time of transfection (30,000 cells/well for a 96-well plate, 24 hrs before transfection). Lipofectamine 3000 reagent master mix was prepared as follows, where reagent volumes listed are per each well undergoing transfected. In an Eppendorf tube (Tube 1), 10 µl of Gibco™ Opti-MEM™ Medium (Fisher Scientific Cat. No. 11524456) and 0.3 µl of Lipofectamine™ 3000 reagent (Invitrogen Cat. No. L3000008) were added and mixed by pipetting. In a separate Eppendorf tube (Tube 2), 10 µl of Gibco™ Opti-MEM™ Medium, 0.4 µl of P3000™ reagent (Invitrogen Cat. No. L3000008) and 0.2 µg of relevant plasmid DNA were added and mixed by pipetting. Reagents from Tube 1 were then added to the reagents in Tube 2 and the mixture was incubated for 15 mins at RT. After incubation, 10 µl of the reagent mixture was added to each well for transfection, and cells were incubated at 37°C in 5% CO_2, overnight before experimental treatment.

2.14.2 Generation of stable cell lines

DU145 cells were transfected with reporter constructs using Lipofectamine 3000™ (Invitrogen Cat. No. L3000008). Cells were seeded in a 10 cm dish to be 70-90% confluent at the time of transfection (2 x 10^6 cells per dish, 24 hrs before transfection) and transfected with relevant reporter construct using Lipofectamine 3000™. Briefly, 1 ml of Gibco™ Opti-MEM™ Medium and 43.4 µl of Lipofectamine 3000™ reagent were added to an Eppendorf tube (Tube 1) and mixed by pipetting. To a fresh Eppendorf tube (Tube 2), 1 ml of Gibco™ Opti-MEM™ Medium, 40 µl of P3000™ reagent and 20 µg of relevant plasmid DNA were added and mixed by pipetting. The reagents in Tube 1 were

then added to Tube 2, mixed by pipetting, and incubated for 15 mins at RT. The total volume of the mixture was then added to the 10 cm dish of cells to be transfected, and cells were incubated at 37ºC in 5% CO_2. After 48 hrs, culture medium was replaced with hygromycin selection medium (RPMI-1640 supplemented with 10% FBS, 100 units/ml of penicillin, 0.1 mg/ml streptomycin and 500 µg/ml hygromycin) to select for transfected cells, and selection medium was replaced every 3 days. When cell colonies formed, the monolayer was briefly trypsinised (30 sec) and cells from individual colonies were transferred to a 6-well plate where they were then cultured and expanded. Expanded cells were tested for the presence of transfected luciferase reporter by ONE-Glo™ EX Luciferase assay (Promega Cat. No. E8110, see below).

2.15 Luciferase Assays

2.15.1 Testing of transiently transfected cells

ONE-Glo™ EX Luciferase assay (Promega Cat. No. E8110) was used for testing IGF-1 responsiveness of transiently transfected reporter constructs and stable cell lines, as per the manufacturer's instructions. Briefly, DU145 cells were seeded at 30,000 cells/well of a 96-well plate and the following day were transfected with the relevant promoter reporter construct using Lipofectamine 3000™ (Invitrogen Cat. No. L3000008) as described in Section 2.14.1. To test response to IGF-1, the following day cells were serum starved for 24 hrs before treatment with HCl solvent control (4.5 µM, 24 hrs) or IGF-1 (50 nM, 24 hrs). To test response to IGF-1 inhibition in full medium, 24 hrs following transfection, cells were treated with 1 µM PBS solvent control or xentuzumab, an IGF-1 and IGF-2 ligand neutralising antibody (BI 845, 1 µM) (Friedbichler *et al.*, 2014). BI 845 antibody or 1 µM PBS solvent control was pre-incubated with culture medium (RPMI-1640 supplemented with 10% FBS, 100 units/ml of penicillin and 0.1 mg/ml streptomycin) for

15 mins, RT before culture medium was then removed from cells and replaced with this pre-incubated medium. Following addition of either IGF-1 or BI 845, cells were incubated overnight at 37ºC in 5% CO_2 before being tested with ONE-Glo™ EX Luciferase assay reagent (Promega Cat. No. E8110). Briefly, treated cells and ONE-Glo™ EX Luciferase assay reagent were equilibrated to RT before addition of ONE-Glo™ EX Luciferase assay reagent in 1:1 ratio of reagent to medium. Cells were incubated in luciferase reagent for 5 mins, RT on a rocker and shielded from light, and luminescence was measured on a POLARstar Omega plate reader (BMG Labtech). The protein content of the lysate was then quantified by Pierce BCA protein assay (ThermoFisher Cat. No. 23225) and luciferase activity was expressed as relative light units per µg protein.

2.15.2 Testing of stable reporter cell lines

Stably transfected cell lines were seeded at 40,000 cells/well of a 96-well plate and incubated overnight at 37ºC in 5% CO_2. Cells were then treated with either 4.5 µM HCl or 1 µM PBS solvent control, IGF-1 (50 nM, 24 hrs) or BI 845 (1 µM, 24 hrs) as described in Section 2.15.1. Treated cells were tested with ONE-Glo™ EX Luciferase assay reagent and luminescence was measured on a POLARstar Omega plate reader (BMG Labtech) as described in Section 2.15.1. The protein content of the lysate was then quantified by Pierce BCA protein assay and luciferase activity was expressed as relative light units per µg protein.

2.16 Mass Spectrometric Analysis of Interactome

2.16.1 Preparation of samples

Both WT 22Rv1 and 22Rv1 IGF-1R null CRISPR knockout cell lines were fractionated using NE-PER™ Nuclear and Cytoplasmic Extraction Reagent kit (10 x 15 cm dishes per cell line, >85% confluency) as in Section 2.5. Nuclear extracts were used for IGF-1R co-

IP, using IGF-1Rβ (CST 3027) antibody or IgG antibody as control (CST-2729) as described in Section 2.8. IPs were collected with Protein A agarose beads and after the final wash, 5-10% of the beads were removed and prepared for SDS-PAGE as described in Section 2.3. The remaining beads, representing 90-95% of the precipitate, were then washed with 20 mM HEPES for 5 mins at 4^{o}C with end-over-end rotation, before collection by centrifugation at 3000 x g, 3 mins at 4^{o}C. Supernatant was discarded, and dry beads stored at -80^{o}C until use.

2.16.2 Silver staining and Western blot analysis of co-IPs

From the 5-10% sample of beads retained for analysis, 50% were separated by SDS-PAGE alongside nuclear and whole cell extract input controls and analysed by Western blot as described in Section 2.3. This was to check successful immunoprecipitation of IGF-1R, and fractionation of nuclear and cytoplasmic extracts by detection of fractionation markers Lamin A/C (nuclear marker) and β-tubulin (cytoplasmic marker). The remaining 50% of retained beads were separated using SDS-PAGE and the gel was stained using Pierce™ Silver Stain for Mass Spectrometry (ThermoFisher Cat. No. 24600) for detection of co-immunoprecipitated proteins as per the manufacturer's protocol. Briefly, the SDS-PAGE gel was washed in ultrapure water for 2 x 5 mins, RT on a rocker. The gel was then incubated for 2 x 15 mins at RT on a rocker in Fixing Solution (30% ethanol, 10% acetic acid in ultrapure water). The gel was then washed 2 x 5 mins in ethanol wash (10% ethanol in ultrapure water) and 2 x 5 mins in ultrapure water at RT on a rocker. The wash was removed, and the gel was then incubated with Sensitizer Working Solution (1:500 Sensitizer in ultrapure water, ThermoFisher Cat. No. 24600) and washed with ultrapure water for 2 x 1 min at RT on a rocker. Silver Stain Working Solution (1:100 Silver Stain Enhancer in Silver Stain, ThermoFisher Cat. No. 24600) was then immediately added to the gel for a 5 min incubation at RT on a rocker. The gel was then washed in ultrapure

water for 2 x 20 secs, and Developer Working Solution (1:100 Silver Stain Enhancer in Silver Stain Developer, ThermoFisher Cat. No. 24600) was immediately added and incubated at RT on a rocker until protein bands began to appear, approximately 4 -5 mins. When staining had reached the desired intensity, Developer Working Solution was removed and replaced with Stop Solution (5% acetic acid in ultrapure water). After a brief wash in Stop Solution, the wash was replaced with fresh Stop Solution and incubated for 10 mins at RT on a rocker. An image of the silver-stained gel was then taken for analysis, where bands present were representative of immunoprecipitated proteins.

2.16.3 On-bead digest and processing of samples

Subsequent steps were performed with the assistance of Dr Iolanda Vendrell (Mass Spectrometry Scientist, MRC Oxford Institute for Radiation Oncology, University of Oxford). Samples containing 90-95% of each precipitate, which had been stored at -80ºC, were defrosted, resuspended in 50 µl of 2 M urea in 20 mM HEPES pH 8 and 1.3 µl of DTT (200 mM, final concentration of 5 mM) and incubated for 30 min at RT. After incubation, 5 µl of indole-3-acetic acid (200 mM IAA, final concentration of 20mM. Sigma Aldrich Cat. No. I1149) was added and samples were incubated for a further 30 mins at RT, shielded from light. To reduce the concentration of urea to <2 M to allow trypsin to function correctly, 100 µl of HEPES pH 8 (20 mM) was added to each sample, along with 5 µl of trypsin enzyme (0.2 µg/µl, Promega Cat. No. V5111). Samples were then incubated at 37ºC overnight in a ThermoMixer with agitation (900 rpm). The trypsin digestion reaction was stopped with addition of 1.7 µl of trifluoroacetic acid (TFA, 1% final concentration), samples were then gently vortexed and centrifuged at 2000 x g for 5 mins at 4ºC. Supernatants (tryptic digests) were then transferred to fresh Eppendorf tubes and desalted using SOLA-HRP cartridges (ThermoFisher). Briefly, 500 µl Solvent B (70% acetonitrile (ACN), 0.1% TFA in ultrapure water, SMART Digest Trypsin Kit,

ThermoFisher Cat. No. 60109-103-B) was loaded on to the SOLA-HRP cartridge (SMART Digest Trypsin Kit, ThermoFisher) and eluted dropwise by pressing with a syringe plunger and the flowthrough was then discarded. The cartridge was then washed with 1 ml of Solvent A (2% ACN, 0.1% TFA in ultrapure water, SMART Digest Trypsin Kit, ThermoFisher) which was filtered through the cartridge dropwise by pressing with a syringe plunger and flowthrough discarded. Samples were then diluted 1:1 with Solvent A, loaded 1 ml at a time onto SOLA-HRP cartridge and eluted dropwise by pressing with a syringe plunger. Samples loaded on to the cartridges were then washed with 1 ml Solvent A as above, and then eluted into a clean Eppendorf tube with 2 x 300 µl of Solvent B, eluting dropwise each time as previously. Eluted peptide samples were then dried in a Savant™ SpeedVac™ SPD120 and stored at -20^{o}C until use.

2.16.4 Mass Spectrometry Analysis

Liquid Chromatography tandem mass spectrometry (LC-MS/MS) analysis was performed by Dr Iolanda Vendrell using an Ultimate 3000-Ultra High Performance Liquid Chromatography (UHPLC) system connected to Orbitrap Fusion-Lumos Tribid Mass Spectrometer (ThermoFisher), located at the Proteomics Facility, Target Discovery Institute, Nuffield Department of Medicine Research Building, Oxford.

Initial analysis by Dr Vendrell used Mascot protein identification software (*http://www.matrixscience.com/*) and the Swiss-Prot protein database (*https://www.uniprot.org/*) without defining a species or database for the peptides present using the parameters outlined in

Table **2.3**. Mascot uses a probabilistic scoring algorithm to rate peptides and proteins according to the level of confidence of the identification, and the level of confidence of the identification is based on the application of a sequential series of score cut offs including:

- Ion score cut off (20) – to discard peptides with low score or random matches

- False discovery rate (FDR) – to remove all peptides that fall out the FDR cut off, and each FDR has an assigned p value
- Number of peptides – a protein identity is accepted when at least 2 peptides are identified
- Protein score – degree of confidence in protein identifications

This initial analysis showed that 35% of identified peptides were from the Staphylococcus aureus bacterial species. To account for this contamination, Dr Vendrell used the PEAKS proteomics software (*https://www.bioinfor.com/peaks-studio/*) to analyse the data against the Swiss-Prot Human protein database with the Swiss-Prot Staphylococcus aureus protein database listed as a contaminant (*https://www.uniprot.org/*). Overall, this generated a list of potential nuclear IGF-1R interacting proteins with approximately 350 detected in WT samples only, 175 detected in at least one WT and one IGF-1R null sample and less than 60 detected in either or both IGF-1R null samples only.

Database	SwissProt 2019_11
Taxonomy	Homo sapiens (human) (20368 sequences)
Type of search	MS/MS Ion Search
Enzyme	Trypsin
Fixed modifications	Carbamidomethyl (C)
Variable modifications	Oxidation (M), Deamidation (NQ)
Mass values	Monoisotopic
Protein mass	Unrestricted
Peptide charge	+2, +3, +4
Decoy database	✓
Peptide mass tolerance	10 ppm
Fragment mass tolerance	0.05 Da
Max missed cleavages	1
Instrument type	ESI-Trap (for Lumos)
#C13	+1
Significance threshold p<	0.5
Max. number of families	AUTO
Ions score cut-off	20
FDR	1%
Threshold	Homology threshold

Table 2.3 Mascot Data Search Parameters
Table showing the search parameters used by Dr Vendrell when performing the UniProt database search using Mascot protein identification software to identify peptides present in nuclear IGF-1R IP samples.

2.17 ChIP-sequencing Analysis

Samples generated from ChIP from tissue were sequenced by the Oxford Genomics Centre ((OGC), Nuffield Department of Medicine, University of Oxford) with the help of Dr Simon Engledow at a depth of 40 – 60 million reads. Following processing by OGC, data was analysed in our lab by Dr Avigail Taylor, post-doctoral bioinformatics researcher. ChIP-Seq reads were mapped using Bowtie2 (Langmead and Salzberg, 2012) and aligned to the human reference genome (hg19) from UCSC. Aligned reads were filtered against Beads Only control DNA and analysed using the peak calling software MACS2 (Zhang *et al.*, 2008) to identify IGF-1R and H3K4me1 binding sites using both "Narrow Peak" and "Broad Peak" parameters. Only peaks that passed significance value (p-value < 0.01) were included in downstream analysis. Peaks that were not mapped to a known chromosome were not included. These IGF-1R binding site peaks were then uploaded to, and visualised using, the UCSC genome browser. ChIP-seq data was also analysed by Dr Taylor using LanceOtron peak calling software (Hentges *et al.*, 2021), to identify and visualise enrichment peaks. Peaks were filtered to include only those with a LanceOtron peak score of $\geq$0.8.

2.18 Statistical Analysis

Data were analysed and processed using Office Excel 2017 (Microsoft) or GraphPad Prism 8 (GraphPad Software Inc, USA). For testing of differences between two treatment groups, a paired or unpaired Student t-test was used as appropriate, and for differences between three or more treatment groups a one-way or two-way ANOVA test was used as appropriate. A p-value for significance was calculated in all cases, and $p<0.05$ was considered significant.

3 Chapter III: Detection of IGF-1Rα-subunit in the nucleus

3.1 Introduction

As discussed in Section 1.6, previous work from our lab and others has shown the presence of IGF-1R in the nucleus of a range of different cell types. While both full length IGF-1Rα- and β-subunits have been detected in the nucleus (Aleksic *et al.*, 2010), most of the previous work to elucidate the function of nuclear IGF-1R has been done via detection of the β-subunit only. This includes detection of interaction with chromatin (Sehat *et al.*, 2010; Wu, Zhu and Robertson, 2012; Warsito *et al.*, 2016; Aleksic *et al.*, 2018), with other nuclear proteins and transcription factors (Warsito *et al.*, 2012; Waraky *et al.*, 2017; Aleksic *et al.*, 2018; Solomon-Zemler *et al.*, 2019) and with proteins involved in the translocation of IGF-1R to the nucleus (Sehat *et al.*, 2010; Packham *et al.*, 2014). Therefore, we decided to further investigate whether the IGF-1Rα-subunit is present in the nucleus, and if so, whether the receptor translocates from the cell surface as a complex of both its α- and β-subunits, and whether the α-subunit is involved in recruitment to nuclear IGF-1R chromatin binding sites. This is analogous to the recent work shown with the insulin receptor (Hancock *et al.*, 2019). Determination of the role of IGF-1Rα in the nucleus will help to further elucidate the role of nuclear IGF-1R and may lead to discovery of novel interactions or functions that could act as potential treatment targets.

3.2 Results

3.2.1 Testing for the presence of cell surface originating IGF-1Rα and β and their interaction in the nucleus

Initial experiments tested for the presence of IGF-1Rα in the nucleus of DU145 and 22Rv1 prostate cancer cell lines. Following starvation, cells were treated with HCl solvent control

(4.5 μM) or IGF-1 (50 nM) and fractionated into nuclear and cytoplasmic fractions. These fractions were then probed for the presence of IGF-1Rα- and β-subunits. Both subunits, as expected, were detected in all cytoplasmic fractions and whole cell extract (WCE) control samples. The presence of both subunits was also detectable in the nucleus of both cell lines, in starved and IGF-1 treated conditions, however no increase in levels of either subunit in the nucleus was seen on treatment with IGF-1 (Figure **3.1**). However, this may be due to the sensitivity of the antibodies used for Western blotting, or the non-linearity of the technique.

It is widely assumed that IGF-1R undergoes ligand stimulation at the cell surface before translocation to the nucleus (Aleksic *et al.*, 2010, 2018; Sehat *et al.*, 2010; Sarfstein *et al.*, 2012; Packham *et al.*, 2014), but this has never been directly tested. Given that the outer nuclear membrane is in continuity with the endoplasmic reticulum membrane, it has been proposed that some nuclear proteins could undergo nuclear import via direct lateral diffusion, the rapid process of lateral movement of proteins within a membrane (Ungricht *et al.*, 2015).

To determine if IGF-1R subunits detected in the nucleus originate from the plasma membrane at the cell surface, DU145 and 22Rv1 cells underwent biotinylation of cell surface proteins followed by ligand stimulation and subcellular fractionation. Biotinylated proteins were isolated from nuclear extract and probed by Western blot for presence of IGF-1Rα- and β-subunits. The biotinylation labelling reagent used is membrane impermeable and labels proteins via formation of an amide bond between the primary amine of lysine residues and the biotin label (*Pierce Cell Surface Protein Biotinylation and Isolation Kit User Guide*, 2020). The IGF-1Rα-subunit is completely extracellular (Figure **3.2**a) (Ullrich *et al.*, 1986; Adams *et al.*, 2000) and contains multiple primary amine residues that should undergo labelling in the presence of the external biotinylation reagent.

The IGF-1Rβ-subunit is almost completely intracellular, although does contain a small extracellular domain (Figure **3.2**a) that contains multiple lysine residues within the fibronectin type III (FnIII)-2b and -3 domains at Lys-782, -821, -838, -857 and -897 (Ullrich *et al.*, 1986; Le Roith *et al.*, 1995; Adams *et al.*, 2000; Li *et al.*, 2019). Therefore, both subunits were predicted to undergo biotinylation.

Both subunits could be detected in nuclear, cytoplasmic and WCE protein input controls in both cell lines. Furthermore, both the α- and β-subunits were also detectable in nuclear extracts from cells that had undergone cell surface protein biotinylation. Neither subunit could be detected in control extracts that had undergone incubation with PBS rather than biotinylation reagent (Figure **3.2**b and c). As a positive control, nuclear extracts were also shown to contain cell surface biotinylated EGFR, a protein well characterised to translocate from the cell surface to the nucleus (S. Lin *et al.*, 2001; Bryant and Stow, 2005; Wang and Hung, 2009). As a negative control, there was no detection of biotinylated lamin and, in 22Rv1, AR, which are both nuclear proteins that do not traffic from the cell surface. Given that only cell surface proteins had been exposed to biotinylation, the absence of both IGF-1R subunits in control samples and presence in nuclear extracts from surface biotin-labelled cells confirms that IGF-1R subunits detectable in the nucleus have translocated from the cell surface.

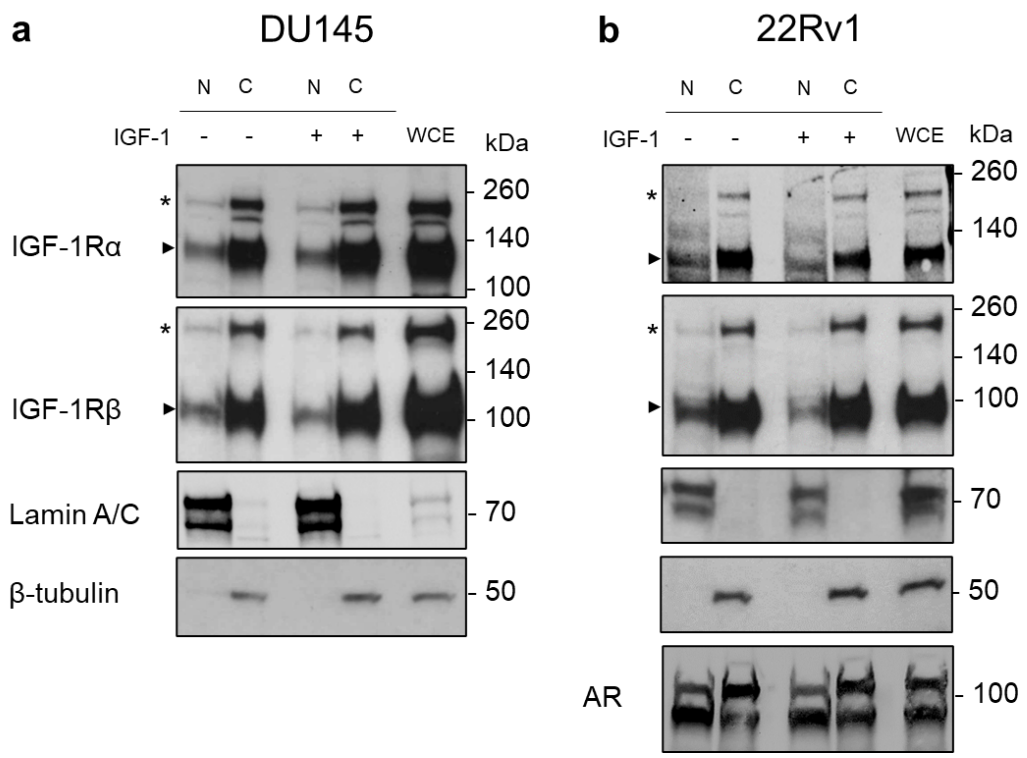


Figure 3.1 IGF-1Rα- and β-subunits are present in the nucleus of DU145 and 22Rv1 cells

Western blots showing detection of both IGF-1Rα- and β-subunits in the nucleus of DU145 (**a**) and 22Rv1 (**b**) cells. Cells were serum-starved for 24 hrs, treated with solvent control (4.5 µM HCl) or IGF-1 (50 nM) for 20 min before fractionation. Cells were then fractionated into nuclear (N) and cytoplasmic (C) fractions and analysed alongside WCE control. Lysates were probed using antibody for IGF-1Rα and IGF-1Rβ. Successful fractionation of nuclear and cytoplasmic extracts was determined by detection of fractionation markers Lamin A/C (nuclear marker) and β-tubulin (cytoplasmic marker). Detection of IGF-1Rα- and β-subunits in the nucleus was not dependent on IGF-1 treatment. All western blots shown are representative of 3 independent biological repeats. Arrowheads: corresponding IGF-1Rα- and β-subunits. Asterisks: 220 kDa IGF-1R proreceptor. (This figure was previously generated by me and published in (Mills *et al.*, 2021). It is reused here under the Creative Commons licence CC BY 4.0 (*https://creativecommons.org/licenses/by/4.0/legalcode*)).

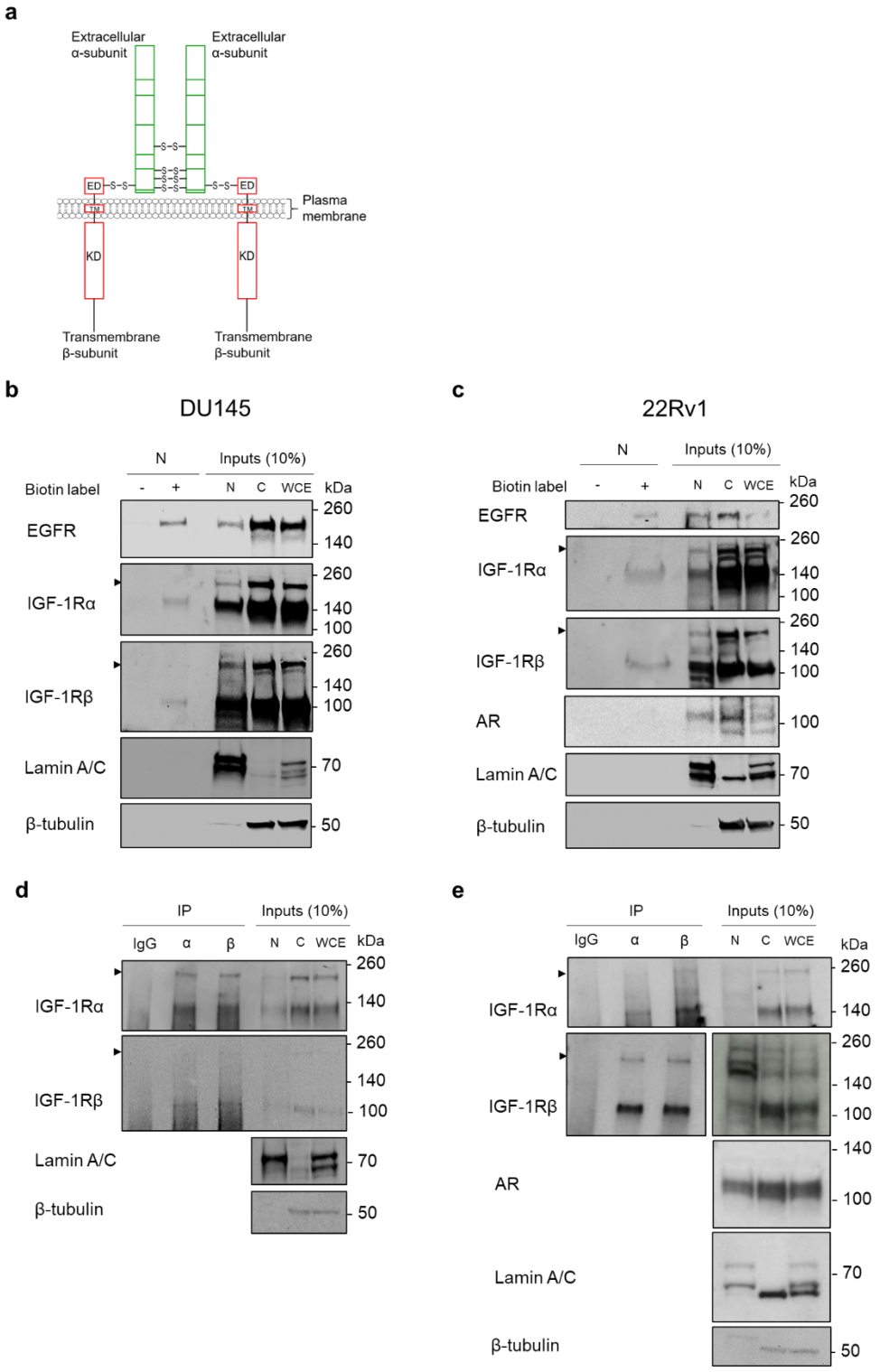


Figure 3.2 Nuclear IGF-1Rα- and β-subunits originate from the cell surface and interact in the nucleus

a Structure of IGF-1R at the cell membrane (adapted from (Adams *et al.*, 2000)), showing extracellular α-subunit and the extracellular portion of the β-subunit that can undergo biotinylation **b, c** DU145 (**b**) and 22Rv1 (**c**) cells were incubated for 10 mins with PBS control or EZ-Link™ Sulfo-NHS-SS-Biotin label, to label cell surface proteins, and then treated with RPMI-1640 medium supplemented with 10% FBS for 20 mins. Cells were fractionated into nuclear (N) and cytoplasmic (C) fractions, and biotinylated proteins were isolated from these fractions and

analysed by Western blot alongside N, C and WCE input controls. Lysates were probed using antibody for IGF-1Rα and IGF-1Rβ. Detection of cell surface biotinylated EGFR in nuclear fractions acts as a positive control and absence of cell surface biotinylated lamin and/or AR acts as a negative control. **d, e** DU145 (**d**) and 22Rv1 (**e**) cells grown in normal culture medium were fractionated into nuclear (N) and cytoplasmic (C) fractions and nuclear lysates were immunoprecipitated with antibody for IGF-1Rα, IGF-1Rβ or IgG control. IPs were analysed by Western blot alongside N, C and WCE input controls (10% of IP input) and were probed using antibody for IGF-1Rα and IGF-1Rβ. In all cases, Western blots shown are representative of 3 independent biological repeats and successful fractionation of nuclear and cytoplasmic extracts was determined by detection of fractionation markers Lamin A/C (nuclear marker) and β-tubulin (cytoplasmic marker). Arrowheads: 220 kDa IGF-1R proreceptor. (This figure was previously generated by me and published in (Mills *et al.*, 2021). It is reused here under the Creative Commons licence CC BY 4.0 (*https://creativecommons.org/licenses/by/4.0/legalcode*)).

As previously outlined in Section 1.2.1, IGF-1R is present at the cell surface as a heterotetrameric complex of two α- and two β-subunits (Figure **3.2**a). Following detection of the IGF-1R subunits in the nucleus that originated from the cell surface, experiments were then undertaken to investigate whether the α- and β-subunits retain an interaction following internalisation and translocation.

Following cellular fractionation of DU145 and 22Rv1 cells, α- or β-subunits were immunoprecipitated from nuclear extracts. As before, both subunits were detected in the nuclear, cytoplasmic and WCE protein input controls. Following immunoprecipitation from nuclear extract, the α-subunit of IGF-1R could be detected in both DU145 and 22Rv1 immunoprecipitates. The IGF-1Rβ-subunit could also clearly be detected following co-immunoprecipitation using α-subunit antibody. Reciprocal β-subunit immunoprecipitation also detected both IGF-1Rα- and β-subunits in DU145 and 22Rv1 nuclear extracts (Figure **3.2**d and e). These experiments showed that IGF-1Rα- and β-subunits maintain an interaction in the nucleus of prostate cancer cells.

Overall, these results suggest the presence of nuclear α-β complexes that have originated from the cell surface. To further support these results, experiments were then planned to visualise nuclear IGF-1R by IF, to test for any IGF induced changes in levels of nuclear

IGF-1R, and for co-localisation of the two subunits in the nucleus following detection of their interaction in the nucleus.

3.2.2 Immunofluorescence detection of nuclear IGF-1Rα- and β-subunits

Previous IF work has shown detection of nuclear IGF-1Rβ in DU145 prostate cancer cells, with levels of nuclear IGF-1R shown to be responsive to both ligand stimulation and IGF-1R inhibition. In these current experiments, IF antibody for IGF-1Rα was optimised with the aim of performing a proximity ligation assay (PLA) to further test for co-localisation of the IGF-1Rα- and β-subunits in the nucleus, and support the results seen in Figure **3.2**d and e. PLA is performed via detection of two distinct antigens with primary antibodies of different species, followed by addition of PLA probe secondary antibodies that have a short specific DNA strand attached to them. If the two antigens are within close proximity of each other, the DNA strands from the PLA probes are joined by hybridizing connector oligos and form a closed, circle DNA template that is required for rolling-circle amplification. The circle DNA template attached to the PLA probes then acts as a primer for DNA polymerase which results in several-hundredfold amplification of the DNA circle. Fluorescent-labelled complementary oligonucleotide probes are then added which bind to the amplified DNA and can be visualised as distinct spots and quantified by fluorescent microscopy (*https://www.sigmaaldrich.com/technical-documents/protocols/biology/how-pla-works.html*, Sigma Aldrich, 2020). These so-called PLA signals should therefore only be visible when primary antibody antigen targets are co-localised or in close proximity with each other. This method has previously been used by others to show co-localisation of IGF-1Rβ-subunit with EEA-1 (Packham *et al.*, 2014), E-cadherin (Nagle *et al.*, 2018), histone H3 (Warsito *et al.*, 2016) and LEF1 transcription factor (Warsito *et al.*, 2012).

A selection of IGF-1Rα-subunit antibodies were tested at a range of different primary and secondary antibody dilutions and are listed in Table **3.1** The IGF-1Rα antibody (24-60) (MA5-13817, ThermoFisher), was thought to be the most specific of the antibodies tested due to the highly reduced signal in IGF-1R null CRISPR knockout DU145 cells (previously generated in our lab by Dr Eliot Osher) versus WT DU145 cells, although some non-specific background staining was present in the IGF-1R null cell line (Figure **3.3**). This antibody was also of a different species origin (mouse) to that of the IGF-1Rβ antibody (CST 9750, rabbit), previously optimised and used in our lab for IF, as required for PLA. IGF-1Rα antibody ((24-60), MA5-13817) was therefore tested in IGF-1 stimulation and inhibition experiments to further optimise antibody dilutions and test specificity.

IGF-1Rα primary antibody	Dilution of primary antibody tested	Dilution of secondary antibody tested
(24-60) MA5-13817	1:50, 1:250, 1:500	1:1000 and 1:2000
αIR-3	1:250, 1:500, 1:1000	1:1000 and 1:2000
sc-712	1:250, 1:500, 1:1000	1:1000 and 1:2000

Table 3.1 List of the IGF-1Rα IF primary antibodies used and the various dilutions at which they were tested

List of the IGF-1Rα primary antibodies tested in IF experiments including (24-60) (MA5-13817, monoclonal, mouse, ThermoFisher), αIR-3 (monoclonal, mouse, Abcam (ab16890)) and sc-717 (polyclonal, rabbit, Santa Cruz). Primary antibodies were tested at the indicated dilutions and in all cases were counterstained with secondary antibody diluted at both 1:1000 and 1:2000 in separate experiments. The optimised primary antibody selected was (24-60) MA5-13817 diluted at 1:250, with secondary antibody diluted at 1:2000.

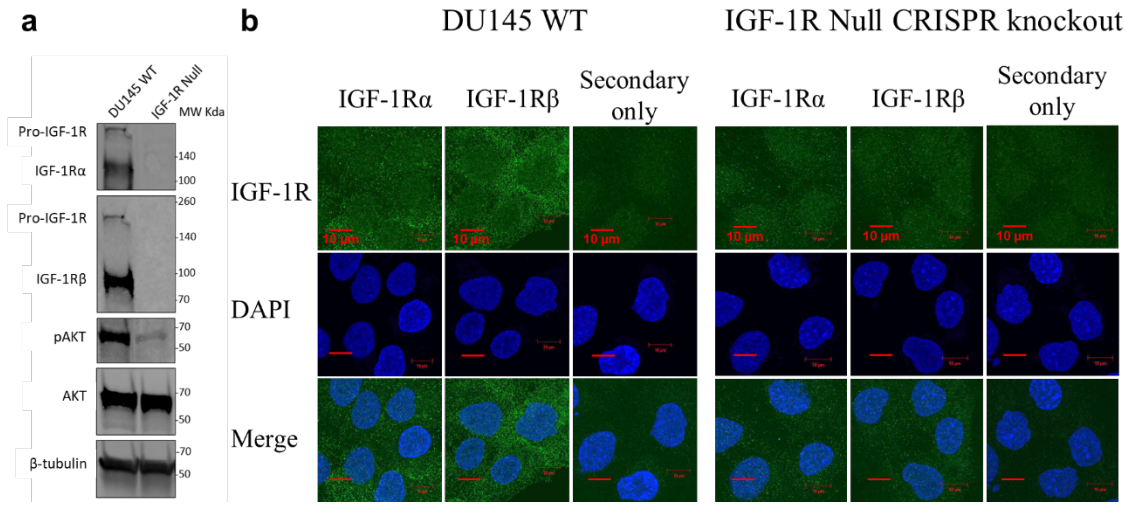


Figure 3.3 Antibodies for IGF-1Rα- and β-subunits give specific immunofluorescent staining

a Western blot showing lack of IGF-1R receptor and reduced pAKT in IGF-1R null CRISPR knockout cell line vs WT DU145 positive control. Lysates were probed using antibodies for IGF-1Rα, IGF-1Rβ, pAKT, AKT and β-tubulin loading control. IGF-1R null CRISPR knockout cell lines were previously generated in our lab by Dr Eliot Osher. **b** IF of IGF-1Rα and β (green) and nuclei stained with DAPI in WT and IGF-1R null DU145 cells. Cells were fixed and incubated overnight with primary antibody for either IGF-1Rα ((24-60), MA5-13817) at 1:250, IGF-1Rβ at 1:500 or blocking solution only (secondary antibody only control). Visualisation was performed on a Zeiss LSM 780 Confocal microscope. Scale bar (red) 10 µm.

To further test the specificity of IGF-1Rα IF staining, and to test the optimisation of primary antibody dilution before performing PLA, experiments were performed to measure the levels of nuclear IGF-1Rα in response to IGF-1 stimulation and IGF-1R tyrosine kinase inhibition. Our lab previously used immunofluorescence to assess changes in nuclear IGF-1R subcellular localisation for both α- and β- subunits, showing an increase in nuclear levels of both subunits in response to IGF-1 treatment. However, we previously tested the response of only nuclear IGF-1Rβ-subunit to IGF-1R kinase inhibition, showing a decrease in nuclear IGF-1Rβ alongside a concurrent increase in IGF-1Rβ at the plasma membrane in response to the inhibitor (Aleksic *et al.*, 2010). In these current experiments, IF staining confirmed detection of IGF-1R in the nucleus with evidence that both IGF-1Rα- and IGF-1Rβ-subunits were IGF-1 responsive, again showing a significant increase of both subunits in the nucleus upon IGF-1 treatment (Figure **3.4**a) as seen previously (Aleksic *et al.*, 2010). Further experiments also found evidence of a significant decrease in nuclear IGF-1Rα-subunit on treatment with IGF-1R tyrosine kinase inhibitor BMS-754807 alongside accumulation of IGF-1R on the plasma membrane for the first time (Figure **3.4**b), as previously seen with the IGF-1Rβ-subunit (Aleksic *et al.*, 2010) and again shown in experiments here (Figure **3.4**b).

While quantification of nuclear IGF-1R showed significant alterations in both experiments, the staining for IGF-1Rα appears to contain some non-specificity due to the similar, ubiquitous staining seen in both experimental conditions (Figure **3.4**). This contrasts with the visible difference in staining localisation of IGF-1Rβ seen with both experimental conditions (Figure **3.4**). This staining pattern for IGF-1Rα was consistent throughout the range of antibody dilutions tested (Table **3.1**). Primary antibodies for PLA are usually required to be highly specific and optimised to provide credible results, so it was therefore decided that the primary antibodies tested here would not be suitable to proceed with PLA

experiments to determine co-localisation of IGF-1Rα- and β-subunits in the nucleus. However, following detection of nuclear IGF-1Rα both by Western blot and IF, experiments were then performed to test if the α-subunit is involved in nuclear IGF-1R function, namely, recruitment of IGF-1R to chromatin.

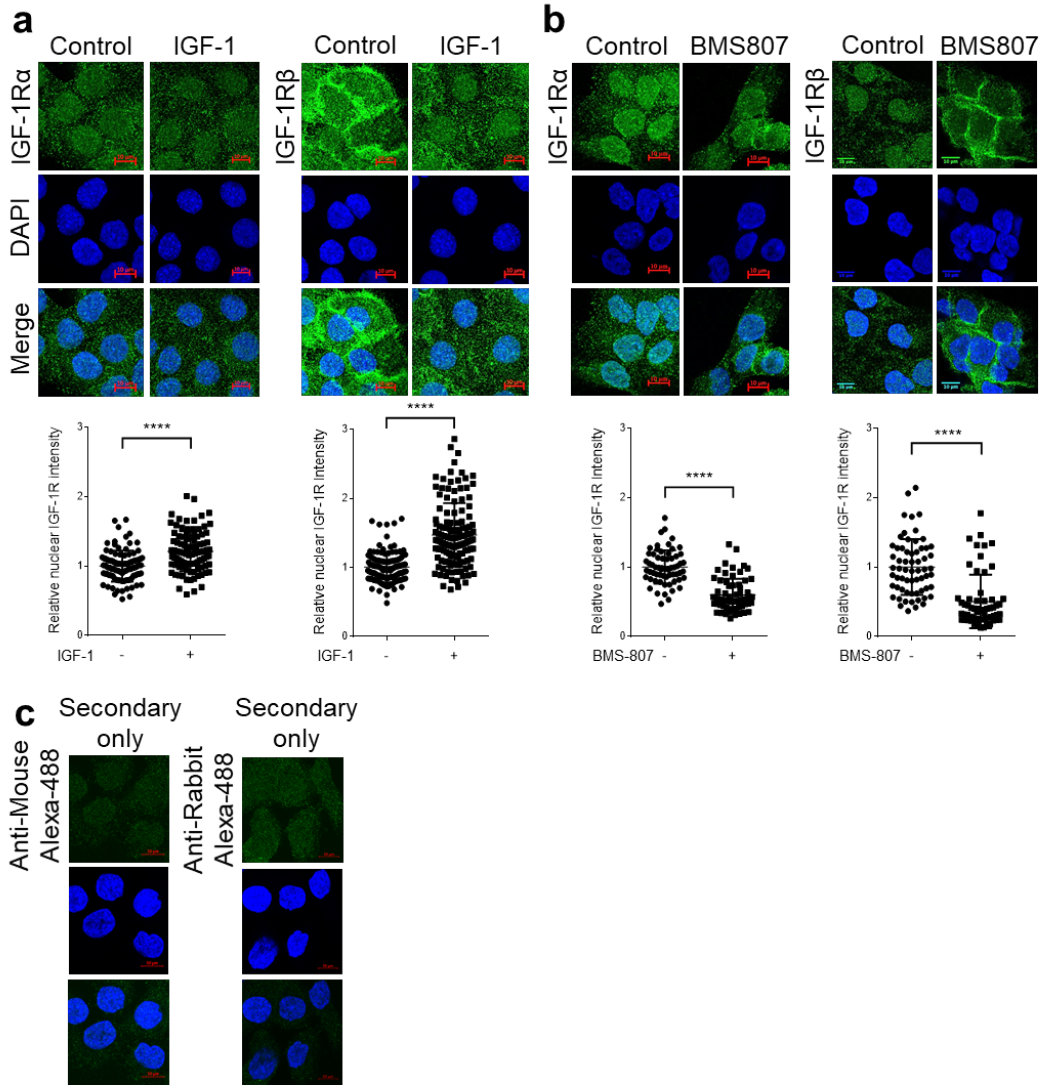


Figure 3.4 Changes in levels of nuclear IGF-1Rα- and β-subunits are detectable by immunofluorescence

a, b Images showing immunofluorescence staining of IGF-1Rα and IGF-1Rβ in DU145 cells. DU145 cells were serum-starved for 24 hrs, treated with solvent (4.5 µM HCl) or IGF-1 (50 nM) for 20 min (**a**) or incubated with solvent (0.1% DMSO) or IGF-1R inhibitor BMS-754807 (100 nM) for 6 hr at 37°C (**b**) and processed for immunofluorescence staining. Graphs: mean ± SD nuclear IGF-1Rα- and β-subunits (n≥ 30 cells per condition across n=3 biological repeats) and data were analysed by unpaired student's t test (*p<0.05; **p<0.005; ***p<0.001; ****p< 0.0001). **c** Images showing cultured DU145 cells stained with Alexa-488 secondary antibodies as used in **a** and **b** in the absence of primary antibody. These images represent a negative control for immunofluorescence staining and demonstrate the specificity of the IGF-1Rα- and β-subunit signals shown in **a** and **b**. In all cases visualisation was performed on a Zeiss LSM 780 Confocal microscope (Scale bars 10 µm) and image analysis was performed using ImageJ software. (This figure was previously generated by me and published in (Mills *et al.*, 2021). It is reused here under the Creative Commons licence CC BY 4.0 (*https://creativecommons.org/licenses/by/4.0/legalcode*)).

3.2.3 Detection of recruitment of IGF-1Rα to known IGF-1R chromatin binding regions

Previous work in our lab using ChIP-seq in DU145 cells showed IGF-1Rβ-subunit recruitment to regulatory regions of chromatin. At most of these sites, IGF-1Rβ enrichment was coincident with recruitment of RNAPolII, and direct interaction between IGF-1Rβ and RNAPolII was also detected. Both IGF-1Rβ recruitment to chromatin and this RNAPolII interaction were shown to be IGF-dependent (Aleksic *et al.*, 2018). Having detected an interaction between nuclear IGF-1Rα- and β-subunits (Figure **3.2**d and e), experiments to investigate whether the IGF-1Rα-subunit is also involved in recruitment to IGF-1Rβ-subunit binding sites were undertaken. ChIP-qPCR was performed for detection of recruitment of the α-subunit to two regions previously identified as sites of IGF-1Rβ enrichment (Aleksic *et al.*, 2018). One is the promoter of the *JUN* oncogene, which our lab previously validated and confirmed to contribute to prostate cancer cell growth and motility (Aleksic *et al.*, 2018), and the other an intergenic region of chromosome 17 (IntChr17) that is enriched for H3K27 acetylation, suggesting putative enhancer function (Calo and Wysocka, 2013), but not RNAPolII recruitment (Figure **3.5**a**)**,.

As previously shown by our lab (Aleksic *et al.*, 2018), ChIP-qPCR in DU145 cells was able to detect significant recruitment of IGF-1Rβ to the *JUN* promoter (Figure **3.5**b). These current experiments also showed recruitment of IGF-1Rβ to IntChr17 by ChIP-qPCR, validating this previous ChIP-seq finding for the first time (Figure **3.5**c). At the *JUN* promoter region both IGF-1Rα- and β-subunits showed significant increase in recruitment versus IgG negative control, however α-subunit recruitment was found to be at a significantly lower level than that of the β-subunit (Figure **3.5**b). In contrast, at the IntChr17 binding site, both subunits showed significant increase in recruitment versus IgG

negative control at approximately equal levels (Figure **3.5**c). Overall, these results suggest that the IGF-1Rα-subunit is also involved in recruitment of IGF-1R to chromatin.

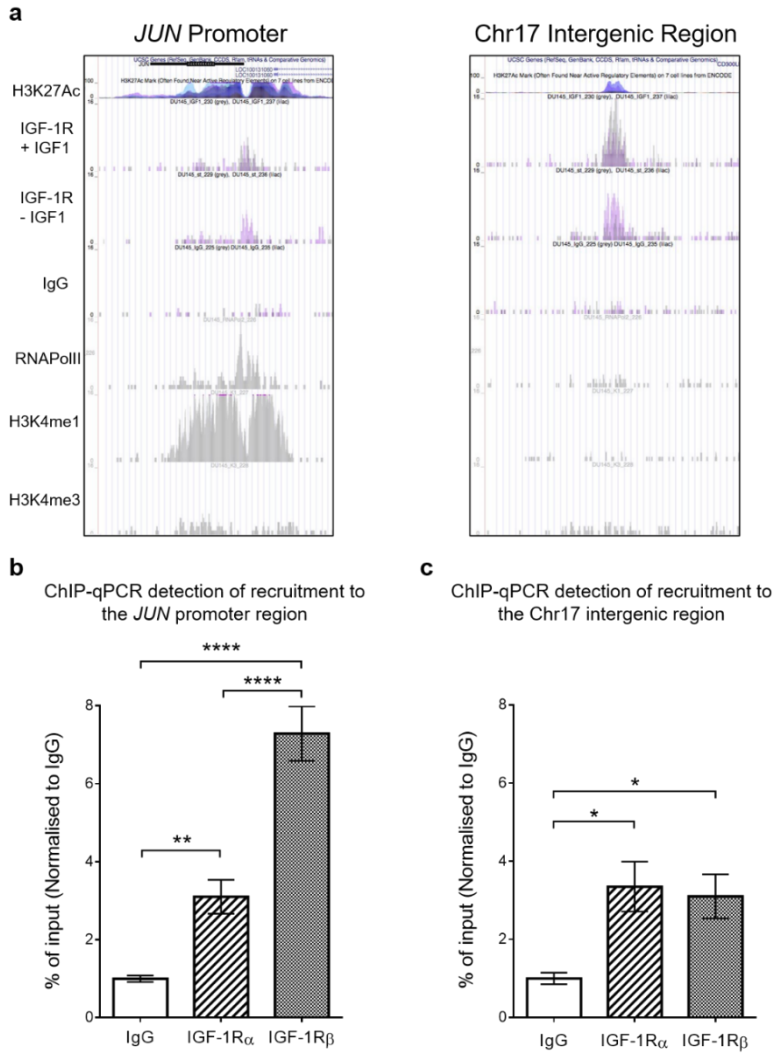


Figure 3.5 Recruitment of IGF-1Rα is detectable at IGF-1Rβ DNA binding sites
a Images from the UCSC genome browser of previously obtained ChIP-seq data showing IGF-1R binding peaks that denote recruitment of RNAPolII and IGF-1Rβ to the *JUN* promoter and IntChr17 (Aleksic *et al.*, 2018). **b-c** Quantification of recruitment of IGF-1Rα or IGF-1Rβ vs IgG negative control to IGF-1Rβ binding regions, detected by ChIP-qPCR. Results represent mean ± SEM of triplicate independent experiments, each with 3 technical replicates (p*<0.05, p**<0.005, p**** < 0.0001, Tukey's multiple comparisons test). Recruitment of both IGF-1Rα and IGF-1Rβ vs IgG was detected at the JUN promoter (**b**) and putative IntChr17 enhancer (**c).** (This figure was previously generated by me and published in (Mills *et al.*, 2021). It is reused here under the Creative Commons licence CC BY 4.0 (*https://creativecommons.org/licenses/by/4.0/legalcode*)).

3.3 Conclusion

These experiments confirmed the presence of IGF-1Rα- and β-subunits in the nucleus of 22Rv1 prostate cancer cells, as previously shown in our lab in DU145 cells (Aleksic *et al.*, 2010). Western blot analysis showed detection of both IGF-1Rα- and β-subunits regardless of the presence of IGF-1 ligand stimulation (Figure **3.1**). However, IF staining showed significant changes in nuclear IGF-1R levels in response to IGF-1 stimulation and IGF-1R inhibition (Figure **3.4**).

Cell surface protein biotinylation experiments directly confirmed for the first time that IGF-1Rs detectable in the nucleus originate from the plasma membrane (Figure **3.2**), in line with the widely accepted hypothesis in which the receptor undergoes translocation to the nucleus following ligand stimulation at the cell surface. IP of the IGF-1R subunits from nuclear extract also showed that the α- and β-subunits of the receptor interact within the nucleus (Figure **3.2**). This finding could suggest that IGF-1R translocates as an $\alpha_2\beta_2$ holoreceptor.

As discussed in Section 1.5, the majority of RTKs that undergo nuclear import, including fibroblast growth factor and EGFR family members, translocate after juxta-membrane proteolytic release of cytoplasmic domain or nuclear import of full-length receptor monomers (S. Lin *et al.*, 2001; Bryant and Stow, 2005; Wang and Hung, 2009). In contrast, IGF-1R and the closely related INSR are heterotetramers in which the $\alpha_2\beta_2$ structure is maintained by disulphide bonds (Adams *et al.*, 2000). Nuclear INSR was reported originally by (Goldfine *et al.*, 1977; Podlecki *et al.*, 1987) and recently by (Hancock *et al.*, 2019), who detected INSR interaction with RNAPolII, consistent with previous data from our lab for IGF-1R (Aleksic *et al.*, 2018), and showed by immunogold electron microscopy that a subset of nuclear INSRα- and β-chains were sufficiently close to each other for direct interaction (Hancock *et al.*, 2019). The co-IP experiments in this

thesis (Figure **3.2**), imply retention of disulphide-bonds between IGF-1Rα- and β-subunits during trafficking from the endosomal compartment via the cytosol to the nucleus. The cytosol is a mildly reducing environment in which most thiols are in a reduced state but which can maintain disulphide-bonds in proteins transferred from other cellular compartments (Sevier and Kaiser, 2002). IGF-1R and INSR contain similar numbers of alpha and beta cysteines and mild INSR reduction is known to cleave a small number of disulphides, generating disulphide-linked αβ monomers that can still bind ligand, while more vigorous INSR reduction generates free alpha and beta chains (Adams *et al.*, 2000). The detection here of the interaction between IGF-1Rα- and β-subunits in nuclear extract implies existence of similar IGF-1R αβ dimer or $\alpha_2\beta_2$ holoreceptor complexes.

Unlike in fractionation and Western blotting experiments, IF staining showed a significant, IGF-1 dependent, increase in levels of both subunits of nuclear IGF-1R in DU145 cells, and a reciprocal significant decrease on inhibition of IGF-1R (Figure **3.4**). However, staining for IGF-1Rα did not show sufficient specificity to be used in PLA experiments to further confirm co-localisation of the two subunits in the nucleus.

Time permitting, further optimisation experiments could have been done for PLA for IGF-1Rα- and β-subunits. As the antibodies for each target must be of different species origin, different IGF-1Rβ-subunit antibodies could be tested that do not originate from rabbit. This would then allow for testing of further IGF-1Rα-subunit primary antibodies that do not have to be of mouse origin. Optimisation of these antibodies may provide staining of better specificity for the α-subunit than that seen here, and that may be stringent enough to perform PLA experiments. Successful PLA experiments may then provide further evidence to support the co-IP results showing interaction of nuclear IGF-1Rα- and β-subunits (Figure **3.2**d and e).

The IF experiments discussed above were all performed in DU145 cells. Parallel IF staining experiments in 22Rv1 cells proved to be unsuccessful due to reduced cell adherence causing rounding of the cells. As a result, the images obtained for 22Rv1 cells showed only a small number of cells had successfully undergone fixation, staining, and mounting. The small number that could be visualised had not flattened, and therefore levels of nuclear IGF-1R could not be accurately quantified. Future IF staining for this cell line could use Poly-L-Lysine or Matrigel coated coverslips to increase the adherence and flattening of 22Rv1 cells potentially allowing for successful visualisation and quantification of nuclear IGF-1R. This would allow for parallel IGF-stimulation and kinase inhibition experiments as shown in DU145 cells, and the potential to carry out PLA experiments.

The complete mechanism of translocation for IGF-1R has not currently been fully elucidated, so it is currently unclear how the receptor would retain the disulphide bonds between α- and β-subunits during nuclear translocation. It is possible that, following ligand stimulation, the whole receptor undergoes internalisation via clathrin-dependent endocytosis into a vesicle, where the disulphide bonds of the receptor are protected from the reducing environment of the cytosol. The whole receptor is then trafficked to the nucleus inside this vesicle, therefore preventing reduction of the disulphide bonds between IGF-1R subunits and retaining its structure. As indicated by Step 4 of Figure **3.6**, which summarises the possible translocation mechanism of IGF-1R, the receptor is currently presumed to undergo endosomal escape into the cytosol. However, detection of nuclear IGF-1Rα-β complexes in this thesis now suggests that the subunits retain their disulphide bonds during transit through the cytosol. With time permitting, the method by which this occurs, and whether the whole trafficking process occurs within a vesicle, could have been further investigated by electron microscopy, testing for the presence of IGF-1Rα- and β-

subunits within vesicles undergoing translocation, as well as testing for the presence of membrane components within the nucleus.

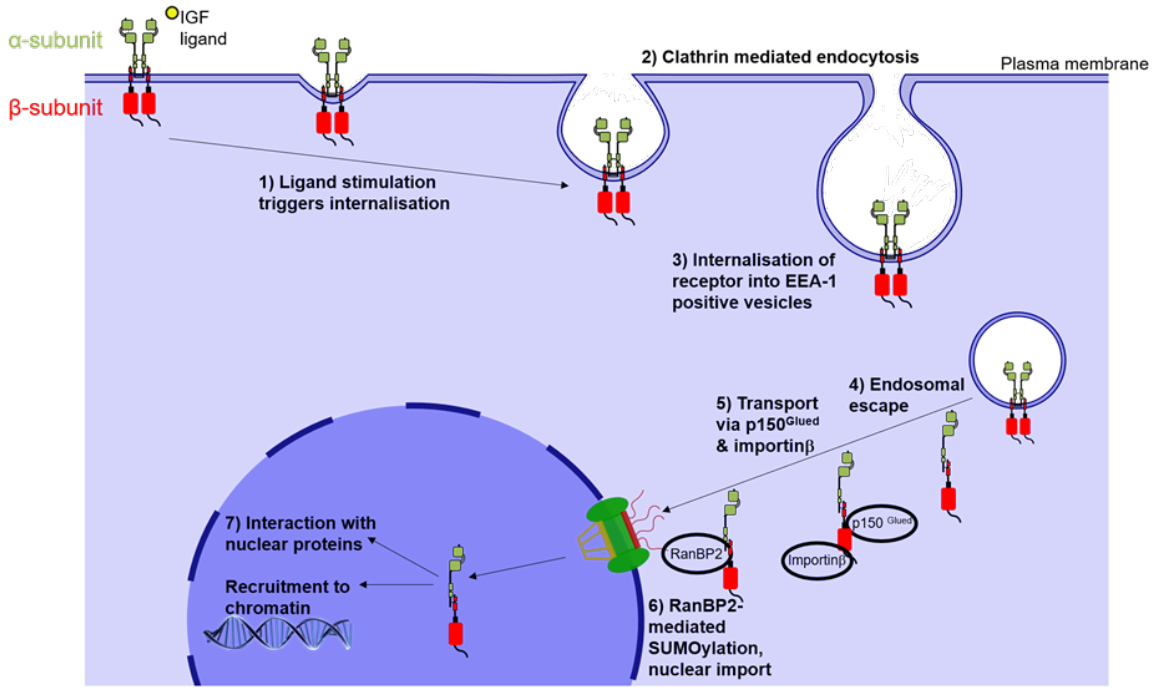


Figure 3.6 Model of potential nuclear translocation mechanism of IGF-1R in its holoreceptor form
1 – 3. Ligand stimulation of IGF-1R triggers clathrin-mediated endocytosis of the receptor into EEA-1 positive vesicles (Aleksic *et al.*, 2010; Packham *et al.*, 2014). **4**. IGF-1R is presumed to undergo endosomal escape into the cytosol. Detection of nuclear IGF-1Rα-β complexes in this thesis suggests retention of disulphide bonded-subunits during transit through the cytosol. **5 – 6**. Cytosolic IGF-1R interacts with $p150^{Glued}$ and is transported to the nucleus via microtubule-dependent dynactin activity where it interacts with importin-β followed by RanBP2. RanBP2 E3 SUMO ligase catalyses the tri-SUMOylation of 3 conserved lysine residues of the β-subunit (Sehat *et al.*, 2010; Packham *et al.*, 2014). **6.** SUMOylation mediates IGF-1R translocation across the nuclear pore complex and into the nucleus. **7.** Nuclear IGF-1R interacts with nuclear proteins including PCNA, nucleolar protein NOM1, transcriptional regulators including TCF/LEF1, Histone H3, RNAPolII, GATA2 and with regulatory regions of chromatin to influence gene transcription and protein function (Warsito *et al.*, 2012, 2016; Waraky *et al.*, 2017; Aleksic *et al.*, 2018; Solomon-Zemler *et al.*, 2019). (This figure was previously generated by me and published in (Mills *et al.*, 2021). It is reused here under the Creative Commons licence CC BY 4.0 (*https://creativecommons.org/licenses/by/4.0/legalcode*)).

Finally, recruitment of IGF-1Rα to known IGF-1Rβ-subunit chromatin binding regions was also detected in these experiments. This mirrors the closely related INSR, which shares significant sequence homology, similar structure and overlapping functions with IGF-1R (Ullrich *et al.*, 1986; Adams *et al.*, 2000; Brzozowski *et al.*, 2002; De Meyts and Whittaker, 2002). As previously mentioned, recent work reported similar levels of

recruitment of both α- and β- INSR subunits to INSR chromatin binding sites validated by ChIP-qPCR (Hancock *et al.*, 2019). In the experiments carried out here, recruitment of both IGF-1R subunits to IntChr17 was found to be at similar levels, however recruitment of IGF-1Rβ-subunit was found to be at a higher level than IGF-1Rα-subunit at the *JUN* promoter region (Figure **3.5**b and c). It is worth noting that RNAPolII is not recruited to the IntChr17 region tested here, in contrast to the RNAPolII recruitment seen at the *JUN* promoter region (Aleksic *et al.*, 2018) (Figure **3.5**a). As previously mentioned, our lab has shown direct interaction of RNAPolII and IGF-1R (Aleksic *et al.*, 2018), therefore it is possible that this interaction is disrupting immunoprecipitation and detection of the α-subunit at the *JUN* promoter region, resulting in differing levels of detected recruitment for the α- and β-subunits at this site. These differences could also be due to technical factors such as different efficiency of antibodies for immunoprecipitation from chromatin, masking of DNA-interacting domain by antibody binding, or interaction of the α-subunit with chromatin indirectly via the β-subunit. Further experiments could test some of these factors by using Protein G agarose beads in IGF-1Rα ChIP as these are optimised for antibodies of mouse origin (Fishman and Berg, 2019), as well as testing a range of other IGF-1Rα antibodies and comparing detected recruitment levels. Further experiments are needed to validate IGF-1Rα recruitment to other previously identified IGF-1Rβ chromatin binding sites, as well as ChIP-seq for the α-subunit itself to potentially identify any further IGF-1R chromatin binding sites that may not yet have been identified via detection of recruitment of the β-subunit.

Future work is now needed to determine what further nuclear IGF-1R chromatin binding sites and protein interactions can be detected via the α-subunit that may further elucidate the role of nuclear IGF-1R in cancer progression.

4 Chapter IV: Assessment of assays for use in high throughput screening for inhibitors of nuclear IGF-1R

4.1 Introduction

As previously discussed in Section 1.6.4, nuclear IGF-1R has been found to be associated with advanced tumour stage, treatment resistance and worse clinical outcomes in a range of cancer types (Aleksic *et al.*, 2010, 2018; van Gaal *et al.*, 2013; Codony-servat *et al.*, 2017), as well as being rarely found in benign tissue (Aleksic *et al.*, 2010, 2018). Therefore, it is possible that nuclear IGF-1R may be a tumour selective property of the IGF-axis that could act as a novel target for treatment. The aim of these following experiments was to develop a screening platform that could be used to screen a library of small molecule drugs for potential novel inhibitors of nuclear IGF-1R, for example compounds that block receptor translocation or DNA binding. Following identification, any potential inhibitors would then be tested to validate their activity, if any, against the pro-tumorigenic effects of nuclear IGF-1R.

Novel inhibitors identified in this screen could also potentially help to elucidate the translocation mechanism of the receptor. As discussed in Section 1.6.1, the translocation mechanism of IGF-1R is partially but incompletely understood, involving clathrin-dependent endocytosis, followed by SUMOylation of IGF-1Rβ and activities of p150 Glued and importin-β/RanBP2 (Aleksic *et al.*, 2010; Sehat *et al.*, 2010; Packham *et al.*, 2014). It was also only until the previous findings in this thesis (Section 3.2.1), that the long-held speculation that nuclear IGF-1R originates from the cell surface was confirmed. Any translocation inhibitors identified in this screen may identify previously undetected proteins that interact with IGF-1R following internalisation. This could provide information on how the receptor is targeted from internalisation into a vesicle at the cell

surface to transportation to the nucleus. In this case, it is possible that any novel inhibitors would therefore also be more specific for inhibition of the action of IGF-1R if they disrupt unique components found in the IGF-1R translocation pathway. This would prevent cross reactivity with the closely related INSR, a common problem with previously trialled anti-IGF-1R therapies, as discussed in Section 1.4.4 (Carboni *et al.*, 2009; Tognon, 2012; Simpson *et al.*, 2017; Osher and Macaulay, 2019).

Two methods were used for development of this screening tool, the first involving IF staining and quantification of nuclear IGF-1R and the second using quantitative luciferase assay reporters containing IGF-1R DNA binding regions. Development of both methods are discussed in full in the following sections.

4.2 Results

4.2.1 Immunofluorescence based screening platform

Previous work in our lab has shown detection of quantifiable changes in levels of nuclear IGF-1R both in response to IGF-1 stimulation and inhibition using IF microscopy (Section 3.2.2 and (Aleksic *et al.*, 2010, 2018)). We therefore aimed to test the feasibility of using this method as a screening tool for small molecule inhibitors of nuclear IGF-1R.

Initial work involved confirming our previous results in the detection of a decrease in nuclear IGF-1R in response to inhibition on a 6-well plate scale. DU145 cells were seeded onto cover slips in a 6-well plate and treated with either BMS-754807, an IGF-1R TKI, or Bafilomycin A1 (BafA1) an inhibitor of V-ATPase, a proton pump involved in a variety of processes including endocytosis, vesicular trafficking and receptor recycling (Huss and Wieczorek, 2009). Cells were then fluorescently stained for IGF-1R, and levels of nuclear IGF-1R were quantified via measuring the signal contained within DAPI-stained nuclei. These results showed a significant decrease in levels of nuclear IGF-1R on treatment with

BMS-754807 or BafA1 (Figure **4.1**), as well as increased accumulation of IGF-1R at the plasma membrane, as seen in our previous experiments (Aleksic *et al.*, 2010).

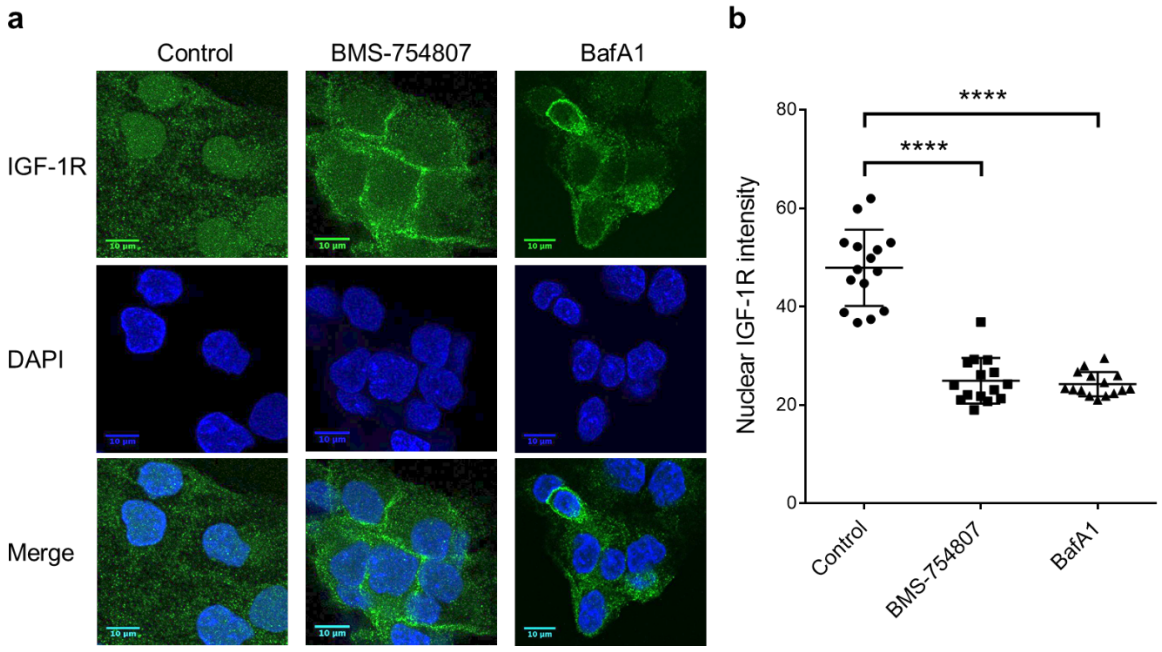


Figure 4.1 Reduction in nuclear IGF-1R in response to inhibitors is detectable by immunofluorescence

a Representative images showing immunofluorescent staining of IGF-1R in DU145 cells. DU145 cells were cultured for 24 hrs in a 6-well plate before treatment with solvent control (0.1% DMSO), BMS-754807 (100 nM) or BafA1 (50 nM) for 6 hrs at 37°C followed by immunofluorescent staining for IGF-1Rβ (1:500). Visualisation was performed on a Zeiss LSM 780 Confocal microscope. Scale bar 10 µm. **b** Quantification of nuclear IGF-1R showing a significant decrease on treatment with BMS-754807 and BafA1 ($n \geq 10$ cells per condition for n=2 biological repeats). Image analysis was performed using ImageJ software and data were analysed by one-way ANOVA (****$p < 0.0001$).

Following confirmation of reduction of nuclear IGF-1R in response to inhibitors, we then aimed to scale this method to a 96-well plate, as a high throughput small molecule screen would require at least a 96-well format or potentially even higher throughput of 384-wells. Following seeding in a 96-well plate, DU145 cells were stained for IGF-1R, however visualisation showed only faint detection of fluorescent signals (Figure **4.2**). To improve IGF-1R detection a range of primary antibody dilutions were tested. Following these optimisation experiments, a 1:250 dilution of primary antibody, increased from 1:500 (as used in Figure **4.1** and Figure **4.2**) was determined to give the clearest signal and BMS-754807 and BafA1 treatment experiments were repeated. Here, cells were co-stained for actin to visualise the plasma membrane, with the intention of quantifying IGF-1R located at the membrane vs nucleus. While staining for IGF-1R could now easily be visualised (Figure **4.3**), it appeared that the specificity required to detect changes in levels of nuclear IGF-1R had been lost, as there was only a small reduction in nuclear IGF-1R detected in cells treated with BMS-754807 and no significant changes in cells treated with BafA1 (Figure **4.3**).

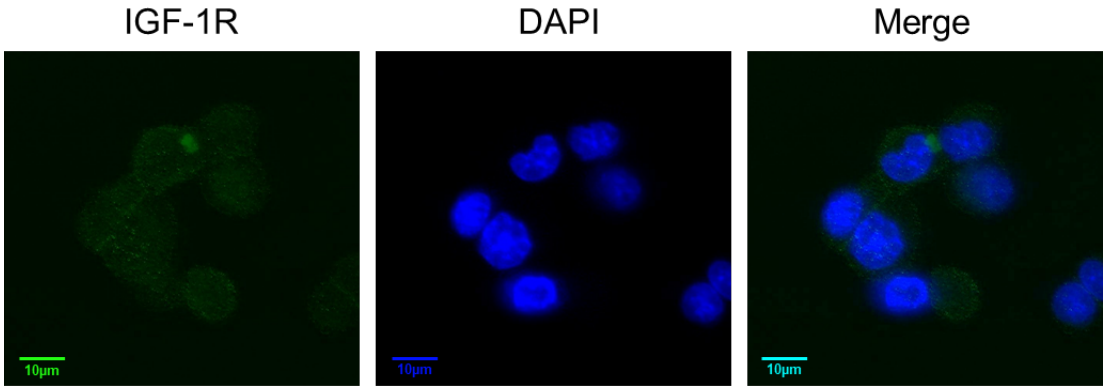


Figure 4.2 Visualisation of IGF-1R staining in 96-well plate
Images showing immunofluorescence staining of IGF-1R in DU145 cells seeded in a 96-well plate and stained with primary antibody for IGF-1Rβ (1:500). Visualisation was performed using an IN Cell Analyzer 6000, scale bar 10 µm. Unlike previous staining in 6-well plate format (Figure **4.1**), the cells showed only a weak fluorescent signal.

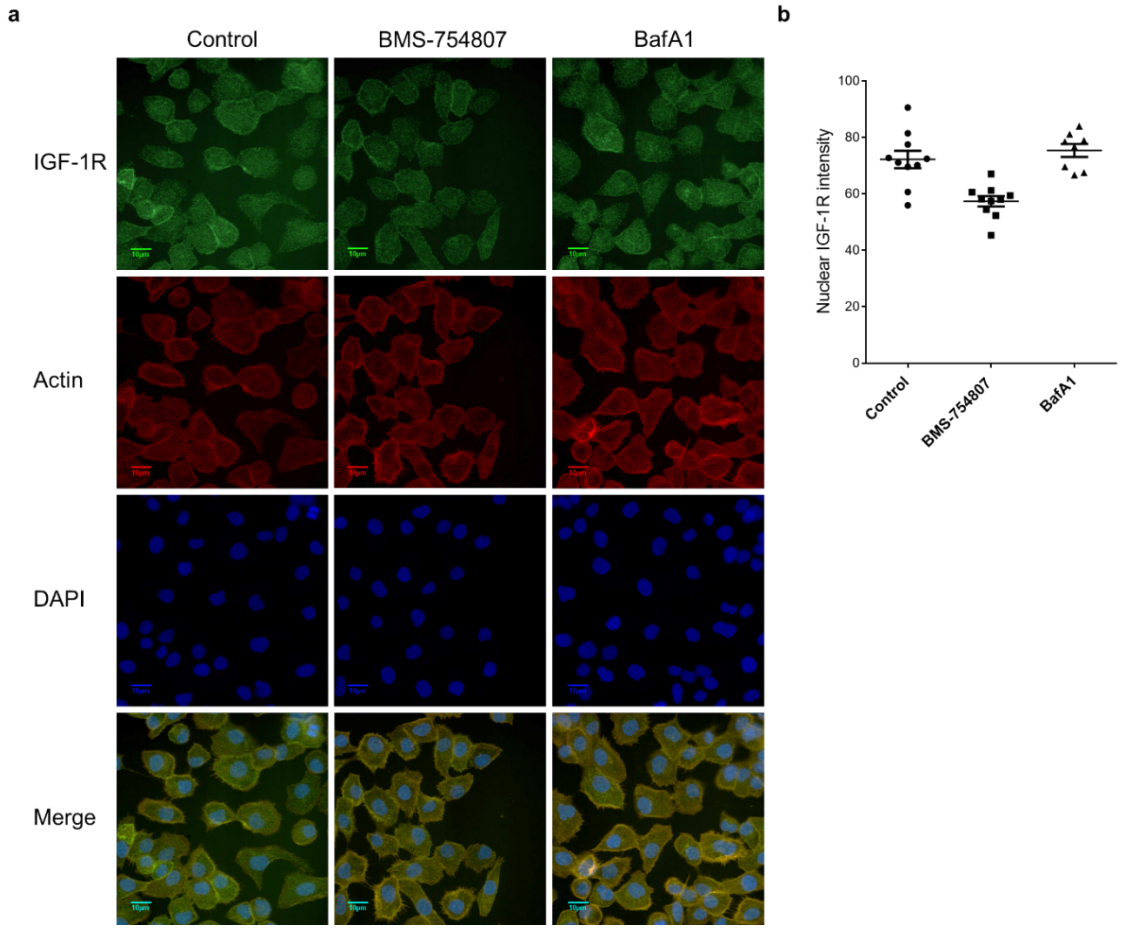


Figure 4.3 Changes in nuclear IGF-1R are not detected by immunofluorescence in a 96-well plate format

a Images showing immunofluorescent staining of IGF-1R and actin in DU145 cells. DU145 cells were treated as in Figure **4.1** and stained for IGF-1Rβ (1:250) and actin phalloidin (1:100) for visualisation of actin filaments. Visualisation was performed using an IN Cell Analyzer 6000, scale bar 10 μm **b** Quantification of nuclear IGF-1R using ImageJ, showing no significant changes on treatment with BMS-754807 or BafA1 ($n \geq 10$ cells per condition. Data shown is representative of results also seen in a second independent repeat and were analysed by one-way ANOVA *$p<0.05$).

Aiming to explore different and possibly more sensitive and specific methods of staining for IGF-1R in a 96-well plate format, Dr Eliot Osher, post-doctoral researcher in our lab, generated an IGF-1R construct with a C-terminal His tag. Dr Osher also generated a His-L-tag, containing a GGSGGS linker between the C-terminus of IGF-1R and the His tag, as direct tagging of a protein without a linker has been shown to potentially cause misfolding of the tagged protein, low yield in protein production, or impaired bioactivity (Chen, Zaro and Shen, 2013). Using IGF-1R null CRISPR knock-out DU145 cells (also generated by

Dr Osher) I performed transient transfections with empty vector, untagged IGF1R or the His-tagged IGF-1R constructs. Initial Western blotting of transfected cell lysates confirmed that the transfected IGF-1R cDNAs were expressed, appropriately processed, and phosphorylated, showing bioactivity of both His-tagged constructs (Figure **4.4**a). Parallel cultures were transfected with either untagged IGF-1R or His-tagged IGF-1R (no linker), stained, and visualised by IF using anti-His-tag primary antibody. While there was more signal in His-tagged IGF-1R transfected cells vs untagged IGF-1R, the signal in cells containing untagged IGF-1R suggested some non-specific staining was present. This was also supported by the presence of staining in every cell of the His-tagged IGF-1R transfected condition, as it is unlikely that the transfection efficiency of this construct was 100%. This staining was largely absent when cells transfected with His-tagged IGF-1R were stained with secondary antibody only (Figure **4.4**c), suggesting that the anti-His primary antibody was the source of non-specific signals.

To reduce this non-specific staining, NTA-Atto 488, a nickel-based compound for specific fluorescence detection of His-tagged proteins (Lai *et al.*, 2015), was also tested. As previously, cells were transfected with either His-tagged or untagged IGF-1R before visualisation with NTA-Atto 488. However, similar high levels of staining were seen with both His-tagged and untagged IGF-1R transfected cells (Figure **4.5**) and, as in Figure **4.4**, staining was present in all cells in the His-tagged IGF-1R transfected conditions when transfection efficiency is unlikely to be 100% (Figure **4.5**). Overall, the NTA-Atto 488 compound therefore also showed a high level of background staining.

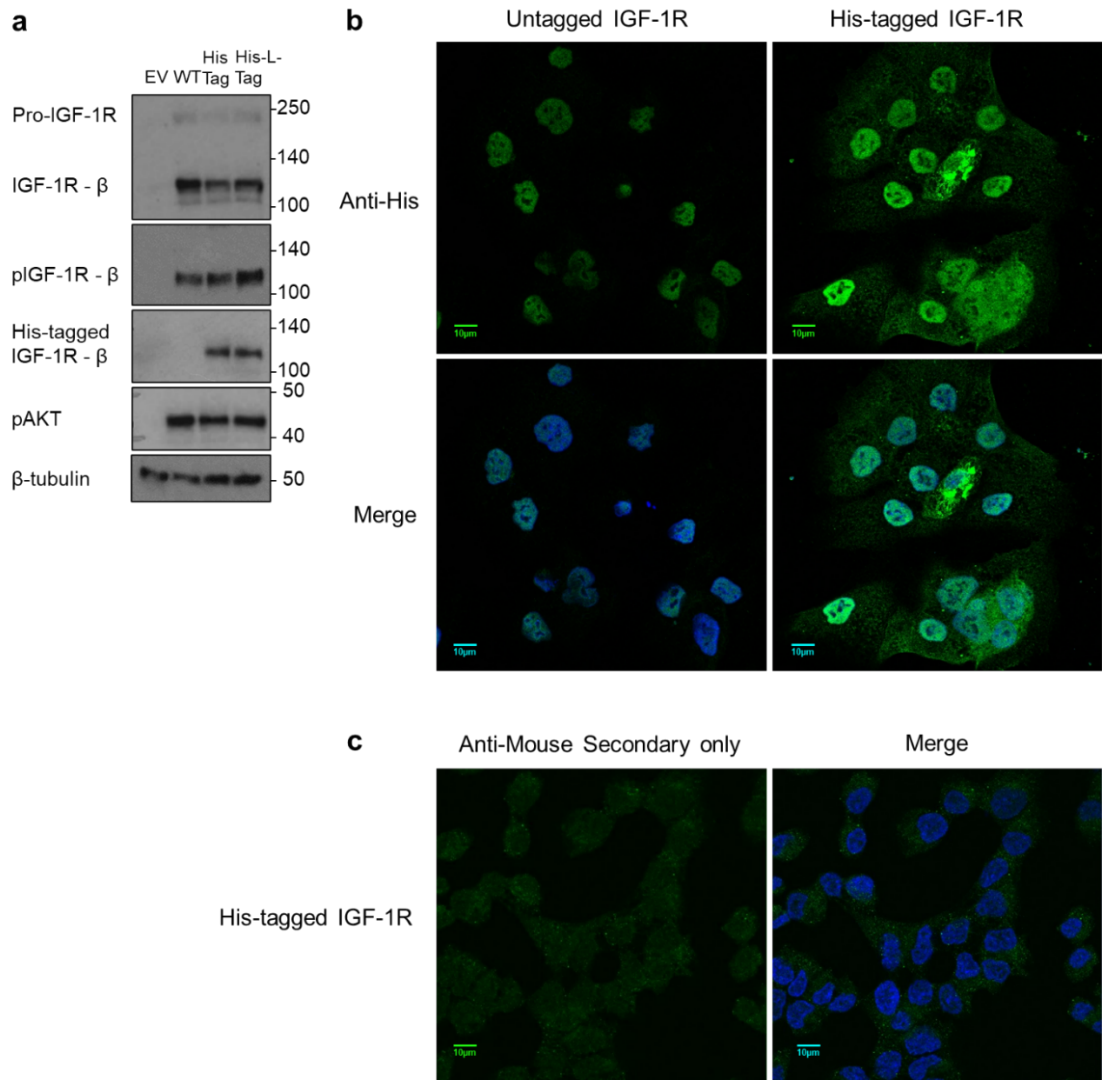


Figure 4.4 Immunofluorescent staining of His-tagged IGF-1R
a Western blot of IGF-1R null DU145 cells-transiently transfected with either empty vector (EV) negative control, WT untagged IGF-1R positive control or one of 2 His-tagged IGF-1R constructs. After 24 hrs cells were lysed and lysates were analysed by Western blot for IGF-1Rβ, phospho-IGF-1Rβ, anti-His and phospho-AKT. Both phospho- and total IGF-1R could be detected in cells transiently transfected with WT or His-tagged IGF-1R constructs, but not in those transfected with EV. The His-tag could only be detected in cells transiently transfected with His-tagged IGF-1R. Detection of phospho-AKT and phospho-IGF-1R in cells transfected with His-tagged IGF-1R suggests the receptor is bioactive. **b** Images showing immunofluorescence staining of His-tag in IGF-1R null DU145 cells transiently transfected with either untagged or His-tagged IGF-1R. After 24 hrs cells were stained with primary antibody for His-tag (1:500). As shown, in cells transfected with untagged IGF-1R (left images), nuclear His-staining was detected. **c** Images showing IGF-1R null DU145 cells transiently transfected with His-tagged IGF-1R. Cells were cultured and transfected as in (**b)** before processing for immunofluorescent staining in the absence of primary antibody. In these cells, nuclear staining previously seen in (**b**) was not present, suggesting that the nuclear staining was not due to non-specificity of the secondary antibody.

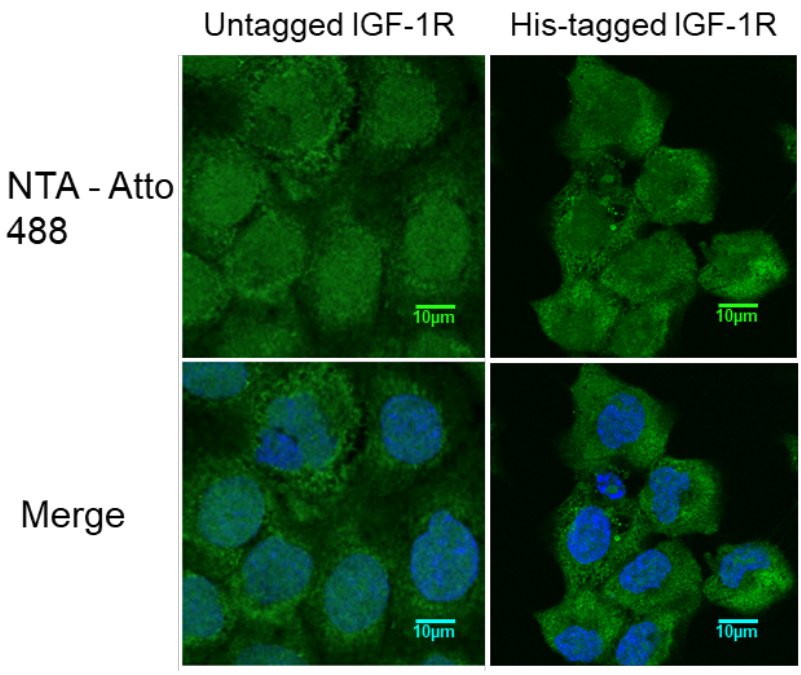


Figure 4.5 Immunofluorescent staining of His-tagged IGF-1R with NTA-Atto 488
Images showing immunofluorescence staining of IGF-1R null cells transiently transfected with either untagged (left) or His-tagged (right) IGF-1R constructs. After 24 hrs cells were stained with NTA-Atto 488, a compound for specific fluorescence detection of His-tagged proteins (Lai *et al.*, 2015). As shown, signal was present in both untagged and His-tagged IGF-1R, suggesting non-specific staining was present.

This IF based method therefore presented multiple challenges regarding practicality for a high throughput screen. Loss of specificity of staining on scaling to a 96-well plate, shown in part by no apparent change in nuclear IGF-1R on treatment with BMS-754807 (Figure **4.3**) and inability to counteract this with staining for a tagged receptor construct (Figure **4.4** and Figure **4.5**), made it unusable for screening a small molecule library. As well as this, the quantification of nuclear IGF-1R via IF would be done using a PerkinElmer Operetta High Content imager in collaboration with Daniel Ebner (Director of the High Throughput Screening facility at the Target Discovery Institute). It is likely further optimisation experiments would also have been needed to set up robust automated analysis and nuclear IGF-1R quantification via this method. It was therefore decided that IF was unsuitable for use as a high throughput screening assay but would be better suited as a

validation step, as in Figure **4.1** for any potential inhibitors that may be identified using a different high throughput screen.

4.2.2 Luciferase reporter assay-based screening platform

Alongside IF based screening, another technique for a nuclear IGF-1R screening platform was also tested. This involved more quantitative methods in development of a luciferase assay-based platform, using luciferase reporter plasmid constructs containing DNA regions of known IGF-1R binding sites from previously performed ChIP-seq experiments in our lab (Aleksic *et al.*, 2018). This is analogous to previous work done in the discovery and characterisation of nifuroxazide, an anti-cancer drug that acts as an inhibitor to STAT3 (Nelson *et al.*, 2008). The aim was to then test the luciferase activity of the constructs in response to IGF-1 stimulation and inhibition to develop an IGF-1 responsive reporter. Any IGF-induced changes in luciferase activity of the reporter could be due to IGF-induced translocation to the nucleus and interaction of IGF-1R with the cloned IGF-1R DNA binding site in the reporter, thereby triggering luciferase expression. IGF responsive reporters could then be stably transfected into DU145 cells for use as a screening tool for small molecule inhibitors of nuclear IGF-1R.

4.2.2.1 *JUN* promoter luciferase reporter

Initial work by Dr Eliot Osher involved cloning a portion of the *JUN* promoter region on chromosome 1 (chr1: 59249322 – 59250750), previously identified and validated as an IGF-1R binding site (Aleksic *et al.*, 2018), into the pNLCol2 luciferase assay vector. This vector was chosen due to having a minimal promoter and a multiple cloning region for insertion of custom promoter elements. Also, the reporter had dual luciferase expression, optimised for high throughput screening as genuine hits show similar responses in both reporters, helping to reduce false positives (*pNLCoI2 [luc2-P2A-NlucP/minP/Hygro] Vector: Promega Certificate of Analysis*, 2012). The *JUN* promoter construct or an empty

vector (EV) negative control were transfected into DU145 cells, selected with hygromycin, and expanded to give two separate stable clones by Dr Osher. Initial luciferase assay experiments by Dr Osher demonstrated that the *JUN* promoter stable cell line showed significantly increased luciferase activity compared to the EV negative control cell line, as expected (Figure **4.6**a). Further experiments undertaken by Dr Osher and me showed that the *JUN* promoter cell line was responsive to IGF-1 stimulation following serum starvation, with an increase in luciferase activity. Conversely, IGF-1 inhibition using BI 845 (xentuzumab, Boehringer Ingelheim), an IGF ligand neutralising antibody (Friedbichler *et al.*, 2014), showed a decrease in luciferase activity (Figure **4.6**b and c). These results showed that the *JUN* promoter construct was responsive to IGF-1, which could be due to the alteration in IGF-1R recruitment to the *JUN* promoter region.

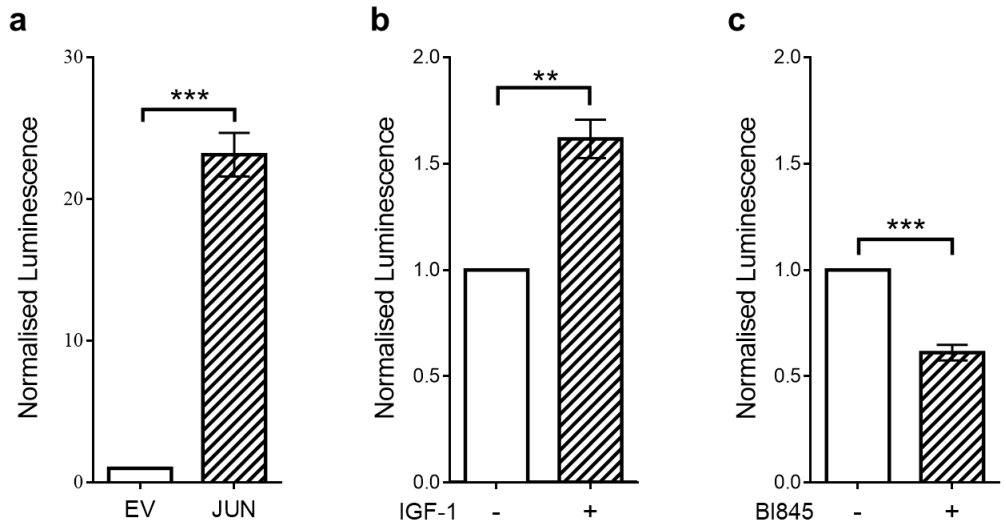


Figure 4.6 *JUN* promoter is IGF-1 responsive
a DU145 clones were cultured in RPMI-1640 medium supplemented with 10% FBS, and luciferase assays performed. Graphs show quantification of the increased luciferase activity of the *JUN* promoter reporter clone vs empty vector (EV) clone. **b-c** *JUN* promoter reporter cells were either serum starved for 24 hrs before treatment with solvent control (4.5 µM HCl) or IGF-1 (50 nM) for 24 hrs (**b)** or cultured in full medium for 24 hrs before culture medium was then removed from cells and replaced with RPMI-1640 medium supplemented with 10% FBS and preincubated with either solvent control (1 µM PBS) or BI 845 (1 µM) for 15 mins before addition to cells for 24 hrs (**c**). Graphs show a significant increase in luminescence of the *JUN* promoter reporter clone on treatment with IGF-1 (**b**) and a reciprocal significant decrease in luminescence on treatment with BI 845 (**c**). In each case luminescence per µg of protein was calculated before being normalised to the controls (white bars on each graph). Results represent mean ± SEM of triplicate independent experiments, each with 2 or more technical replicates. In each case data were analysed by unpaired student's t test (**p<0.005; ***p<0.001). Taken together these results show that the *JUN* promoter reporter stable cell line was IGF-1 responsive.

The difference in luciferase activity on IGF-1 stimulation or inhibition of the *JUN* promoter construct was found to be approximately 1.5-fold. On the advice of our collaborator Daniel Ebner in the HTS facility, this was lower than the approximate 2-3-fold change that would be desirable for a large enough screening window to reduce the risk of false positive hits. Further IGF-1 treatment time points were tested at 10 min, 30 min, 1 hr, 6 hrs, 48 hrs and 72 hrs treatment to investigate whether this affected the fold change in luciferase activity of the *JUN* promoter construct, however no significant difference in luciferase activity was detected between serum starved and IGF- treatments at these time points (data not shown). However, the data at 24 hrs, shown in Figure **4.6**, did support the

potential approach of using IGF-1R DNA binding sites in a luciferase reporter vector. This therefore led to the testing of further binding sites and their use in potential reporters.

4.2.2.2 Validation and cloning of further potential reporter regions

Previous work in our lab showed that many IGF-1R binding sites coincide with sites of RNAPolII recruitment, and that RNAPolII recruitment to these binding sites is IGF-1 dependent (Aleksic *et al.*, 2018). RNAPolII was also shown to be recruited to the *JUN* promoter region previously tested in the luciferase reporter, as described in Section 4.2.2.1. The IGF-1 dependent recruitment of RNAPolII to this region may have resulted in background luciferase activity from the *JUN* promoter reporter, limiting the fold change in luciferase activity, and therefore the screening window in response to IGF-1 stimulation. Therefore, from the IGF-1R chromatin binding sites previously identified in our lab (Aleksic *et al.*, 2018), regions were selected based on absence of or minimal RNAPolII binding peaks in the presence of IGF-1R binding and presence of one of the chromatin marks for active enhancers or promoters including H3K4me1, H3K4me3 or H3K27Ac (discussed in Section 1.6.2). The *FAM21A* promoter region was selected due to its previous characterisation in our lab (Aleksic *et al.*, 2018), an intergenic region of Chromosome 17 was chosen for the absence of RNAPolII binding but the presence of the active enhancer mark H3K27Ac, and the *DUSP8* promoter was chosen also due to lack of RNAPolII binding and the presence of the H3K4me1 enhancer mark (Figure **4.7**a). Recruitment of the receptor to these regions was validated in response to IGF-1 stimulation by ChIP-qPCR and IGF-1R recruitment to all four regions was shown to be increased on treatment with IGF-1 versus untreated control cells (Figure **4.7**b).

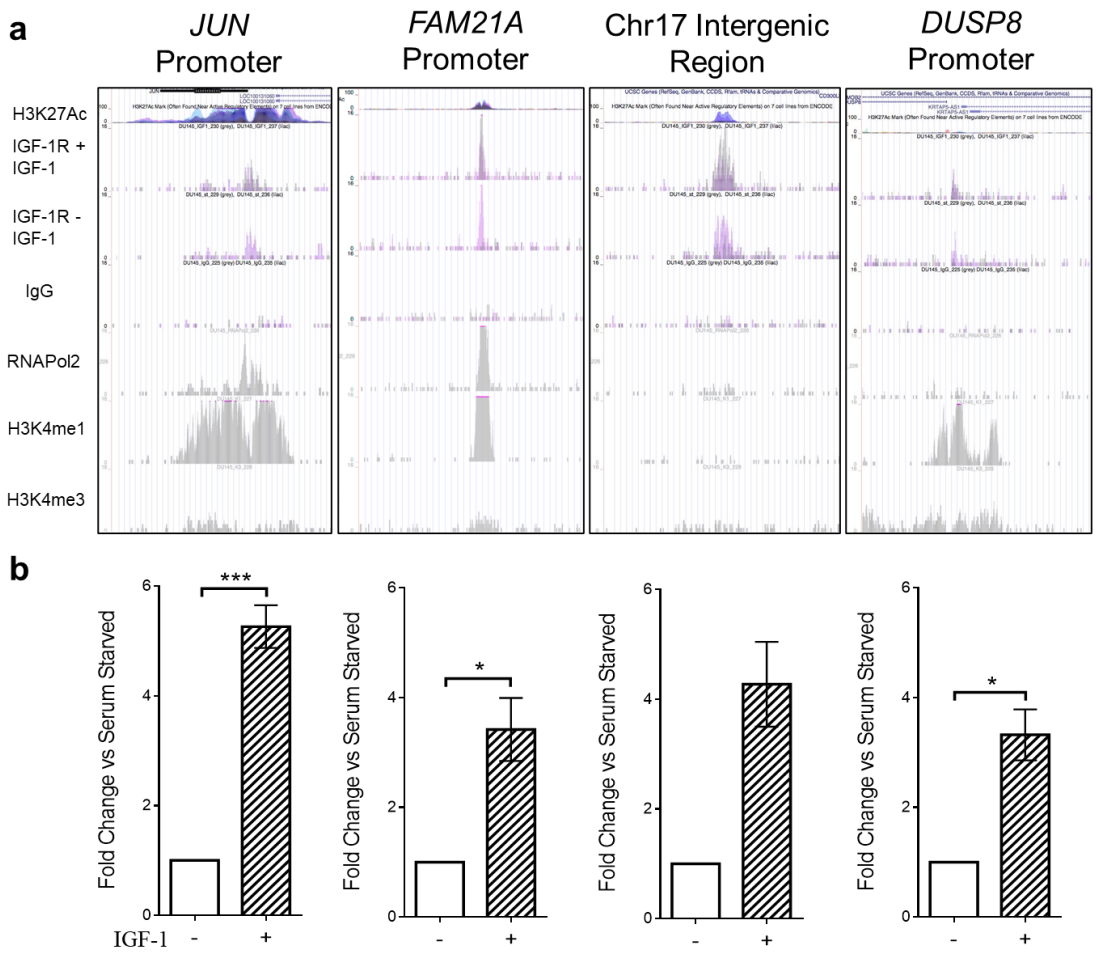


Figure 4.7 Recruitment of IGF-1R to IGF-1R chromatin binding sites is IGF-1 dependent

a UCSC genome browser images showing previously identified IGF-1R chromatin binding sites (Aleksic *et al.*, 2018). Images show binding peaks for IGF-1R ± IGF-1 and RNAPolII. Images also show peaks for H3K4me1 and H3K27Ac, markers for sites of active enhancer regions, as well as H3K4me3 a marker for promoter regions. It is worth noting the minimal RNAPolII binding and presence of H3K27Ac active enhancer mark for the Chromosome 17 Intergenic region. **b** ChIP-qPCR validation of the IGF-1R chromatin binding sites shown in the corresponding UCSC genome browser images above each graph. DU145 cells were serum starved for 24 hrs and treated with solvent control (4.5 µM HCl) or IGF-1 (50 nM) for 10 mins and ChIP-qPCR was performed using antibody for IGF-1Rβ-subunit and primers shown in Materials and Methods (Section 2.12). Graphs show increased recruitment of IGF-1R to all endogenous chromatin binding regions on treatment with IGF-1. Results represent mean ± SEM of triplicate independent experiments and data were analysed in each case using an unpaired student's t test (*$p<0.05$; ***$p<0.001$). These results confirm that recruitment of IGF-1R to the selected DNA binding sites is IGF-1 responsive.

PCR amplification primers were then designed for the regions validated in Figure **4.7**, as well as further IGF-1R sites listed in Table **4.1**. These regions were amplified from DU145 genomic DNA to be used in a luciferase reporter plasmid. Due to the highly repetitive nature of the Chromosome 17 intergenic region, multiple primer sets were tested before successful cloning of an approximately 1100 bp region, shown in Figure **4.8**. The repetitive sequence of the *DUSP8* promoter region also meant that this region could not be amplified by PCR for use in a luciferase reporter vector as specific primers could not be designed. The further cloned regions that are listed in Table **4.1** were selected on the basis of a lack of RNAPolII binding, and presence of an enhancer or promoter chromatin marker, as discussed for the regions validated in Figure **4.7**.

Six of the selected regions were successfully amplified by PCR using primers incorporating sites for restriction enzymes HindiIII and Xho1, showing products at the correct expected sizes (Figure **4.8**). These products were column purified and then digested alongside pNLCol2 luciferase reporter vector before ligation of the vector and IGF-1R binding region. Following transformation of the luciferase reporter constructs, bacterial colonies were analysed by PCR for presence of the correctly cloned vector. Figure **4.9** shows products of colony PCR amplification of the Chromosome 17 luciferase reporter plasmid. Lanes 2 and 6 of Figure **4.9** show products at the correct size, approximately 1100 bp, and successful cloning of the IGF-1R binding region was confirmed with Sanger Sequencing. Colony PCR amplification also showed products at the predicted sizes for the *FAM21A* and *FAM21C* promoter regions, the *ARG2* promoter, Laptm5, and LOC79999 (Table **4.2**). Correct insert sequence was confirmed by Sanger Sequencing before all cloned constructs were then tested by luciferase assay.

Lane Number	Selected Regions	Gene Co-ordinates	Size (bp)
1	Laptm5	chr1: 31297026 – 31297640	614
2	ARG2	chr14: 68085973 – 68086869	896
3	*IGF2R* promoter	chr6: 160389594 – 160390540	946
4	*FAM21A* promoter	chr10: 51827228 – 51828123	895
5	*FAM21C* promoter	chr10: 46222227 – 46223137	910
6	LAMP1	chr13: 113952397 – 113953402	1005
7	HES4	chr1: 935870 - 936484	614
8	LOC79999	chr17: 19093243 – 19093687	444
9	NEURL2	chr20: 44519133 – 44520191	1058
10	UBE2H	chr7: 129592162 – 129593199	1037
11	*FAM21C* promoter	chr10: 46222227 – 46223137	910
12	GOLGA6A	chr15: 74392121 – 74393133	1012
13	Chromosome 17 intergenic region	chr17: 72509997 - 72511095	1098

Table 4.1 Cloned IGF-1R binding sites for testing as luciferase reporters
Table showing the IGF-1R binding regions cloned for use in luciferase reporter constructs. Regions are shown with their chromosomal co-ordinates, predicted sizes in base pairs (bp), and labelled with the corresponding lane that PCR products were run on the agarose gels shown in Figure **4.8**.

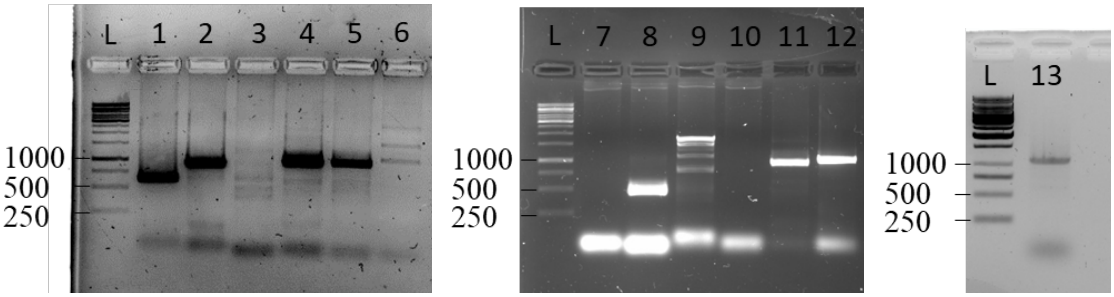


Figure 4.8 Cloning of IGF-1R binding regions for potential luciferase reporters
Agarose gels showing PCR amplification products from cloning of IGF-1R binding sites for testing in luciferase reporters. Numbered lanes correspond to cloned regions listed in Table **4.1**. Lane L: GeneRuler 1 kb DNA Ladder, and labelled products show sizes in bp. Lanes 1, 2, 4, 5, 8 and 11-13 show products at expected sizes.

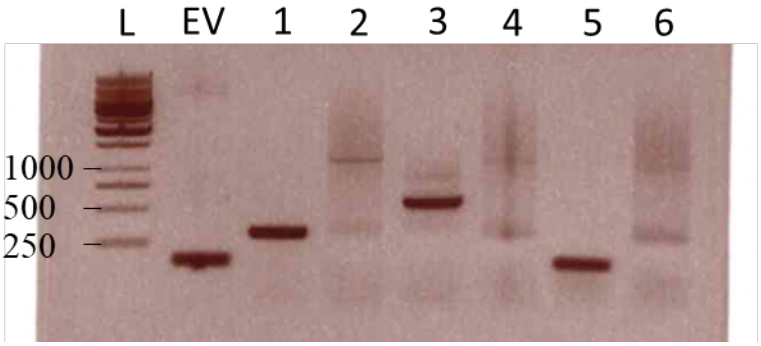


Figure 4.9 Colony PCR amplification of Chromosome 17 intergenic region
Agarose gel showing PCR product from bacterial colonies transformed with Chromosome 17 luciferase reporter plasmid. Numbered lanes correspond to colony number from transformation plate and EV shows empty vector negative control. GeneRuler 1 kb DNA Ladder is shown in lane labelled 'L', and labelled bands show sizes in bp. Lanes 2 and 6 show products at expected size for the Chromosome 17 region (approx. 1100 bp) and were analysed by Sanger Sequencing to confirm correct sequence of the reporter insert. Image is representative of results also seen for other successfully cloned IGF-1R binding regions to generate reporter constructs to be tested by luciferase assay, listed in Table **4.2** and shown in Figure **4.10**.

Cloned Region	Size (bp)
Laptm5	614
ARG2	896
IGF2R promoter	946
FAM21A promoter	895
LOC79999	444
Chromosome 17 intergenic region	1098

Table 4.2 Successfully cloned IGF-1R binding sites
Table listing the regions that were successfully cloned into the pNLCol2 luciferase reporter plasmid from the IGF-1R binding regions listed in Table **4.1** and shown in Figure **4.8**.

DU145 cells were transiently transfected with either EV, or one of the luciferase reporter constructs containing an IGF-1R DNA binding site listed in Table **4.2**. Luciferase activity of transfected cells was then measured following 24 hrs incubation with solvent control (4.5 μM HCl) or IGF-1 (50 nM) to test the IGF responsiveness of the luciferase reporters (Figure **4.10**). As expected, EV transfected cells showed minimal luciferase activity, and no response to IGF-1 treatment. The Chromosome 17 construct showed a significant, approximate 2-fold increase in luciferase activity on treatment with IGF-1, a larger fold increase than that previously seen with IGF-1 treatment of *JUN* promoter stable cell lines (Figure **4.6**). However, the remaining constructs showed minimal luciferase activity above that of EV negative control and no significant differences on treatment with IGF-1 (Figure **4.10**). The lack of IGF-1 responsiveness could be due to the recruitment of currently

unidentified transcription factors to the cloned IGF-1R DNA binding sites, or that the region did not span the entire IGF-1R binding site, influencing levels of luciferase activity. Due to the significant response and increase in luciferase activity of the Chromosome 17 reporter, this construct was then chosen to be tested in further assays.

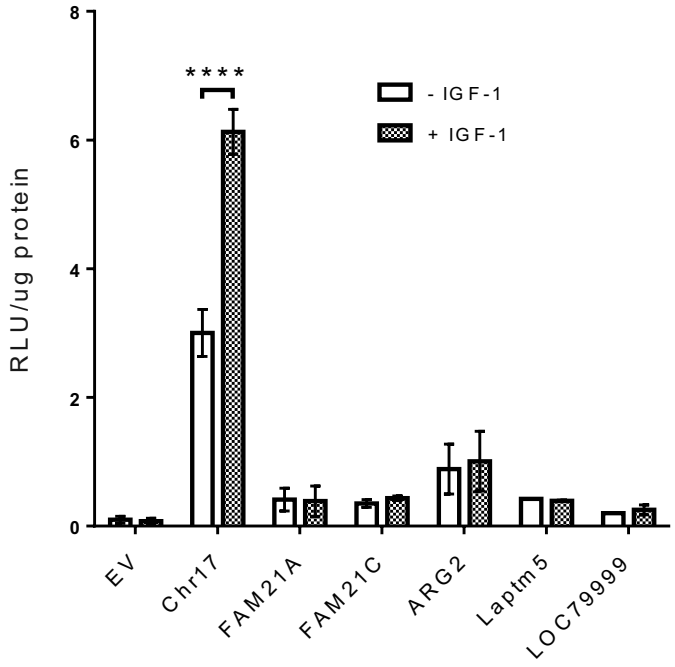


Figure 4.10 Luciferase assay testing IGF-1 responsiveness of nuclear IGF-1R reporters

DU145 cells were transiently transfected with empty vector (EV) or luciferase reporter plasmid containing indicated IGF-1R binding region. Cells were then serum starved for 24 hrs before treatment with solvent control (4.5 µM HCl) or IGF-1 (50 nM) for 24 hrs. Graph shows relative luminescence units (RLU) generated by each reporter construct corrected for µg protein in the presence or absence of IGF-1. Results represent mean ± SEM of triplicate independent experiments with at least 2 technical replicates. Data were analysed in each case using two-way ANOVA comparing untreated vs IGF-1 treated cells (****$p<0.0001$). Of the six reporter constructs tested, only the Chromosome 17 intergenic region construct showed a significant increase in luminescence on treatment with IGF-1, showing potential as an IGF-1 responsive reporter.

4.2.2.3 Luciferase assay testing and development of stable cell line for Chromosome 17 reporter

Following the initial results in Figure **4.10** showing luciferase activity of the Chromosome 17 reporter construct, experiments to confirm IGF-1 responsiveness were then performed. DU145 cells were transiently transfected with the reporter, serum-starved and treated with

either IGF-1 ligand (Figure **4.11**a) or the IGF ligand neutralising antibody BI 845 (Figure **4.11**b). IGF-1 was found to cause an approximately 2-fold increase in luminescence vs solvent-treated control cells, although the response was variable and not statistically significant. The reciprocal experiment with BI 845 also showed an approximately 2-fold decrease in luminescence on inhibition of IGF ligand (Figure **4.11**b). These results confirmed the IGF responsiveness of the Chromosome 17 reporter plasmid and showed a fold change in luminescence closer to the 2-3-fold difference suggested by collaborators as appropriate for a screening window.

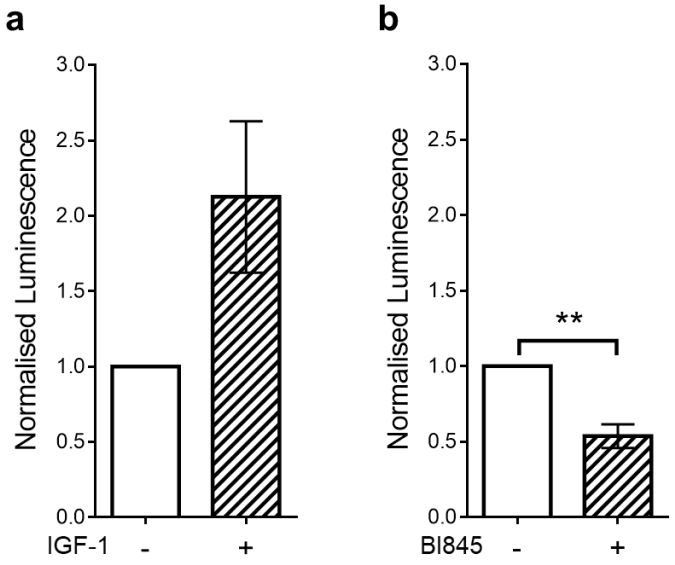


Figure 4.11 Transiently transfected Chromosome 17 intergenic region reporter is IGF-1 responsive

a-b DU145 cells transiently transfected with the Chromosome 17 intergenic region reporter were either serum starved for 24 hrs before treatment with solvent control (4.5 µM HCl) or IGF-1 (50 nM) for 24 hrs (**a)** or cultured for 24 hrs in full medium (RPMI-1640 with 10% FBS) before culture in full medium preincubated with solvent control (1 µM PBS) or BI 845 (1 µM) for 15 mins before addition to cells for 24 hrs (**b)**. Graphs show an increase approaching statistical significance (p=0.0887) in luminescence on treatment with IGF-1 (**a**) and a reciprocal significant decrease in luminescence on treatment with BI 845 (**b**). In each case luminescence per µg of protein was calculated before being normalised to the controls shown in white on each graph. Results represent mean ± SEM of triplicate independent experiments, each with 2 or more technical replicates. In each case data were analysed by unpaired student's t test (*$p<0.05$, **$p<0.005$). Taken together these results show that the Chromosome 17 intergenic region reporter plasmid was IGF-1 responsive.

However, these results were obtained using transient transfections, likely introducing variation between biological repeats for example due to differences in transfection efficiency. To generate stable clones to check the IGF responsiveness of the Chromosome 17 reporter, DU145 cells were transfected with the reporter plasmid and cultured in antibiotic selection medium. Stable clones would also be required in the small molecule screening platform for novel inhibitors of nuclear IGF-1R, to avoid potential variation due to transfection efficiency and the impracticality of transfecting large quantities of cells before each round of screening.

Following transfection and culture in selection medium, selected colonies of surviving transfected cells were expanded for use in luciferase assays to test for the IGF-response of the Chromosome 17 reporter plasmid. Colonies were tested alongside the previously generated EV and *JUN* promoter stable cell line constructs, used as a negative and positive control respectively, and cells were stimulated with IGF-1 before relative luminescence measurements were taken. As shown previously in Figure **4.6**, the EV clone did not respond to IGF-1, while the *JUN* promoter stable clone showed significant luminescence above that of the EV control with a further significant increase in luminescence on treatment with IGF-1(Figure **4.12**).

Approximately 25 different Chromosome 17 reporter transfected clones were expanded and tested by luciferase assay. The graph in Figure **4.12** shows luciferase assay results for colonies 2-4 and are representative of the results seen in all colonies tested. In contrast to the results following transient transfection (Figure **4.11**), the stably transfected Chromosome 17 reporters showed minimal to no luciferase activity at a level lower than that of even the EV negative control, with no response to IGF-1 stimulation. This

suggested either that the Chromosome 17 reporter had not been retained or that the luciferase reporter had undergone silencing while retaining hygromycin resistance.

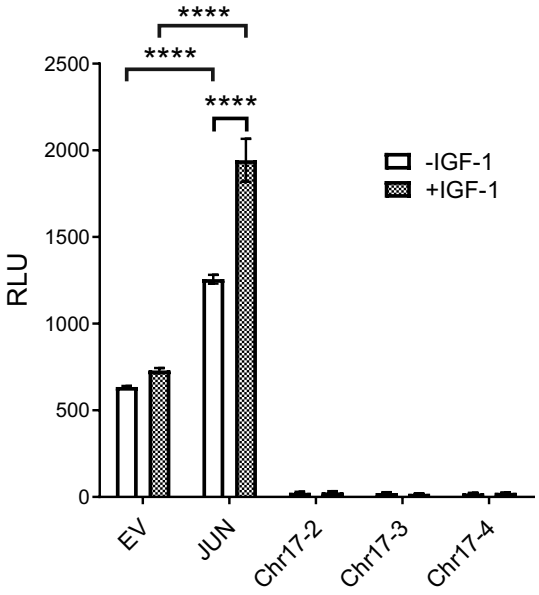


Figure 4.12 Chromosome 17 intergenic region reporter showed no luciferase expression in stable clones

EV and *JUN* promoter reporter clones (negative and positive controls respectively) were seeded alongside an equal number of Chromosome 17 intergenic region reporter stable clones and tested for luciferase activity in response to IGF-1 as in previous experiments (Figure **4.6**Figure **4.10**Figure **4.11**). The graph shows three different Chromosome 17 intergenic region reporter clones that are representative of the approximately 25 different clones tested, showing negligible luminescence activity with no response to IGF-1. Graph shows relative luminescence units (RLU), mean ± SEM from 3 independent assays each with 2 or more technical replicates. Data were analysed by 2way ANOVA comparing untreated vs IGF-1 treated cells (****$p<0.0001$) and Tukey's multiple comparison test for EV vs *JUN* promoter reporter clones (****$p<0.0001$).

After testing ~25 different stable clones, it was clear that none generated luciferase signal that was above or even equal to EV negative controls, or comparable to previous results with the transiently transfected Chromosome 17 intergenic region reporter shown in Figure **4.11**. The causes for the difference in signal between transient transfections and stable integration of the reporter are unclear. Due to the highly repetitive nature of the Chromosome 17 intergenic region that makes up the IGF-1R binding site, it is possible there was a high amount of non-specific binding at the region cloned into the reporter. This could result in high levels of luciferase expression, likely to be toxic to any cells that showed long term expression from the reporter plasmid. To counteract this, a second reporter plasmid was used, pGL4.27, into which the same region of the Chromosome 17 IGF-1R binding site was cloned. Unlike the previously used pNLCol2, the pGL4.27 plasmid backbone contains only one luciferase reporter gene rather than two, which also contains a PEST sequence which signals for degradation of the luciferase protein, reducing its half-life (Rechsteiner and Rogers, 1996; García-Alai *et al.*, 2006). This would therefore reduce the potentially toxic build-up of luciferase within the cell and could increase the chance of survival of clones that stably integrate the reporter plasmid. However, upon transfection of the pGL4.27 construct containing the Chromosome 17 region, no colonies survived antibiotic selection after multiple attempts (data not shown).

Therefore, it was decided to take a third approach to generate a stable clone incorporating the Chromosome 17 region. This involved cloning a smaller, more central region of the IGF-1R binding region on Chromosome 17. The aim was to reduce the amount of non-specific binding, therefore reducing excess and potentially toxic luciferase production.

4.2.2.4 Cloning and testing of Chromosome 17 Peak Region reporter

The UCSC genome browser was used to visualise the IGF-1R binding peak present on Chromosome 17 (Figure **4.13**). A 533 bp region (chr17: 72510364 – 72510897) was selected for amplification as it spanned the centre of the IGF-1R binding peak, and it was thought that this may minimise the non-specific binding while still retaining IGF-1R binding to the reporter. This would prevent build-up of background luciferase that may be toxic to the cell, therefore increasing the chances of generating a surviving stable construct, as mentioned previously. This 533 bp sequence was designated the 'Chromosome 17 Peak Region'.

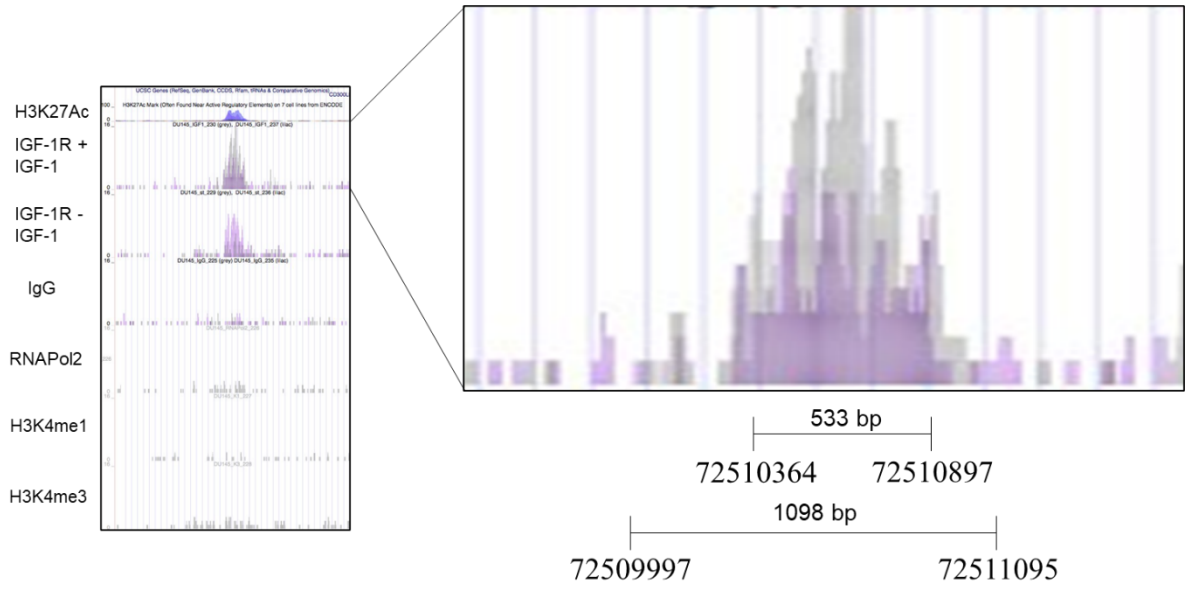


Figure 4.13 UCSC Genome Browser image of IGF-1R binding site in Chromosome 17 intergenic region
Left: UCSC genome browser image showing previously identified IGF-1R chromatin binding region in Chromosome 17 intergenic region, as shown in Figure **4.7**a (Aleksic *et al.*, 2018). Right: expanded view of IGF-1R binding region showing original 1098 bp region cloned to generate reporters tested in Figure **4.11**, and the centre of the IGF-1R binding peak, designated the 'Chromosome 17 Peak Region'. Primers were designed to clone this Peak Region, spanning chr17: 72510364 – 72510897.

As with the previous constructs described in this chapter, the Chromosome 17 Peak region was amplified by PCR from DU145 genomic DNA. PCR products were analysed on an agarose gel and were found to contain products at approximately the expected size of 533 bp (Figure **4.14**a). The amplified regions were digested and ligated alongside the pNLCol2 reporter plasmid and, following transformation, colonies were amplified by PCR with primers for the Chromosome 17 Peak Region and analysed on an agarose gel (Figure **4.14**b). Each numbered lane in Figure **4.14**b denotes a different bacterial colony tested by PCR, and colonies 2 and 5 showed product bands approximately at the expected size of 533 bp. The reporter constructs from colonies 2 and 5 were analysed by Sanger Sequencing and were confirmed to contain the reporter plasmid with the correct Chromosome 17 Peak Region sequence.

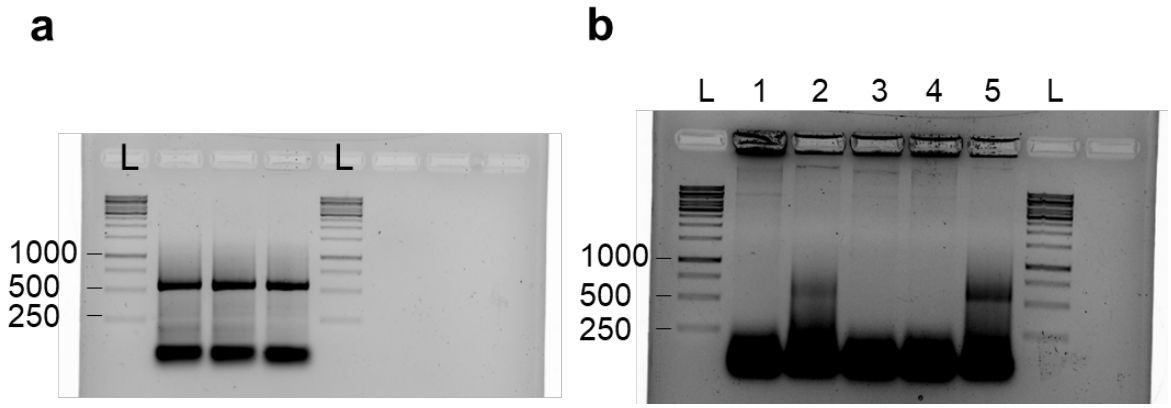


Figure 4.14 Cloning and colony PCR amplification of Chromosome 17 Peak region for luciferase reporter
a Agarose gel showing PCR product from amplification of Chromosome 17 Peak region from genomic DNA. All three of the triplicate amplifications from genomic DNA experiments show products at the expected size (approx. 533 bp). **b** Agarose gel showing colony PCR from 5 colonies transformed with Chromosome 17 luciferase reporter plasmid. Colonies 2 and 5 show products at the correct size (approx. 533 bp) and were analysed by Sanger Sequencing, confirming successful cloning of the Peak Region. GeneRuler 1 kb DNA Ladder is shown in lanes labelled 'L', with sizes in bp.

Following confirmation of the correct sequence, the Chromosome 17 Peak Region construct was tested in a luciferase assay. DU145 cells were transiently transfected with either EV negative control, the previously developed Chromosome 17 construct tested in Section 4.2.2.3 as a positive control, or the Chromosome 17 Peak Region construct. Cells were then treated with IGF-1 following serum starvation (Figure **4.15**a) or with IGF ligand neutralising antibody BI 845 (Figure **4.15**b). As shown in Figure **4.15**, EV negative control cells showed minimal luminescence activity and no significant response to IGF-1 stimulation or inhibition, as expected, and the previously tested Chromosome 17 construct showed luminescence activity similar to previous experiments (Figure **4.10** and Figure **4.11**). The Chromosome 17 Peak Region construct showed luminescence activity above the EV negative control but lower than the ~1100 bp Chromosome 17 construct, with no significant response to either IGF-1 stimulation or IGF ligand inhibition (Figure **4.15**).

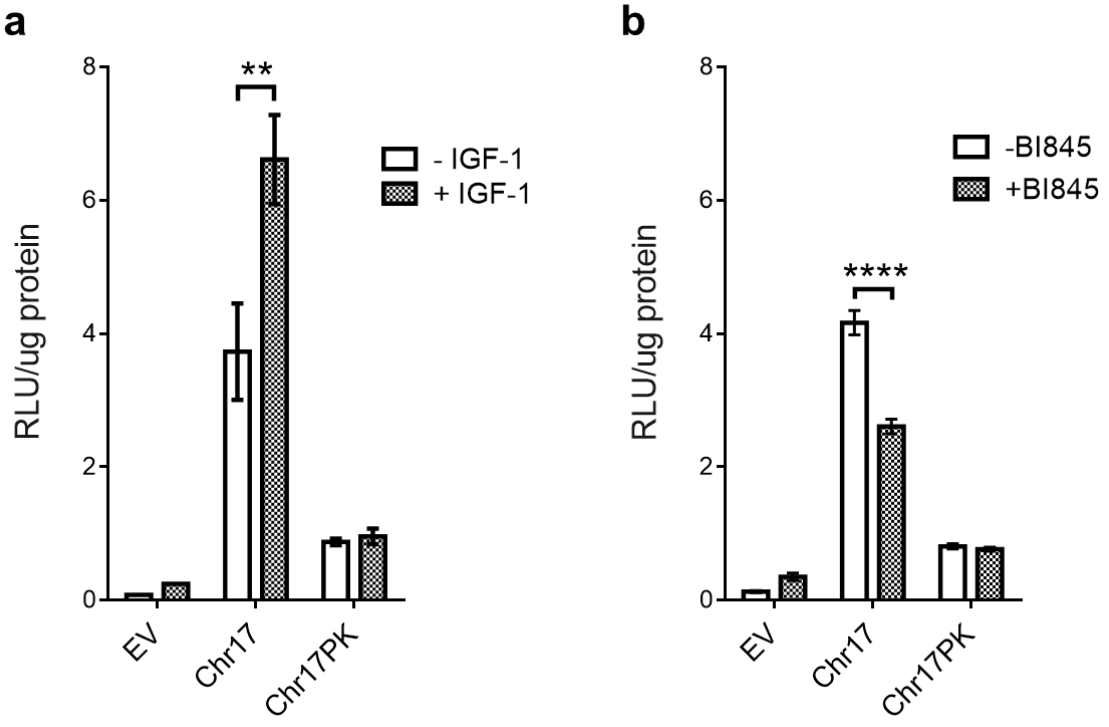


Figure 4.15 Chromosome 17 Peak region luciferase reporter did not show IGF-1 responsiveness

a-b DU145 cells were transiently transfected with empty vector (EV) negative control, previously tested Chromosome 17 intergenic region (Chr17) positive control or Chromosome 17 peak region (Chr17PK) constructs. Cells were either serum starved for 24 hrs before treatment with solvent control (4.5 μM HCl) or IGF-1 (50 nM) for 24 hrs (**a)** or cultured for 24 hrs before culture medium was then removed from cells and replaced with RPMI-1640 medium supplemented with 10% FBS and preincubated with either solvent control (1 μM PBS) or BI 845 (1 μM) for 15 mins before addition to cells for 24 hrs (**b)**. Results represent mean ± SEM of triplicate independent experiments, each with 2 or more technical replicates. Data were analysed using two-way ANOVA comparing untreated vs IGF-1 or BI 845 treated cells (**p<0.005; ****p<0.0001). Taken together these data show that the Chromosome 17 Peak region reporter construct was not responsive to IGF-1.

Overall, this suggests that IGF-1R was not able to bind to this smaller peak region of the IGF-1R binding site identified in the intergenic region of Chromosome 17. The lower luminescence activity of the 533 bp construct compared to the ~1100 bp region suggests that non-specific binding may have been reduced, however it seems IGF-1R binding to the region has also been disrupted. Due to the inability of the Chromosome 17 Peak construct to show IGF responsiveness in transient transfection experiments, no attempt was made to try and generate a stable cell line. Therefore, despite multiple attempts it did not prove possible to generate an IGF-responsive stable reporter cell line for use as a small molecule drug screening tool.

4.3 Conclusion

Overall, the initial aim of these experiments was to generate a tool for screening of a small molecule library for novel inhibitors of nuclear IGF-1R. Initial approaches used IF analysis, which on a smaller scale showed quantifiable differences in nuclear IGF-1R levels on treatment with, or inhibition of, IGF-1 and IGF-1R respectively. However, scaling this to a higher throughput method that would be required for a screening platform resulted in a loss of specificity for this technique. It is possible this could be improved by testing a further range of primary antibody dilutions and staining conditions as well as testing other primary antibodies for IGF-1R to reduce background staining and potentially improve specificity. Given the specificity of the IF staining, it is likely this technique would have been better suited to be used for low throughput validation of any small molecule nuclear IGF-1R inhibitors identified from a high throughput screen.

A more quantitative approach was also tested for development of a screening assay, involving luciferase-based reporter plasmids containing previously identified IGF-1R DNA binding regions. A stable cell line expressing a luciferase-based reporter plasmid

containing one of these binding regions, a portion of the *JUN* promoter, showed significant responsiveness both to IGF-1 stimulation and IGF-ligand inhibition. However, the fold change of these responses was deemed too small for use in a high throughput screen.

The *JUN* promoter construct did however represent a proof of concept for the luciferase assay-based screen, leading to cloning and testing of further IGF-1R DNA binding regions by this method. While most of these regions did not show luciferase activity or IGF-1 responsiveness, an IGF-1R binding site in the intergenic region of Chromosome 17 showed responsiveness to both IGF-1 stimulation and IGF ligand inhibition in transient transfections. However, a stable cell line for this construct could not be generated.

For the tested IGF-1R DNA binding regions that did not show luciferase activity, it is possible that the cloned regions did not span the entirety of the region required for IGF-1R binding. This is supported by the fact that regions that did not show luminescence activity were a much shorter length than both the Chromosome 17 intergenic region and region of the *JUN* promoter used in IGF-responsive reporters. These shorter regions were dictated by the repetitive nature of the sequences present, and therefore represented regions for which specific primers could be designed. Further work could expand the size of these cloned regions to ensure the entire IGF-1R binding site is present or, if possible, it would also be useful to identify an IGF-1R DNA binding motif, as previously done with the closely related INSR (GGGAXXTGTAGT) (Hancock *et al.*, 2019). However, accurate motif identification typically requires analysis of thousands of binding regions (McLeay and Bailey, 2010; Machanick and Bailey, 2011), whereas the data from our lab identified fewer than 100 (Aleksic *et al.*, 2018). This would require further ChIP-seq data to add to the currently obtained data set from our lab to enable accurate motif prediction.

If time had been permitting, the Chromosome 17 intergenic region could have been cloned into a lentiviral vector, which have increased infection efficiency compared to the plasmid

vectors tested here, therefore increasing the likelihood of generating stable clones that integrate the desired reporter construct.

Future work would involve testing of remaining IGF-1R DNA binding sites identified by ChIP-seq or expanded regions of those tested here as previously mentioned, in similar reporter assays. The ChIP-qPCR validation shown in Figure **4.7**b shows that recruitment of IGF-1R to some of these regions is responsive to IGF-1 treatment at an approximately 3-fold increase. It is unclear why this translates to a less than 2-fold change at regions tested in luciferase reporter assays but may be due to background binding of other transcription factors or proteins at these regions. It is possible that other IGF-1R DNA binding regions that were not tested here do not have this issue. It is also possible that any change in reporter activity may not necessarily be due to changes in nuclear IGF-1R, but due to indirect effects such as IGF-signalling influencing nuclear import or chromatin binding of alternative transcriptional regulators that bind to the same region.

Although a high throughput screen was not undertaken in this case, some potential flaws in this screening method may have included detection of false positives due to compound inhibition of luciferase. However, the risk of this was reduced due to the use of the pNLCol2 dual luciferase reporter, as mentioned previously (*pNLCoI2 [luc2-P2A-NlucP/minP/Hygro] Vector: Promega Certificate of Analysis*, 2012). Inhibition of nuclear IGF-1R could also occur via inhibition of endocytosis, trafficking, transport through nuclear pores, or binding to chromatin and possibly to other proteins that promote IGF-1R recruitment. Therefore, it is unlikely in retrospect that inhibitors of any of these processes would be specific for IGF-1R. Had high throughput screening been undertaken, this non-specificity could have been reduced by counter-screening using a reporter responsive to changes in the closely related INSR and with an NF-κB responsive reporter to screen out

compounds that were general inhibitors of transcription, analogous to the work done by (Nelson *et al.*, 2008).

The overall aim of these experiments was to generate a small molecule screening platform for inhibitors of IGF-1R. While the reporters generated could not be used for this function, we have generated two different IGF responsive luciferase reporters. It is possible that future work could use this same concept to develop a screening tool for small molecule inhibitors of nuclear IGF-1R, and the work here has shown that this method can also be used as a validation tool for future studies. Confirming this, we used similar methods to design a luciferase reporter for the *RRM2* promoter to help to assess the role of the IGF-axis in enhancing RRM2 expression (Rieunier *et al.*, 2021).

5 Chapter V: Recruitment of IGF-1R to chromatin binding sites *in vivo*

5.1 Introduction

As discussed in Section 1.6.2, our lab and others have detected recruitment of nuclear IGF-1R to chromatin (Aleksic *et al.*, 2010; Sehat *et al.*, 2010). The more recent work from our lab showed, in DU145 prostate cancer cells, that IGF-1R chromatin binding sites clustered at or near TSSs and 95% were coincident with RNAPolII binding. We showed that recruitment of both IGF-1R and RNAPolII to these regions was IGF-1 dependent, including recruitment to the *JUN* and *FAM21A* promoters. These genes were upregulated in response to IGF-1 and act as mediators of cell survival and IGF-induced migration, factors required by tumours to progress to an advanced stage (Aleksic *et al.*, 2018). Given these functions and the association of nuclear IGF-1R with adverse survival in renal cancer (Aleksic *et al.*, 2010), and advanced tumour stage in prostate cancer (Aleksic *et al.*, 2018), as well as the relatively low number (62) of unique IGF-1R chromatin binding sites detected in DU145 (Aleksic *et al.*, 2018), we therefore wanted to investigate the functional contribution of IGF-1R recruitment to chromatin *in vivo.* Notably, study of AR recruitment showed over 9000 extra chromatin binding sites for AR detected in clinical tissue compared to cell lines (Sharma *et al.*, 2013). We therefore aimed to perform IGF-1R ChIP-seq from fresh frozen prostate tissue, analysing levels of recruitment in comparison to the *in vitro* cell line data. We also aimed to assess recruitment of IGF-1R to AREs, in light of the crosstalk between AR signalling and the IGF-axis (Krueckl *et al.*, 2004; Turney *et al.*, 2011) and the contribution of the IGF-axis to androgen independence, as previously discussed in Section 1.4. This could not be assessed in cell line data as the cell line used, DU145, is AR negative. We also planned to analyse any detected sites of IGF-1R

recruitment in comparison to publicly available data on RNAPolII recruitment sites, given the interaction between RNAPolII and IGF-1R and the IGF-dependent RNAPolII recruitment to chromatin, previously reported by our lab (Aleksic *et al.*, 2018).

Overall, these experiments aimed to assess the contribution of nuclear IGF-1R to activation of genes involved in growth, proliferation, and cancer progression via direct interaction with regulatory regions of chromatin *in vivo.* The first aim was to validate and optimise IGF-1R ChIP from fresh frozen tissue samples obtained from either biopsy from radical prostatectomies (RPs) or tissue surplus to diagnostic need from transurethral resection of the prostate (TURP) operations.

5.2 Results

5.2.1 Testing for IGF-1R ChIP from TURP tissue samples

Initial tissue samples were obtained from surplus tissue from TURP operations (Table 5.1). These samples were cut on ice using scalpels, before fixation followed by homogenisation using a FastPrep Tissue homogeniser, as described in Materials and Methods (see Section 2.11.2). These tissues consisted of approximately 0.7-2.0 g of material, generating enough chromatin for at least a negative control and IGF-1R ChIP, and in some cases also an RNAPolII ChIP positive control.

Following homogenisation and before sonication, DNA fragment size was assessed by analysing a small amount of chromatin by agarose gel electrophoresis. In these cases, following homogenisation, fragment size was found to be approximately within the desired range of 150–500 bp for ChIP (Figure 5.1). Therefore, these samples did not undergo sonication to further fragment the DNA, and chromatin was processed using antibodies for the relevant ChIP condition or beads only negative control.

Sample Number	Malignant/Benign	Gleason Grade	Grade Group	Castrate resistant prostate cancer?
TURP 1	>80% of chippings contain prostatic adenocarcinoma	4+5 = 9*	5*	Yes
TURP 2	Approx 50% of chippings contain prostatic adenocarcinoma	N/A**	N/A**	Yes
TURP 3	Benign	-	-	Yes
RP 1	Benign	7 (3 + 4)	2	No
	Malignant			
RP 2	Benign	7 (3 + 4)	2	No
	Malignant			
	Malignant			
RP 3	Benign	7 (3 + 4)	2	No
	Malignant			
RP 4	Benign	7 (3 + 4)	2	No
	Malignant			
RP 5	Benign	7 (3 + 4)	2	No
	Benign			
RP 6	Benign	7 (3 + 4)	2	No
	Malignant			

Table 5.1 List of fresh frozen human prostate tissue samples collected for ChIP
List of TURP tissue samples (TURP 1-3) and tissue biopsies from radical prostatectomies (RP 1-6) collected for ChIP experiments. Sample number was assigned based on the order in which tissue samples were collected. Benign vs malignant status and Gleason grade for collected biopsies was confirmed histologically by Oxford Centre for Histopathology Research (OCHRe). This status could not be confidently assigned for TURP samples as the tissue collected was that which was surplus to diagnostic need (i.e., not the same chippings processed for routine Uro-Pathology assessment), and due to the nature of the procedure results in a mixture of tissue types. These patients had rising PSA on endocrine therapy indicating castrate resistant prostate cancer. *Gleason score may not be reliable in patients treated with endocrine therapy. **Gleason grade not assigned. Patients donating RP biopsies 1-6 were all previously untreated.

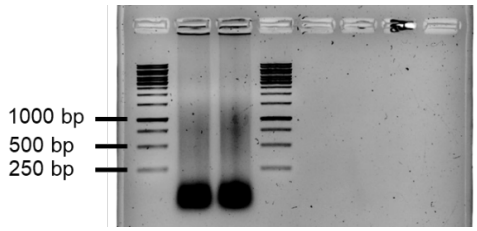


Figure 5.1 Agarose gel showing DNA fragment sizes of homogenised TURP tissue
Agarose gel showing DNA fragment size of TURP tissue sample that had been homogenised but not sonicated. Both lanes are from the same TURP sample and 2.5% of obtained chromatin was loaded (5 µl out of 200 µl used for ChIP).

To test for successful ChIP, qPCR was used with primers for the *JUN* and *FAM21A* promoters, known and validated regions of both IGF-1R and RNAPolII recruitment from the previous *in vitro* data (Aleksic *et al.*, 2018) and confirmed in this project (Section 4.2.2.2, Figure **4.7**). Results from these initial TURP samples were mixed, showing: no RNAPolII recruitment at either region but recruitment of IGF-1R (TURP 1, Figure 5.2a), recruitment of RNAPolII and IGF-1R, but with IGF-1R recruitment at a much higher level than RNAPolII (TURP 2, Figure 5.2b) or a low level of recruitment of IGF-1R to both regions (TURP 3, Figure 5.2c).

As the previous *in vitro* data showed, RNAPolII recruitment was detected at both *JUN* and *FAM21A* promoter regions (Aleksic *et al.*, 2018). However, no RNAPolII recruitment at all could be detected in the sample from TURP 1, raising potential questions about the validity of the result seen for IGF-1R recruitment (Figure 5.2a). In the sample from TURP 2 there was an approximate 4-fold enrichment for RNAPolII recruitment, similar to results in DU145 cells (Aleksic *et al.*, 2018), but the approximately 200-fold increase in recruitment of IGF-1R vs control at the *JUN* promoter does not seem credible (Figure 5.2b). These findings contrast with the *in vitro* data, as the level of IGF-1R recruitment seen here was much higher than those detected in DU145 cells (6 – 8-fold enrichment) (Aleksic *et al.*, 2018). The data for recruitment of both RNAPolII and IGF-1R to the *JUN* promoter in TURP 2 are in contrast to the 4-fold increase in RNAPolII and 2-fold increase in IGF-1R recruitment at the *FAM21A* promoter from the same sample (Figure 5.2b), data which were more in line with previous results *in vitro* (Section 4.2.2.2, Figure **4.7** and (Aleksic *et al.*, 2018)). Finally, TURP 3 had a smaller amount of starting tissue, and therefore generated enough chromatin for only a negative control and IGF-1R ChIP. In this case, IGF-1R recruitment could be detected at both promoter regions at 1.5-2-fold above that of control, although with lower fold enrichment than in the other samples. (Figure

5.2c). Lower levels of IGF-1R recruitment may be due to the benign histology of the tissue for this case (Table 5.1) although the chippings obtained for ChIP may have contained a small amount of cancer.

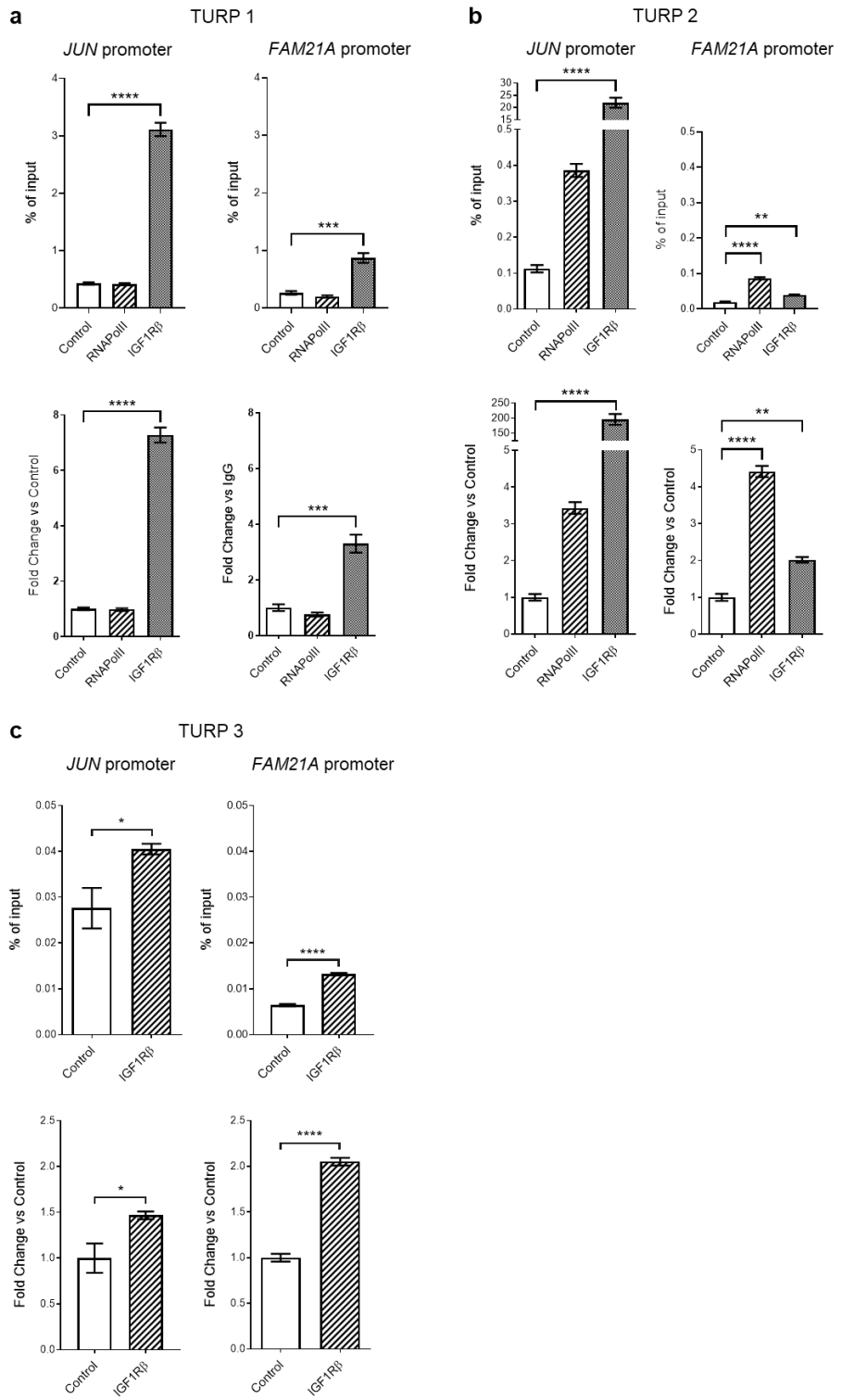


Figure 5.2 ChIP-qPCR validation of recruitment of RNAPolII and IGF-1Rβ at the *JUN* and *FAM21A* promoter regions in TURP tissue samples

a-c Graphs showing ChIP-qPCR quantification of fold change recruitment of RNAPolII and IGF-1R to the *JUN* and *FAM21A* promoters in tissue samples from TURP 1 (**a**), 2 (**b**) and 3(**c**). Tissue samples were homogenised and processed for ChIP-qPCR with beads only control or with antibodies for IGF-1R or phospho-RNAPolII (RNA polymerase II CTD repeat YSPTSPS (phospho S2)). Results represent mean ± SEM of 3 technical replicates from a single experiment. (p*<0.05, p**<0.005, p*** < 0.0005, p**** < 0.0001, One-way ANOVA (**a** and **b**) or unpaired t test (**c**)).

This variation in results may have been due to a variety of factors. Firstly, the tissue obtained from TURPs was tissue surplus to diagnostic need, and due to the nature of the operation, was likely to be a mixture of both benign and malignant tissue. Previous work from our lab has shown that nuclear IGF-1R is more frequently detected in malignant prostate epithelia and rarely detected in benign epithelia (Aleksic *et al.*, 2018), therefore the difference in detected IGF-1R recruitment between samples may have been due to differing proportions of malignant vs benign tissue present. It is also likely that there was a difference in levels of nuclear IGF-1R within and between malignant portions of collected samples, which could have been assessed if parallel samples were available for IHC staining. As the tissue samples were initially sliced by hand using a scalpel it is likely that tissues were not sliced into the same size tissue fragments each time. This therefore would have also affected downstream processes including fixation and homogenisation of the tissue, processes that may have been less efficient with larger portions of tissue, potentially resulting in different ChIP efficiency.

Due to the COVID-19 related national restrictions, non-essential operations including TURPs were put on hold, thereby limiting the collection of these tissue samples. On resumption of lab work, we decided to proceed with ChIP from tissue samples obtained via biopsies from RPs only, due to a variety of factors. While the mass of tissue obtained from a biopsy, approximately 0.1-0.3g, was lower than that obtained from excess TURP tissue, the biopsy tissues obtained were confirmed by histology to be benign or malignant tissue. This avoids the issue of having a mix of tissue types as was the case with TURP tissue samples. Alongside the biopsy samples, parallel tissue sections can also be taken from these RPs for IHC, allowing staining and quantification of levels of IGF-1R. This would allow for assessment of levels of nuclear IGF-1R in each case and may explain any differences in levels of IGF-1R recruitment to chromatin between samples. From a

practical standpoint, RP procedures also resumed at a quicker and more regular rate than TURPs following easing of COVID-19 restrictions, allowing for quicker collection of samples. The following section outlines the optimisation of ChIP experiments from these small tissue biopsy samples.

5.2.2 Validation of IGF-1R ChIP from biopsy tissues from radical prostatectomies

From each RP, both a benign and a malignant biopsy was obtained for experimental work (Table 5.1). Initial optimisation experiments used benign biopsy samples to ensure the ChIP protocol worked correctly, before using malignant biopsies to generate samples for IGF-1R ChIP-seq.

As with TURP tissue, biopsy tissues were initially sliced by hand using a scalpel and homogenised using the FastPrep tissue homogeniser (see Section 2.11.2). A small volume of chromatin (2.5% of material used for ChIP) was analysed by agarose gel electrophoresis to assess DNA fragment size, as before, showing that fragments ranged from 600 bp and over. To improve fragmentation, chromatin was sonicated using a Pico Sonicator which reduced the fragment size to between 150-500 bp (Figure **5.3**). For initial optimisation, ChIP was then performed for RNAPolII as a positive control, however enrichment of RNAPolII at the *JUN* promoter region could not be detected by qPCR and input samples gave high Ct values in an initially tested benign biopsy (RP 1,

Table **5.2**). ChIP DNA sample concentrations were then measured, and input DNA concentration was found to be much lower (19 – 25 ng/µl) than those from previous *in vitro* cell line samples (235.5 ng/µl) (

Table **5.3**). High Ct values and low DNA concentrations suggested there was a low concentration of starting material, potentially due to inefficient lysis of biopsy tissue.

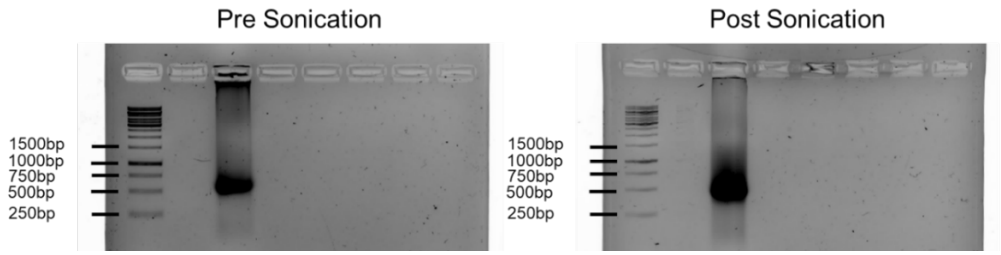


Figure 5.3 Agarose gels showing DNA fragment size pre- and post-sonication
Agarose gels showing DNA fragment size of processed RP 1 benign biopsy sample. DNA fragment size was found to be approx. 600 bp following homogenisation (Pre sonication, left). The sample was then sonicated, reducing fragment size ≤ 500 bp (Post sonication, right), before being processed for ChIP.

ChIP Condition	Ct Values	Average Ct Value
Input	28.17216	
	28.15791	
	28.12923	28.1531
Beads only control	30.02311	
	29.64405	
	29.77071	29.81262
RNAPolII	29.82051	
	29.7242	
	29.76894	29.77122

Table 5.2 ChIP-qPCR Ct values from benign biopsy sample
Table showing ChIP-qPCR Ct values from RP 1 benign biopsy using primers for the *JUN* promoter. Similar average Ct values for both beads only control and RNAPolII ChIP conditions shows there was no enrichment of RNAPolII. Similarly high Ct values for input samples suggests low amounts of starting material.

Sample	ChIP Condition	Concentration (ng/µl)	260/280
DU145 (*in vitro* ChIP)	Input	235.5	1.47
	Beads only control	68.1	1.76
	RNAPolII	74.0	1.51
RP 1 Benign Biopsy	Input	19.9	1.46
	Beads only control	22.8	1.53
	RNAPolII	6.8	1.49
RP 2 Benign Biopsy	Input	25.0	1.59
	Beads only control	15.7	1.48
	RNAPolII	14.7	1.42

Table 5.3 Concentration of ChIP DNA samples from DU145 and benign biopsy samples
Table showing concentrations of ChIP DNA generated from DU145 cells and benign tissue biopsies from RP 1 and 2. Concentration of Input DNA samples from tissue biopsies were much lower than the input DNA generated from DU145.

To improve this method, the tissue biopsy ChIP protocol published by (Singh *et al.*, 2019), was adapted for use here. As outlined in Materials and Methods (see Section 2.11.3), tissue samples were now sliced using a Leica CM1950 cryostat into 30 µm slices at -20ºC, before fixation and homogenisation using a pellet pestle homogeniser. This ensured consistent slicing thickness of tissue, and the thinner tissue slices also likely increased efficiency of fixation and homogenisation. To check whether suitable starting material for ChIP was now present, 10% of chromatin following homogenisation of an initially tested benign biopsy (RP 4) was analysed by Western blot alongside 22Rv1 whole cell extract. Both IGF-1R and histone H3, another protein detectable by ChIP at the *JUN* and *FAM21A* promoters (Figure 5.4a), could be successfully detected in the chromatin sample from homogenised benign biopsy tissue, therefore suggesting enough protein was present for ChIP (Figure 5.4b).
DNA fragment size was again analysed by agarose gel electrophoresis, and the chromatin was sonicated to give fragments 150-500 bp in size, before being processed for ChIP using beads only (control) or H3K4me1 antibody. ChIP DNAs were then analysed by qPCR using primers for both the *JUN* and *FAM21A* promoter regions and showed approximately 18- and 200-fold H3K4me1 enrichment respectively in H3K4me1 ChIP vs control at both regions (Figure 5.4c).
Furthermore, the input Ct values were much lower (range 20-23 compared with 28-30 previously,
Table **5.2**) indicating that the new protocol had improved tissue lysis and chromatin yield considerably.

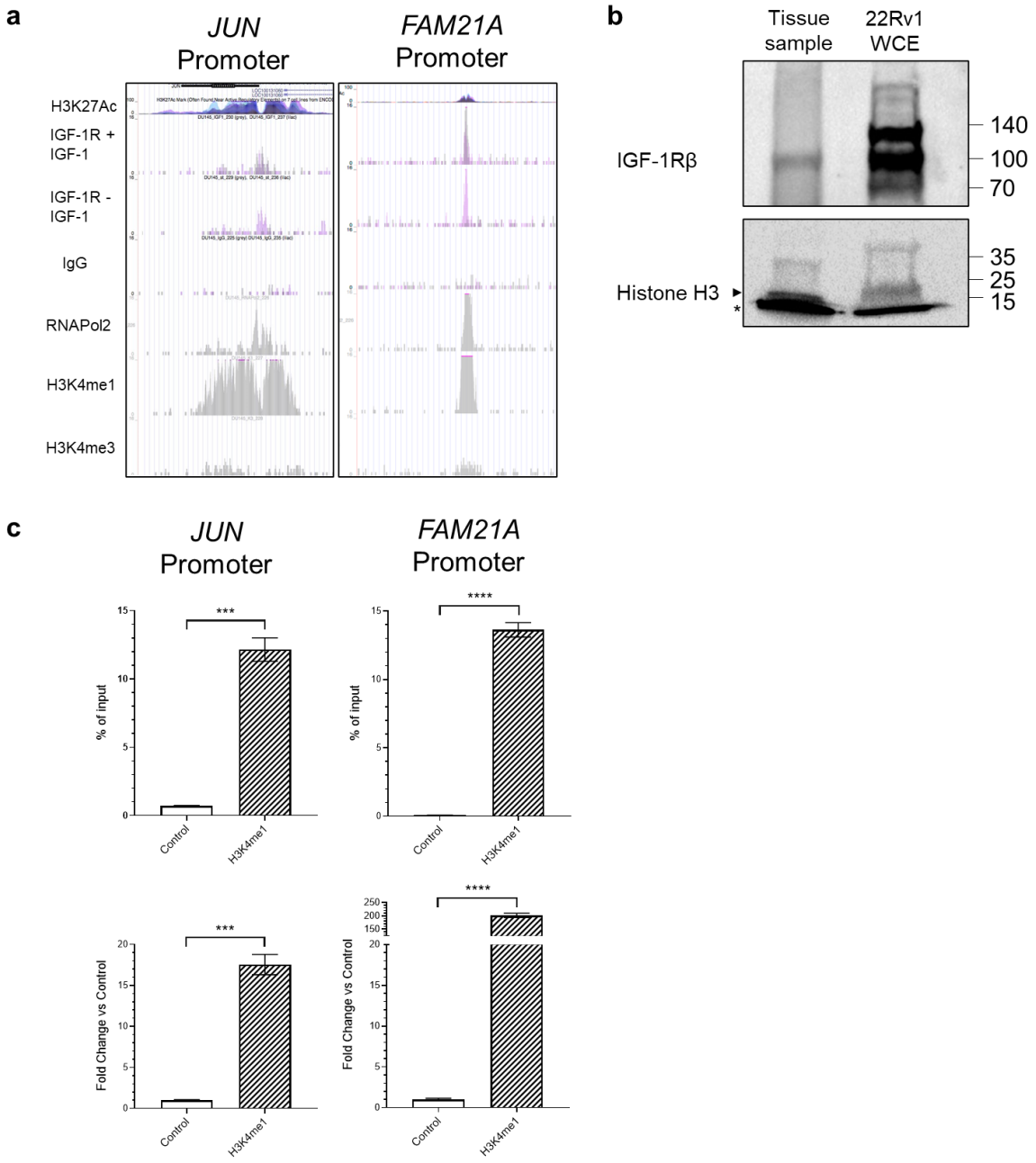


Figure 5.4 Western blot validation and ChIP-qPCR from benign tissue biopsy
a UCSC genome browser image showing recruitment of H3K4me1 to the *JUN* and *FAM21A* promoter regions which are also sites of IGF-1R recruitment (Aleksic *et al.*, 2018). **b** Western blot showing detection of IGF-1Rβ and Histone H3 in RP 4 benign biopsy sample (50 µg) homogenised using the method from (Singh *et al.*, 2019), alongside 22Rv1 whole cell extract (WCE, 70 µg) positive control. Arrowhead: histone H3. Asterisk: signal likely due to dye front. **c** ChIP-qPCR quantification showing enrichment of H3K4me1 histone mark at both the *JUN* and *FAM21A* promoter regions in the RP 4 benign biopsy analysed in **b**. Graphs show both % of input (top) and Fold Change vs Beads only control values (bottom). Results represent mean ± SEM of triplicate technical replicates. (p*** < 0.0005, p**** < 0.0001, One-way ANOVA).

Following this successful detection of enrichment of H3K4me1 from ChIP performed on chromatin extracted from a benign biopsy, collected malignant biopsies were then processed for ChIP using the modified method from (Singh *et al.*, 2019) and chromatin was processed for ChIP using beads only (control) or IGF-1R antibody. However, enrichment of DNA in IGF-1R ChIP vs control could not be detected by qPCR using primers for the *JUN* promoter (Figure 5.5a).

To determine if the ChIP process was working correctly, further malignant biopsy samples were processed for control (beads only) and IGF-1R ChIP, as previously, as well as H3K4me1 as a positive control. ChIP-qPCR using primers for the *FAM21A* promoter region showed detectable H3K4me1 enrichment vs control ChIP in all tissue samples processed, suggesting that the protocol was fundamentally sound (Figure 5.5b). IGF-1R recruitment could be detected in only one of the samples (RP 5) and not in the other 5 malignant samples. The reasons for this difference are unclear. Although samples were processed using the same protocol, homogenisation and sonication may have resulted in DNA fragments of varying sizes that were not spanned by the primers used. Lack of detected IGF-1Rβ recruitment may also be due to differing levels of nuclear IGF-1R between tissue samples.

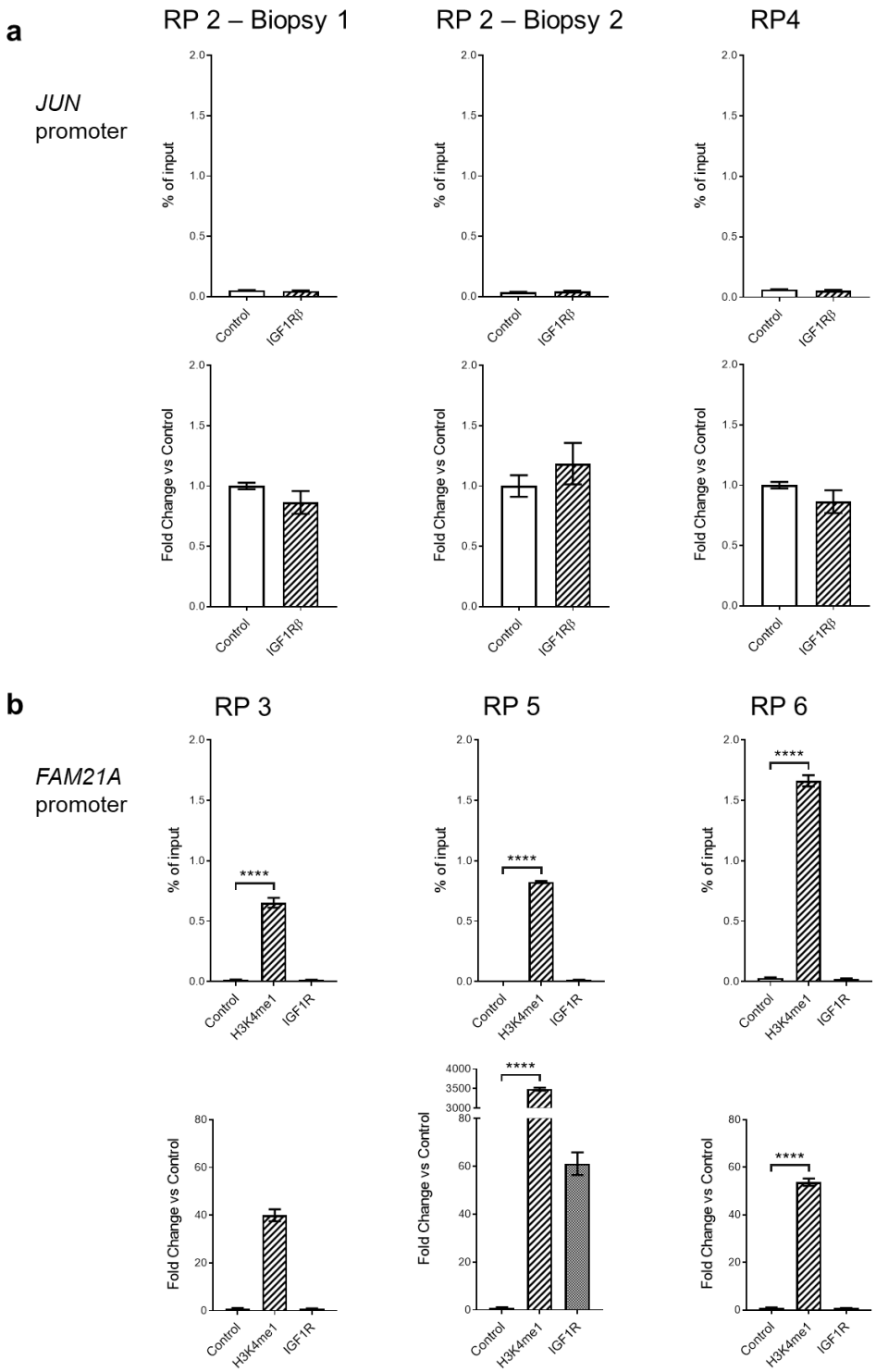


Figure 5.5 ChIP-qPCR quantification of IGF-1Rβ ChIP from malignant tissue biopsies

a ChIP-qPCR quantification showing no enrichment of IGF-1Rβ from the indicated patient malignant biopsies using primers for the *JUN* promoter, showing both % of input (top) and Fold Change vs Beads only control (bottom). Results represent mean ± SEM of triplicate technical replicates and differences in data were not found to be significant by unpaired t test. **b** ChIP-qPCR quantification showing enrichment of IGF-1R and H3K4me1 histone marker from the indicated malignant biopsies at the *FAM21A* promoter, showing both % of input (top) and Fold Change vs Beads only control (bottom). Results represent mean ± SEM of 3 technical replicates. (p**** < 0.0001, One-way ANOVA).

Detectable H3K4me1 enrichment in these ChIP experiments suggests that the ChIP protocol was sound. Therefore, the ChIP DNAs after ChIP-qPCRs shown above were sent for sequencing. In total, 16 samples were sequenced including an input control and samples from the 3 malignant biopsies processed for control (beads only), H3K4me1 and IGF-1R ChIP (9 DNA samples, Figure 5.5b). The ChIP DNAs from the 3 initially processed malignant biopsies that were processed for control and IGF-1R ChIP (6 DNA samples, Figure 5.5a) were also sent for sequencing. These samples are summarised in Table 5.4. The malignant sample from RP 1 was used during protocol optimisation, and therefore was not sent for sequencing analysis.

Sample No.	IGF-1R recruitment		H3K4me1 recruitment	
	Tested	Detected	Tested	Detected
RP 2 – biopsy 1	Yes	No	No	No
RP 2 – biopsy 2	Yes	No	No	No
RP 3	Yes	No	Yes	Yes
RP 4	Yes	No	No	No
RP 5	Yes	Yes	Yes	Yes
RP 6	Yes	No	Yes	Yes

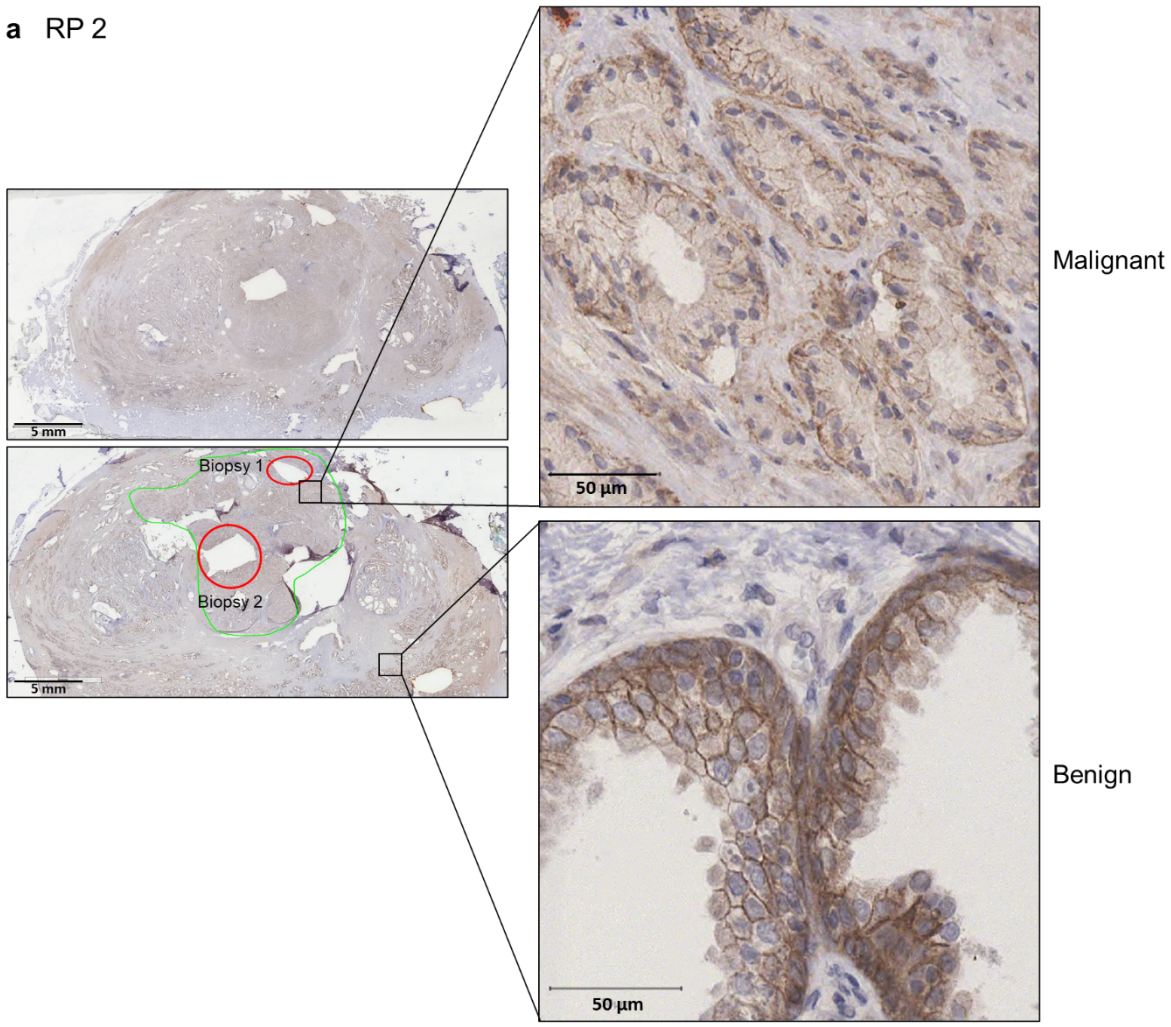
Table 5.4 Table summarising the RP biopsy samples tested by ChIP-qPCR and sent for sequencing
Table summarising the RP biopsy samples analysed by ChIP-qPCR, as shown in (Figure 5.5) and sent for sequencing analysis. Both of the RP 2 biopsies were malignant biopsies taken from the same RP patient.

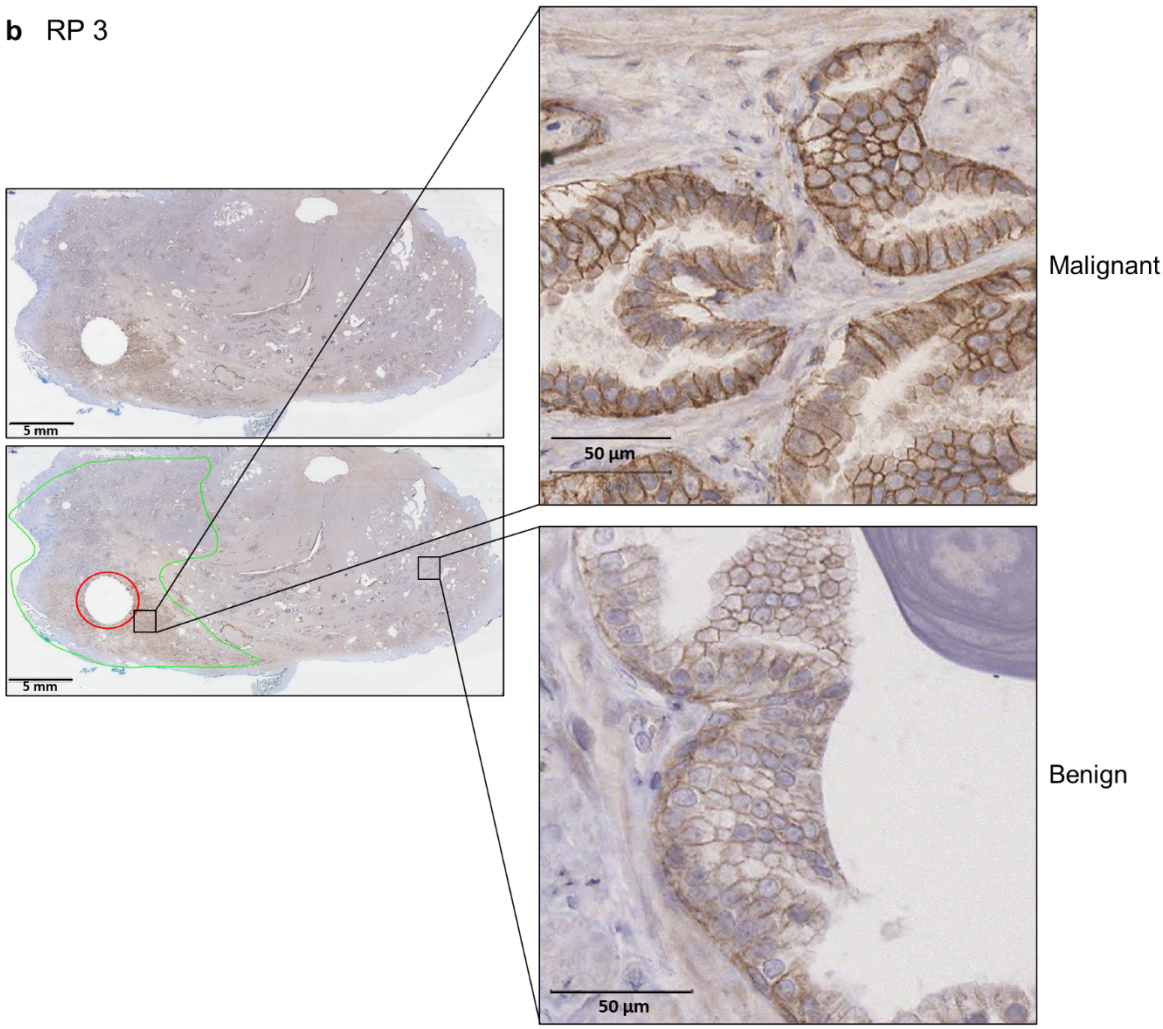
5.2.3 IGF-1R IHC staining of parallel RP tissue sections

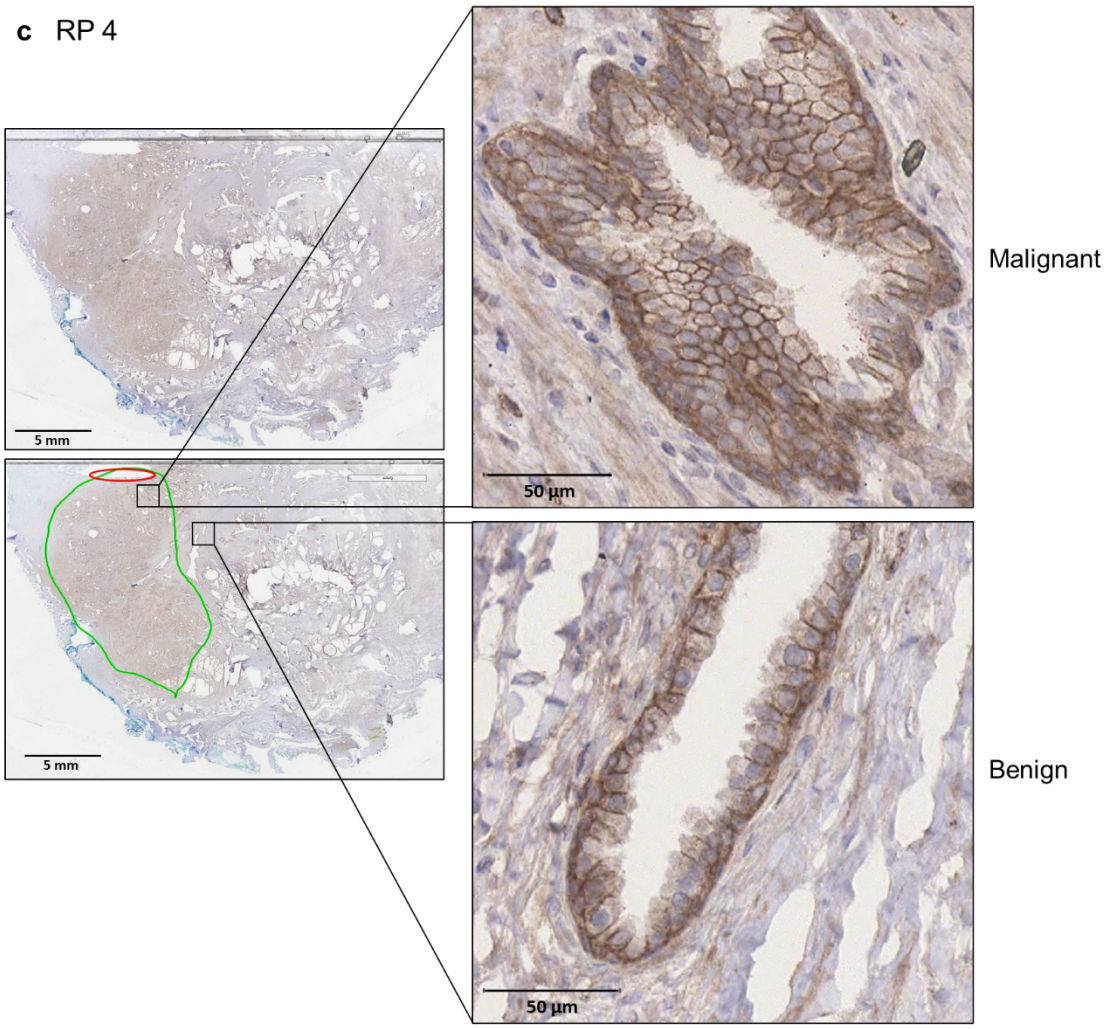
Along with fresh frozen biopsy samples, parallel FFPE sections from the same RPs were obtained, stained by IHC for IGF-1R and scored by Prof Verrill, focusing on the areas around the punch biopsy sites (Figure 5.6). There was more IGF-1R staining in malignant versus benign areas (Figure 5.6), consistent with previous work from our lab (Hellawell *et al.*, 2002) and in all cases at least 80% of cells were positive for cytoplasmic IGF-1R staining, and at least 90% of cells were positive for membrane IGF-1R staining (Table 5.5). However, Prof Verrill detected no nuclear IGF-1R in any of the stained RP sections

(Table 5.5). This lack of nuclear IGF-1R contrasts with our previous work which detected strong nuclear staining by IHC in ~50% of a much larger set (n = 137) of cases treated by radical prostatectomy (Aleksic *et al.*, 2018). This may explain the lack of detected recruitment of IGF-1R to chromatin by ChIP-qPCR from the biopsy tissues processed for ChIP-seq (Figure 5.5).

Absence of detectable nuclear IGF-1R here could be due firstly to the small number of cases processed. The cases collected were from a limited range of grades and stages (Table 5.6), the majority of which were localised to the prostate (pT2). As nuclear IGF-1R is associated with a more advanced tumour stage in prostate cancer (Aleksic *et al.*, 2018), these cases may have contained levels of nuclear IGF-1R that were below the threshold of detection by IHC. Secondly, there may be different sensitivity thresholds for IGF-1R detection in the nucleus by IHC vs recruitment to chromatin by ChIP-qPCR, as suggested by positive signal for IGF-1R recruitment in RP 5 with negative nuclear IGF-1R by IHC (Figure 5.5d, Table 5.5). Thirdly, while Prof Verrill commented that the IHC looked acceptable and consistent with previous patterns (aside from lack of nuclear signal), there may have been technical issues such as small differences in antigen retrieval or different lots of antibody (although the antibody used is monoclonal), that affected ability to detect nuclear IGF-1R signal. Due to time constraints, FFPE sections for IHC (Figure 5.6) could not be obtained until after biopsy samples had been processed for ChIP-seq. If time and finances had permitted, a larger number of biopsy samples from a wider range of cases at different tumour stages would have been obtained. Staining of parallel FFPE sections would then have been performed first, to identify samples with positive nuclear IGF-1R staining. Biopsies from these samples would have then been selected for IGF-1R ChIP-qPCR and ChIP-seq to increase the likelihood of positive ChIP signals.


a RP 2
5 mm
Biopsy 1
Biopsy 2
5 mm
50 µm
Malignant
50 µm
Benign


b RP 3
5 mm
5 mm
50 µm
50 µm
Malignant
Benign


c RP 4
5 mm
5 mm
50 µm
50 µm
Malignant
Benign

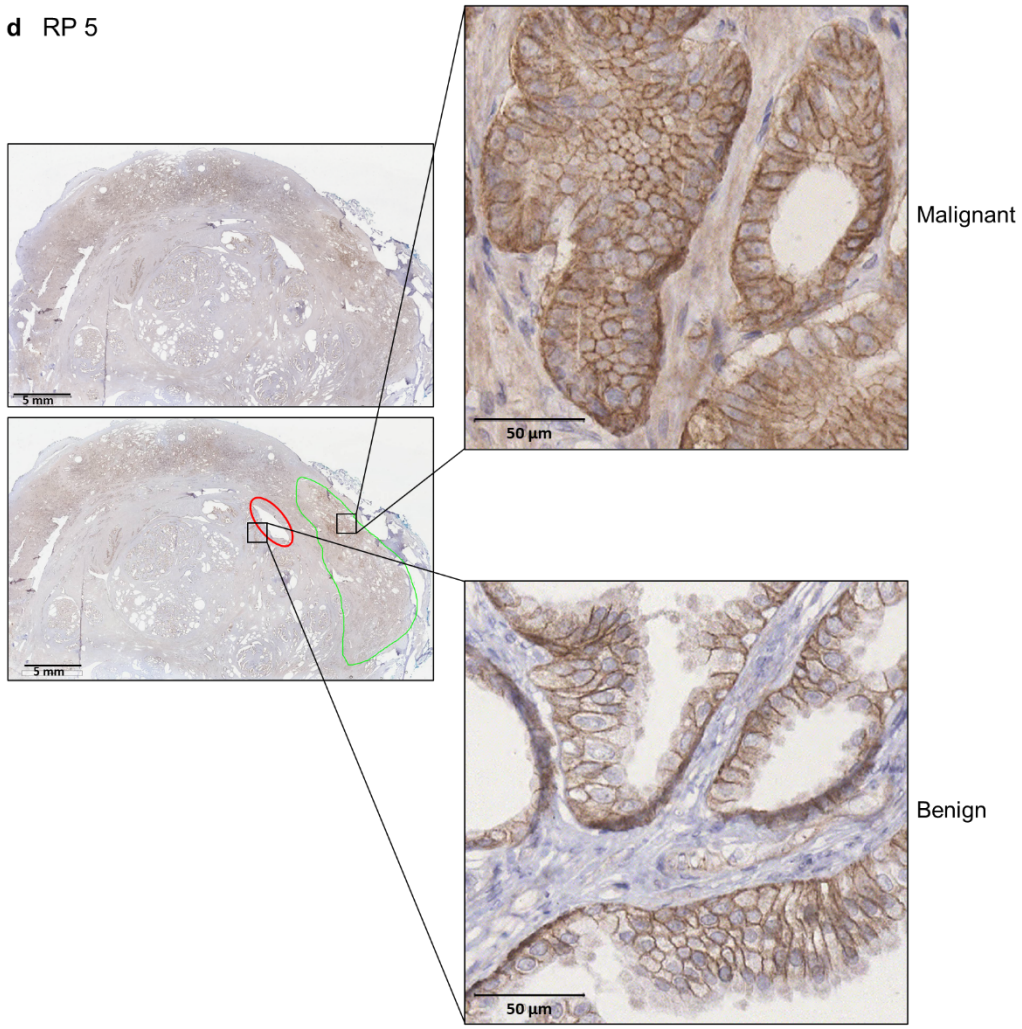


Figure 5.6 IHC staining of IGF-1R in FFPE sections of RPs from which biopsies were analysed by ChIP-seq

a-e IHC staining of IGF-1R in FFPE sections taken from RPs from which biopsies were obtained and processed for ChIP-seq. Images represent sections from RPs from RP 2 (**a**), 3 (**b**), 4 (**c**) and 5 (**d**). Left: images of whole stained sections, lower image shows same images annotated for malignant areas (encircled by green line) and site of biopsy punch processed for ChIP-seq (red circle). Scale bar 5 mm. Right: higher power images of malignant (top) and benign (bottom) areas, as indicated, of the stained tissue section. Scale bar 50 µm. Although initially identified as containing tumour, biopsy punch from RP 5 (**d**) appeared to have been taken on the borderline of the malignant area of tissue. IHC staining was performed with the help of Jinseon Kim (Selena), Research Assistant in our lab, and identification of malignant areas was performed by Prof Clare Verrill.

Patient No.	Nuclear Score	Nuclear Percentage	Nuclear Percentage Score	Nuclear IR Score	Cytoplasmic Score	Cytoplasmic Percentage	Cytoplasmic Percentage Score	Cytoplasmic IR Score	Membrane Score	Membrane Percentage	Membrane Percentage Score	Membrane IR Score	H3K4me1 recruitment detected?	IGF-1R recruitment detected?
RP 2	0	0	0	0	1	100	4	4	2	80	3	6	Yes	No
RP 3	0	0	0	0	1	100	4	4	3	100	4	12	Yes	No
RP 4	0	0	0	0	2	100	4	8	3	100	4	12	Yes	No
RP 5	0	0	0	0	3	100	4	12	3	100	4	12	Yes	Yes

Table 5.5 IHC scoring of IGF-1R in FFPE tissue sections

Scoring of IGF-1R IHC shown in Figure 5.6. Scoring was performed by Prof Clare Verrill as per (Aleksic *et al.*, 2018) (See Section 2.10.2). Nuclear, cytoplasmic and membrane scores were ranked as 0, nil; 1, weak; 2, moderate; 3, heavy. Percentage scores were calculated from the percentage of cells showing relevant subcellular staining and ranked as 0: 0%; 1: 1-10%; 2: 11-50%; 3: 51-80%; 4: 81-100%. Immunoreactivity (IR) scores were calculated from relevant subcellular score multiplied by percentage score. ChIP-qPCR detection of H3K4me1 and IGF-1R recruitment in relevant paired biopsies (shown in Figure 5.5) is also indicated. No nuclear IGF-1R staining could be convincingly identified in RPs 2-5. An FFPE section for RP 6 could not be obtained.

Patient No.	Cancer Type	Gleason Grade	Grade Group	Tumour Stage
RP 2	Prostatic Adenocarcinoma	7 (3 + 4)	2	pT2
RP 3	Prostatic Adenocarcinoma	7 (3 + 4)	2	pT3a
RP 4	Prostatic Adenocarcinoma	7 (3 + 4)	2	pT2
RP 5	Prostatic Adenocarcinoma	7 (3 + 4)	2	pT2
RP 6	Prostatic Adenocarcinoma	7 (3 + 4)	2	pT3a

Table 5.6 Clinical data for cases from which biopsies were obtained

Grade and pathological stage (pT) data for all cases from which biopsies were obtained and processed for ChIP-seq. As shown, all cases were of the same Gleason Grade, and most cancers were localised to the prostate (pT2). pT3a indicates extraprostatic extension.

5.2.4 Analysis of *in vivo* IGF-1R ChIP-seq data

Traditionally, the peak calling software MACS2 (Zhang *et al.*, 2008) is used as the gold standard when analysing ChIP-seq data sets. MACS2 uses statistical tests to differentiate enrichment at the region versus background using a matched negative control. This simplifies signal at a given region from information-dense peak shapes into a single standardised value (maximum peak height) which is then used to calculate a p value for enrichment. Regions that are found to be statistically significantly enriched are identified as peaks and then visualised using the separate UCSC genome browser (Zhang *et al.*, 2008). However, this statistical approach can lead to the presence of false negatives due to failed detection of differently shaped regions of enrichment, which on further analysis can be consistently and correctly identified as an enriched peak by visual assessment in a genome browser programme (Hocking *et al.*, 2017). This limitation has led to the development of LanceOtron, a deep-learning based peak caller optimised for open chromatin, transcription factor and chromatin modification ChIP-seq data (Hentges *et al.*, 2021). This web browser-based tool combines enrichment calculations with the shape of the signal peak to identify enriched regions and calculate their peak score, p-value, peak height and peak width. An in-built peak visualisation interface is used to visualise enrichment peaks and set specific detection thresholds for each dataset. Optimisation of this programme showed that LanceOtron outperformed MACS2 across a range of datasets and data types, with peaks uniquely identified by LanceOtron found to be enriched for enhancers or promoters (Hentges *et al.*, 2021).

To investigate potential use of this software to analyse the *in vivo* IGF-1R ChIP-seq data generated here, Dr Avigail Taylor, Post-Doctoral Bioinformatician in our lab, used LanceOtron to re-analyse previously obtained *in vitro* IGF-1R ChIP-seq data from DU145 cells (Aleksic *et al.*, 2018). In the original analysis, performed by Dr Nicki Gray,

(Computational Biology Research Group, Weatherall Institute of Molecular Medicine), the 'Narrow Peaks' caller function of MACS2 was used to identify peaks of IGF-1R enrichment in duplicate independent IGF-1R ChIPs (sample numbers 230, 237) each called against duplicate control IgG ChIPs (samples 225, 235). IGF-1R ChIP was performed on both DU145 prostate cancer cells and SK-N-MC Ewing sarcoma cells. ChIP-seq analysis detected 62 and 66 IGF-1R chromatin binding sites in each cell line respectively, with 25 sites common between the two cell lines. ChIP was performed on serum-starved and IGF-treated DU145 cells, but analysis focused on peaks in the IGF-treated ChIP-seq samples, with IGF-1R recruitment to the *JUN* and *FAM21* promoters undergoing validation (Aleksic *et al.*, 2018).

In addition to the 'Narrow Peaks' caller function of MACS2, re-analysis by Dr Taylor also used the 'Broad Peaks' function, which had not been used in the previous analysis and identifies broader enrichment peaks that do not match the narrow and sharp peak enrichment profile of traditional transcription factors (Zhang *et al.*, 2008). This analysis showed that all peaks previously identified in Narrow Peaks MACS2 analysis were identified in both Broad Peaks MACS2 and in LanceOtron (Figure 5.7b). A higher number of IGF-1R enriched peaks were identified in Broad Peaks MACS2 analysis (69) versus Narrow Peaks MACS2 (42) (Figure 5.7a), the majority of which were also identified by LanceOtron (Figure 5.7c). A much higher number of binding peaks were identified by LanceOtron, with 1922 peaks identified in total (Figure 5.7a), the majority of which were identified by LanceOtron only (Figure 5.7d). These findings are illustrated by the detection of the previously validated IGF-1R binding region at the *JUN* promoter (Aleksic *et al.*, 2018), detected by both MACS2 and LanceOtron (Figure 5.8a), and a potential IGF-1R binding site identified only by LanceOtron within the *TRIO* gene (Figure 5.8b), a gene involved in cell growth and migration (Bellanger *et al.*, 2000).

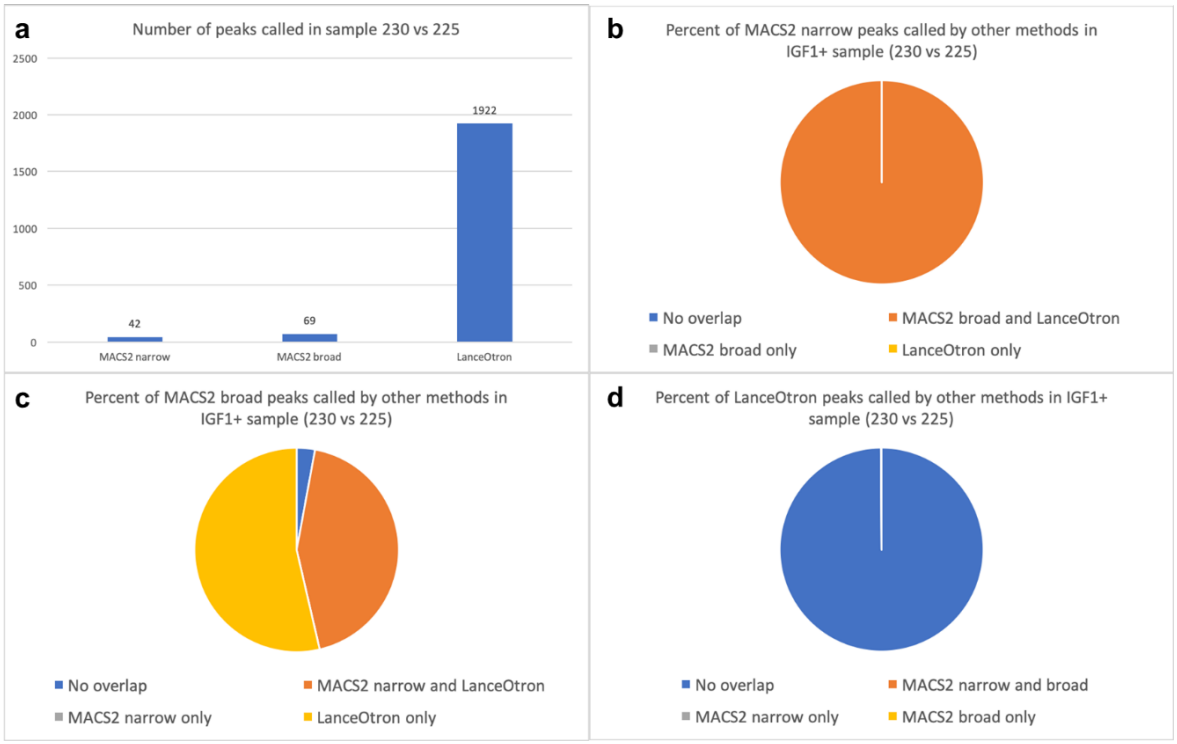


Figure 5.7 Peak calling by MACS2 and LanceOtron in IGF-1R ChIP-seq *in vitro* data
a The number of enrichment peaks from IGF-1R ChIP-seq in DU145 cells called by either MACS2 Narrow Peak parameters (42), Broad Peak parameters (69) or by LanceOtron (1922). **b-d** Pie charts showing the proportion of peaks identified by either MACS2 Narrow Peak parameters (**b**), MACS2 Broad Peak parameters (**c**) or LanceOtron (**d**) that were also identified by other indicated peak calling software. Sample 230 indicates IGF-1R ChIP sample, and Sample 225 indicates IgG control sample. Analysis and charts were generated by Dr Avigail Taylor. Peaks identified in differing peak calling software were deemed to be the same peak if they overlapped by at least 50%, but reciprocity was not required (See Section 2.17).

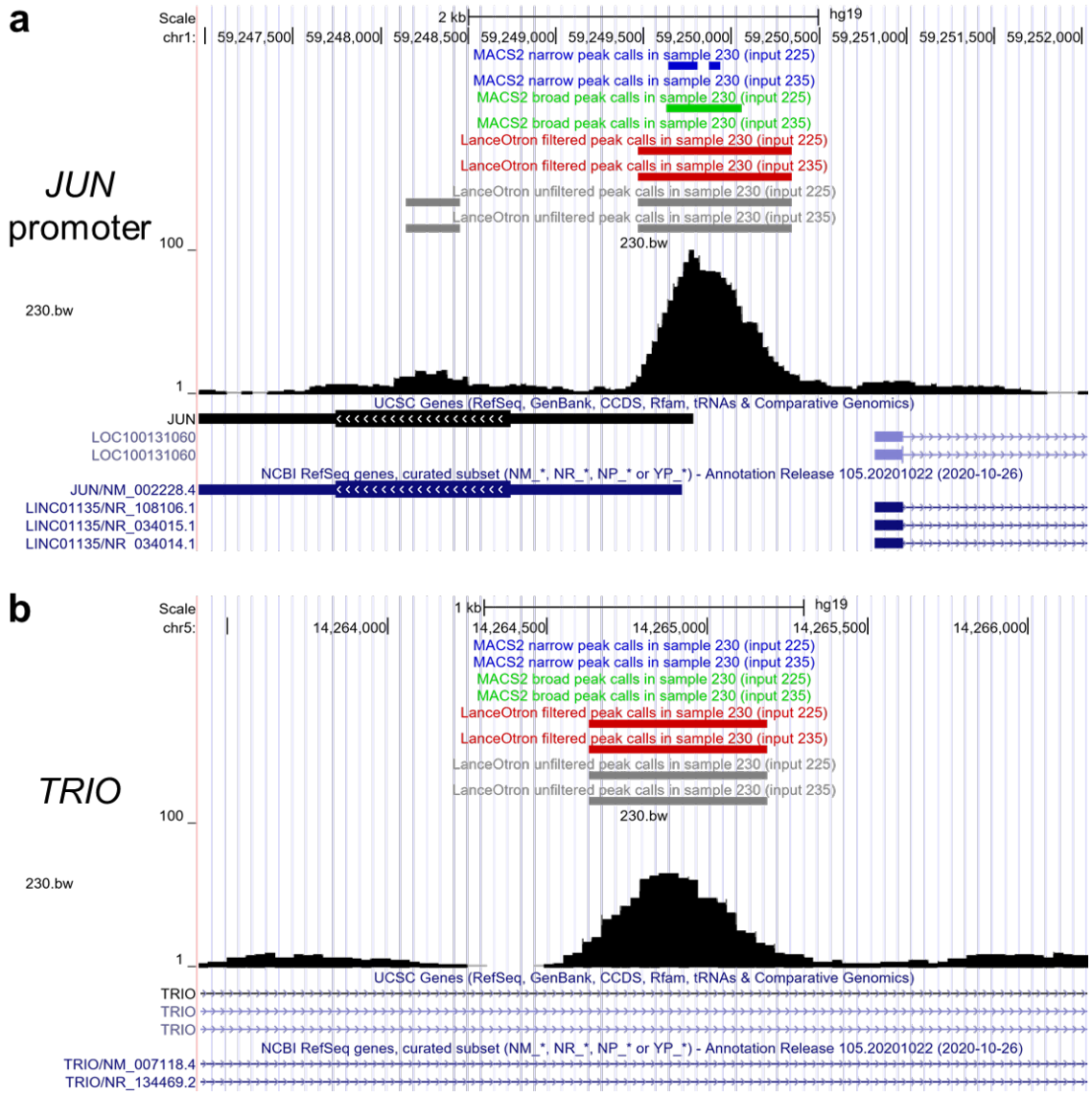


Figure 5.8 UCSC Genome Browser images showing IGF-1R binding peaks identified in MACS2 and LanceOtron

a-b UCSC genome browser images showing IGF-1R enrichment peaks at the *JUN* promoter on chromosome 1 (**a**) and within the gene *TRIO* on chromosome 5 (**b**). Blue and green bars above the enrichment peak at the *JUN* promoter (**a**) indicates identification of this region as an enrichment peak by MACS2 Narrow and Broad Peak parameters respectively. Absence of these bars above the enrichment peak in *TRIO* (**b**) indicates that this region was not identified as an enrichment peak by MACS2. In both cases, presence of red and grey bars indicates detection of these regions as enrichment peaks by LanceOtron both before and after filtering of the data (See Section 2.17). UCSC genome browser images were generated by Dr Avigail Taylor.

While the additional IGF-1R binding sites identified by LanceOtron still need validation by ChIP-qPCR, this analysis suggests that many potential IGF-1R binding regions may have previously been missed. Therefore, both MACS2 and LanceOtron were used by Dr Avigail Taylor to analyse the *in vivo* IGF-1R ChIP-seq data generated here.

ChIP-seq reads were aligned to the human reference genome (hg19), to allow for comparison to the previous *in vitro* ChIP-seq data which had been aligned to hg19. It is worth noting that on the advice of Dr Simon Engledow (OGC, University of Oxford), a 'Beads Only' negative control condition was used for this *in vivo* work, in contrast to an IgG negative control used in the previous *in vitro* work in our lab (Figure 5.7) (Aleksic *et al.*, 2018). Following filtering against enrichment in 'Beads Only' negative control samples, initial peak calling identified significantly enriched peaks in the order of tens of thousands for H3K4me1 positive control ChIP across all peak calling software programmes, consistent with the previous *in vitro* work in our lab (Aleksic *et al.*, 2018), and other work in the field (Sharma *et al.*, 2013; Hancock *et al.*, 2019; Singh *et al.*, 2019). Analysis also showed identification of peaks for IGF-1R binding in both Narrow and Broad peak MACS2 parameters, with between 23 – 878 IGF-1R peaks detected in the tissue samples (Table 5.7). Using Narrow peak parameters, the number of peaks detected were at a level similar to or greater than those identified in the *in vitro* cell line data (42) (Figure 5.7). Broad peak parameters identified ≥100 peaks in nearly all tissue samples, a higher number than previously identified *in vitro* (69) (Figure 5.7). Identification of these peaks represented successful detection of IGF-1R recruitment across the genome in clinical cancers for the first time.

Patient No.	ChIP Condition	MACS2 Narrow Peaks	MACS2 Broad Peaks
RP 2 – biopsy 1	IGF-1R	42	118
RP 2 – biopsy 2	IGF-1R	144	225
RP 3	H3K4me1	45385	86660
	IGF-1R	188	269
RP 4	IGF-1R	46	179
RP 5	H3K4me1	68794	104027
	IGF-1R	230	878
RP 6	H3K4me1	40483	74206
	IGF-1R	23	52

Table 5.7 Number of enrichment peaks identified by MACS2 from *in vivo* ChIP-seq data

Table showing the number of enrichment peaks identified by MACS2 using Narrow or Broad Peak parameters for both H3K4me1 and IGF-1R ChIP from malignant biopsy tissues processed in Figure 5.5. Both RP 2 biopsies were malignant biopsies taken from the same RP case. Peak calling was performed by Dr Avigail Taylor.

Using LanceOtron, initial analysis identified tens to hundreds of thousands of IGF-1R binding peaks across all samples (Table 5.8). Hits were then filtered using a peak quality score of 0.8 or greater, where 0 represents no peak and 1.0 represents a perfect peak. Only 13-65 peaks were detected by LanceOtron in the clinical samples (Table 5.8). Therefore, a lower number of peaks from *in vivo* IGF-1R ChIP-seq were identified by LanceOtron compared to MACS2, in contrast to the much higher number of peaks detected by only LanceOtron from the cell line data (Table 5.8). It is possible that a LanceOtron peak score cut off of 0.8 may be too high, potentially excluding legitimate enrichment peaks. While subsequent analysis used this data set filtered for a peak score of ≥0.8, if time had permitted, peak visualisation within LanceOtron would have been used, together with experimental peak validation, to optimise filter thresholds for peak scores.

Patient No.	ChIP Condition	LanceOtron (Unfiltered)	LanceOtron (Peak score ≥0.8)
RP 2 – biopsy 1	IGF-1R	142336	13
RP 2 – biopsy 2	IGF-1R	40473	41
RP 3	H3K4me1	124690	24550
	IGF-1R	127520	14
RP 4	IGF-1R	18066	37
RP 5	H3K4me1	133986	31924
	IGF-1R	121059	65
RP 6	H3K4me1	98515	16718
	IGF-1R	110857	17

Table 5.8 Number of enrichment peaks identified by LanceOtron from *in vivo* ChIP-seq data
Table showing the number of binding peaks identified by LanceOtron for H3K4me1 and IGF-1R ChIP from biopsy tissues processed in Figure 5.5. Table shows both the number of unfiltered peaks identified and the number of peaks remaining when filtering for peak score of 0.8 or over. Peak calling was performed by Dr Avigail Taylor.

Comparison of the IGF-1R peaks identified by each peak calling software showed that the majority of peaks identified by Narrow Peak MACS2 parameters were also identified by Broad Peak MACS2 parameters (Figure 5.9) Although a much lower number of peaks were identified *in vivo* by LanceOtron, as with previous analysis most of these peaks were identified by LanceOtron only. However, in contrast to *in vitro* data analysis, LanceOtron did not identify the majority of Broad parameter MACS2 peaks (Figure 5.9).

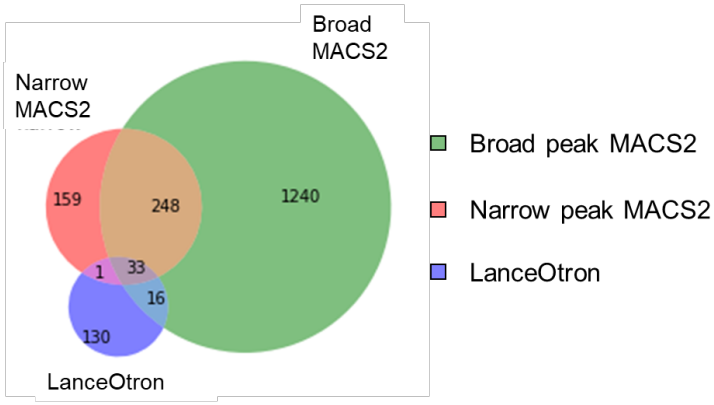


Figure 5.9 Overlap of peaks identified by MACS2 parameters and LanceOtron from IGF-1R ChIP-seq *in vivo*
Venn diagram generated by Dr Avigail Taylor showing the indicated number of peaks identified by Narrow peak MACS2 parameters, Broad peak MACS2 parameters, LanceOtron or 2 or more of the peak calling software programmes. Peaks identified across all tissue samples by each specific peak calling software were merged. These merged lists for each peak calling software were then combined to give a set of unique peak regions used to generate the Venn diagram shown.

From the peaks identified in the *in vitro* work on DU145 cells, only a small number were also identified in this current *in vivo* ChIP-seq. Only 3 peaks from DU145 were also identified *in vivo* by Narrow Peak MACS2 parameters, 5 by Broad Peak MACS2 parameters and 52 by LanceOtron (Figure 5.10). The full list of these peaks and their genomic coordinates are listed in the appendix in Section 8.1.

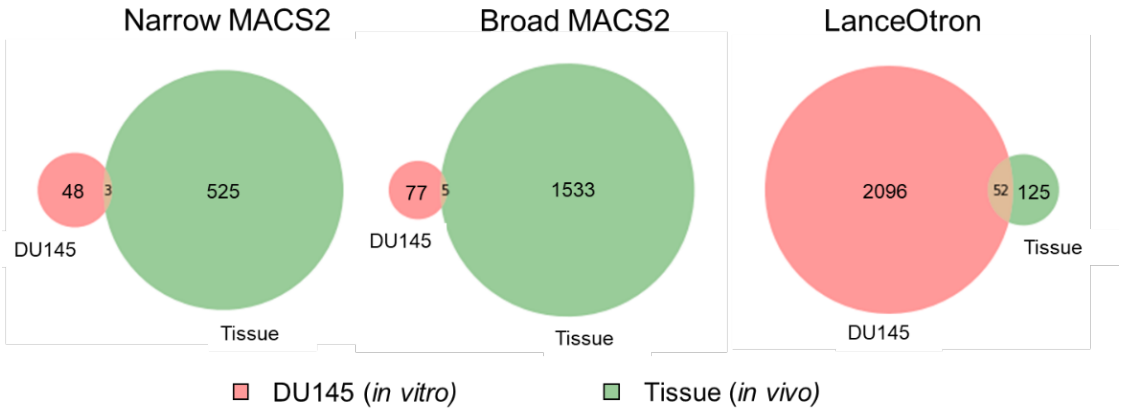


Figure 5.10 Overlap of peaks identified by indicated peak calling software from IGF-1R ChIP-seq *in vitro* and *in vivo*
Venn diagrams generated by Dr Avigail Taylor showing the overlap of the peaks identified by indicated peak calling software from *in vitro* and *in vivo* IGF-1R ChIP-seq data. As shown, only a small number of peaks were identified in both DU145 cell line and clinical tissue data, with 3, 5 and 52 identified in both by Narrow Peak MACS2 parameters, Broad Peak MACS2 parameters and LanceOtron respectively. Peaks identified across all tissue samples by each specific peak calling software were merged, this merged list was then compared to the list of peaks identified by the same peak calling software from the DU145 cell line data to generate the diagrams shown.

The previous *in vitro* IGF-1R ChIP-seq data showed that IGF-1R peaks clustered near TSS of genes, and the majority were coincident with RNAPolII or H3K4me1 binding sites, suggesting the sites were regulatory DNA regions (Aleksic *et al.*, 2018). For the *in vivo* IGF-1R ChIP-seq data generated here, the peaks identified using the different peak calling parameters were analysed to assess distance from TSS and therefore similar recruitment to regulatory DNA regions. As expected, H3K4me1 peaks identified in all peak calling parameters clustered near TSSs (Figure 5.11). Consistent with the *in vitro* data the majority of IGF-1R binding sites identified were also found to cluster near gene TSSs (Figure 5.11). Of the 1827 merged peaks called across all IGF-1R samples by both MACS2 and

LanceOtron, 690 (38%) were coincident with merged peaks called for H3K4me1, a mark of active enhancers (Yu *et al.*, 2010). Proximity of these IGF-1R peaks to TSS and their coincidence with H3K4me1 suggests a potential role influencing gene expression *in vivo* by IGF-1R recruitment to chromatin.

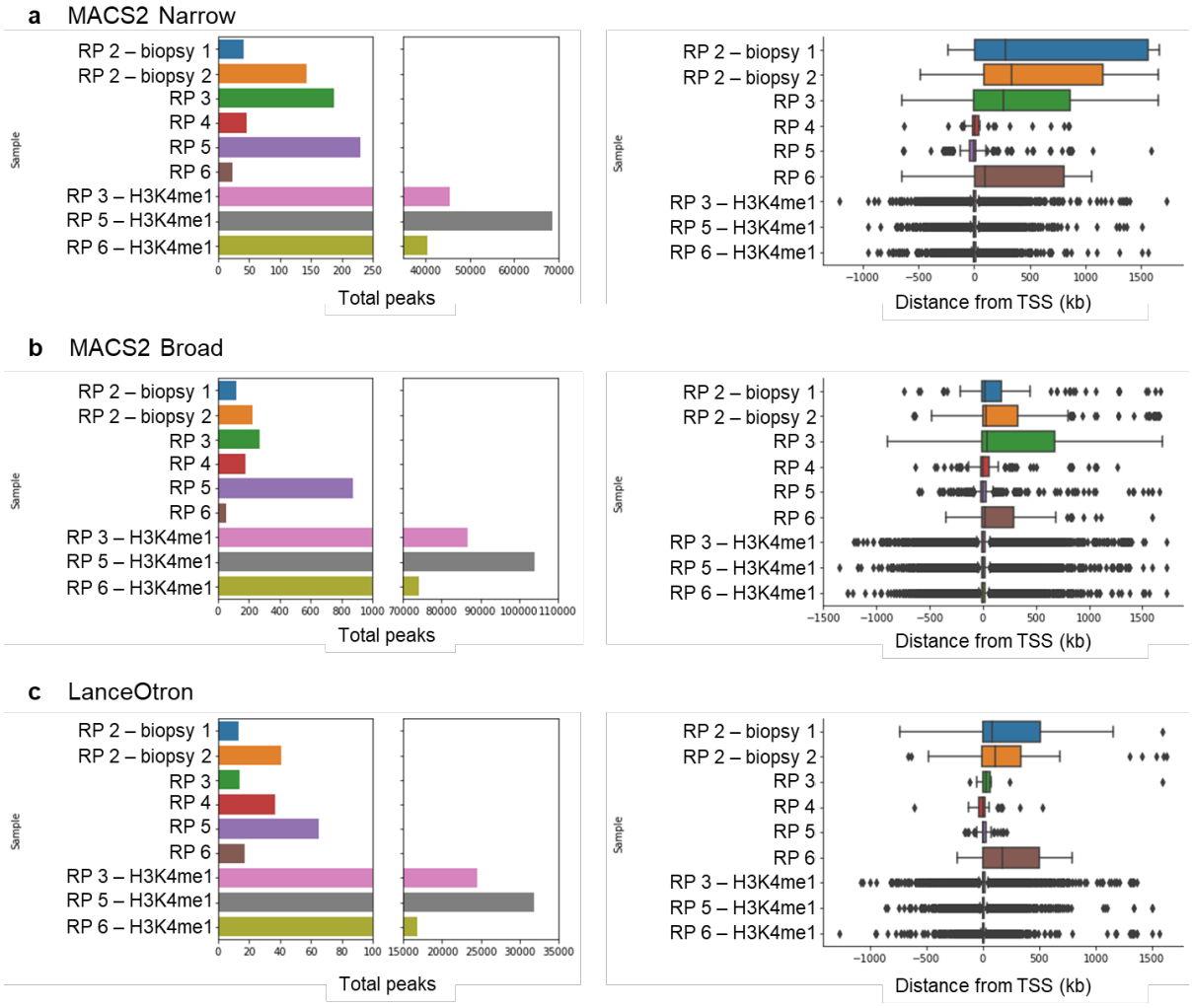


Figure 5.11 Distance from TSS of ChIP-seq peaks identified *in vivo*
Bar charts showing the number of ChIP-seq peaks identified for IGF-1R or H3K4me1 from each indicated sample (left), and the distance of these identified peaks from the nearest TSS (right) for the peaks identified using Narrow Peak MACS2 parameters (**a**), Broad Peak MACS2 parameters (**b**) and LanceOtron (**c**). Plots were generated by Dr Avigail Taylor. Box and whisker plots show the median, range and interquartile range.

It is worth noting that the highest number of peaks for IGF-1R binding across all peak calling software was detected in the biopsy sample from RP 5, the only sample in which IGF-1R recruitment to chromatin could be detected by ChIP-qPCR (Figure 5.5). While initial correspondence from ORB suggested this sample was a malignant biopsy, upon evaluation of IGF-1R IHC staining this biopsy was identified as on the borderline of the area identified as malignant tissue (Figure 5.6d, red circle denotes biopsy site). The differences in number of IGF-1R binding peaks between the samples could be explained by differing levels of nuclear IGF-1R. This would have been assessed had nuclear IGF-1R been detectable by IHC (Figure 5.6, Table 5.5), although, as noted above, the thresholds for detection of nuclear IGF-1R by IHC and ChIP-qPCR are likely to be different.

The IGF-1R peaks identified in the tissues (Figure 5.11) as being proximal to a TSS in each peak caller, were then combined into a 'consensus gene set' made up of genes with a TSS proximal to corresponding IGF-1R peaks detected by any of the peak calling parameters in more than one tissue sample. As shown in Figure 5.12, the majority of these IGF-1R peaks were within 500 - 1000 kb of a TSS of these consensus genes.

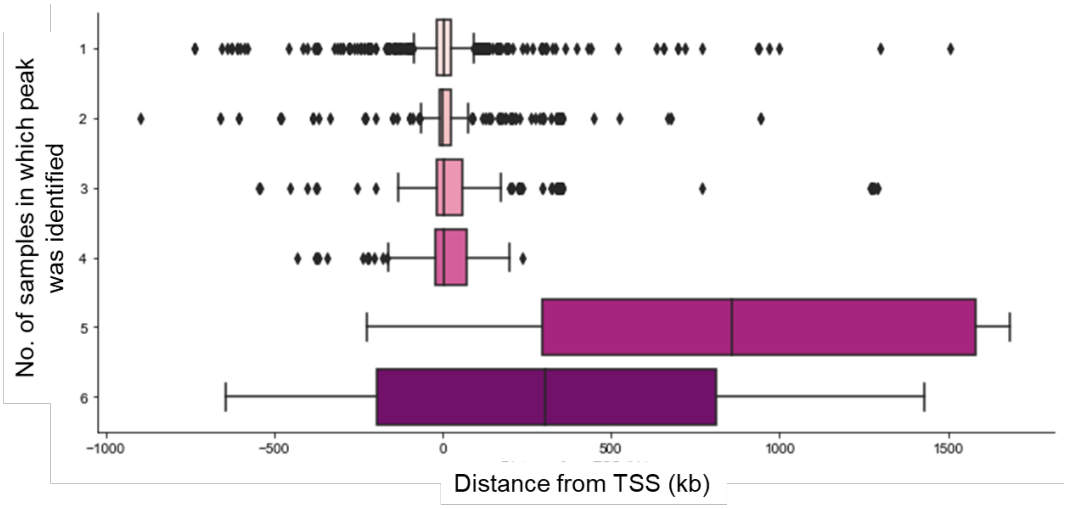


Figure 5.12 Distance of IGF-1R peaks from TSS of consensus genes
Box plot showing the distance of IGF-1R peaks from the TSS of consensus genes. Consensus genes were those with a TSS proximal to an IGF-1R peak that was identified in more than one of the processed tissue samples. Peaks from different tissue samples were considered to be the same if the peak overlapped by a minimum of one nucleotide. Box plot was generated by Dr Avigail Taylor. Box and whisker plots show the median, range and interquartile range.

Consensus genes that had an IGF-1R peak proximal to their TSS in 4 or more of the processed tissue samples were identified and are listed in Table 5.9. Strip plots showed that most of these peaks were found to be less than 500 kb from the nearest TSS, many of them downstream not upstream of the TSS (Figure 5.13). For consensus genes identified to have an IGF-1R peak proximal to their TSS in 4 or more tissue samples, PANTHER Classification System analysis showed that most of these genes encoded proteins involved in gene specific transcriptional regulation or scaffold/adaptor proteins (Figure 5.14a). The proteins encoded by these genes were also classified as playing a role in a range of biological pathways (Figure 5.14b).

No. of samples containing IGF-1R peak at TSS	Gene name	Function
4	ACTR3BP2 (ARP3 Actin-Related Protein 3 Homolog B Pseudogene 2)	Pseudogene
	BMS1P22 (BMS1, Ribosome Biogenesis Factor Pseudogene 22)	Pseudogene
	CRLF2 (Cytokine Receptor Like Factor 2)	Encodes a type I cytokine receptor
	FAM90A7P	Pseudogene
	LOC102723769	Uncharacterised RNA gene
	LOC646652	Pseudogene
	MIR3648-2	Micro RNA gene
	NKX1-1 (NK1 Homeobox 1)	NKX transcription factor protein (regulators of organ development)
	ROCK1 (Rho Associated Coiled-Coil Containing Protein Kinase 1)	Serine/threonine kinase (key regulator of the actin cytoskeleton and cell polarity)
	TEKT4P2	Pseudogene
	ZNF558 (Zinc Finger Protein 558)	Potentially involved in transcriptional regulation
5	ANKRD20A12P	Pseudogene
	ANKRD26P1	Pseudogene
	ASNSP1	Pseudogene
	EMB (Embigin)	Transmembrane glycoprotein, may play a role in cell growth and development
	LOC441666	Pseudogene
	LSP1P4	Pseudogene
	MIR9901	Micro RNA gene
	SPIN4 (Spindlin Family Member 4)	Expressed protein exhibits H3K4me3-binding activity
	ZNF733P (Zinc Finger Protein 733, Pseudogene)	Pseudogene
6	CWH43 (Cell Wall Biogenesis 43 C-Terminal Homolog)	Lipid remodelling
	EMBP1 (Embigin Pseudogene 1)	Pseudogene
	GYG2P1	Pseudogene
	POTEA (POTE Ankyrin Domain Family Member A)	Cancer/Testis antigen

No. of samples containing IGF-1R peak at TSS	Gene name	Function
6	SPRY3 (Sprouty RTK Signaling Antagonist 3)	Negatively regulates MAPK signalling. Inhibits EGF-mediated ERK signalling, and may function as an antagonist of FGF signalling
	TPTE (Transmembrane Phosphatase with Tensin Homology)	PTEN-related tyrosine phosphatase that plays a role in testis function. Identified as a cancer/testis antigen
	ZXDA (Zinc Finger X-Linked Duplicated A)	Zinc finger gene, promotes transcription of MHC class I and MHC class II genes

Table 5.9 Genes containing IGF-1R peak proximal to their TSS in 4 or more tissue ChIP-seq samples

Table listing the genes identified as having an IGF-1R peak proximal to their TSS in 4 or more of the tissue samples processed for IGF-1R ChIP-seq. Table shows the number of samples that contained an IGF-1R peak within the gene TSS, the gene name and basic description of the gene's function. Information was compiled from GeneCards: The Human Gene Database (https://www.genecards.org/).

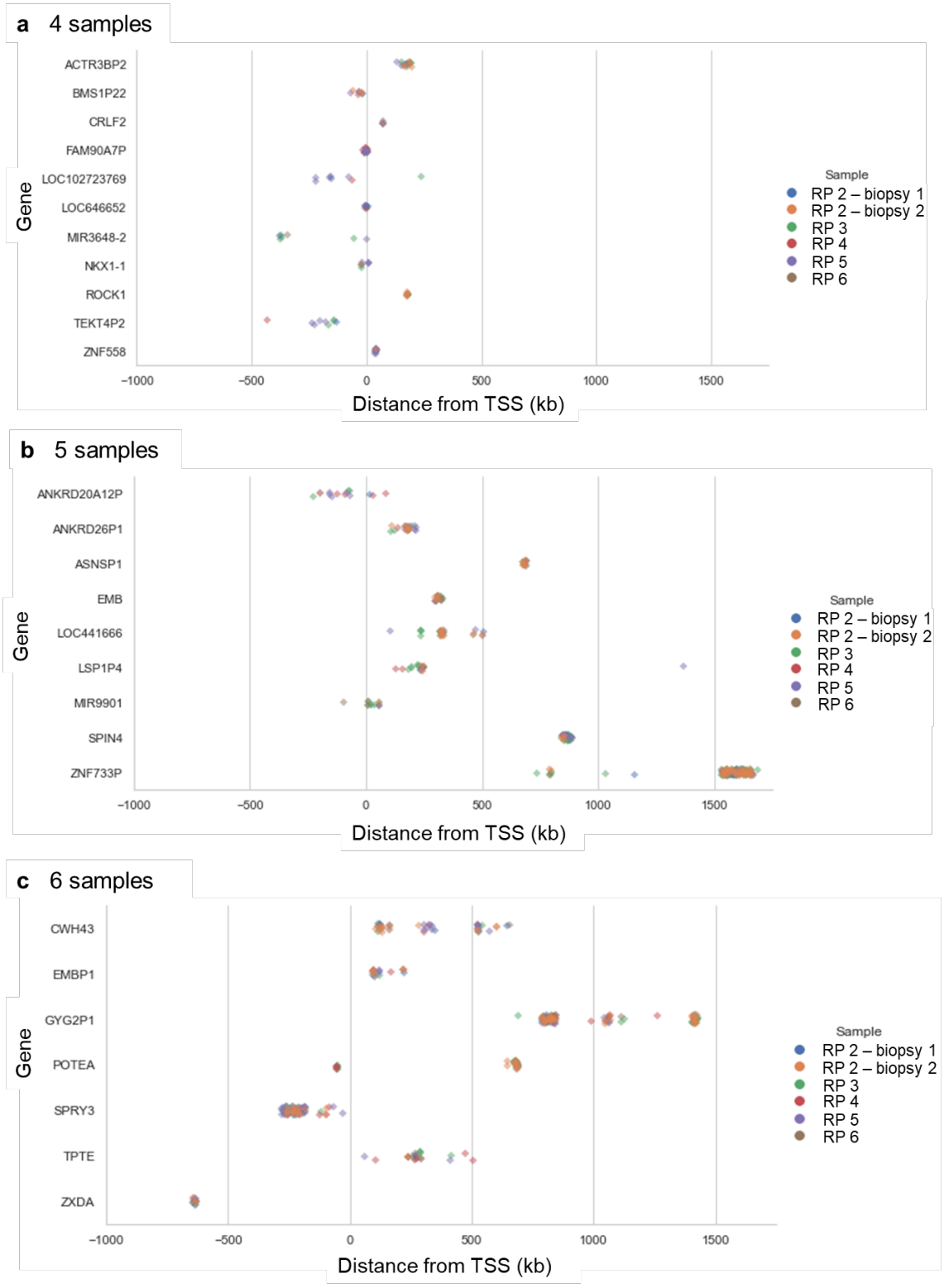
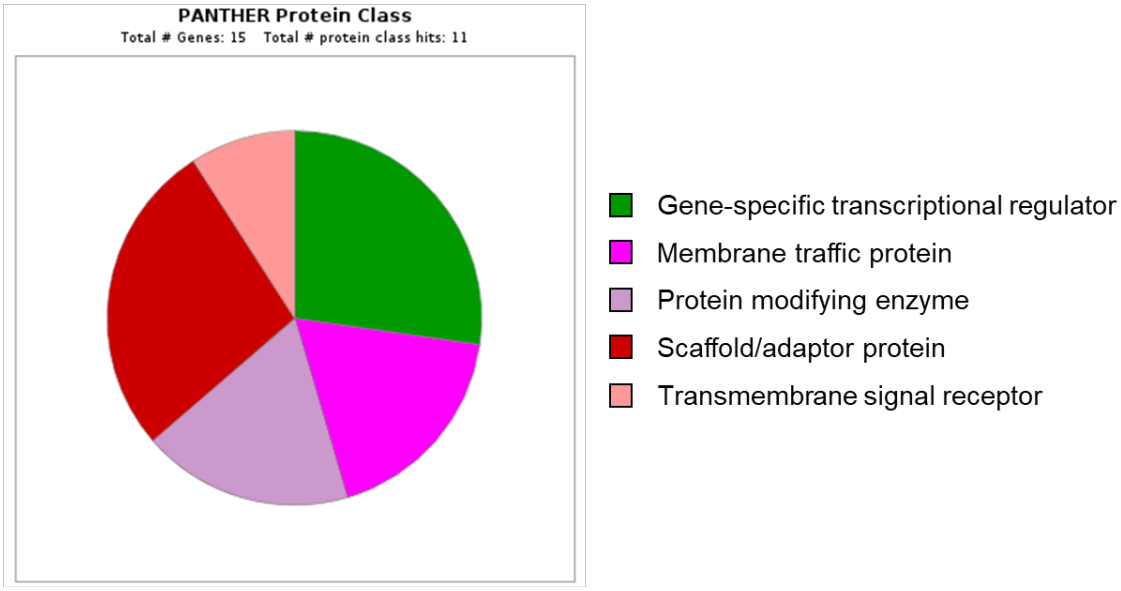


Figure 5.13 Distance of IGF-1R peaks from TSS of specific consensus genes identified in multiple tissue samples

Strip plots showing the distance of IGF-1R peaks from TSS of indicated consensus genes identified in either 4 (**a**), 5 (**b**) or all 6 (**c**) of the processed tissue samples. Strip plots were generated by Dr Avigail Taylor.

a



b

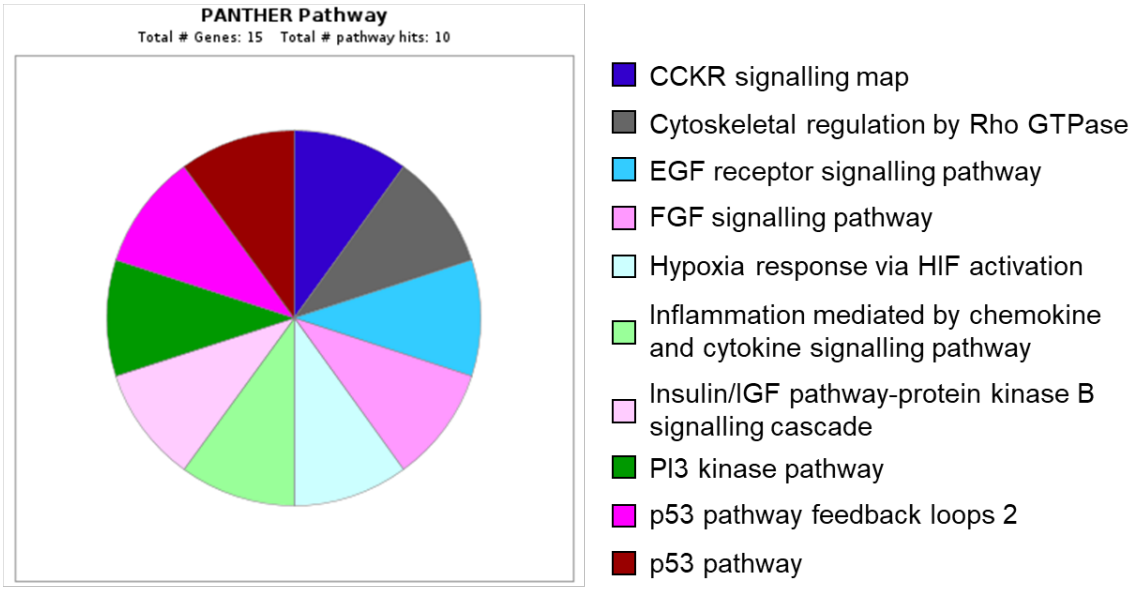


Figure 5.14 PANTHER classification of protein class and biological pathways of identified consensus genes

PANTHER analysis showing the protein class (**a**) and biological pathway processes (**b**) of consensus genes identified to have corresponding IGF-1R peaks proximal to their TSS in 4 or more of the tissue samples processed for ChIP-seq as identified in Figure 5.13. PANTHER pathway analysis was performed by me.

Of the consensus genes identified to a have an IGF-1R peak proximal to their TSS, 4 out of the 7 IGF-1R peaks identified in all 6 tissue samples processed for IGF-1R ChIP-seq (Figure 5.13c, Table 5.9) were also identified in our previous *in vitro* ChIP-seq dataset. These were proximal to the TSS for the genes POTEA, SPRY3, TPTE and ZXDA (Table 5.10).

Peak Calling Method	**Gene**	**Genomic co-ordinates of IGF-1R peak**	**Distance to TSS (kb)**	**Annotation**
Narrow Peak MACS2	POTEA	chr8: 43094777 - 43094988	-53	Intergenic
Broad Peak MACS2	POTEA	chr8: 43092770 - 43093158	-55	Intergenic
	POTEA	chr8: 43094668 - 43095233	-53	Intergenic
	POTEA	chr8: 43096704 - 43097052	-51	Intergenic
LanceOtron	POTEA	chr8: 43092520 - 43094147	-54	Intergenic
	POTEA	chr8: 43094426 - 43095554	-53	Intergenic
	POTEA	chr8: 43095573 - 43097305	-51	Intergenic
	TPTE	chr21: 10698445 - 10699726	292	Intergenic
	TPTE	chr21: 10699913 - 10700591	291	Intergenic
	ZXDA	chrX: 58570140 - 58571226	-634	Intergenic
	ZXDA	chrX: 58574279 - 58577198	-639	Intergenic
	SPRY3	chrY: 58819386 - 58905579	-238	Intergenic
	SPRY3	chrY: 58974649 - 58977529	-124	Intergenic
	SPRY3	chrY: 58981575 - 58983329	-118	Intergenic

Table 5.10 IGF-1R binding peaks identified proximal to gene TSS *in vitro* and in all *in vivo* samples
Table showing the genomic co-ordinates of IGF-1R peaks identified in all 6 tissue samples processed for ChIP-seq as well as our previous *in vitro* data (Aleksic *et al.*, 2018). Table shows the name of associated gene, co-ordinates of IGF-1R peak and distance of IGF-1R peak from the TSS to the nearest kb. Distances from TSS shown here match those for *in vivo* IGF-1R peaks shown in (Figure 5.13c).

The IGF-1R peak proximal to the TSS of the Transmembrane Phosphatase with Tensin Homology (TPTE) gene was identified in all 6 of the processed tissue samples as well as in the *in vitro* cell line data. TPTE was classified as playing a role in the Insulin/IGF pathway-protein kinase B signalling cascade, the PI3K pathway and the p53 pathway (Figure 5.14b), all functions related to IGF-1R signalling. TPTE is strongly expressed exclusively in the testis (Chen *et al.*, 1999), but has previously been identified as a cancer-testis specific antigen that is aberrantly transcribed in human cancers of the liver, lung and

prostate (Dong *et al.*, 2003; Singh *et al.*, 2008). This IGF-1R peak detected proximal to the TSS of TPTE was also coincident with a H3K4me1 peak, a marker for an active enhancer region, as well as a small peak for H3K27ac, a marker for an active promoter region (Yu *et al.*, 2010) (Figure 5.15). Therefore, recruitment of IGF-1R to this region may have a regulatory role in expression of TPTE in prostate cancer.

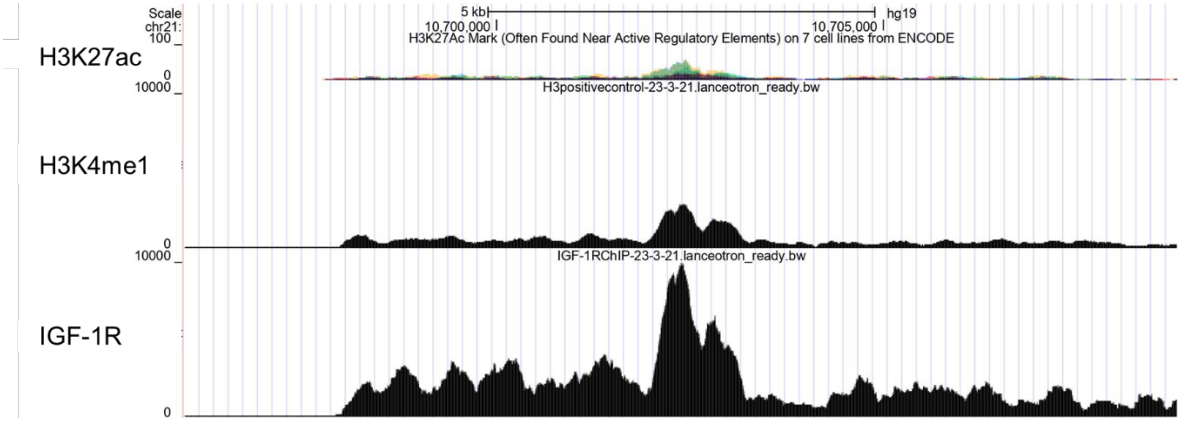


Figure 5.15 UCSC genome browser image of binding peaks identified at TPTE TSS
UCSC genome browser images showing IGF-1R and H3K4me1 peaks identified by ChIP-seq from RP5 biopsy sample. Browser image shows coincidence of IGF-1R and H3K4me1 peak at TSS of TPTE gene as listed in Table 5.10. Publicly available data for H3K27ac available within the UCSC genome browser also shows a small peak at the same region. H3K4me1 and H3K27ac are markers for active enhancer regions (Yu *et al.*, 2010), suggesting recruitment of IGF-1R to this region may have a regulatory function. Browser image is representative of peaks detected in all processed biopsy samples.

These peaks did not include the IGF-1R binding sites at the *JUN* and *FAM21A/C* promoters that were previously validated *in vitro* by our lab (Aleksic *et al.*, 2018), and in this thesis (Section 4.2.2.2). Interestingly, one of the peaks identified both *in vitro* and *in vivo* by both Narrow and Broad peak MACS2 parameters, was the region of chromosome 17 previously validated *in vitro* by ChIP-qPCR in this thesis and used to generate IGF-responsive luciferase reporters (Table 5.11, see Section 4.2.2.2) This peak was detected in all clinical tissues.

Peak Calling Method	Genomic co-ordinates of IGF-1R peak	Annotation
Narrow Peak MACS2	chr17: 72510132 -72510908	Intergenic
Broad Peak MACS2	chr17: 72510125 -72511132	Intergenic

Table 5.11 Peak Co-ordinates of IGF-1R binding site identified both *in vitro* and *in vivo* in an intergenic region of chromosome 17
Co-ordinates of IGF-1R binding site peak within an intergenic region of chromosome 17 identified by both Narrow and Broad Peak parameters in MACS2 in both *in vitro* and *in vivo* data. This IGF-1R binding site was previously validated *in vitro* by ChIP-qPCR in this thesis, and the relevant region of DNA was used to generate an IGF-responsive luciferase reporter (see Section 4.2.2.2).

We also analysed whether IGF-1R recruitment was detected coincident with sites of AR binding. This was done using AR ChIP-seq data from 2 samples of prostate cancer tissue from treatment naïve prostate cancer patients previously reported by the lab of Prof Ian Mills (NDSS, University of Oxford) (Sharma *et al.*, 2013). Comparing location of AR peaks identified *in vivo* by the work from Prof Mills' lab with all unique IGF-1R peaks identified in our own *in vivo* work here found that 59 of 1827 identified IGF-1R peaks (3%) overlapped with peaks for AR. However, this did include the IGF-1R peak proximal to the TSS of TPTE (see appendix in Section 8.2 for full list of IGF-1R peaks that overlap with AR peaks).

Due to time constraints, identified IGF-1R peaks could not be validated *in vitro* by ChIP-qPCR. If time had permitted this validation would have been undertaken to confirm recruitment of IGF-1R to these identified regions.

5.3 Discussion

For the first time we have characterised genome-wide recruitment of IGF-1R to chromatin binding sites *in vivo* in prostate cancer biopsy tissue. Most of the identified IGF-1R peaks were shown to cluster near TSSs, suggesting these regions have potential regulatory function. Most of the consensus genes containing IGF-1R peaks proximal to their TSS encoded transcriptional regulators.

Protocols used for this study required considerable troubleshooting and optimisation, and there were persistent technical issues. TURPs were used initially because larger amounts of tissue were available per patient, and results showed potential detection of IGF-1R enrichment by ChIP-qPCR (Figure 5.2). In contrast, IGF-1R enrichment could only be detected by qPCR in one small RP biopsy sample (Figure 5.5). Although the method adapted for use here (Singh *et al.*, 2019) used similar amounts of starting material, IGF-1R is not a traditional transcription factor, and the probability of detecting IGF-1R recruitment by ChIP-qPCR may be improved by using larger tissue samples. Further modifications could include more accurate quantification and optimisation of DNA fragment sizes post-sonication using a Fragment Analyzer (Sabatel, 2017). As previously discussed in Section 5.2.3, it may be informative to collect more cases at a wider range of cancer grades and stages, selecting cases with detectable nuclear IGF-1R by IHC.

It is unclear why IGF-1R recruitment could be detected by ChIP-seq but not ChIP-qPCR. It is possible this may be due to differences in sensitivity between qPCR and sequencing analysis or use of inappropriate qPCR primers. In ChIP-qPCR validation, primers for the *JUN* and *FAM21A* promoter regions were used to check for IGF-1R recruitment. However, these primers were designed for use in cell lines and subsequent *in vivo* IGF-1R ChIP-seq data did not detect an IGF-1R peak at either of these regions. This suggests these primers may not have been suitable to confirm successful IGF-1R ChIP from tissue samples. As

previously discussed in detail in Section 5.2.3 it is also unclear why nuclear IGF-1R could not be detected by IHC, in contrast to our previous work (Aleksic *et al.*, 2010, 2018). As discussed, if time had permitted, a larger number of biopsy samples from a wider range of cases at different tumour stages would have been obtained and those that were positive for nuclear IGF-1R staining would have been processed for ChIP-seq.

If time had permitted, IGF-1R binding sites identified *in vivo* would have been validated by ChIP-qPCR *in vitro*. Initial validation experiments would have focussed on the regions identified proximal to TSSs in 4 or more of the processed tissue samples (Figure 5.13), including the previously mentioned region proximal to the TSS of TPTE. Detection of IGF-1R peaks in multiple samples suggests these regions may play a consistent role in the actions of nuclear IGF-1R recruitment to chromatin, especially those also detected *in vitro*. The proximity of these peaks to gene TSSs may also suggest they are regulatory regions of DNA. Experiments to test the potential functional relevance of recruitment of IGF-1R to validated sites would also have been undertaken. Gene expression levels and relevant phenotypic responses would have been assessed in response to IGF-1 stimulation or inhibition of IGF-1R internalisation, analogous to our previous *in vitro* work with the *JUN* promoter (Aleksic *et al.*, 2018). This would determine if recruitment of IGF-1R to these regions is IGF-1 dependent, and whether there is functional relevance to recruitment of IGF-1R to these regions. Validation of such a role in activation of known oncogenes or genes involved in cell growth, could then shed light on the role of nuclear IGF-1R in promoting prostate cancer progression *in vivo*.

It is unclear why only a small number of IGF-1R peaks previously identified *in vitro* (Aleksic *et al.*, 2018) were detected *in vivo*. As mentioned previously, there is crosstalk between the IGF-axis and AR signalling (Krueckl *et al.*, 2004; Turney *et al.*, 2011). The cell line used in the previous *in vitro* work (Aleksic *et al.*, 2018), DU145, is AR negative,

which could result in recruitment of IGF-1R to a different set of chromatin binding sites. To further investigate this, if time had permitted, further work would have been undertaken to optimise DNA fragmentation and enable IGF-1R ChIP-seq in the 22Rv1 prostate cancer cell line that is AR positive. (Repeated attempts to optimise this DNA fragmentation were not successful (data not shown)). IGF-1R peaks identified by ChIP-seq in DU145, 22Rv1 and *in vivo* could then have been compared.

If time had permitted, further analysis would have been undertaken of the ChIP-seq dataset generated here. The IGF-1R peaks from the *in vivo* ChIP-seq data, and our previously generated *in vitro* ChIP-seq data would have been aligned to the most up to date human reference genome (hg38). Also, in light of the exclusion by LanceOtron of a large number of MACS2-IGF-1R peaks identified in tissues, experimental validation and optimisation of LanceOtron peak score cut off would have been carried out, together with the LanceOtron peak visualisation tool to guide identification of authentic IGF-1R binding sites. The visualisation tool within LanceOtron allows optimisation of peak calling for features of specific datasets, i.e., peak shape, rather than using fixed criteria as with MACS2 (Zhang *et al.*, 2008; Hentges *et al.*, 2021). Therefore, correct optimisation of LanceOtron will likely have identified peaks that may be excluded by MACS2. However, the novelty of LanceOtron means that it currently lacks robust experimental validation by its developers (Hentges *et al.*, 2021), and therefore any identified peaks would require further validation. As mentioned previously, work by (Sharma *et al.*, 2013) on the AR detected an extra 9000 AR chromatin binding sites in prostate cancer tissue vs cell lines using MACS2. In total, 1827 unique IGF-1R peaks were identified from all tissue samples processed here using both MACS2 and LanceOtron. Narrow Peaks MACS2 identified 23-230 peaks *in vivo* (Table 5.7) but only 42 *in vitro* (Figure 5.7), similarly Broad Peaks MACS2 identified 52-878 peaks *in vivo* (Table 5.7) but only 69 *in vitro* (Figure 5.7). Therefore, a higher average

number of IGF-1R peaks were identified by MACS2 *in vivo* versus *in vitro* but to a lower magnitude than the number of extra AR sites detected by (Sharma *et al.*, 2013). LanceOtron detected 13-65 peaks across all tissue samples (Table 5.8), a much lower number than the 1922 detected *in vitro* (Figure 5.7). However, as discussed above, this may be due to incorrect optimisation of the LanceOtron peak parameters used. The number of IGF-1R binding sites identified by both MACS2 both *in vivo* and *in vitro* are much lower than the 3976 high confidence peaks identified by MACS2 following *in vitro* ChIP-seq for the closely related INSR in HepG2 human hepatocellular carcinoma cells (Hancock *et al.*, 2019). However, data from the same work detected only 572 INSR binding sites in SH-SY5Y neuroblastoma cells (Hancock *et al.*, 2019), a similar amount to the number of IGF-1R sites detected here. Of the INSR binding sites identified, only 422 were common between both cell lines suggesting INSR binding to chromatin may be cell type specific. Similarly, the previous *in vitro* data generated by our lab detected 62 IGF-1R peaks in DU145 prostate cancer cells and 66 in SK-N-MC Ewing sarcoma cells, of which only 25 were common between both cell lines (Aleksic *et al.*, 2018). Of the INSR binding sites identified in HepG2 cells, 82% of peaks were within gene promoter regions (defined as ±500 bp from TSS) (Hancock *et al.*, 2019), and were therefore clustered at gene TSS, analogous to IGF-1R peaks identified here and in the previous *in vitro* data. The genes with INSR-bound promoters were also found to be strongly enriched for insulin-related functions. Analysis also showed 73% of INSR peaks were coincident with RNAPolII binding sites (Hancock *et al.*, 2019), analogous to previous *in vitro* data from our lab for IGF-1R, showing 95% of IGF-1R binding sites were coincident with binding sites for RNAPolII (Aleksic *et al.*, 2018). Work with EGFR, another RTK that undergoes nuclear translocation, has shown approximately 489 EGFR chromatin binding sites in HeLa cells (Wong, 2018). *In vitro* work by (Sehat *et al.*, 2010) also detected 568 IGF-1R binding sites

in melanoma cells, however these were found to be mostly intergenic away from gene TSSs. The number of IGF-1R binding sites identified in this thesis therefore appears to be at a slightly lower range than those identified for other nuclear RTKs and are much lower than those for traditional transcription factors such as FOXA1 (approx. 57 000) (Singh *et al.*, 2019).

Analysis showed that 38% of identified IGF-1R peaks *in vivo* were coincident with peaks identified for H3K4me1, a marker for active enhancers. This suggests that IGF-1R recruitment to these regions may have enhancer function. This could be true particularly for the intergenic site identified on chromosome 17 in DU145 cells that is coincident with H3K27ac enrichment (Aleksic *et al.*, 2018) and that was also detected in all tissues analysed here. It would also be interesting to use publicly available datasets to assess coincidence of all detected IGF-1R peaks with peaks for RNAPolII and regulatory histone marks, such as the H3K27ac mark of active enhancers, H3K4me1 that can mark enhancers and promoters, and H3K4me3 that marks promoters (Yu *et al.*, 2010; Benayoun *et al.*, 2014; Bae and Lesch, 2020).

Analysis also showed that only 3% of identified IGF-1R peaks *in vivo* overlapped with AR peaks previously identified in prostate cancer tissues from treatment naïve patients by (Sharma *et al.*, 2013). This suggests that the contribution of the IGF-axis to androgen independence (Krueckl *et al.*, 2004; Turney *et al.*, 2011) is unlikely to be via recruitment to and activation of AREs. Development of castrate resistant and anti-androgen drug resistant prostate cancer is thought to arise from sustained AR related signalling via androgen-independent mechanisms (Mitchell and Neal, 2015; Wang *et al.*, 2018). As the biopsies processed for IGF-1R ChIP-seq here were from cases that were localised and previously untreated (Table 5.1, Table 5.6), they were highly unlikely to have developed androgen independence. Therefore, it is possible that the cancers processed here were not

undergoing sustained androgen independent AR signalling, which could limit hypothesised compensatory recruitment of IGF-1R to AREs. To assess this, prostate cancer tissue from a range of cases could be processed for IGF-1R ChIP including tumours at a more advanced stage, higher Gleason grade and CRPC. Data could then be analysed to determine if IGF-1R is recruited to AREs in cancers that are more likely to be undergoing AR signalling via androgen independent mechanisms, as well as analysing whether IGF-1R recruitment is different at different tumour stages. Further AR ChIP-seq datasets could also be used to analyse overlap of any AR peaks not identified by (Sharma *et al.*, 2013) with IGF-1R peaks identified in this thesis.

Overall, we have shown genome-wide recruitment of IGF-1R to chromatin *in vivo* for the first time using prostate cancer biopsy samples. Detection of IGF-1R peaks was found to be proximal to gene TSSs, suggesting a potential regulatory role for IGF-1R recruitment to chromatin. Further validation experiments are needed to confirm IGF-1R binding at these regions, and test whether there is a link between IGF-1R recruitment and gene expression at the transcriptional and/or epigenetic level. If IGF-1R recruitment to chromatin is confirmed to regulate genes involved in cancer growth and progression, this will help to explain the link between levels of nuclear IGF-1R and more advanced cancer stage in prostate cancer (Aleksic *et al.*, 2018).

6 Chapter VI: Investigating the nuclear interactome of IGF-1R

6.1 Introduction

As previously mentioned in Section 1.6.3, following translocation to the nucleus, IGF-1R has been shown to interact with other nuclear proteins including transcription factors (Aleksic *et al.*, 2018; Solomon-Zemler *et al.*, 2019), an IGF-1 dependent interaction with RNAPolII shown by our lab (Aleksic *et al.*, 2018) and direct phosphorylation of PCNA by nuclear IGF-1R in work by the Larsson lab (Waraky *et al.*, 2017). These proteins are involved in activating gene transcription and DNA replication, and therefore likely contribute to cell growth and proliferation.

As previously discussed in this thesis (Section 1.6.4), higher levels of nuclear IGF-1R were detected in malignant compared to benign epithelium and were associated with a more advanced tumour stage in prostate cancer (Aleksic *et al.*, 2010, 2018). Nuclear IGF-1R has also previously been suggested as a potential marker for tumours that may be more responsive to anti-IGF-1R targeted treatment (Asmane *et al.*, 2012). As the nuclear IGF-1R interacting proteins mentioned above all likely contribute to cell growth, it is possible that these functional interactions contribute to the advanced cancer phenotype associated with nuclear IGF-1R. Therefore, we decided to investigate the nuclear interactome of IGF-1R, to identify potential novel interactors of nuclear IGF-1R. Identification of currently unidentified nuclear IGF-1R interacting proteins, and validation of the functional relevance, will help to further elucidate the role of IGF-1R in the nucleus. This may identify additional interacting proteins that contribute to cancer growth and progression, act as potential treatment targets and help to understand clinical responses to anti-IGF-1R treatments.

6.2 Results

6.2.1 Immunoprecipitation of nuclear IGF-1R

Initial experiments involved the IP of IGF-1R from nuclear extract. We chose the prostate cancer cell line 22Rv1 for these experiments. This was because 22Rv1 cells are AR positive, making them more clinically relevant than the AR negative DU145 cells used previously to investigate nuclear IGF-1R functions (Aleksic *et al.*, 2018). In addition, we had a 22Rv1 IGF-1R null clone, generated in our lab by DPhil student Matthew Ellis using CRISPR knockout, that could be used as a negative control for IP and mass spectrometry analysis. Our experimental plan involved performing duplicate independent IPs of IGF-1Rβ-subunit from nuclear extract from both WT and IGF-1R null cells, before analysing the co-IP'd proteins by mass spectrometry. The data obtained from the IGF-1R null cells were likely to contain non-specific proteins that may also be co-IP'd, aiming to provide an additional and more robust negative control than using only an IgG IP of nuclear lysate extracted from WT IGF-1R cells.

The IGF-1R WT and IGF-1R null cells were grown in full medium and fractionated into nuclear and cytoplasmic fractions. Equal amounts of pre-cleared nuclear extract were used for IP of IGF-1Rβ-subunit from both WT and null cells, alongside an IgG negative control from WT nuclear lysate. Following IP, 80% of each sample was stored as dry Protein A agarose beads at -80^{o}C, and 20% was used to check suitability for mass spectrometry analysis.

Western blot analysis was performed with 10% of IP samples analysed in parallel with nuclear, cytoplasmic and WCE input controls, probing for the presence of the IGF-1Rβ-subunit and markers for successful fractionation. As expected, IGF-1Rβ was detected in nuclear, cytoplasmic and WCE input samples from WT 22Rv1, but was absent in the input samples from the IGF-1R null cells. Western blotting also detected IGF-1Rβ in the IP from

WT cells, but not in the IgG negative control or the IPs from the IGF-1R null cell line, showing successful IP of IGF-1R (Figure **6.1**a). The band for IGF-1Rβ detected in the IP of WT nuclear extract was relatively faint compared to previous nuclear IP experiments in this thesis (Section 3.2.1, Figure **3.2**d and e). This is because only 10% of the IP sample was used for Western blotting, and most of the sample was retained for mass spectrometry. The presence of Lamin A/C and β-tubulin in only the nuclear and cytoplasmic extracts respectively suggests successful cell fractionation, therefore suggesting that IP'd proteins were likely to be those interacting with the receptor in the nucleus.

The remaining 10% of each IP sample, including IgG negative control, was analysed by silver staining. A definitive protein band in the WT IP sample at ~100kDa, which might represent IGF-1R, could not be identified. This is likely due to the small amount of protein sample loaded, only 10% of each IP. However, the WT and IGF-1R null samples showed differing patterns of protein bands, with more bands being present in the WT versus the IGF-1R null IP (Figure **6.1**b). While the IGF-1R null IP sample showed the presence of more protein bands than that of the IgG negative control sample, the differences between the IGF-1Rβ-subunit IPs from the IGF-1R WT and null cells suggested a different set of proteins had undergone IP in each case. Combined with the detection of IGF-1Rβ by Western blot in only the WT IP, these results suggested the samples would be suitable for mass spectrometry analysis.

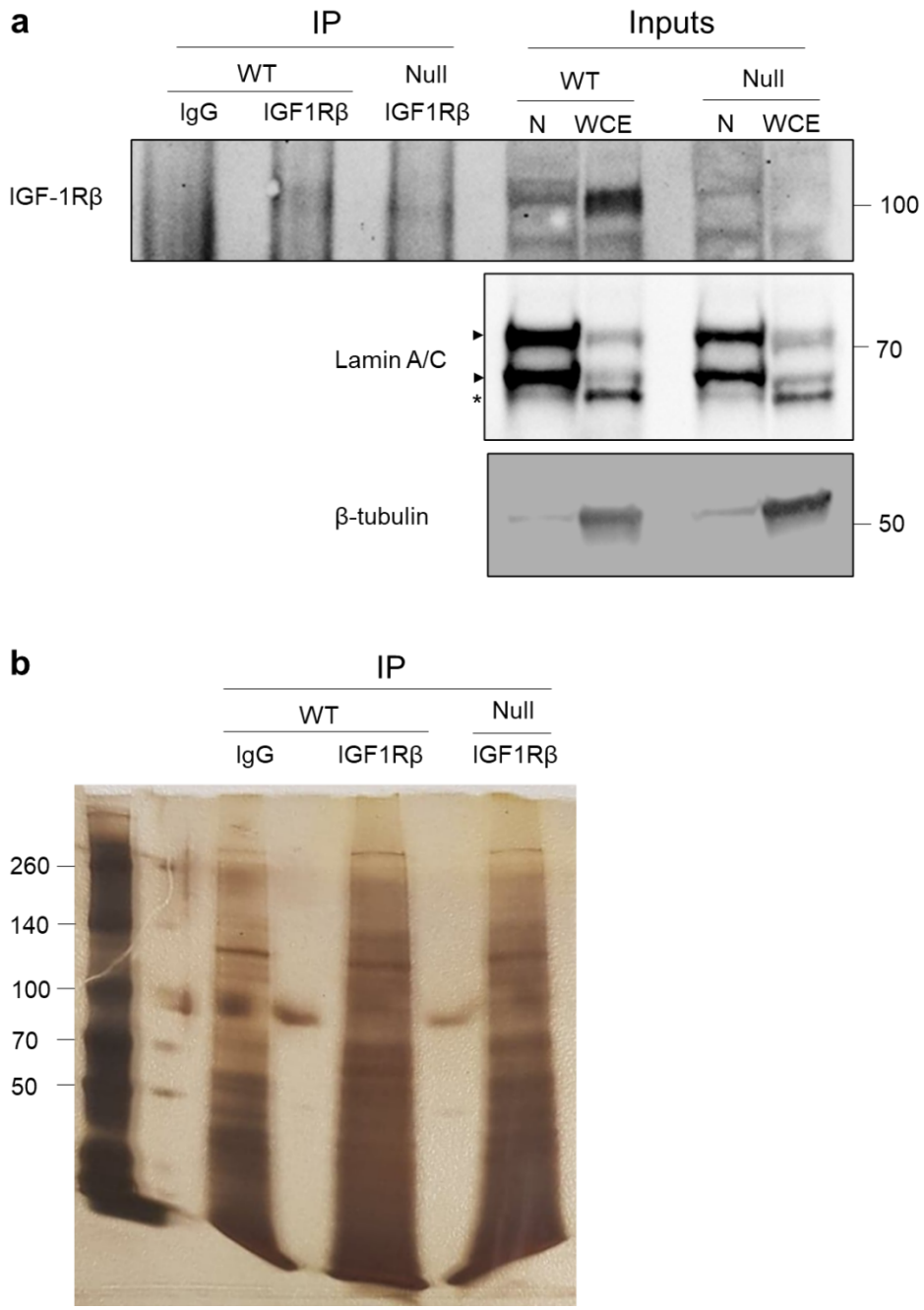


Figure 6.1 Testing nuclear IGF-1R IP for suitability for mass spectrometry analysis
a Western blot showing detection of IGF-1Rβ-subunit in WT 22Rv1 cells only, following IP of IGF-1Rβ from nuclear extract of WT and IGF-1R null 22Rv1 cells. Nuclear (N) lysates were immunoprecipitated with antibody for IGF-1Rβ or IgG control (WT only) and analysed alongside N and WCE input controls (10% of IP input) using antibody for IGF-1Rβ. Successful fractionation of nuclear and cytoplasmic extracts was determined by detection of fractionation markers Lamin A/C (Arrowheads: doublet at 74, 63 kDa respectively, nuclear marker) and β-tubulin (55 kDa, cytoplasmic marker). Asterisk: β-tubulin signal (50kDa) visible on re-probing same membrane for Lamin. **b** A silver-stained gel of the same IGF-1R IPs shown in (**a**). IGF-1R IPs from WT and IGF-1R null cells appeared to contain more proteins compared to the IgG control. The different pattern of bands in the IPs from IGF-1R WT and null cells suggested that a different set of proteins was present in each sample. Similar results in both WB and silver staining were obtained in the second set of IGF-1R IPs, providing two WT and two IGF-1R null samples for mass spectrometry analysis.

6.2.2 Mass Spectrometry analysis of nuclear IGF-1R interactome

Following successful detection of IGF-1R in IP from nuclear extract, the remaining 80% of samples stored at -80ºC were then processed for mass spectrometry via on bead tryptic digest, followed by desalting using SOLA-HRP cartridges. LC-MS/MS analysis was then performed by Dr Iolanda Vendrell using a Thermo Scientific Orbitrap Fusion Lumos Tribrid Mass Spectrometer (see Section 2.16.4).

Initial analysis by Dr Vendrell using Mascot protein identification software showed a high false discovery rate of over 35% for the peptides detected, suggesting that contaminants were present. To further investigate this, Dr Vendrell then analysed the data against the Swiss-Prot protein database without defining a species or database. This analysis showed that 35% of the identified peptides were from *Staphylococcus aureus*. It is possible that this contamination came from the Protein A agarose beads used to perform the initial IP of IGF-1R from nuclear extract, as Protein A is a surface protein from the cell wall of *Staphylococcus aureus* (Schneewind, Model and Fischetti, 1992).

To circumvent difficulties in analysis caused by this contamination, Dr Vendrell used the PEAKS proteomics software to analyse the data against the Swiss-Prot Human protein database with the Swiss-Prot *Staphylococcus aureus* protein database listed as a contaminant (see Section 2.16.4). This then removed detected *Staphylococcus aureus* proteins leaving only those of human origin, including those that had been filtered out in initial Mascot analysis due to the high false discovery rate. Overall, LC-MS/MS detected peptides representing potential nuclear IGF-1R interacting proteins with approximately 100 and 152 proteins in each WT sample only, with a further 107 detected in both, and in IGF-1R null cells 17 and 38 with a further 2 detected in both (Figure **6.2**).

Of note, no IGF-1R peptides were detected in any of the samples.

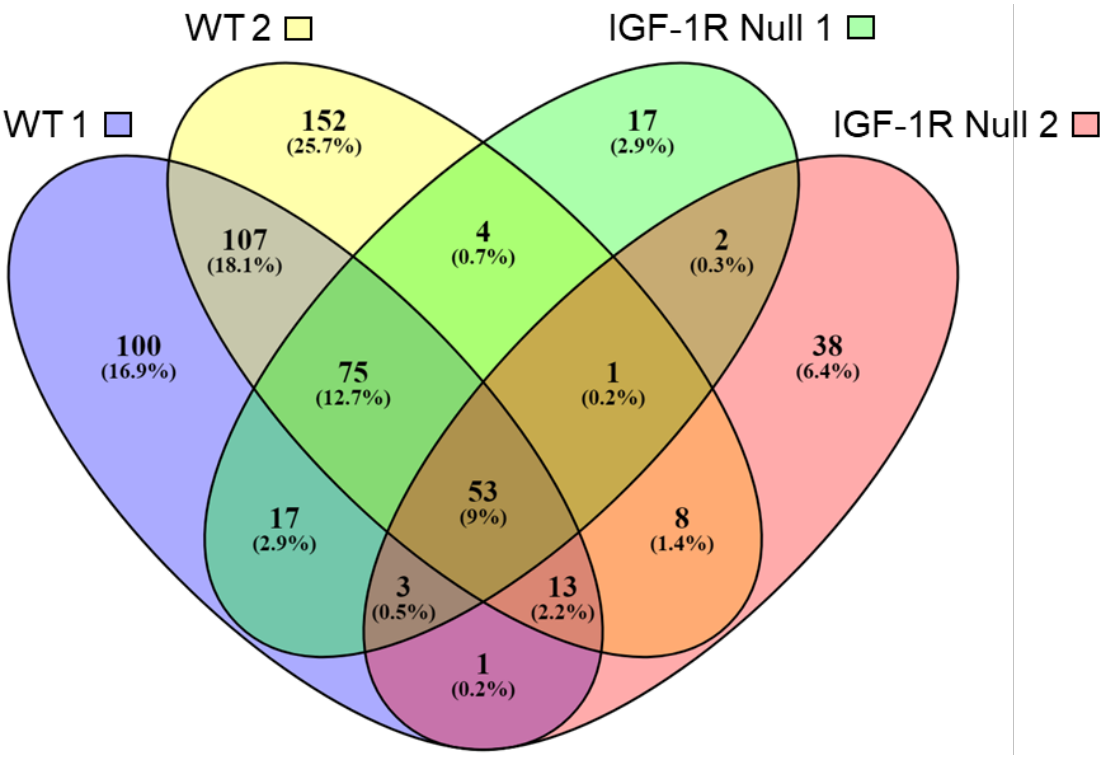


Figure 6.2 Distribution of the number of protein hits detected in WT and IGF-1R null IPs by mass spectrometry
Venn diagram showing the distribution of different proteins identified by mass spectrometry in each of the two WT and two IGF-1R null samples. Overlapping sections indicate hits that were detected in 2 or more samples. As shown, most hits, approximately 60%, were identified in either of the WT samples or both. The hits that were identified in only IGF-1R null samples (approximately 12%) were excluded from further analysis as they represent potential false positive hits. The full list of hits is listed in appendices (Section 8.1).

The lack of detection of IGF-1R and presence of contaminants raised doubts about successful detection of the IGF-1R nuclear interactome. However, this dataset did identify previously known interactors of nuclear IGF-1R including PCNA (Waraky *et al.*, 2017), importin-β and Ran-BP2 (Packham *et al.*, 2014), NOM1 (Solomon-Zemler *et al.*, 2019) and GATA2 (Aleksic *et al.*, 2018), as discussed in Section 1.6.3. These findings suggested that some genuine nuclear IGF-1R interacting proteins had been detected. Therefore, we further analysed the data to identify potential hits of interest for validation.

Proteins that were identified in the two IGF-1R null samples only were excluded from analysis, as these were likely to be non-specific, along with those for which only 1 peptide was detected in both WT samples as the low level of detection suggested the hit may have

been a false positive. Average peptide numbers were then calculated for each detected protein across both the two WT and two IGF-1R null samples. The data were analysed by two-way ANOVA to test for hits for which a statistically significant increase in average peptide number could be detected in WT vs IGF-1R null samples. This generated a list of 10 proteins that were detected at a statistically significantly higher level in WT cells than IGF-1R null cells. While this analysis excluded a large portion (>98%) of the dataset, this method was thought to give more confidence in deciding which hits to initially investigate and validate (Dr Vendrell, personal communication). These remaining proteins were then sorted by the difference in average peptide number between the WT vs IGF-1R null samples (Table **6.1**).

Acc Number	Description	WT 1 No. of peptides	WT 2 No. of peptides	Null 1 No. of peptides	Null 2 No. of peptides	Mean Diff. No. of peptides	Summary	Adjusted P Value
P78527	DNA-dependent protein kinase catalytic subunit	33	79	8	11	46.5	****	<0.0001
P52272	Heterogeneous nuclear ribonucleoprotein M	32	27	13	2	22	****	<0.0001
Q08211	ATP-dependent RNA helicase A	20	18	2	4	16	****	<0.0001
P02545	Prelamin-A/C	15	21	3	1	16	****	<0.0001
Q6W2J9	BCL-6 corepressor	12	20	2	0	15	***	0.0003
Q00839	Heterogeneous nuclear ribonucleoprotein U	16	21	8	1	14	**	0.0013
Q14498	RNA-binding protein 39	5	30	4	4	13.5	**	0.0026
P11142	Heat shock cognate 71 kDa protein	19	16	9	2	12	*	0.0206
P10809	60 kDa heat shock protein mitochondrial	19	12	5	3	11.5	*	0.0389
Q9BQG0	Myb-binding protein 1A	14	10	1	0	11.5	*	0.0389

Table 6.1 Table of potential nuclear IGF-1R interactome proteins
Table listing the nuclear IGF-1R interacting protein hits that were enriched to a statistically significant higher level in IGF-1R IP from WT vs IGF-1R null 22Rv1 cells analysed by mass spectrometry. Analysis was performed on the full data set listed in appendices (Section 8.1), excluding hits identified in only IGF-1R null samples, or those identified in either of the WT samples with a peptide number of only 1. (p*<0.05, p**<0.005, p*** < 0.0005, p**** < 0.0001, Two-way ANOVA).

The analysis shown in Table **6.1** identified DNA-PKcs as the top ranked hit. DNA-PKcs is the catalytic subunit of the DNA-dependent serine/threonine protein kinase DNA-PK. DNA-PKcs forms a complex with the Ku70/Ku80 heterodimer to form the DNA-PK holoenzyme, which is required for NHEJ of the broken DNA ends at DSBs (Lieber, 2010).

NHEJ is initiated via binding of broken DNA ends by the Ku70/Ku80 heterodimer, followed by recruitment of DNA-PKcs through its interaction with Ku70/Ku80 and DNA. Binding to DNA promotes activation of DNA-PKcs kinase activity and activated DNA-PKcs phosphorylates Ser139 on histone variant H2AX (γH2AX), a well-known marker of DNA damage (Paull *et al.*, 2000) that aids in recruitment of DSB repair proteins. DNA-PKcs recruitment to DNA ends to form the DNA-PK holoenzyme promotes DNA-end tethering (Graham, Walter and Loparo, 2016), triggers phosphorylation of DNA-PKcs and recruits other NHEJ core proteins including XRCC4 (Li *et al.*, 1995), XLF (Ahnesorg, Smith and Jackson, 2006; Buck *et al.*, 2006) and DNA ligase IV (Critchlow, Bowater and Jackson, 1997; Grawunder *et al.*, 1997), which align and ligate the DNA ends (Blackford and Jackson, 2017).

Previous work from our lab found that IGF-1R depletion enhances the radiosensitivity of prostate cancer cells (Rochester *et al.*, 2005), and delays repair of DSBs by both homologous recombination (HR) (Turney *et al.*, 2012) and NHEJ (Chitnis *et al.*, 2014). Given this finding and the important role of DNA-PKcs in NHEJ (Blackford and Jackson, 2017), this protein was therefore chosen as the focus for validation.

6.2.3 Validation of DNA-PKcs interaction

Initial validation experiments involved IP of IGF-1R followed by Western blotting for DNA-PKcs. As in Section 6.2.1, 22Rv1 cells were first fractionated into nuclear and cytoplasmic extracts and analysed by Western blotting to confirm detection of DNA-PKcs in the nucleus (Figure **6.3**a). IP for IGF-1Rβ was then performed from precleared nuclear protein and the immunoprecipitates were then analysed to test for the presence of DNA-PKcs using western blotting transfer conditions adjusted for the high molecular weight (450 kDa) of the protein (see Section 2.3).

As shown in Figure **6.3**b, both DNA-PKcs and IGF-1Rβ were detected in the input samples, as expected. IGF-1Rβ was detected in the IP of IGF-1Rβ but not in the IgG negative control suggesting successful immunoprecipitation of the receptor. DNA-PKcs could also be detected in the IGF-1Rβ IP, but not in the IgG control IP, therefore supporting the detection of interaction with IGF-1Rβ by mass spectrometry. Immunoprecipitates were also probed for two additional DNA repair proteins: PARP-1, another hit in the mass spectrometry dataset (Section 8.1) but found not to be significantly enriched vs IGF-1R null control samples (Table **6.1**), and Ku80 which was not a mass spectrometry hit but is a protein well characterised to interact with DNA-PKcs (Lieber, 2010). Both proteins could be detected in nuclear, cytoplasmic, and whole cell extract inputs, but could not be detected in any of the IPs. These negative results add more weight to the positive result seen for interaction of IGF-1R with DNA-PKcs.

In light of the previous results in this thesis showing interaction of IGF-1Rα- and β-subunits in the nucleus (Section 3.2.1, Figure **3.2**d and e), an IP for IGF-1Rα was also performed to test whether the α-subunit is involved in the interaction with DNA-PKcs. DNA-PKcs could not be detected in the IGF-1Rα IP, however the faint band for IGF-1Rβ in this IP (Figure **6.3**b), in contrast to previous experiments (Section 3.2.1, Figure **3.2**d and e), suggests that the IP for the α-subunit was potentially not successful. If time had permitted, further repeats of this experiment would have been performed to confirm the presence or absence of an interaction between IGF-1Rα and DNA-PKcs. Given time constraints and that the mass spectrometry dataset was generated from an IP of IGF-1Rβ, further validation experiments focused on the interaction between DNA-PKcs and the β-subunit.

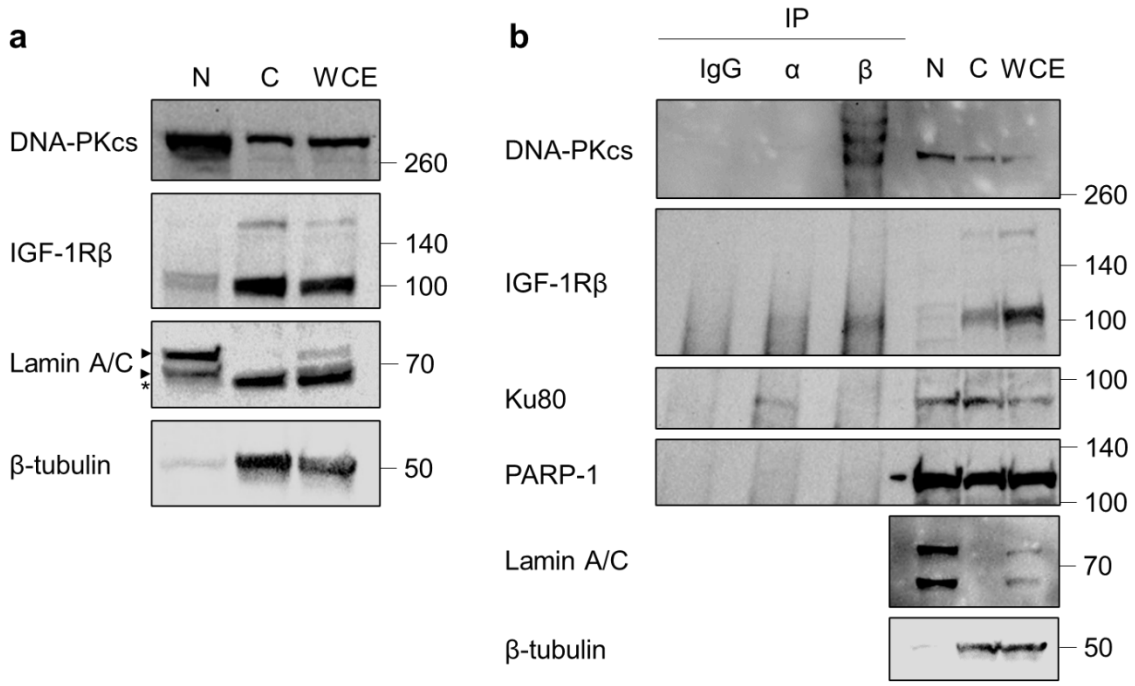


Figure 6.3 IGF-1Rβ-subunit interacts with DNA-PKcs in the nucleus of 22Rv1 cells
a Cells were lysed and fractionated to give nuclear, cytoplasmic, and whole cell extracts which were analysed by Western blot for DNA-PKcs and IGF-1Rβ. A similar result was obtained in a second independent set of immunoprecipitates. Successful fractionation of nuclear and cytoplasmic extracts was determined by detection of fractionation markers Lamin A/C (Arrowheads: doublet at 74, 63 kDa respectively, nuclear marker) and β-tubulin (55 kDa, cytoplasmic marker). Asterisk: β-tubulin signal (50kDa) visible on re-probing the same membrane for Lamin. **b** Cells grown in normal culture medium were fractionated and nuclear lysates were immunoprecipitated with IgG (control) or antibody to IGF-1Rα or IGF-1Rβ. IPs were analysed by Western blot in parallel with N, C and WCE input controls (10% of IP input) using antibodies for IGF-1Rβ, DNA-PKcs, Ku80 and PARP-1. A similar result was obtained in a second independent set of immunoprecipitates, and fractionation of nuclear and cytoplasmic extracts was determined as in (**a**).

Concurrent and independent phospho-proteomics data obtained by another DPhil student in our lab, Matthew Ellis, also showed by mass spectrometry a difference in phosphorylation of DNA-PKcs at residue S3205 in 22Rv1 IGF-1R WT vs null cells in response to IR. This finding suggested a decreased level of S3205 phosphorylation in the IGF-1R null vs WT clones 1 hr after 2 Gy IR. The S3205 phospho-site is less well characterised than other DNA-PKcs phosphorylations but had been identified by the lab of Prof Susan Lees-Miller, University of Calgary (Douglas *et al.*, 2002; Neal *et al.*, 2011). For this work they had generated a polyclonal antibody to pS3205 DNA-PKcs (Douglas *et al.*, 2002), which they kindly donated to us. However, despite varying Western blotting

conditions to probe whole cell extracts, it was not possible to detect any signal using this antibody, which Prof Lees-Miller had warned us was old and had not been used in their lab for many years. In parallel, Matthew Ellis tested antibodies to other better-characterised DNA-PKcs phospho-sites S2056 and T2609 (Chan *et al.*, 2002; Chen *et al.*, 2005). The latter gave no signal, but he did detect phosphorylation of DNA-PKcs at S2056 in response to IR, with decreased DNA-PKcs phosphorylation in IGF-1R null cells vs WT cells and maximum difference at 8 Gy (Figure **6.4**). Lysates were also probed for phosphorylation of RPA32 on S4/8, reported to be a DNA-PK specific phospho-site (Ashley *et al.*, 2014; Leimbacher *et al.*, 2019). This signal was also reduced in IGF-1R null 22Rv1 cells (Figure **6.4**).

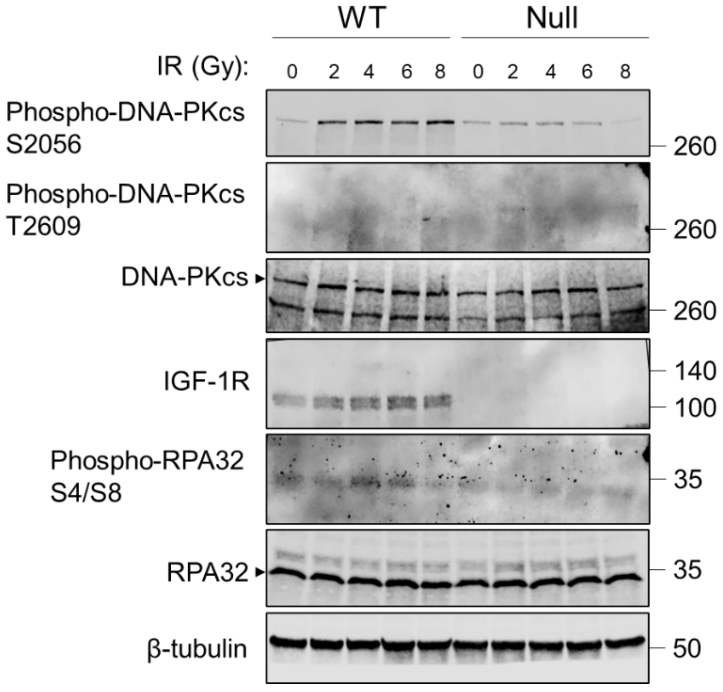


Figure 6.4 DNA-PKcs shows differential phosphorylation following IR in WT vs IGF-1R null 22Rv1 clones
Cells were grown in full culture medium (with 10% FBS) and treated with indicated IR dose before collection 1 hr post treatment. Whole cell lysates were then analysed by Western blot using antibodies for DNA-PKcs, pS2056-DNA-PKcs, pT2609-DNA-PKcs, IGF-1Rβ, pRPA32 (S4/8) and total RPA32. Blot is representative of 3 independent biological repeats completed by Matthew Ellis, with β-tubulin as a loading control.

I then used these antibodies to test for interaction between nuclear IGF-1R and phosphorylated DNA-PKcs. I could not detect pS3205 DNA-PKcs, the specific site detected to be differentially phosphorylated by mass spectrometry, in nuclear, cytoplasmic or WCE inputs (Figure **6.5**a). I re-probed this same IGF-1R IP for pS2056 DNA-PKcs to test for interaction of the receptor with the S2056 phosphorylated form of DNA-PKcs (Figure **6.5**a). This phosphorylated form of DNA-PKcs could be detected in input controls and was present in IGF-1Rβ IP but not in IgG negative control (Figure **6.5**a), suggesting that IGF-1R is interacting with the phosphorylated form of DNA-PKcs. This suggestion was supported by results of IP from WCE of DNA-PKcs and IGF-1Rβ (Figure **6.5**b). DNA-PKcs IP showed successful pull down of both total DNA-PKcs and pS2056 DNA-PKcs, as would be expected. IGF-1Rβ IP also showed presence of pS2056 DNA-PKcs, supporting the result shown in Figure **6.5**a, although IGF-1R itself was only weakly detected. Total DNA-PKcs was not detected (Figure **6.5**b), unlike previous IP experiments from nuclear extract (Figure **6.3**). However, given that this IP was from WCE and only a small proportion of the total IGF-1R is in the nucleus (Aleksic *et al.*, 2010, 2018) the amount of nuclear IGF-1R available for IP is likely to be very low, and therefore so is the proportion of IP'd receptor interacting with DNA-PKcs. Detection of pS2056 DNA-PKcs but not total DNA-PKcs here was potentially due to difference in sensitivity of the Western blotting antibodies used. With time permitting, future experiments would be performed to repeat this experiment from nuclear extract rather than WCE, aiming to improve the clarity of IGF-1Rβ detection and obtain more support for interaction of IGF-1R with pS2056 DNA-PKcs.

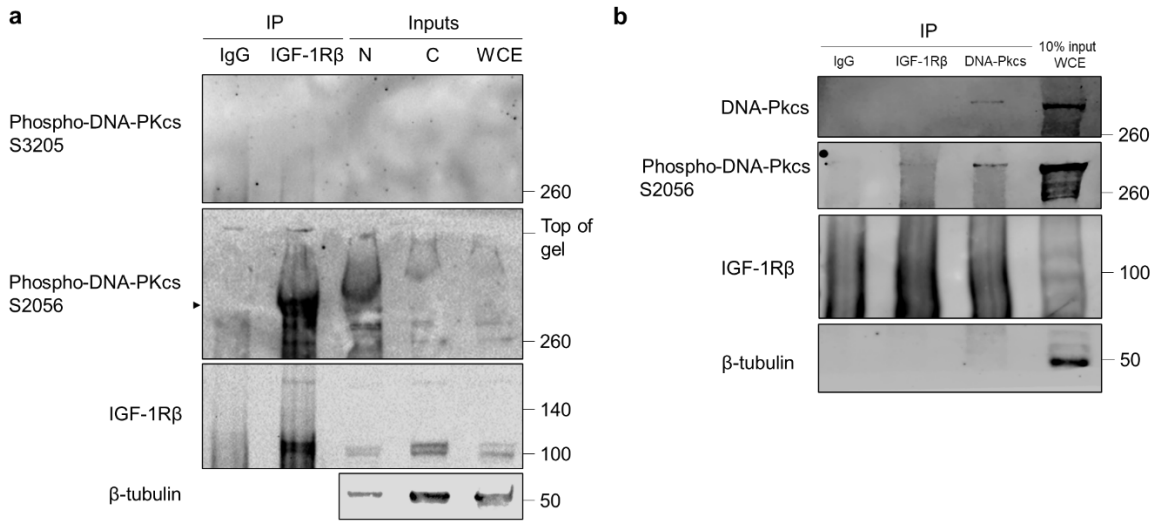


Figure 6.5 IGF-1R interacts with phosphorylated DNA-PKcs in 22Rv1 cells
a Cells were grown in normal culture medium as in Figure **6.3** and fractionated into nuclear (N) and cytoplasmic (C) fractions. Nuclear lysates were immunoprecipitated with IgG control antibody or IGF-1Rβ antibody and analysed by Western blot alongside N, C and WCE input controls (10% of IP input) using antibodies to pS3205 or pS2056 DNA-PKcs (Arrowhead: Phospho-DNA-PKcs 2056, 450 kDa). A similar result was obtained in a second independent set of immunoprecipitates and separation of nuclear extract from cytoplasmic contaminants was determined by detection of β-tubulin (cytoplasmic marker). **b** Cells were grown in normal culture medium and whole cell extracts were immunoprecipitated with IgG (control), IGF-1Rβ or DNA-PKcs as indicated. IPs were analysed by Western blot alongside input controls in 2 independent biological repeats as in (**b**).

To investigate the potential functionality of IGF-1R – DNA-PKcs interaction, and given the importance of DNA-PK in the DNA damage response, I performed IP of IGF-1R from nuclear extract in unirradiated cells or following treatment with 5 Gy or 10 Gy IR. One-hour post-IR, cells were fractionated and IGF-1Rβ IP was performed from nuclear extract (Figure **6.6**). No change in the levels of interaction of the two proteins could be detected in response to IR, as DNA-PKcs was detected at similar levels in the IPs from all 3 conditions, suggesting damage-independent interaction. The IPs were also probed for Ku80 that complexes with DNA-PKcs and Ku70 to form the DNA-PK holoenzyme. Ku80 was detected in the inputs as expected, but not in the IPs suggesting IGF-1R does not interact with the total DNA-PK complex. Although not performed here, future repeats of this experiment should include an IR-treated IgG negative control IP.

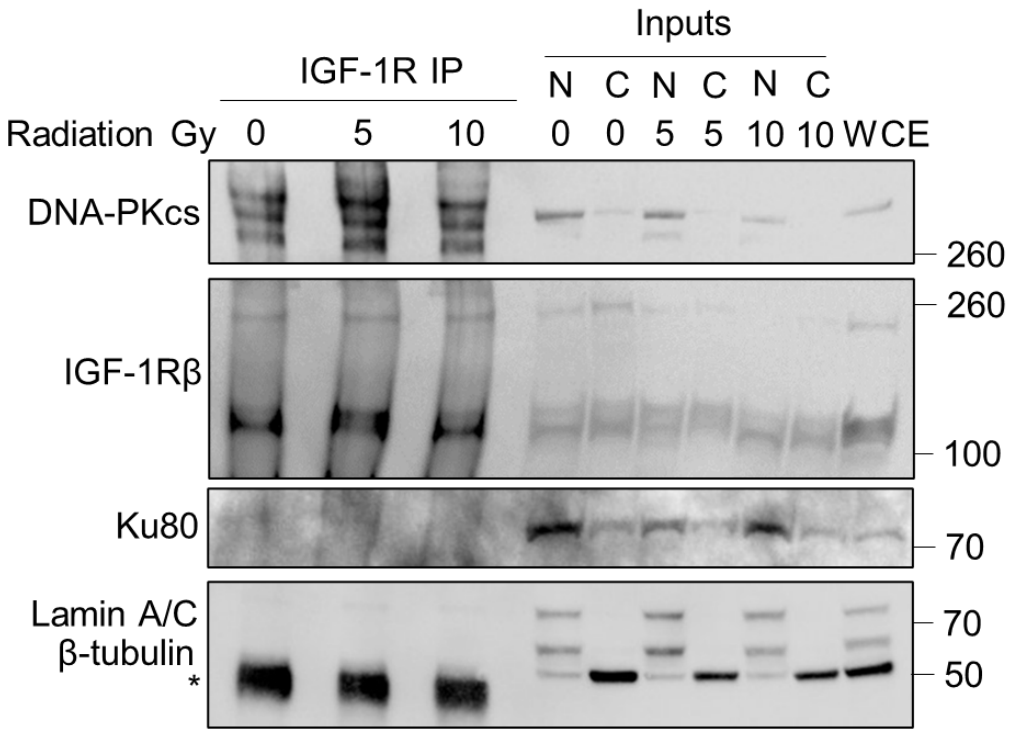


Figure 6.6 IGF-1R and DNA-PKcs interaction is independent of IR
22Rv1 cells were treated with 0, 5 or 10 Gy and 1 hr post IR were fractionated into nuclear (N) and cytoplasmic (C) fractions. Nuclear lysates were immunoprecipitated with antibody for IGF-1Rβ and analysed by Western blot alongside N, C and WCE input controls (10% of IP input) using antibodies for IGF-1Rβ, DNA-PKcs and Ku80. A similar result was obtained in a second independent set of immunoprecipitates, and fractionation of nuclear and cytoplasmic extracts was determined by detection of fractionation markers Lamin A/C (doublet at 74, 63 kDa respectively, nuclear marker) and β-tubulin (55 kDa, cytoplasmic marker). Asterisk: band for IgG isotypes released from beads during IP procedure.

In further functional experiments performed with Matthew Ellis, we investigated recruitment of DNA-PKcs to chromatin in response to IR, given that DNA-PKcs is recruited to chromatin to promote DSB repair via NHEJ (Gell and Jackson, 1999; Lieber, 2010; Jette and Lees-Miller, 2015). WT and IGF-1R null 22Rv1 cells were irradiated at 8 Gy by Matthew Ellis as this dose showed the maximum difference in DNA-PKcs S2056 phosphorylation in his previous experiment (Figure **6.4**). Then we both collected cells 10 mins, 1 hr and 4 hr post IR and on parallel cultures performed chromatin fractionation or whole cell lysis alongside unirradiated controls. Western blot analysis of WCEs confirmed loss of IGF-1R in the null cells, and showed reduced phosphorylation of S2056 DNA-PKcs and S4/8 RPA32 in IGF-1R null cells (Figure **6.7**a), as shown previously by

Matthew (Figure **6.4**). We noted that chromatin fractions showed no detectable recruitment of DNA-PKcs to chromatin in IGF-1R null vs WT cells (Figure **6.7**b). IGF-1R itself was not detected on chromatin extracted from WT cells. The Ku70/80 signal was weak, detectable only on long exposure, in contrast to the clear signals in WCE, suggesting the signals may be non-specific as no changes in recruitment to chromatin of Ku70/80 could be detected in response to IR. We also detected γH2AX on chromatin with increased signal in both WT and IGF-1R null cells, consistent with induction of, and response to, DNA damage.

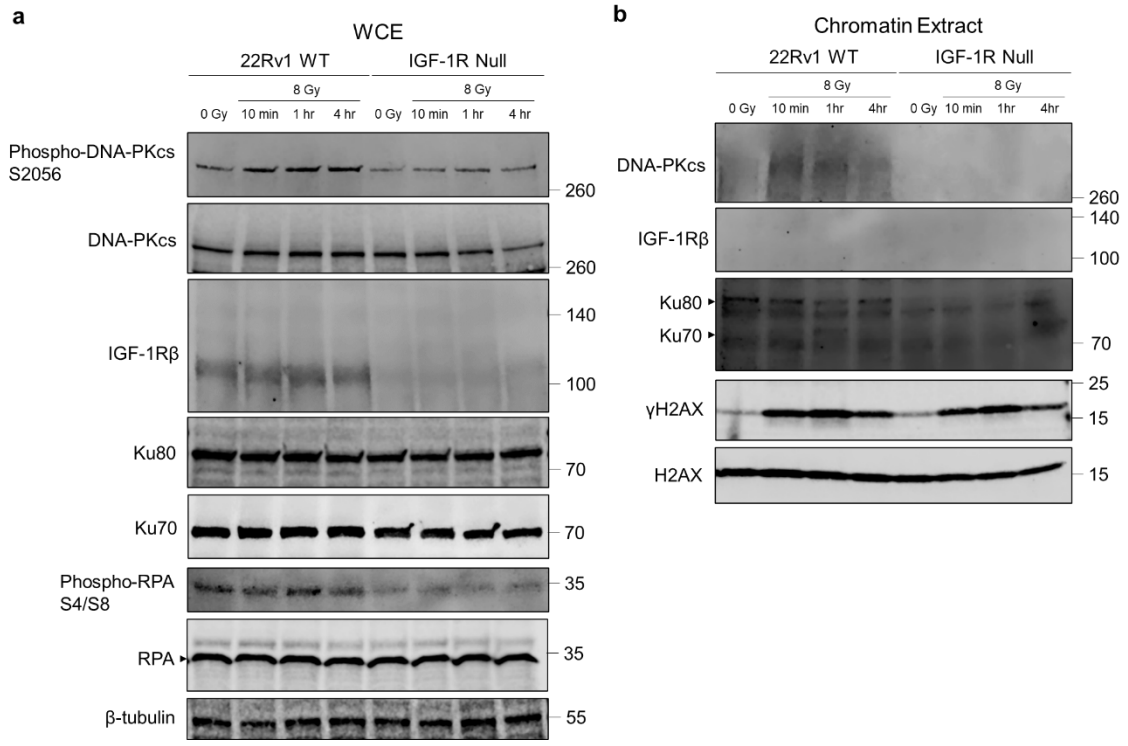


Figure 6.7 DNA-PKcs recruitment to chromatin is reduced in IGF-1R null cells
22Rv1 WT cells and a 22Rv1 IGF-1R null CRISPR knockout cell line were grown in normal culture media before treatment with 8 Gy IR. Both cell lines were then collected at the indicated time points post-IR and either processed for whole cell lysis (**a**) or chromatin extraction (**b**). Samples were then analysed by Western blot using antibodies for DNA-PKcs, pS2056 DNA-PKcs, IGF-1Rβ, pIGF-1R (Tyr1135/1136), Ku70/80, Ku80, pRPA (S4/8), RPA and γH2AX. For WCE (**a**) and chromatin (**b**) samples respectively, β-tubulin and H2AX acted as loading controls. Due to time constraints this Western blot was not repeated.

6.3 Discussion

Overall, the initial aim of this work was to use mass spectrometry to generate an interactome data set for nuclear IGF-1R. Nuclear fractionation and IP of IGF-1Rβ-subunit were performed, and IP'd proteins were analysed by mass spectrometry. Interaction of nuclear IGF-1R with the DNA repair related protein DNA-PKcs, has now been initially validated for the first time. Nuclear IGF-1R was shown to interact with pS2056 DNA-PKcs in a novel finding, and the same site was shown to be differentially phosphorylated in WT vs IGF-1R null clones by Matthew Ellis. No changes in interaction between IGF-1R and DNA-PKcs could be detected post-IR, but initial experiments in cells lacking IGF-1R, recruitment of DNA-PKcs to chromatin in response to IR was shown to be reduced, consistent with previous findings from our lab showing that IGF-1R inhibition delays DSB repair by NHEJ (Chitnis *et al.*, 2014).

The mass spectrometry dataset generated here was found to contain *Staphylococcus aureus* contaminants. To improve the quality of this dataset, magnetic beads could have been used for IGF-1R IP. While magnetic beads have a lower binding capacity for antibody as they are non-porous, they do not interact with each other to form a protein complex as agarose beads do. This means all bound antibodies are accessible to antigen, so magnetic beads may offer greater antigen yield. The use of a magnet rather than centrifugation to separate beads from supernatant also makes it easier to remove buffers without disturbing the bead pellet, which increases the efficiency of washes, the reproducibility of the experiment, and may decrease the chances of contamination (*https://www.thermofisher.com/uk/en/home/life-science/protein-biology/protein-biology-learning-center/protein-biology-resource-library/pierce-protein-methods/immunoprecipitation-ip.html*). Extra cellular input for IP could also be used to increase the chance of detecting IGF-1R by mass spectrometry. If time had permitted, these modifications would have been assessed.

Although DNA-PKcs could be detected in IGF-1R IP (Figure **6.3**b), IGF-1R was detected only weakly in reciprocal DNA-PK IP (Figure **6.5**b). Recent work by Yang *et al*., published during the completion of this thesis write up, also investigated the interactome of IGF-1R, focussing on validating the interaction of IGF-1R with nuclear mitotic apparatus protein (NuMA). However, in the initial nuclear IGF-1R interactome mass spectrometry generated as part of this work, DNA-PKcs was also detected, although not further validated (Yang *et al.*, 2021), therefore supporting the finding in this thesis. If time had been permitting, DNA-PKcs IP experiments would have been repeated to further confirm this. These experiments could have used magnetic beads to improve IP, as discussed above, or Protein G agarose beads which are optimised for IP of antibodies of mouse origin (Fishman and Berg, 2019) such as the DNA-PKcs antibody used here. *In vitro* pull-down assays using 2 differently tagged IGF-1R and DNA-PKcs recombinant proteins, which would provide a cleaner IP, could also be used to confirm this interaction, or similarly, experiments using one recombinant protein incubated with IP of the other. Subsequent experiments could explore which domains of the proteins interact using differently truncated versions of IGF-1R and/or DNA-PKcs *in vitro*. X-ray crystallography could also be used to assess the exact structure of the interaction between proteins. *In vitro* work would also determine whether IGF-1R needs to be phosphorylated to interact with DNA-PKcs, and thus whether the interaction is IGF ligand dependent.

Previous work from our lab found that in the context of DSB repair by NHEJ, IGF-1R and DNA-PKcs function in the same pathway. IGF-1R inhibition was found to enhance the radiosensitivity of M059K, a glioblastoma cell line, but in a DNA-PKcs deficient cell line (M059J) established from the same tumour (Allalunis-Turner *et al.*, 1995), IGF-1R inhibition had no effect on radiosensitivity. Experiments in DU145 prostate cancer cells also found that IGF-1R inhibition increased the radiosensitivity of control treated cells but

had no effect on the radiosensitivity of cells pre-treated with an inhibitor of DNA-PKcs (Chitnis *et al.*, 2014). Overall, these results suggested there is epistasis between IGF-1R activation and NHEJ however it is unclear whether this functional link is via IGF-1R signalling pathway activation (Cosaceanu *et al.*, 2007; Valenciano *et al.*, 2012; Xu *et al.*, 2012). The detection of DNA-PKcs as a nuclear IGF-1R interactor raises the possibility that the functional link may be due to the physical interaction of nuclear IGF-1R and DNA-PKcs. This would be analogous to increased activation of DNA-PKcs in response to DNA damage via interaction with nuclear EGFR (Dittmann *et al.*, 2005; Liccardi, Hartley and Hochhauser, 2011), another RTK that undergoes nuclear translocation (S. Lin *et al.*, 2001) (Section 1.5.1).

Of the three DNA-PKcs phosphorylation sites probed for by Western blot, S2056 and T2609 are the most well characterised and undergo autophosphorylation when DNA-PKcs is activated (Chan *et al.*, 2002; Chen *et al.*, 2005), although T2609 may also undergo phosphorylation by ATM and ATR under certain circumstances (Yajima, Lee and Chen, 2006; Chen *et al.*, 2007). It is thought that both sites are important for DNA repair (Jette and Lees-Miller, 2015) and it is suggested that S2056 phosphorylation may regulate Ku80 binding (Sibanda *et al.*, 2017). The S3205 phospho-site is less well characterised but has also been shown to undergo autophosphorylation *in vitro* (Douglas *et al.*, 2002), is phosphorylated in an ATM-dependent manner after IR (Neal *et al.*, 2011), and undergoes phosphorylation by polo-like kinase 1 during mitosis, although the effects of this phosphorylation remain unclear (Douglas *et al.*, 2014).

It is worth noting that despite detecting an interaction between IGF-1R and p2056 DNA-PKcs (Figure **6.5**) an interaction between IGF-1R and Ku80 could not be detected (Figure **6.3**), potentially suggesting IGF-1R interacts with DNA-PKcs when it is not interacting with the Ku70/Ku80 heterodimer on chromatin to form the DNA-PK holoenzyme.

Consistent with this, recruitment of IGF-1R to chromatin could not be detected by Western blot (Figure **6.7**b). It is unclear whether the apparent lack of recruitment of DNA-PKcs to chromatin seen in IGF-1R null cells (Figure **6.7**b) is due to the loss of the direct interaction between IGF-1Rβ and DNA-PKcs or due to changes in IGF-mediated signalling. DNA-PKcs is recruited to chromatin and then undergoes S2056 auto-phosphorylation (Chen *et al.*, 2005), so the reduced phosphorylation of DNA-PKcs seen in IGF-1R null cells (Figure **6.4**) implies reduced recruitment, consistent with the reduced recruitment seen in Figure **6.7**b. With time permitting further experiments would have been carried out to investigate this, including repeating the chromatin fractionation experiment in Figure **6.7**. Advice from Prof. Andrew Blackford (Department of Oncology, University of Oxford), suggested that due to the lack of changes in Ku70/80 recruitment to chromatin following IR, the signal detected in Figure **6.7**b may be non-specific, and more DNA damage may be needed to induce detectable recruitment. If time had permitted, future repeats of these experiments could have used radiomimetic drug phleomycin to induce these higher levels of DNA damage, as in (Ochi *et al.*, 2015), to assess differences in Ku70/80 and subsequent DNA-PKcs recruitment to chromatin. Further chromatin fractionation experiments would also have been carried out in the presence of inhibitors of IGF-1R and downstream kinases Akt and ERK. If downstream kinase inhibitors induced the phenotype seen in IGF-1R null cells, then this would imply that DNA-PKcs recruitment to chromatin requires signalling downstream of IGF-1R. Conversely, if DNA-PKcs chromatin recruitment is unaffected by downstream kinase inhibition but is impaired by inhibition of IGF-1R kinase activation and internalisation, this may suggest the direct interaction with IGF-1R is required to promote DNA-PKcs chromatin recruitment. This would therefore support a functional role for the interaction between IGF-1R and DNA-PKcs, although previous work has already shown that Akt interacts with DNA-PKcs to promote autophosphorylation of DNA-PKcs

at S2056 (Toulany *et al.*, 2012) and therefore DNA repair (Jette and Lees-Miller, 2015). This could be further investigated using deletion or point mutation IGF-1R constructs that do not show kinase activity but maintain the structural integrity and subcellular localisation of the receptor, such as those generated by (Zhang et al., 2015; Jamwal et al., 2018), or the TSM IGF-1R constructs used by (Sehat *et al.*, 2010; Warsito *et al.*, 2012; Lin *et al.*, 2017), that maintain kinase activity but show reduced nuclear translocation (discussed in Sections 1.6.1 and 1.6.4). Whether IGF-1R directly phosphorylates DNA-PKcs could also be tested using recombinant forms of the two proteins in an *in vitro* kinase assay.

Further experimental work will be needed to investigate the impact on changes in the function of the DNA-PK complex in DNA repair via NHEJ. The reduction in DNA-PKcs recruitment to chromatin in IGF-1R null cells could contribute to the reduced NHEJ in IGF-1R inhibited cells as previously shown by our lab (Chitnis *et al.*, 2014). This could be tested using assays for NHEJ activity such as the GFP NHEJ reporter cassette (Seluanov, Mao and Gorbunova, 2010). Further work is also needed to validate this interaction in other prostate cancer cell lines, such as DU145 used in Chapters 3 and 4, as well as other cancer types.

7 Chapter VII: Conclusion and Future Directions

The main aim of the work in this thesis was to gain a better understanding of the biology of nuclear IGF-1R in prostate cancer. This included investigating the role of the α-subunit of the receptor in the nucleus, generating a screening platform for small molecule inhibitors of nuclear IGF-1R, investigating recruitment of IGF-1R to chromatin *in vivo* and the protein interactome of the nuclear receptor.

Initial work showed detection of IGF-dependent changes in nuclear IGF-1Rα-subunit in DU145 and 22Rv1 prostate cancer cells, confirming previous work from our lab showing detection of nuclear α-subunit by IHC (Aleksic *et al.*, 2010). In novel findings, work here showed an interaction between IGF-1Rα- and β-subunits in the nucleus and that the α-subunit of the receptor is also recruited to IGF-1R DNA binding sites, only previously shown for the β-subunit of the receptor (Sehat *et al.*, 2010; Wu, Zhu and Robertson, 2012; Warsito *et al.*, 2016; Aleksic *et al.*, 2018). These novel findings therefore raise the question of what further, currently unidentified, interactions of nuclear IGF-1R can be detected via the α-subunit of the receptor. If time had been permitting, ChIP-seq for IGF-1Rα-subunit would have been carried out to try and assess this question, with the possibility that there are further IGF-1R DNA binding sites that can be detected via recruitment of the α-subunit. IGF-dependent recruitment of the α-subunit to these regions could be tested, as with the β-subunit (Warsito *et al.*, 2016; Aleksic *et al.*, 2018), and contribution to promoting activation of genes associated with cancer growth and progression could be measured by qPCR. It is possible that both subunits bind a distinct set of DNA binding sites, but the detected recruitment here of the α-subunit to known β-subunit binding sites raises the question of whether both subunits remain in a complex when interacting with chromatin. ChIP for the α-subunit would help to answer part of this question alongside further work to identify which domains of IGF-1R interact with DNA.

This could be determined using EMSA with different recombinant IGF-1R constructs, such as 486STOP, a construct encoding a portion of the α-subunit (Dunn *et al.*, 1998; Reiss *et al.*, 1998), and 952STOP, a construct truncated at residue 952 within the β-subunit (Prager *et al.*, 1992). An adapted surface plasmon resonance technique, previously used to investigate the interaction between ER and DNA, could also be used with these truncated versions of IGF-1R to potentially identify DNA binding domains (Teh *et al.*, 2007).

The presence of the ligand binding α-subunit in the nucleus also raises the question of whether IGF-1 ligand is still bound to nuclear IGF-1R. Previous work has shown EGF ligand bound to EGFR in the nucleus of breast cancer cells (S. Lin *et al.*, 2001), and proliferating hepatocytes (Grasl-Kraupp *et al.*, 2002; de Angelis Campos *et al.*, 2011), and the presence of insulin ligand in the nucleus in human lymphocyte cells has also been shown (Goldfine *et al.*, 1977). EGF, PDGF and nerve growth factor ligands have also been detected in the nucleus and shown to bind to chromatin in colorectal cancer cells (Rakowicz-Szulczynska *et al.*, 1986). To our knowledge, the presence of nuclear IGF-1 ligand has not previously been detected. This could be investigated by fractionation and Western blotting or by IF to determine the presence of nuclear IGF-1. Whether this ligand is bound by nuclear IGF-1R could also be investigated by PLA or co-IP.

It is still unclear which subunit and domains of nuclear IGF-1R mediate interactions with other nuclear proteins and recruitment to chromatin. Previous work with EGFR identified a strong transactivation domain within the carboxy terminus of the receptor (S. Lin *et al.*, 2001). Transactivation domains contain binding sites for other proteins such as transcription coregulators (Triezenberg, 1995) and are therefore likely involved in chromatin and nuclear protein interactions. While a transactivation domain has not currently been identified within IGF-1R, identification of domains that mediate nuclear IGF-1R interactions, via experiments outlined above, will help to identify the regions of

the receptor required for these interactions. This will help to further understand nuclear IGF-1R function, and its contribution to cancer progression.

The second aim of this thesis was to use a screening platform to identify small molecule inhibitors of nuclear IGF-1R function that could have identified potential new tumour-selective IGF-1R inhibitor treatments. There may also have been potential to elucidate as yet unknown aspects of the IGF-1R nuclear translocation mechanism, via identification of proteins whose inhibition blocked IGF-1R translocation, and which may themselves be targets for cancer treatment. A suitable stable clone containing one of the tested IGF-1R DNA binding sites could not be generated, and a small molecule screen was not undertaken. However, as previously discussed (Section 4.3), this method may not have identified small molecule inhibitors specific for nuclear IGF-1R, given likely use of translocation mechanisms similar or identical to other RTKs including INSR. Furthermore, such a screen could have identified direct inhibitors of luciferase (although as discussed, the choice of reporter plasmid was designed to reduce this risk), or drugs that were general inhibitors of translocation or chromatin binding.

To investigate IGF-1R DNA binding sites *in vivo*, IGF-1R ChIP-seq was performed from malignant biopsies from patients undergoing RP. In novel findings, this work detected recruitment of IGF-1R to chromatin *in vivo*. Identified IGF-1R peaks were proximal to gene TSS, and 38% of peaks were coincident with H3K4me1 peaks, a marker for active gene enhancer regions (Yu *et al.*, 2010), suggesting IGF-1R is recruited to regulatory DNA regions at these sites and may influence gene expression. However, only 3% of identified IGF-1R peaks overlapped with those identified for AR in samples from two untreated patients by (Sharma *et al.*, 2013).

Future work is now needed to validate these identified IGF-1R binding sites by ChIP-qPCR *in vitro* and to test whether there is a link between IGF-1R recruitment and gene

expression at the transcriptional and/or epigenetic level. Analogous to our previous work (Aleksic *et al.*, 2018), recruitment of IGF-1R to identified regions could be tested for IGF-dependency via IGF ligand stimulation and inhibition experiments. Direct activation and upregulation of gene expression by recruitment of IGF-1R to identified gene promoters, rather than indirect activation via IGF-1R signalling, could also be tested. Experiments using a kinase dead receptor construct that retains nuclear but not signalling function, such as the construct identified by (Jamwal *et al.*, 2018), or a construct which retains signalling function but shows reduced nuclear translocation, such as the TSM IGF-1R developed and used by the Larsson lab (Sehat *et al.*, 2010; Warsito *et al.*, 2012; Lin *et al.*, 2017), could be used to test this. Constructs could be expressed in IGF-1R null cell lines generated by our lab and used in this thesis, and recruitment of these IGF-1R constructs to identified binding sites could be tested and expression of related genes could be assessed using qPCR. Confirmation of gene upregulation by nuclear IGF-1R recruitment to chromatin would further confirm the clinical relevance of nuclear IGF-1R in cancer biology.

As discussed previously (Sections 5.2.3 and 5.3), if time had been permitting, a higher number of patient cases would have been assessed including cases with cancers at a range of stages. Previous work has shown an association of nuclear IGF-1R with a more advanced prostate cancer stage (Aleksic *et al.*, 2018). Therefore IGF-1R ChIP-seq from more advanced cancers may show a different set of IGF-1R chromatin binding sites that explains this association. This may involve binding to a higher number of gene promoters associated with functions that contribute to cancer progression including cell growth, cell motility and cell survival. Validation of the novel detection here of IGF-1R recruitment to chromatin *in vivo*, will further confirm the clinical relevance of IGF-1R and the mechanisms by which nuclear IGF-1R contributes to cancer progression.

Finally, we also investigated the nuclear interactome of the receptor. Work in this thesis used immunoprecipitation of the β-subunit of IGF-1R from nuclear extract and mass spectrometry to identify nuclear proteins interacting with IGF-1R. DNA-PKcs was successfully identified and validated as an interactor of nuclear IGF-1R. While work recently published during the completion of this thesis also detected DNA-PKcs amongst the nuclear IGF-1R interactors by mass spectrometry (Yang *et al.*, 2021), the validation of the interaction in this thesis represents a novel finding. A phospho-proteomics dataset obtained by Matthew Ellis, DPhil student in our lab, also showed differential phosphorylation of DNA-PKcs in WT 22Rv1 vs IGF-1R null cells in response to IR. Validation experiments showed that nuclear IGF-1R was interacting with the phosphorylated form of DNA-PKcs, and work we performed together revealed that IR-induced recruitment of DNA-PKcs to chromatin was detected in WT 22Rv1 cells but not in IGF-1R null cells. However, it is unclear whether the functionality of the IGF-1R-DNA-PKcs interaction is required to trigger DNA-PKcs recruitment to chromatin and phosphorylation. If time had permitted, pull-down experiments would have been performed to test for direct interaction between recombinant IGF-1R and IP'd DNA-PK. IGF-1R contains only a tyrosine kinase domain and has only previously been shown to phosphorylate proteins at tyrosine residues, including histone H3 at Y41 (Warsito *et al.*, 2016), and PCNA at Y60, Y133, and Y250 (Waraky *et al.*, 2017). Therefore, S2056 of DNA-PKcs is likely not directly phosphorylated by IGF-1R. However, if time had been permitting, *in vitro* kinase assays could have been used to assess if DNA-PKcs is phosphorylated via direct interaction with IGF-1R. Truncated versions of either DNA-PKcs or IGF-1R could also have been used to assess which specific domains of the two proteins interact, as discussed in Section 6.3.

Experiments performed here showed no change in the interaction of IGF-1R and DNA-PKcs in response to IR, and no interaction between IGF-1R and Ku70/80 could be detected. Overall, this suggests that IGF-1R does not interact with the DNA-PK holoenzyme when bound to chromatin at sites of DSBs. Indeed, no recruitment of IGF-1R to chromatin could be detected by Western blot, suggesting that IGF-1R interacts with DNA-PKcs in the nucleoplasm. This could be confirmed by PLA for the two proteins, which would visualise intracellular sites of protein:protein interaction, and could also be applied *in situ* to clinical tumours as with previous work by the Larsson lab to validate the IGF-1R-PCNA interaction (Waraky *et al.*, 2017; Yang *et al.*, 2020). Although IGF-1R recruitment to chromatin could not be detected by Western blot, other experiments in this thesis detected recruitment of IGF-1R to chromatin by ChIP-qPCR. This discrepancy is likely due to higher levels of cellular input used for ChIP-qPCR experiments, and the higher sensitivity of ChIP versus Western blotting. Cross-linking steps in the ChIP protocol also likely increased retention of IGF-1R interactions with chromatin. Together with the novel findings described here, the proposed future experiments may support a functional role for IGF-1R in recruitment of DNA-PKcs to chromatin, potentially explaining the epistasis between IGF-1R and NHEJ identified in our lab's previous work (Chitnis *et al.*, 2014) and data from Matthew Ellis (unpublished).

DNA-PK has also been shown to play a role in transcriptional regulation and has been shown to directly interact with and phosphorylate RNAPolII (Dvir *et al.*, 1992; Maldonado *et al.*, 1996), which our lab has shown also interacts with nuclear IGF-1R (Aleksic *et al.*, 2018). DNA-PK expression has been correlated with poor outcome in certain cancer types including NSCLC (Xing *et al.*, 2008) hepatocellular carcinoma (Evert *et al.*, 2013; Cornell *et al.*, 2015) and B-cell chronic lymphocytic leukaemia (Willmore *et al.*, 2008). DNA-PK also plays a role in genome stability, promoting tumour cell survival and progression

regardless of genomic damage (Goodwin and Knudsen, 2014). It is possible that the IGF-1R – DNA-PKcs interaction identified here may play a role in regulating DNA-PKcs activity in these processes as well as NHEJ, that may contribute to the association of nuclear IGF-1R with adverse clinical outcomes (Aleksic *et al.*, 2010, 2018; van Gaal *et al.*, 2013; Codony-servat *et al.*, 2017).

Overall, this project aimed to improve the current understanding of nuclear IGF-1R function, its role in cancer biology and its contribution to cancer progression. In summary, work in this thesis has shown that IGF-1Rα-subunit interacts with IGF-1Rβ-subunit in the nucleus of prostate cancer cells and is recruited to previously identified IGF-1Rβ-subunit DNA binding sites. For the first time, IGF-1R chromatin binding sites were identified *in vivo* in malignant prostate cancer biopsies. The majority of these regions were proximal to gene TSS and 38% were coincident with a histone marker for active enhancers, suggesting a potential regulatory role for nuclear IGF-1R recruitment to chromatin *in vivo*. IGF-1R has also been shown to directly interact with DNA-PKcs, potentially playing a role in DNA-PKcs recruitment to chromatin and contribution to DSB repair by NHEJ. Further work is now needed to determine the wider implications of these findings, including how these functions contribute to cancer progression, and how these findings may be utilised to improve IGF-axis targeted treatment for patients with cancer.

8 Appendices

8.1 List of IGF-1R ChIP-seq hits identified both *in vitro* and *in vivo*

Full list of IGF-1R peaks identified in both our lab's previous *in vitro* ChIP-seq (Aleksic *et al.*, 2018) and the *in vivo* ChIP-seq data generated in this thesis. Table shows the peak calling software used to identify each peak, chromosome co-ordinates for each peak, annotation of relevant region, distance of peak from nearest TSS, nearest promoter ID, gene name, description and gene type for genes in which peaks are present within the TSS.

Peak Calling Method	Chr	Start	End	Annotation	Distance to TSS	Nearest Promoter ID	Entrez ID	Nearest Ensembl	Gene Name	Gene Description	Gene Type
MACS2 Narrow	chr8	43094777	43094988	Intergenic	-52703	NM_001005365	340441	ENSG00000188877	POTEA	POTE ankyrin domain family member A	protein-coding
	chr17	72510132	72510908	Intergenic	17094	NM_174892	124599	ENSG00000178789	CD300LB	CD300 molecule like family member b	protein-coding
	chr21	9825665	9826363	promoter-TSS (NR_162111)	182	NR_128711	103504731	ENSG00000264462	MIR3648-2	microRNA 3648-2	ncRNA
MACS2 Broad	chr8	43092770	43093158	Intergenic	-54621	NM_001005365	340441	ENSG00000188877	POTEA	POTE ankyrin domain family member A	protein-coding
	chr8	43094668	43095233	Intergenic	-52635	NM_001005365	340441	ENSG00000188877	POTEA	POTE ankyrin domain family member A	protein-coding
	chr8	43096704	43097052	Intergenic	-50707	NM_001005365	340441	ENSG00000188877	POTEA	POTE ankyrin domain family member A	protein-coding
	chr17	72510125	72511132	Intergenic	16986	NM_174892	124599	ENSG00000178789	CD300LB	CD300 molecule like family member b	protein-coding
	chr21	9825660	9826382	promoter-TSS (NR_162111)	189	NR_128711	103504731	ENSG00000264462	MIR3648-2	microRNA 3648-2	ncRNA
	chr21	9826859	9827047	TTS (NR_037421)	503	NR_162105	113218501	N/A	MIR10396A	microRNA 10396a	ncRNA
LanceOtron	chr1	34712833	34713391	Intergenic	70604	NM_001134734	84970	ENSG00000142698	C1orf94	chromosome 1 open reading frame 94	protein-coding
	chr1	155160947	155161805	intron (NM_001204285, intron 3 of 8)	1324	NM_001044390	4582	ENSG00000185499	MUC1	mucin 1, cell surface associated	protein-coding
	chr1	228744545	228746603	TTS (NR_023363)	559	NR_023373	100169762	ENSG00000199334	RNA5S11	RNA, 5S ribosomal 11	rRNA
	chr1	228770290	228771894	Intergenic	-7079	NR_023371	100169760	ENSG00000201321	RNA5S9	RNA, 5S ribosomal 9	rRNA
	chr1	228779892	228782191	TTS (NR_023363).10	384	NR_002834	574029	N/A	DUSP5P1	dual specificity phosphatase 5 pseudogene 1	pseudo

Peak Calling Method	Chr	Start	End	Annotation	Distance to TSS	Nearest Promoter ID	Entrez ID	Nearest Ensembl	Gene Name	Gene Description	Gene Type
LanceOtron	chr2	45642693	45643109	intron (NM_018079, intron 18 of 20)	-160821	NR_033831	400952	ENSG00000205054	LINC01121	long intergenic non-protein coding RNA 1121	ncRNA
	chr2	91608489	91610427	Intergenic	238517	NR_027238	654342	N/A	LSP1P4	LSP1 pseudogene 4	pseudo
	chr4	2245312	2246026	Intergenic	-1821	NM_001303143	79441	ENSG00000214367	HAUS3	HAUS augmin like complex subunit 3	protein-coding
	chr4	49093389	49095866	Intergenic	105968	NM_001286791	80157	ENSG00000109182	CWH43	cell wall biogenesis 43 C-terminal homolog	protein-coding
	chr4	49108878	49113060	Intergenic	122310	NM_001286791	80157	ENSG00000109182	CWH43	cell wall biogenesis 43 C-terminal homolog	protein-coding
	chr4	49115129	49117077	Intergenic	127444	NM_001286791	80157	ENSG00000109182	CWH43	cell wall biogenesis 43 C-terminal homolog	protein-coding
	chr4	49117108	49117514	Intergenic	128652	NM_001286791	80157	ENSG00000109182	CWH43	cell wall biogenesis 43 C-terminal homolog	protein-coding
	chr4	49117615	49117707	Intergenic	129002	NM_001286791	80157	ENSG00000109182	CWH43	cell wall biogenesis 43 C-terminal homolog	protein-coding
	chr4	49150698	49152244	Intergenic	162812	NM_001286791	80157	ENSG00000109182	CWH43	cell wall biogenesis 43 C-terminal homolog	protein-coding
	chr4	49633352	49634220	Intergenic	645127	NM_001286791	80157	ENSG00000109182	CWH43	cell wall biogenesis 43 C-terminal homolog	protein-coding
	chr4	49640872	49645155	Intergenic	654354	NM_001286791	80157	ENSG00000109182	CWH43	cell wall biogenesis 43 C-terminal homolog	protein-coding
	chr5	17527244	17528471	Intergenic	83738	NR_134271	102723526	ENSG00000249662	LINC02218	long intergenic non-protein coding RNA 2218	ncRNA
	chr5	17596821	17598246	Intergenic	58214	NM_001355258	391769	ENSG00000269466	H3.Y	histone cluster 2, H3c pseudogene	protein-coding
	chr7	61967151	61971319	Intergenic	795199	NR_003952	643955	ENSG00000185037	ZNF733P	zinc finger protein 733, pseudogene	pseudo

Peak Calling Method	Chr	Start	End	Annotation	Distance to TSS	Nearest Promoter ID	Entrez ID	Nearest Ensembl	Gene Name	Gene Description	Gene Type
LanceOtron	chr7	90524507	90524921	intron (NM_001287136, intron 5 of 13)	185584	NM_001287136	5218	ENSG00000058091	CDK14	cyclin dependent kinase 14	protein-coding
	chr7	158152771	158153884	intron (NM_130842, intron 1 of 21)	172178	NR_030325	693180	ENSG00000207637	MIR595	microRNA 595	ncRNA
	chr8	9113710	9114355	Intergenic	67523	NR_125431	101929128	ENSG00000248538	LOC101929128	uncharacterized LOC101929128	ncRNA
	chr8	43092520	43094147	Intergenic	-54252	NM_001005365	340441	ENSG00000188877	POTEA	POTE ankyrin domain family member A	protein-coding
	chr8	43094426	43095554	Intergenic	-52595	NM_001005365	340441	ENSG00000188877	POTEA	POTE ankyrin domain family member A	protein-coding
	chr8	43095573	43097305	Intergenic	-51146	NM_001005365	340441	ENSG00000188877	POTEA	POTE ankyrin domain family member A	protein-coding
	chr8	46842846	46843648	Intergenic	686018	NR_146077	389652	ENSG00000248498	ASNSP1	asparagine synthetase pseudogene 1	pseudo
	chr8	46843920	46845952	Intergenic	684329	NR_146077	389652	ENSG00000248498	ASNSP1	asparagine synthetase pseudogene 1	pseudo
	chr8	46848907	46851554	Intergenic	679035	NR_146077	389652	ENSG00000248498	ASNSP1	asparagine synthetase pseudogene 1	pseudo
	chr8	85948779	85949170	Intergenic	-70499	NM_001349639	85444	ENSG00000133739	LRRCC1	leucine rich repeat and coiled-coil centrosomal protein 1	protein-coding
	chr8	86569543	86571218	Intergenic	-2475	NR_003594	100288527	N/A	REXO1L2P	REXO1 like 2, pseudogene	pseudo
	chr8	86788545	86790357	Intergenic	-1129	NR_003594	100288527	N/A	REXO1L2P	REXO1 like 2, pseudogene	pseudo
	chr8	144119593	144120298	promoter-TSS (NR_149322)	-681	NR_126399	286122	ENSG00000177335	C8orf31	chromosome 8 open reading frame 31	ncRNA
	chr9	68426932	68427462	TTS (NR_033907)	-11809	NR_039688	100616184	ENSG00000276029	MIR4477A	microRNA 4477a	ncRNA

Peak Calling Method	Chr	Start	End	Annotation	Distance to TSS	Nearest Promoter ID	Entrez ID	Nearest Ensembl	Gene Name	Gene Description	Gene Type
LanceOtron	chr10	42359916	42361664	Intergenic	502703	NR_024380	441666	ENSG00000215146	LOC441666	zinc finger protein 91 pseudogene	pseudo
	chr10	42361887	42363024	Intergenic	501038	NR_024380	441666	ENSG00000215146	LOC441666	zinc finger protein 91 pseudogene	pseudo
	chr10	134924805	134925641	intron (NM_001083909, intron 5 of 6)	9473	NM_001291085	84435	ENSG00000197177	ADGRA1	adhesion G protein-coupled receptor A1	protein-coding
	chr12	34852076	34852943	Intergenic	677078	NM_032834	84920	ENSG00000139133	ALG10	ALG10 alpha-1,2-glucosyltransferase	protein-coding
	chr16	33869586	33870256	Intergenic	-96124	NR_162093	113218496	N/A	MIR9901	microRNA 9901	ncRNA
	chr16	33973706	33974132	Intergenic	7874	NR_162093	113218496	N/A	MIR9901	microRNA 9901	ncRNA
	chr16	35279434	35279920	Intergenic	298754	NR_033985	400533	ENSG00000261122	LINC02167	long intergenic non-protein coding RNA 2167	ncRNA
	chr16	46419353	46429437	Intergenic	178614	NR_026556	124149	N/A	ANKRD26P1	ankyrin repeat domain 26 pseudogene 1	pseudo
	chr16	46430378	46430469	Intergenic	172586	NR_026556	124149	N/A	ANKRD26P1	ankyrin repeat domain 26 pseudogene 1	pseudo
	chr17	22259234	22261794	Intergenic	238077	NM_001190452	100462977	ENSG00000256618	MTRNR2L1	MT-RNR2 like 1	protein-coding
	chr18	63448994	63449374	intron (NM_001317214, intron 2 of 10)	30936	NM_001362438	1005	ENSG00000081138	CDH7	cadherin 7	protein-coding
	chr19	51001851	51003605	Intergenic	11720	NM_138334	126119	ENSG00000161677	JOSD2	Josephin domain containing 2	protein-coding
	chr20	62323901	62325246	non-coding (NR_037882, exon 30 of 38)	-3432	NM_003823	8771	ENSG00000243509	TNFRSF6B	TNF receptor superfamily member 6b	protein-coding
	chr21	10698445	10699726	Intergenic	291858	NM_199260	7179	ENSG00000274391	TPTE	transmembrane phosphatase with tensin homology	protein-coding

Peak Calling Method	Chr	Start	End	Annotation	Distance to TSS	Nearest Promoter ID	Entrez ID	Nearest Ensembl	Gene Name	Gene Description	Gene Type
LanceOtron	chr21	10699913	10700591	Intergenic	290691	NM_199260	7179	ENSG00000274391	TPTE	transmembrane phosphatase with tensin homology	protein-coding
	chr22	25489444	25490109	intron (NM_001145206, intron 4 of 10)	18883	NR_038941	100128531	ENSG00000203280	LOC100128531	uncharacterized LOC100128531	ncRNA
	chrX	58570140	58571226	Intergenic	-633616	NM_007156	7789	ENSG00000198205	ZXDA	zinc finger X-linked duplicated A	protein-coding
	chrX	58574279	58577198	Intergenic	-638671	NM_007156	7789	ENSG00000198205	ZXDA	zinc finger X-linked duplicated A	protein-coding
	chrY	58819386	58905579	Intergenic	-237921	NM_005840	10251	ENSG00000168939	SPRY3	sprouty RTK signaling antagonist 3	protein-coding
	chrY	58974649	58977529	Intergenic	-124314	NM_005840	10251	ENSG00000168939	SPRY3	sprouty RTK signaling antagonist 3	protein-coding
	chrY	58981575	58983329	Intergenic	-117951	NM_005840	10251	ENSG00000168939	SPRY3	sprouty RTK signaling antagonist 3	protein-coding

8.2 List of *in vivo* IGF-1R ChIP-seq hits coincident with *in vivo* AR binding sites

Full list of IGF-1R peaks identified *in vivo* by ChIP-seq in this thesis that overlap with AR binding site peaks identified *in vivo* from untreated prostate cancer tissue by (Sharma *et al.*, 2013). The table shows the chromosome co-ordinates for each peak, annotation of relevant region, distance of peak from nearest TSS, nearest promoter ID, and gene name, description and gene type for proximal gene.

Chr	Start	End	Annotation	Distance to TSS	Nearest PromoterID	Entrez ID	Nearest Ensembl	Gene Name	Gene Description	Gene Type
chr1	91852810	91853078	intron (NM_001017975, intron 4 of 38)	17450	NM_001017975	164045	ENSG00000162669	HFM1	helicase for meiosis 1	proteincoding
chr1	121357848	121358130	Intergenic	97079	NR_003955	647121	ENSG00000231752	EMBP1	embigin pseudogene 1	pseudo
chr1	121483128	121483428	Intergenic	222368	NR_003955	647121	ENSG00000231752	EMBP1	embigin pseudogene 1	pseudo
chr2	72028745	72029507	Intergenic	335297	NM_001130984	8291	ENSG00000135636	DYSF	dysferlin	proteincoding
chr2	91606908	91607776	Intergenic	240633	NR_027238	654342	-	LSP1P4	LSP1 pseudogene 4	pseudo
chr2	91610160	91610319	Intergenic	237736	NR_027238	654342	-	LSP1P4	LSP1 pseudogene 4	pseudo
chr2	91613684	91614513	Intergenic	233877	NR_027238	654342	-	LSP1P4	LSP1 pseudogene 4	pseudo
chr2	92281253	92281503	Intergenic	152219	NR_027714	440888	-	ACTR3BP2	ACTR3B pseudogene 2	pseudo
chr2	92305551	92305814	Intergenic	176523	NR_027714	440888	-	ACTR3BP2	ACTR3B pseudogene 2	pseudo
chr2	162135185	162139073	Intergenic	-25975	NR_110593	101929512	-	LOC101929512	uncharacterized LOC101929512	ncRNA
chr3	75718207	75718572	Intergenic	-3043	NR_040005	401074	ENSG00000242516	LINC00960	long intergenic non-protein coding RNA 960	ncRNA

Chr	Start	End	Annotation	Distance to TSS	Nearest PromoterID	Entrez ID	Nearest Ensembl	Gene Name	Gene Description	Gene Type
chr4	49151296	49151753	Intergenic	162865	NM_001286791	80157	ENSG00000109182	CWH43	cell wall biogenesis 43 Cterminal homolog	proteincoding
chr4	49512192	49512695	Intergenic	523784	NM_001286791	80157	ENSG00000109182	CWH43	cell wall biogenesis 43 Cterminal homolog	proteincoding
chr4	68265476	68265792	Intergenic	22084	NR_110747	101927237	ENSG00000250075	LOC101927237	uncharacterized LOC101927237	ncRNA
chr6	169277937	169278259	Intergenic	86379	NR_136249	105378146	-	LOC105378146	uncharacterized LOC105378146	ncRNA
chr7	61967224	61967654	Intergenic	796995	NR_003952	643955	ENSG00000185037	ZNF733P	zinc finger protein 733, pseudogene	pseudo
chr7	61971065	61971289	Intergenic	793257	NR_003952	643955	ENSG00000185037	ZNF733P	zinc finger protein 733, pseudogene	pseudo
chr7	61974966	61976385	Intergenic	788759	NR_003952	643955	ENSG00000185037	ZNF733P	zinc finger protein 733, pseudogene	pseudo
chr7	152107750	152108119	intron (NM_170606, intron 1 of 58)	25154	NM_170606	58508	ENSG00000055609	KMT2C	lysine methyltransferase 2C	proteincoding
chr8	43092619	43093369	Intergenic	-54591	NM_001002920	340441	ENSG00000188877	POTEA	POTE ankyrin domain family member A	proteincoding

Chr	Start	End	Annotation	Distance to TSS	Nearest PromoterID	Entrez ID	Nearest Ensembl	Gene Name	Gene Description	Gene Type
chr8	43094570	43095390	Intergenic	-52605	NM_001002920	340441	ENSG00000188877	POTEA	POTE ankyrin domain family member A	proteincoding
chr8	43096527	43097184	Intergenic	-50730	NM_001002920	340441	ENSG00000188877	POTEA	POTE ankyrin domain family member A	proteincoding
chr8	70602142	70602649	intron (NM_030958, intron 6 of 9)	97260	NR_132437	23213	ENSG00000137573	SULF1	sulfatase 1	proteincoding
chr10	42399245	42399522	Intergenic	464110	NR_024380	441666	ENSG00000215146	LOC441666	zinc finger protein 91 pseudogene	pseudo
chr10	42530573	42530797	Intergenic	332808	NR_024380	441666	ENSG00000215146	LOC441666	zinc finger protein 91 pseudogene	pseudo
chr10	42534490	42534813	Intergenic	328842	NR_024380	441666	ENSG00000215146	LOC441666	zinc finger protein 91 pseudogene	pseudo
chr12	34841579	34841929	Intergenic	666323	NM_032834	84920	ENSG00000139133	ALG10	ALG10 alpha-1,2glucosyltransferase	proteincoding
chr16	33973658	33973928	Intergenic	7748	NR_162093	113218496	-	MIR9901	microRNA 9901	ncRNA
chr16	46392914	46393569	Intergenic	209768	NR_026556	124149	-	ANKRD26P1	ankyrin repeat domain 26 pseudogene 1	pseudo
chr16	46407345	46407946	Intergenic	195364	NR_026556	124149	-	ANKRD26P1	ankyrin repeat domain 26 pseudogene 1	pseudo

Chr	Start	End	Annotation	Distance to TSS	Nearest PromoterID	Entrez ID	Nearest Ensembl	Gene Name	Gene Description	Gene Type
chr16	46416765	46417452	Intergenic	185901	NR_026556	124149	-	ANKRD26P1	ankyrin repeat domain 26 pseudogene 1	pseudo
chr16	46426177	46426415	Intergenic	176713	NR_026556	124149	-	ANKRD26P1	ankyrin repeat domain 26 pseudogene 1	pseudo
chr16	46426914	46427682	Intergenic	175711	NR_026556	124149	-	ANKRD26P1	ankyrin repeat domain 26 pseudogene 1	pseudo
chr16	46435187	46435498	Intergenic	167667	NR_026556	124149	-	ANKRD26P1	ankyrin repeat domain 26 pseudogene 1	pseudo
chr16	67251186	67251624	intron (NM_001365159, intron 2 of 6)	9300	NM_001365158	26231	ENSG00000125122	LRRC29	leucine rich repeat containing 29	proteincoding
chr18	18511955	18512409	Intergenic	179592	NM_005406	6093	ENSG00000067900	ROCK1	Rho associated coiled-coil containing protein kinase 1	proteincoding
chr18	18512917	18513150	Intergenic	178741	NM_005406	6093	ENSG00000067900	ROCK1	Rho associated coiled-coil containing protein kinase 1	proteincoding

Chr	Start	End	Annotation	Distance to TSS	Nearest PromoterID	Entrez ID	Nearest Ensembl	Gene Name	Gene Description	Gene Type
chr18	18514712	18515195	Intergenic	176821	NM_005406	6093	ENSG00000067900	ROCK1	Rho associated coiled-coil containing protein kinase 1	proteincoding
chr18	18515785	18516318	Intergenic	175723	NM_005406	6093	ENSG00000067900	ROCK1	Rho associated coiled-coil containing protein kinase 1	proteincoding
chr18	18516835	18517293	Intergenic	174710	NM_005406	6093	ENSG00000067900	ROCK1	Rho associated coiled-coil containing protein kinase 1	proteincoding
chr19	27737301	27737567	Intergenic	-546905	NR_110689	101927151	ENSG00000267575	LOC101927151	uncharacterized LOC101927151	ncRNA
chr19	27740049	27740331	Intergenic	-544149	NR_110689	101927151	ENSG00000267575	LOC101927151	uncharacterized LOC101927151	ncRNA
chr20	29618641	29619028	intron (NR_132316, intron 2 of 5)	6786	NR_132316	102723316	-	FRG1DP	FSHD region gene 1 family member D, pseudogene	pseudo
chr21	9825686	9827555	TTS (NR_037421)	170	NR_162105	113218501	-	MIR10396A	microRNA 10396a	ncRNA
chr21	10701247	10701491	Intergenic	289574	NM_001290224	7179	ENSG00000274391	TPTE	transmembrane phosphatase with tensin homology	proteincoding

Chr	Start	End	Annotation	Distance to TSS	Nearest PromoterID	Entrez ID	Nearest Ensembl	Gene Name	Gene Description	Gene Type
chr21	10702137	10702518	Intergenic	288616	NM_001290224	7179	ENSG00000274391	TPTE	transmembrane phosphatase with tensin homology	proteincoding
chr21	10702813	10703112	Intergenic	287981	NM_001290224	7179	ENSG00000274391	TPTE	transmembrane phosphatase with tensin homology	proteincoding
chr21	10720403	10722705	Intergenic	269389	NM_001290224	7179	ENSG00000274391	TPTE	transmembrane phosphatase with tensin homology	proteincoding
chrY	13464950	13465188	Intergenic	1068320	NR_033667	352887	ENSG00000206159	GYG2P1	glycogenin 2 pseudogene 1	pseudo
chrY	13465935	13466540	Intergenic	1067152	NR_033667	352887	ENSG00000206159	GYG2P1	glycogenin 2 pseudogene 1	pseudo
chrY	13468106	13468388	Intergenic	1065142	NR_033667	352887	ENSG00000206159	GYG2P1	glycogenin 2 pseudogene 1	pseudo
chrY	13469929	13470607	Intergenic	1063121	NR_033667	352887	ENSG00000206159	GYG2P1	glycogenin 2 pseudogene 1	pseudo
chrY	13483261	13484185	Intergenic	1049666	NR_033667	352887	ENSG00000206159	GYG2P1	glycogenin 2 pseudogene 1	pseudo

Chr	Start	End	Annotation	Distance to TSS	Nearest PromoterID	Entrez ID	Nearest Ensembl	Gene Name	Gene Description	Gene Type
chrY	13485510	13485747	Intergenic	1047761	NR_033667	352887	ENSG00000206159	GYG2P1	glycogenin 2 pseudogene 1	pseudo
chrY	13489076	13489955	Intergenic	1043874	NR_033667	352887	ENSG00000206159	GYG2P1	glycogenin 2 pseudogene 1	pseudo
chrY	28816610	28817946	Intergenic	942641	NR_002176	474148	ENSG00000280961	TTTY3B	testis-specific transcript, Ylinked 3B	ncRNA
chrY	58855965	58856888	Intergenic	-243977	NM_005840	10251	ENSG00000168939	SPRY3	sprouty RTK signaling antagonist 3	proteincoding
chrY	58862482	58862798	Intergenic	-237763	NM_005840	10251	ENSG00000168939	SPRY3	sprouty RTK signaling antagonist 3	proteincoding
chrY	58981757	58981817	Intergenic	-118616	NM_005840	10251	ENSG00000168939	SPRY3	sprouty RTK signaling antagonist 3	proteincoding

8.3 List of nuclear IGF-1R interactome hits identified by mass spectrometry

Full list of nuclear IGF-1R interactome hits identified by mass spectrometry in each indicated WT or IGF-1R null sample. Table shows Accession Number for each identified protein and protein name/description including gene code. For each sample in which peptides for indicated protein could be identified the table shows Protein Score (Prot Score - sum of the ion score of all identified peptides), Peptide number (The total number of distinct peptide sequences identified in the protein group) and Unique Peptide number (The number of identified peptide sequences that are unique to a protein group). Columns in which no data is present indicate that the relevant peptide was not detected in that sample.

		WT 1			WT 2			Null 1			Null 2		
Acc Number	**Description**	**Prot score (-10logP)**	**Peptide No.**	**Unique Peptide No.**	**Prot score (-10logP)**	**Peptide No.**	**Unique Peptide No.**	**Prot score (-10logP)**	**Peptide No.**	**Unique Peptide No.**	**Prot score (-10logP)**	**Peptide No.**	**Unique Peptide No.**
P78527	DNA-dependent protein kinase catalytic subunit GN=PRKDC	282	33	33	361.51	79	79	125.84	8	8	158.65	11	11
P52272	Heterogeneous nuclear ribonucleoprotein M GN=HNRNPM	333.25	32	32	313.07	27	27	156.59	13	13	69.83	2	2
Q08211	ATP-dependent RNA helicase A GN=DHX9	242.76	20	20	224.11	18	18	71.54	2	2	101.07	4	4
P10809	60 kDa heat shock protein mitochondrial GN=HSPD1	251.68	19	19	164.65	12	12	90.52	5	5	89.36	3	3
P38646	Stress-70 protein mitochondrial GN=HSPA9	265.78	18	18	120.39	4	4	164.94	9	9	82.66	4	4
P11142	Heat shock cognate 71 kDa protein GN=HSPA8	232.84	19	15	212.31	16	14	147.76	9	8	61.45	2	2
P17844	Probable ATP-dependent RNA helicase DDX5 GN=DDX5	246.9	19	15	188.49	14	12	135.51	9	7	70.21	2	2
P25705	ATP synthase subunit alpha mitochondrial GN=ATP5F1A	240.48	12	12	206.58	9	9	157.17	8	7	104.54	4	4
P23396	40S ribosomal protein S3 GN=RPS3	224.47	12	12	208.84	12	12	121.62	7	7	83.75	3	3
P40939	Trifunctional enzyme subunit alpha mitochondrial GN=HADHA	203.45	10	10	236.85	16	16	116.09	6	6	132.43	7	7
P04406	Glyceraldehyde-3-phosphate dehydrogenase GN=GAPDH	226.38	10	10	210.97	10	10	111.39	3	3	78.53	2	2
P62701	40S ribosomal protein S4 X isoform GN=RPS4X	240.94	12	7	226.14	10	6	130.61	7	3	92.68	3	3
P60709	Actin cytoplasmic 1 GN=ACTB	236.25	11	6	237.35	15	9	146.26	6	6	106.47	4	4
P63261	Actin cytoplasmic 2 GN=ACTG1	236.25	11	6	237.35	15	9	146.26	6	6	106.47	4	4
Q9NVI7	ATPase family AAA domain-containing protein 3A GN=ATAD3A	222.13	13	6	128.91	6	3	107.26	4	4	61.62	2	2
Q9BQG0	Myb-binding protein 1A GN=MYBBP1A	133.74	5	5	307.43	30	30	80.25	4	4	88.45	4	4
P06576	ATP synthase subunit beta mitochondrial GN=ATP5F1B	169.48	6	4	98.76	4	3	82.58	4	3	127.19	8	8
P48047	ATP synthase subunit O mitochondrial GN=ATP5PO	145.58	4	4	135.5	4	4	67.36	2	2	79.03	2	2
P05141	ADP/ATP translocase 2 GN=SLC25A5	127.25	5	3	97.16	5	2	84.21	3	3	60.72	2	2
Q00839	Heterogeneous nuclear ribonucleoprotein U GN=HNRNPU	239.09	16	16	253.46	21	21	129.88	8	8	41.74	1	1
P02545	Prelamin-A/C GN=LMNA	187.98	15	14	249.39	21	20	73.03	3	3	44.05	1	1
Q96PK6	RNA-binding protein 14 GN=RBM14	232.17	13	13	194.91	12	12	141.42	9	9	39.37	1	1
P61978	Heterogeneous nuclear ribonucleoprotein K GN=HNRNPK	224.32	12	12	196.34	10	10	94.69	4	4	37.67	1	1
P33992	DNA replication licensing factor MCM5 GN=MCM5	168.23	11	11	106.17	5	5	84.7	5	5	39.47	1	1
P68363	Tubulin alpha-1B chain GN=TUBA1B	226.06	11	11	185.21	8	8	108.33	5	5	45.07	1	1
O15240	Neurosecretory protein VGF GN=VGF	223.87	10	10	216.18	10	10	94.6	4	4	52.68	1	1
P68104	Elongation factor 1-alpha 1 GN=EEF1A1	160.53	9	9	111.19	6	6	94.57	3	3	38.43	1	1
Q5VTE0	Putative elongation factor 1-alpha-like 3 GN=EEF1A1P5	160.53	9	9	111.19	6	6	94.57	3	3	38.43	1	1
Q9Y230	RuvB-like 2 GN=RUVBL2	129.75	8	8	77.31	3	3	53.73	2	2	41.56	1	1
Q9Y265	RuvB-like 1 GN=RUVBL1	137.63	7	7	124.98	7	7	79.98	4	4	53.47	1	1
Q13151	Heterogeneous nuclear ribonucleoprotein A0 GN=HNRNPA0	174.12	6	6	140.85	5	5	97.03	3	3	43.95	1	1
P06748	Nucleophosmin GN=NPM1	189.66	6	6	151.94	6	6	92.27	3	3	36.78	1	1
P62829	60S ribosomal protein L23 GN=RPL23	170.13	5	5	114.53	2	2	99.92	3	3	40.79	1	1
P36542	ATP synthase subunit gamma mitochondrial GN=ATP5F1C	137.83	5	5	98.87	3	3	72.02	2	2	40.44	1	1
Q14103	Heterogeneous nuclear ribonucleoprotein D0 GN=HNRNPD	135.58	5	4	124.82	3	3	88.75	3	3	41.47	1	1
P22090	40S ribosomal protein S4 Y isoform 1 GN=RPS4Y1	186.02	8	3	180.21	7	3	115.15	6	2	40.5	1	1
Q9Y2R4	Probable ATP-dependent RNA helicase DDX52 GN=DDX52	171.51	7	7	260.36	14	14	31.17	1	1	39.47	1	1
Q96CU9	FAD-dependent oxidoreductase domain-containing protein 1 GN=FOXRED1	140.45	6	6	105.54	4	4	55.61	1	1	44.11	1	1

		WT 1			WT 2			Null 1			Null 2		
Acc Number	Description	Prot score (-10logP)	Peptide No.	Unique Peptide No.	Prot score (-10logP)	Peptide No.	Unique Peptide No.	Prot score (-10logP)	Peptide No.	Unique Peptide No.	Prot score (-10logP)	Peptide No.	Unique Peptide No.
Q9BVJ6	U3 small nucleolar RNA-associated protein a14 homolog A GN=UTP14A	115.79	6	6	176.73	11	11	40.68	1	1	37.01	1	1
P11387	DNA topoisomerase 1 GN=TOP1	104.88	5	5	109.39	4	4	36.39	1	1	35.94	1	1
P60866	40S ribosomal protein S20 GN=RPS20	107.07	4	4	41.44	1	1	48.86	1	1	36.27	1	1
P62266	40S ribosomal protein S23 GN=RPS23	126.67	4	4	81.34	3	3	43.51	1	1	36.51	1	1
Q04837	Single-stranded DNA-binding protein mitochondrial GN=SSBP1	128.23	3	3	123.44	4	4	30.9	1	1	46.64	1	1
Q6P1L8	39S ribosomal protein L14 mitochondrial GN=MRPL14	93.62	2	2	47.37	1	1	36.71	1	1	43.59	1	1
P02768	Serum albumin GN=ALB	98.57	2	2	96.29	3	3	41	1	1	74.4	2	2
Q9H0D6	5'-3' exoribonuclease 2 GN=XRN2	183.01	14	14	181.25	10	10	91.05	3	3			
P25205	DNA replication licensing factor MCM3 GN=MCM3	214.51	13	13	75.25	2	2	84.42	2	2			
Q6W2J9	BCL-6 corepressor GN=BCOR	153.73	12	12	249.45	20	20	64.64	2	2			
P22626	Heterogeneous nuclear ribonucleoproteins A2/B1 GN=HNRNPA2B1	239.48	12	11	181.72	8	8	133.04	8	7			
O00148	ATP-dependent RNA helicase DDX39A GN=DDX39A	161.43	10	10	177.27	9	9	110.62	6	6			
Q13217	DnaJ homolog subfamily C member 3 GN=DNAJC3	177.96	10	10	134.55	4	4	109.56	3	3			
P11021	Endoplasmic reticulum chaperone BiP GN=HSPA5	198.45	12	10	97.58	6	5	76.46	4	3			
Q9Y446	Plakophilin-3 GN=PKP3	167.55	9	9	56.11	2	2	89.97	4	4			
P26599	Polypyrimidine tract-binding protein 1 GN=PTBP1	209.84	9	9	168.43	7	7	69.44	3	3			
P22087	rRNA 2'-O-methyltransferase fibrillarin GN=FBL	169.94	9	9	207.82	11	11	92.31	3	3			
Q9BY77	Polymerase delta-interacting protein 3 GN=POLDIP3	193.19	8	8	168.57	5	5	103.06	4	4			
Q13148	TAR DNA-binding protein 43 GN=TARDBP	181.65	8	8	179.51	6	6	88.15	4	4			
P63244	Receptor of activated protein C kinase 1 GN=RACK1	143.27	7	7	98.45	5	5	71.94	2	2			
P43243	Matrin-3 GN=MATR3	145.43	6	6	172.71	12	12	80.33	3	3			
P09651	Heterogeneous nuclear ribonucleoprotein A1 GN=HNRNPA1	177.44	7	6	129.26	4	4	102.55	3	2			
P22061	Protein-L-isoaspartate(D-aspartate) O-methyltransferase GN=PCMT1	175.96	6	6	53.03	2	2	70.82	2	2			
O00571	ATP-dependent RNA helicase DDX3X GN=DDX3X	161.26	6	5	96.35	3	3	94.35	3	2			
P23528	Cofilin-1 GN=CFL1	151.18	5	5	47.94	1	1	65.4	2	2			
Q92841	Probable ATP-dependent RNA helicase DDX17 GN=DDX17	176.86	9	5	148.51	8	6	99.49	4	2			
Q15233	Non-POU domain-containing octamer-binding protein GN=NONO	159.11	4	4	84.91	2	2	70.1	2	2			
Q14978	Nucleolar and coiled-body phosphoprotein 1 GN=NOLC1	97.47	4	4	76.72	2	2	71.96	2	2			

		WT 1			WT 2			Null 1			Null 2		
Acc Number	Description	Prot score (-10logP)	Peptide No.	Unique Peptide No.	Prot score (-10logP)	Peptide No.	Unique Peptide No.	Prot score (-10logP)	Peptide No.	Unique Peptide No.	Prot score (-10logP)	Peptide No.	Unique Peptide No.
P51648	Aldehyde dehydrogenase family 3 member A2 GN=ALDH3A2	118.23	3	3	146.22	6	6	92.97	4	4			
P52597	Heterogeneous nuclear ribonucleoprotein F GN=HNRNPF	169.03	4	3	139.47	3	2	93.36	3	2			
P68371	Tubulin beta-4B chain GN=TUBB4B	228.76	13	2	191.78	10	2	83.02	3	3			
Q9BSD7	Cancer-related nucleoside-triphosphatase GN=NTPCR	99.58	2	2	84.89	1	1	75.46	2	2			
P0DMV8	Heat shock 70 kDa protein 1A GN=HSPA1A	128.67	6	2	99.16	4	2	59.99	3	2			
P0DMV9	Heat shock 70 kDa protein 1B GN=HSPA1B	128.67	6	2	99.16	4	2	59.99	3	2			
P31943	Heterogeneous nuclear ribonucleoprotein H GN=HNRNPH1	176.11	7	2	176.16	7	2	102.69	3	2			
P33993	DNA replication licensing factor MCM7 GN=MCM7	191.09	14	14	167.84	10	10	36	1	1			
Q9NR30	Nucleolar RNA helicase 2 GN=DDX21	140.64	10	10	159.84	9	9	46.85	1	1			
Q9UL03	Integrator complex subunit 6 GN=INTS6	135.84	8	8	189.72	11	11	36.15	1	1			
Q96EY1	DnaJ homolog subfamily A member 3 mitochondrial GN=DNAJA3	180.72	7	7	129.51	6	6	44.54	1	1			
Q14938	Nuclear factor 1 X-type GN=NFIX	139.17	6	6	123.29	4	4	41.15	1	1			
P23246	Splicing factor proline- and glutamine-rich GN=SFPQ	180.74	6	6	85.7	4	4	60.05	1	1			
P49411	Elongation factor Tu mitochondrial GN=TUFM	171.22	5	5	104.23	3	3	38.49	1	1			
Q8NHM5	Lysine-specific demethylase 2B GN=KDM2B	127.33	5	5	91.2	5	5	46.02	1	1			
Q16795	NADH dehydrogenase [ubiquinone] 1 alpha subcomplex subunit 9 mitochondrial GN=NDUFA9	108.58	5	5	78.39	3	3	35.41	1	1			
Q8NBN7	Retinol dehydrogenase 13 GN=RDH13	113.15	5	5	112.88	4	4	41.25	1	1			
Q14498	RNA-binding protein 39 GN=RBM39	112.81	5	5	161.73	6	6	31.26	1	1			
P31689	DnaJ homolog subfamily A member 1 GN=DNAJA1	109.14	3	3	106.79	2	2	52.45	1	1			
Q9UHB6	LIM domain and actin-binding protein 1 GN=LIMA1	70.72	3	3	110.79	5	5	34.83	1	1			
Q9Y285	Phenylalanine--tRNA ligase alpha subunit GN=FARSA	113.69	3	3	75.84	1	1	67.82	1	1			
Q9UJZ1	Stomatin-like protein 2 mitochondrial GN=STOML2	136.14	3	3	60.93	1	1	45.1	1	1			
P12236	ADP/ATP translocase 3 GN=SLC25A6	114.59	4	2	126.08	5	2	48.96	1	1			
P08574	Cytochrome c1 heme protein mitochondrial GN=CYC1	53.65	2	2	72.75	2	2	31.99	1	1			
P04792	Heat shock protein beta-1 GN=HSPB1	80.82	2	2	58.63	2	2	43.98	1	1			
Q00325	Phosphate carrier protein mitochondrial GN=SLC25A3	61.34	2	2	55.19	1	1	35.72	1	1			

		WT 1			WT 2			Null 1			Null 2		
Acc Number	Description	Prot score (-10logP)	Peptide No.	Unique Peptide No.	Prot score (-10logP)	Peptide No.	Unique Peptide No.	Prot score (-10logP)	Peptide No.	Unique Peptide No.	Prot score (-10logP)	Peptide No.	Unique Peptide No.
Q9UHV9	Prefoldin subunit 2 GN=PFDN2	83.09	2	2	38.63	1	1	44.94	1	1			
Q15365	Poly(rC)-binding protein 1 GN=PCBP1	145.74	5	3	75.01	2	1	32.97	1	0			
Q15366	Poly(rC)-binding protein 2 GN=PCBP2	137.33	4	2	73.7	2	1	32.97	1	0			
Q8N163	Cell cycle and apoptosis regulator protein 2 GN=CCAR2	30.9	1	1	221.85	15	15	47.92	2	2			
Q96BP2	Coiled-coil-helix-coiled-coil-helix domain-containing protein 1 GN=CHCHD1	60.19	1	1	46.23	1	1	44.48	1	1			
P63167	Dynein light chain 1 cytoplasmic GN=DYNLL1	73.62	1	1	94.77	1	1	31.44	1	1			
Q9NY12	H/ACA ribonucleoprotein complex subunit 1 GN=GAR1	29.29	1	1	40.82	1	1	32.69	1	1			
P55795	Heterogeneous nuclear ribonucleoprotein H2 GN=HNRNPH2	150.04	5	1	150.81	5	1	102.69	3	2			
P46013	Proliferation marker protein Ki-67 GN=MKI67	48.11	1	1	169.12	13	13	35.56	1	1			
P32322	Pyrroline-5-carboxylate reductase 1 mitochondrial GN=PYCR1	55.96	2	1	95.85	3	2	57.24	2	2			
P63208	S-phase kinase-associated protein 1 GN=SKP1	48.54	1	1	50.1	1	1	34.25	1	1			
P46783	40S ribosomal protein S10 GN=RPS10	92.13	3	3	77.3	2	2	72.29	2	2			
P62280	40S ribosomal protein S11 GN=RPS11	148.89	5	5	139.55	4	4	63.55	2	2			
P25398	40S ribosomal protein S12 GN=RPS12	76.51	2	2	77.27	2	2	39.64	1	1			
P62263	40S ribosomal protein S14 GN=RPS14	123.41	4	4	94.91	2	2	38.92	1	1			
P62841	40S ribosomal protein S15 GN=RPS15	136.95	4	4	97.54	3	3	64.73	2	2			
P08708	40S ribosomal protein S17 GN=RPS17	202.96	8	8	187.78	7	7	85.81	3	3			
P62269	40S ribosomal protein S18 GN=RPS18	138.13	6	6	120.78	7	7	58.37	2	2			
P62851	40S ribosomal protein S25 GN=RPS25	86.09	4	4	61.62	2	2	37.49	1	1			
P62857	40S ribosomal protein S28 GN=RPS28	46.18	1	1	68.75	1	1	40.46	1	1			
P61247	40S ribosomal protein S3a GN=RPS3A	72.29	3	3	119.08	7	7	48.96	1	1			
P46782	40S ribosomal protein S5 GN=RPS5	170.58	4	4	157.99	5	5	76.77	2	2			
P62913	60S ribosomal protein L11 GN=RPL11	113.87	3	3	92.95	2	2	62.57	2	2			
P26373	60S ribosomal protein L13 GN=RPL13	66.4	2	2	93.8	4	4	33.31	1	1			
Q07020	60S ribosomal protein L18 GN=RPL18	37.58	1	1	49.04	2	2	35.68	1	1			
Q6P5R6	60S ribosomal protein L22-like 1 GN=RPL22L1	89.03	3	3	140.51	3	3	68.71	2	2			

		WT 1			WT 2			Null 1			Null 2		
Acc Number	Description	Prot score (-10logP)	Peptide No.	Unique Peptide No.	Prot score (-10logP)	Peptide No.	Unique Peptide No.	Prot score (-10logP)	Peptide No.	Unique Peptide No.	Prot score (-10logP)	Peptide No.	Unique Peptide No.
P32969	60S ribosomal protein L9 GN=RPL9	158.85	5	5	126.35	4	4	31.11	1	1			
Q9NUL7	Probable ATP-dependent RNA helicase DDX28 GN=DDX28	178.73	9	9	68.45	2	2				50.68	1	1
P12004	Proliferating cell nuclear antigen GN=PCNA	146.66	5	5	101.89	2	2				47.28	1	1
P05388	60S acidic ribosomal protein P0 GN=RPLP0	124.39	4	4	33.04	1	1				48.54	1	1
Q8NHW5	60S acidic ribosomal protein P0-like GN=RPLP0P6	124.39	4	4	33.04	1	1				48.54	1	1
P07437	Tubulin beta chain GN=TUBB	224.36	13	3	183.92	9	1				37.2	1	1
P55084	Trifunctional enzyme subunit beta mitochondrial GN=HADHB	58.91	2	2	87.35	4	4				93.44	3	3
Q9H7Z7	Prostaglandin E synthase 2 GN=PTGES2	72.52	2	2	146.03	5	5				44.59	1	1
O43819	Protein SCO2 homolog mitochondrial GN=SCO2	90.56	1	1	74.79	1	1				38.11	1	1
Q12905	Interleukin enhancer-binding factor 2 GN=ILF2	41.81	1	1	142.93	5	5				43.86	1	1
Q8NBQ5	Estradiol 17-beta-dehydrogenase 11 GN=HSD17B11	29.32	1	1	117.32	2	2				67.04	2	2
P62879	Guanine nucleotide-binding protein G(I)/G(S)/G(T) subunit beta-2 GN=GNB2	33.74	1	1	138.84	5	2				53.45	1	1
P62873	Guanine nucleotide-binding protein G(I)/G(S)/G(T) subunit beta-1 GN=GNB1	33.74	1	1	107.83	4	1				37.58	1	1
Q99729	Heterogeneous nuclear ribonucleoprotein A/B GN=HNRNPAB	51.01	2	1	66.68	1	1				41.47	1	1
Q86YZ3	Hornerin GN=HRNR	114.61	4	4				123.67	4	4	67.48	2	2
P05387	60S acidic ribosomal protein P2 GN=RPLP2	55.1	1	1				31.92	1	1	43.84	1	1
A1L0T0	Acetolactate synthase-like protein GN=ILVBL				115.64	2	2	37.94	1	1			
Q15599	Na(+)/H(+) exchange regulatory cofactor NHE-RF2 GN=SLC9A3R2	165.9	7	7	91.71	2	2						
O15119	T-box transcription factor TBX3 GN=TBX3	167.21	6	6	144.19	5	5						
P22830	Ferrochelatase mitochondrial GN=FECH	92.75	4	4	111.05	4	4						
P55265	Double-stranded RNA-specific adenosine deaminase GN=ADAR	95.37	3	3	210.6	15	15						
O75643	U5 small nuclear ribonucleoprotein 200 kDa helicase GN=SNRNP200	99.28	3	3	161.89	10	10						
P42167	Lamina-associated polypeptide 2 isoforms beta/gamma GN=TMPO	91.63	3	3	249.3	13	7						
P09543	2' 3'-cyclic-nucleotide 3'-phosphodiesterase GN=CNP	92.83	3	3	155.84	5	5						
Q99496	E3 ubiquitin-protein ligase RING2 GN=RNF2	84.45	3	3	160.17	6	4						

		WT 1			WT 2			Null 1			Null 2		
Acc Number	Description	Prot score (-10logP)	Peptide No.	Unique Peptide No.	Prot score (-10logP)	Peptide No.	Unique Peptide No.	Prot score (-10logP)	Peptide No.	Unique Peptide No.	Prot score (-10logP)	Peptide No.	Unique Peptide No.
P14866	Heterogeneous nuclear ribonucleoprotein L GN=HNRNPL	78.7	3	3	88.51	4	4						
P63173	60S ribosomal protein L38 GN=RPL38	89.28	3	3	84.94	3	3						
Q07666	KH domain-containing RNA-binding signal transduction associated protein 1 GN=KHDRBS1	71.48	3	3	81.5	3	3						
Q9NX20	39S ribosomal protein L16 mitochondrial GN=MRPL16	74.14	3	3	77.41	2	2						
P08047	Transcription factor Sp1 GN=SP1	117.36	3	3	92.32	2	2						
P20700	Lamin-B1 GN=LMNB1	91.53	3	2	168.18	13	12						
O00567	Nucleolar protein 56 GN=NOP56	64.22	2	2	185.89	9	9						
Q9Y2X3	Nucleolar protein 58 GN=NOP58	69.71	2	2	162.75	9	9						
Q9H0A0	RNA cytidine acetyltransferase GN=NAT10	87.1	2	2	156.4	7	7						
P36873	Serine/threonine-protein phosphatase PP1-gamma catalytic subunit GN=PPP1CC	58.97	2	2	126.02	6	6						
P23769	Endothelial transcription factor GATA2 GN=GATA2	91.14	2	2	168.34	5	5						
Q8IY67	Ribonucleoprotein PTB-binding 1 GN=RAVER1	61.67	2	2	119.32	4	4						
Q9BSM1	Polycomb group RING finger protein 1 GN=PCGF1	48.21	2	2	111.12	3	3						
P84090	Enhancer of rudimentary homolog GN=ERH	104.19	2	2	103.91	2	2						
Q96EE3	Nucleoporin SEH1 GN=SEH1L	80.69	2	2	99.07	2	2						
P62318	Small nuclear ribonucleoprotein Sm D3 GN=SNRPD3	67.62	2	2	66.91	2	2						
Q5T9A4	ATPase family AAA domain-containing protein 3B GN=ATAD3B	153.2	8	1	74.69	4	1						
P68032	Actin alpha cardiac muscle 1 GN=ACTC1	177.01	6	1	165.91	7	1						
P68133	Actin alpha skeletal muscle GN=ACTA1	177.01	6	1	165.91	7	1						
P62736	Actin aortic smooth muscle GN=ACTA2	177.01	6	1	165.91	7	1						
P63267	Actin gamma-enteric smooth muscle GN=ACTG2	177.01	6	1	165.91	7	1						
Q8IWS0	PHD finger protein 6 GN=PHF6	99.58	5	5	43.39	1	1						
P62249	40S ribosomal protein S16 GN=RPS16	99.02	4	4	29.34	1	1						
Q9NUI1	Peroxisomal 2 4-dienoyl-CoA reductase GN=DECR2	84.47	4	4	30.2	1	1						
P61254	60S ribosomal protein L26 GN=RPL26	72.94	3	3	29.13	1	1						
O43390	Heterogeneous nuclear ribonucleoprotein R GN=HNRNPR	97.68	3	2	74.8	2	1						

		WT 1			WT 2			Null 1			Null 2		
Acc Number	Description	Prot score (-10logP)	Peptide No.	Unique Peptide No.	Prot score (-10logP)	Peptide No.	Unique Peptide No.	Prot score (-10logP)	Peptide No.	Unique Peptide No.	Prot score (-10logP)	Peptide No.	Unique Peptide No.
P18085	ADP-ribosylation factor 4 GN=ARF4	66.89	2	2	55.09	1	1						
P56134	ATP synthase subunit f mitochondrial GN=ATP5MF	70.84	2	2	29.88	1	1						
P13995	Bifunctional methylenetetrahydrofolate dehydrogenase/cyclohydrolase mitochondrial GN=MTHFD2	60.41	2	2	28.52	1	1						
Q96EP5	DAZ-associated protein 1 GN=DAZAP1	84.85	2	2	41.72	1	1						
Q9NV06	DDB1- and CUL4-associated factor 13 GN=DCAF13	48.87	2	2	61.9	1	1						
O60884	DnaJ homolog subfamily A member 2 GN=DNAJA2	68.6	2	2	67.8	1	1						
P26641	Elongation factor 1-gamma GN=EEF1G	48.5	2	2	30.71	1	1						
O95900	Mitochondrial mRNA pseudouridine synthase TRUB2 GN=TRUB2	51.76	2	2	35.53	1	1						
P37108	Signal recognition particle 14 kDa protein GN=SRP14	91.44	2	2	47.76	1	1						
Q9Y2W1	Thyroid hormone receptor-associated protein 3 GN=THRAP3	56.82	2	2	40.37	1	1						
O60506	Heterogeneous nuclear ribonucleoprotein Q GN=SYNCRIP	72.44	2	1	53.97	2	1						
Q15029	116 kDa U5 small nuclear ribonucleoprotein component GN=EFTUD2	64.21	1	1	129.79	5	5						
P51153	Ras-related protein Rab-13 GN=RAB13	40.44	1	1	150.02	5	4						
Q13724	Mannosyl-oligosaccharide glucosidase GN=MOGS	53.5	1	1	141.01	4	4						
Q14527	Helicase-like transcription factor GN=HLTF	29.04	1	1	98.54	3	3						
Q96C36	Pyrroline-5-carboxylate reductase 2 GN=PYCR2	38.49	1	0	80.74	3	2						
P62753	40S ribosomal protein S6 GN=RPS6	50.36	1	1	66.42	2	2						
Q13547	Histone deacetylase 1 GN=HDAC1	29.9	1	1	67.38	2	2						
Q5C9Z4	Nucleolar MIF4G domain-containing protein 1 GN=NOM1	47.92	1	1	71.9	2	2						
Q8IY37	Probable ATP-dependent RNA helicase DHX37 GN=DHX37	46.74	1	1	51.32	2	2						
O43824	Putative GTP-binding protein 6 GN=GTPBP6	73.87	1	1	49.27	2	2						
Q15637	Splicing factor 1 GN=SF1	37.97	1	1	52.39	2	2						
P82930	28S ribosomal protein S34 mitochondrial GN=MRPS34	58.32	1	1	39.18	1	1						
Q9NVE7	4'-phosphopantetheine phosphatase GN=PANK4	33.4	1	1	30.62	1	1						
P40429	60S ribosomal protein L13a GN=RPL13A	29.55	1	1	30.37	1	1						
P50914	60S ribosomal protein L14 GN=RPL14	39.68	1	1	30.96	1	1						

		WT 1			WT 2			Null 1			Null 2		
Acc Number	Description	Prot score (-10logP)	Peptide No.	Unique Peptide No.	Prot score (-10logP)	Peptide No.	Unique Peptide No.	Prot score (-10logP)	Peptide No.	Unique Peptide No.	Prot score (-10logP)	Peptide No.	Unique Peptide No.
P61353	60S ribosomal protein L27 GN=RPL27	32.76	1	1	45.53	1	1						
P62910	60S ribosomal protein L32 GN=RPL32	63.74	1	1	68.82	1	1						
P61513	60S ribosomal protein L37a GN=RPL37A	62.34	1	1	28.48	1	1						
O76031	ATP-dependent Clp protease ATP-binding subunit clpX like mitochondrial GN=CLPX	34.99	1	1	38.27	1	1						
Q9Y3Y2	Chromatin target of PRMT1 protein GN=CHTOP	51.46	1	1	48.88	1	1						
Q07021	Complement component 1 Q subcomponent-binding protein mitochondrial GN=C1QBP	54.53	1	1	32.47	1	1						
Q13363	C-terminal-binding protein 1 GN=CTBP1	34.87	1	1	40.06	1	1						
O60762	Dolichol-phosphate mannosyltransferase subunit 1 GN=DPM1	43.36	1	1	48.56	1	1						
O60832	H/ACA ribonucleoprotein complex subunit DKC1 GN=DKC1	48.55	1	1	40.62	1	1						
P16401	Histone H1.5 GN=H1-5	32.37	1	1	31.91	1	1						
P33778	Histone H2B type 1-B GN=HIST1H2BB	47.62	1	1	43.61	1	1						
P62807	Histone H2B type 1-C/E/F/G/I GN=H2BC4	47.62	1	1	43.61	1	1						
P58876	Histone H2B type 1-D GN=HIST1H2BD	47.62	1	1	43.61	1	1						
Q93079	Histone H2B type 1-H GN=HIST1H2BH	47.62	1	1	43.61	1	1						
P06899	Histone H2B type 1-J GN=H2BC11	47.62	1	1	43.61	1	1						
O60814	Histone H2B type 1-K GN=H2BC12	47.62	1	1	43.61	1	1						
Q99880	Histone H2B type 1-L GN=H2BC13	47.62	1	1	43.61	1	1						
Q99879	Histone H2B type 1-M GN=H2BC14	47.62	1	1	43.61	1	1						
Q99877	Histone H2B type 1-N GN=H2BC15	47.62	1	1	43.61	1	1						
P23527	Histone H2B type 1-O GN=HIST1H2BO	47.62	1	1	43.61	1	1						
Q16778	Histone H2B type 2-E GN=HIST2H2BE	47.62	1	1	43.61	1	1						
Q5QNW6	Histone H2B type 2-F GN=HIST2H2BF	47.62	1	1	43.61	1	1						
Q8N257	Histone H2B type 3-B GN=HIST3H2BB	47.62	1	1	43.61	1	1						
P57053	Histone H2B type F-S GN=H2BFS	47.62	1	1	43.61	1	1						
Q3ZCT8	Kelch repeat and BTB domain-containing protein 12 GN=KBTBD12	31.75	1	1	33.06	1	1						
P56270	Myc-associated zinc finger protein GN=MAZ	44.2	1	1	41.57	1	1						

		WT 1			WT 2			Null 1			Null 2		
Acc Number	Description	Prot score (-10logP)	Peptide No.	Unique Peptide No.	Prot score (-10logP)	Peptide No.	Unique Peptide No.	Prot score (-10logP)	Peptide No.	Unique Peptide No.	Prot score (-10logP)	Peptide No.	Unique Peptide No.
Q8WUK0	Phosphatidylglycerophosphatase and protein-tyrosine phosphatase 1 GN=PTPMT1	50.24	1	1	39.87	1	1						
Q53GA4	Pleckstrin homology-like domain family A member 2 GN=PHLDA2	50.76	1	1	46.48	1	1						
P61619	Protein transport protein Sec61 subunit alpha isoform 1 GN=SEC61A1	39.64	1	1	43.06	1	1						
Q6NVV1	Putative 60S ribosomal protein L13a protein RPL13AP3 GN=RPL13AP3	29.55	1	1	30.37	1	1						
P35250	Replication factor C subunit 2 GN=RFC2	46.85	1	1	57.72	1	1						
Q96T37	RNA-binding protein 15 GN=RBM15	45.44	1	1	41.7	1	1						
P62306	Small nuclear ribonucleoprotein F GN=SNRPF	60.17	1	1	54.12	1	1						
P62314	Small nuclear ribonucleoprotein Sm D1 GN=SNRPD1	71.6	1	1	59.1	1	1						
Q7Z2T5	TRMT1-like protein GN=TRMT1L	50.61	1	1	78.97	1	1						
P15880	40S ribosomal protein S2 GN=RPS2	84.02	5	5	90.68	3	3						
P62277	40S ribosomal protein S13 GN=RPS13	116.84	4	4	99.64	3	3						
P62244	40S ribosomal protein S15a GN=RPS15A	82.04	2	2	75.56	2	2						
P39019	40S ribosomal protein S19 GN=RPS19	72.85	2	2	66.43	2	2						
P62273	40S ribosomal protein S29 GN=RPS29	54.23	2	2	58.9	2	2						
P62081	40S ribosomal protein S7 GN=RPS7	66.75	2	2	65.3	2	2						
P27635	60S ribosomal protein L10 GN=RPL10	81.57	2	2	85.52	3	3						
P18621	60S ribosomal protein L17 GN=RPL17	60.61	2	2	83.81	2	2						
P46778	60S ribosomal protein L21 GN=RPL21	75.33	2	2	51.07	1	1						
P83731	60S ribosomal protein L24 GN=RPL24	82.92	2	2	33.01	1	1						
P46776	60S ribosomal protein L27a GN=RPL27A	49.57	2	2	39.48	1	1						
Q86V81	THO complex subunit 4 GN=ALYREF	212.79	8	8				61.45	2	2			
O95831	Apoptosis-inducing factor 1 mitochondrial GN=AIFM1	125.16	5	5				53.86	2	2			
P08238	Heat shock protein HSP 90-beta GN=HSP90AB1	132.58	5	5				53.38	2	2			
P78347	General transcription factor II-I GN=GTF2I	104.94	4	4				57.92	2	2			
P35637	RNA-binding protein FUS GN=FUS	74.33	3	3				58.84	2	2			
P42704	Leucine-rich PPR motif-containing protein mitochondrial GN=LRPPRC	83.43	2	2				39.48	1	1			

		WT 1			WT 2			Null 1			Null 2		
Acc Number	Description	Prot score (-10logP)	Peptide No.	Unique Peptide No.	Prot score (-10logP)	Peptide No.	Unique Peptide No.	Prot score (-10logP)	Peptide No.	Unique Peptide No.	Prot score (-10logP)	Peptide No.	Unique Peptide No.
O75489	NADH dehydrogenase [ubiquinone] iron-sulphur protein 3 mitochondrial GN=NDUFS3	58.6	2	2				33.62	1	1			
Q9Y4W6	AFG3-like protein 2 GN=AFG3L2	37	1	1				34.16	1	1			
Q02978	Mitochondrial 2-oxoglutarate/malate carrier protein GN=SLC25A11	34.67	1	1				38.08	1	1			
Q9H936	Mitochondrial glutamate carrier 1 GN=SLC25A22	33.13	1	1				40.36	1	1			
Q9H1K4	Mitochondrial glutamate carrier 2 GN=SLC25A18	33.13	1	1				40.36	1	1			
Q15436	Protein transport protein Sec23A GN=SEC23A	45.62	1	1				43.48	1	1			
Q15437	Protein transport protein Sec23B GN=SEC23B	45.62	1	1				43.48	1	1			
Q9GZT3	SRA stem-loop-interacting RNA-binding protein mitochondrial GN=SLIRP	40.26	1	1				36.94	1	1			
P53007	Tricarboxylate transport protein mitochondrial GN=SLC25A1	31.07	1	1				36.26	1	1			
P07477	Trypsin-1 GN=PRSS1	90.83	2	2							51.31	1	1
O00483	Cytochrome c oxidase subunit NDUFA4 GN=NDUFA4				34.38	1	1	45.98	1	1			
P24539	ATP synthase F(0) complex subunit B1 mitochondrial GN=ATP5PB				71.65	2	2	48.66	1	1			
Q15072	Zinc finger protein OZF GN=ZNF146				87.14	3	3	52.02	1	1			
Q9BQE3	Tubulin alpha-1C chain GN=TUBA1C				185.21	8	8				45.07	1	1
P11233	Ras-related protein Ral-A GN=RALA				138.92	4	4				43.35	1	1
P61224	Ras-related protein Rap-1b GN=RAP1B				89.78	3	3				41.45	1	1
P27824	Calnexin GN=CANX				80.86	2	2				37.11	1	1
Q86UE4	Protein LYRIC GN=MTDH				39.11	1	1				35.77	1	1
P51149	Ras-related protein Rab-7a GN=RAB7A				29.04	1	1				49.49	1	1
P22695	Cytochrome b-c1 complex subunit 2 mitochondrial GN=UQCRC2				60.07	1	1				58.95	1	1
O94826	Mitochondrial import receptor subunit TOM70 GN=TOMM70				28.83	1	1				49.54	1	1
Q5D862	Filaggrin-2 GN=FLG2							41.94	1	1	42.08	1	1
Q86U44	N6-adenosine-methyltransferase catalytic subunit GN=METTL3	132.03	4	4									
Q9Y2R9	28S ribosomal protein S7 mitochondrial GN=MRPS7	98.36	3	3									
P62805	Histone H4 GN=H4C1	83.97	3	3									
P67809	Y-box-binding protein 1 GN=YBX1	130.23	3	3									

		WT 1			WT 2			Null 1			Null 2		
Acc Number	Description	Prot score (-10logP)	Peptide No.	Unique Peptide No.	Prot score (-10logP)	Peptide No.	Unique Peptide No.	Prot score (-10logP)	Peptide No.	Unique Peptide No.	Prot score (-10logP)	Peptide No.	Unique Peptide No.
P08195	4F2 cell-surface antigen heavy chain GN=SLC3A2	63.27	2	2									
P62899	60S ribosomal protein L31 GN=RPL31	47.28	2	2									
Q9NXV6	CDKN2A-interacting protein GN=CDKN2AIP	63.3	2	2									
P60981	Destrin GN=DSTN	52.73	2	2									
Q92945	Far upstream element-binding protein 2 GN=KHSRP	57.11	2	2									
P68871	Haemoglobin subunit beta GN=HBB	68.86	2	2									
Q92615	La-related protein 4B GN=LARP4B	52.61	2	2									
Q01650	Large neutral amino acids transporter small subunit 1 GN=SLC7A5	76.71	2	2									
P29966	Myristoylated alanine-rich C-kinase substrate GN=MARCKS	74.64	2	2									
Q9P258	Protein RCC2 GN=RCC2	53.5	2	2									
P62136	Serine/threonine-protein phosphatase PP1-alpha catalytic subunit GN=PPP1CA	58.97	2	2									
P62140	Serine/threonine-protein phosphatase PP1-beta catalytic subunit GN=PPP1CB	58.97	2	2									
P82914	28S ribosomal protein S15 mitochondrial GN=MRPS15	31.07	1	1									
Q9Y399	28S ribosomal protein S2 mitochondrial GN=MRPS2	37.19	1	1									
Q9Y2Q9	28S ribosomal protein S28 mitochondrial GN=MRPS28	30.69	1	1									
P42677	40S ribosomal protein S27 GN=RPS27	39.12	1	1									
P62241	40S ribosomal protein S8 GN=RPS8	38.47	1	1									
P08865	40S ribosomal protein SA GN=RPSA	29.36	1	1									
P30050	60S ribosomal protein L12 GN=RPL12	36.94	1	1									
P61313	60S ribosomal protein L15 GN=RPL15	56.85	1	1									
P84098	60S ribosomal protein L19 GN=RPL19	49.04	1	1									
P46779	60S ribosomal protein L28 GN=RPL28	34.32	1	1									
P47914	60S ribosomal protein L29 GN=RPL29	48.15	1	1									
P83881	60S ribosomal protein L36a GN=RPL36A	38.33	1	1									
Q969Q0	60S ribosomal protein L36a-like GN=RPL36AL	38.33	1	1									
P62424	60S ribosomal protein L7a GN=RPL7A	35.68	1	1									

		WT 1			WT 2			Null 1			Null 2		
Acc Number	Description	Prot score (-10logP)	Peptide No.	Unique Peptide No.	Prot score (-10logP)	Peptide No.	Unique Peptide No.	Prot score (-10logP)	Peptide No.	Unique Peptide No.	Prot score (-10logP)	Peptide No.	Unique Peptide No.
Q9H0C2	ADP/ATP translocase 4 GN=SLC25A31	51.23	2	1									
Q9NXU5	ADP-ribosylation factor-like protein 15 GN=ARL15	30.06	1	1									
O00116	Alkyl dihydroxyacetone phosphate synthase peroxisomal GN=AGPS	44.49	1	1									
Q9NUU7	ATP-dependent RNA helicase DDX19A GN=DDX19A	34.74	1	1									
Q9UMR2	ATP-dependent RNA helicase DDX19B GN=DDX19B	34.74	1	1									
Q96SN8	CDK5 regulatory subunit-associated protein 2 GN=CDK5RAP2	28.95	1	1									
Q96AJ1	Clusterin-associated protein 1 GN=CLUAP1	37.75	1	1									
Q9H845	Complex I assembly factor ACAD9 mitochondrial GN=ACAD9	69.49	1	1									
Q02338	D-beta-hydroxybutyrate dehydrogenase mitochondrial GN=BDH1	44.98	1	1									
Q9UBS4	DnaJ homolog subfamily B member 11 GN=DNAJB11	30.56	1	1									
P24534	Elongation factor 1-beta GN=EEF1B2	61.05	1	1									
Q15375	Ephrin type-A receptor 7 GN=EPHA7	33.74	1	1									
Q9HAV4	Exportin-5 GN=XPO5	42.76	1	1									
P09382	Galectin-1 GN=LGALS1	41.47	1	1									
P11413	Glucose-6-phosphate 1-dehydrogenase GN=G6PD	30.81	1	1									
Q9HAV0	Guanine nucleotide-binding protein subunit beta-4 GN=GNB4	33.74	1	1									
Q92769	Histone deacetylase 2 GN=HDAC2	29.9	1	1									
Q02539	Histone H1.1 GN=H1-1	41.99	1	1									
P16403	Histone H1.2 GN=H1-2	41.99	1	1									
P16402	Histone H1.3 GN=H1-3	41.99	1	1									
P10412	Histone H1.4 GN=H1-4	41.99	1	1									
P22492	Histone H1t GN=HIST1H1T	41.99	1	1									
O00629	Importin subunit alpha-3 GN=KPNA4	29.5	1	1									
Q71RC2	La-related protein 4 GN=LARP4	29.46	1	1									
P24666	Low molecular weight phosphotyrosine protein phosphatase GN=ACP1	37.62	1	1									
Q8WWC4	m-AAA protease-interacting protein 1 mitochondrial GN=MAIP1	32.99	1	1									

		WT 1			WT 2			Null 1			Null 2		
Acc Number	Description	Prot score (-10logP)	Peptide No.	Unique Peptide No.	Prot score (-10logP)	Peptide No.	Unique Peptide No.	Prot score (-10logP)	Peptide No.	Unique Peptide No.	Prot score (-10logP)	Peptide No.	Unique Peptide No.
O43148	mRNA cap guanine-N7 methyltransferase GN=RNMT	29.96	1	1									
Q9HCE5	N6-adenosine-methyltransferase non-catalytic subunit GN=METTL14	28.81	1	1									
P43490	Nicotinamide phosphoribosyltransferase GN=NAMPT	37.09	1	1									
Q9NPP4	NLR family CARD domain-containing protein 4 GN=NLRC4	28.92	1	1									
P19338	Nucleolin GN=NCL	34.31	1	1									
Q9UBD5	Origin recognition complex subunit 3 GN=ORC3	33.42	1	1									
P62937	Peptidyl-prolyl cis-trans isomerase A GN=PPIA	36.96	1	1									
O00750	Phosphatidylinositol 4-phosphate 3-kinase C2 domain containing subunit beta GN=PIK3C2B	29.83	1	1									
P09874	Poly [ADP-ribose] polymerase 1 GN=PARP1	68.85	1	1									
Q9NVV4	Poly(A) RNA polymerase mitochondrial GN=MTPAP	37.49	1	1									
Q8N490	Probable hydrolase PNKD GN=PNKD	47.36	1	1									
Q8WXW3	Progesterone-induced-blocking factor 1 GN=PIBF1	35.12	1	1									
P11171	Protein 4.1 GN=EPB41	28.64	1	1									
Q9BRX2	Protein pelota homolog GN=PELO	43.76	1	1									
P11177	Pyruvate dehydrogenase E1 component subunit beta mitochondrial GN=PDHB	39.55	1	1									
P28702	Retinoic acid receptor RXR-beta GN=RXRB	62.33	1	1									
Q9Y224	RNA transcription translation and transport factor protein GN=RTRAF	44.16	1	1									
A0AV96	RNA-binding protein 47 GN=RBM47	48.45	1	1									
Q01844	RNA-binding protein EWS GN=EWSR1	37.25	1	1									
O14983	Sarcoplasmic/endoplasmic reticulum calcium ATPase 1 GN=ATP2A1	31.96	1	1									
P16615	Sarcoplasmic/endoplasmic reticulum calcium ATPase 2 GN=ATP2A2	31.96	1	1									
P49458	Signal recognition particle 9 kDa protein GN=SRP9	31.17	1	1									
Q8WVI0	Small integral membrane protein 4 GN=SMIM4	44.13	1	1									
Q01081	Splicing factor U2AF 35 kDa subunit GN=U2AF1	42.64	1	1									
P0DN76	Splicing factor U2AF 35 kDa subunit-like protein GN=U2AF1L5	42.64	1	1									
P31040	Succinate dehydrogenase [ubiquinone] flavoprotein subunit mitochondrial GN=SDHA	41.53	1	1									

		WT 1			WT 2			Null 1			Null 2		
Acc Number	Description	Prot score (-10logP)	Peptide No.	Unique Peptide No.	Prot score (-10logP)	Peptide No.	Unique Peptide No.	Prot score (-10logP)	Peptide No.	Unique Peptide No.	Prot score (-10logP)	Peptide No.	Unique Peptide No.
Q16650	T-box brain protein 1 GN=TBR1	29.39	1	1									
P17987	T-complex protein 1 subunit alpha GN=TCP1	30.03	1	1									
Q9ULT0	Tetratricopeptide repeat protein 7A GN=TTC7A	37.64	1	1									
Q02086	Transcription factor Sp2 GN=SP2	30.17	1	1									
Q13428	Treacle protein GN=TCOF1	44.6	1	1									
P35030	Trypsin-3 GN=PRSS3	32.89	1	1									
P49815	Tuberin GN=TSC2	37.35	1	1									
E9PRG8	Uncharacterized protein C11orf98 GN=C11orf98	40.4	1	1									
Q9NW07	Zinc finger protein 358 GN=ZNF358	38.93	1	1									
Q8NDX6	Zinc finger protein 740 GN=ZNF740	52.18	1	1									
P34931	Heat shock 70 kDa protein 1-like GN=HSPA1L	125.13	5	0									
P17066	Heat shock 70 kDa protein 6 GN=HSPA6	97.49	4	0									
Q13885	Tubulin beta-2A chain GN=TUBB2A	203.54	9	0									
Q9BVA1	Tubulin beta-2B chain GN=TUBB2B	203.54	9	0									
Q13509	Tubulin beta-3 chain GN=TUBB3	178.31	6	0									
Q9NZN5	Rho guanine nucleotide exchange factor 12 GN=ARHGEF12				246.12	17	17						
Q5JTH9	RRP12-like protein GN=RRP12				138.68	8	8						
Q96AG4	Leucine-rich repeat-containing protein 59 GN=LRRC59				143	7	7						
P17544	Cyclic AMP-dependent transcription factor ATF-7 GN=ATF7				133.36	7	7						
Q14974	Importin subunit beta-1 GN=KPNB1				114.73	6	6						
P61586	Transforming protein RhoA GN=RHOA				146.78	6	6						
Q6SPF0	Atherin GN=SAMD1				127.47	5	5						
O94906	Pre-mRNA-processing factor 6 GN=PRPF6				104.73	5	5						
Q96QD9	UAP56-interacting factor GN=FYTTD1				116.97	5	5						
Q14690	Protein RRP5 homolog GN=PDCD11				96.11	4	4						
O14980	Exportin-1 GN=XPO1				81.55	4	4						
Q29RF7	Sister chromatid cohesion protein PDS5 homolog A GN=PDS5A				109.4	4	4						

		WT 1			WT 2			Null 1			Null 2		
Acc Number	Description	Prot score (-10logP)	Peptide No.	Unique Peptide No.	Prot score (-10logP)	Peptide No.	Unique Peptide No.	Prot score (-10logP)	Peptide No.	Unique Peptide No.	Prot score (-10logP)	Peptide No.	Unique Peptide No.
Q6P2Q9	Pre-mRNA-processing-splicing factor 8 GN=PRPF8				95.74	4	4						
Q9H0S4	Probable ATP-dependent RNA helicase DDX47 GN=DDX47				94.64	3	3						
Q5JTV8	Torsin-1A-interacting protein 1 GN=TOR1AIP1				86.66	3	3						
Q14980	Nuclear mitotic apparatus protein 1 GN=NUMA1				59.55	3	3						
Q96SI9	Spermatid perinuclear RNA-binding protein GN=STRBP				88.36	3	3						
Q9BUQ8	Probable ATP-dependent RNA helicase DDX23 GN=DDX23				88.41	3	3						
P63000	Ras-related C3 botulinum toxin substrate 1 GN=RAC1				89.08	3	3						
Q14684	Ribosomal RNA processing protein 1 homolog B GN=RRP1B				76.59	3	3						
P04843	Dolichyl-diphospho oligosaccharide protein glycosyltransferase subunit 1 GN=RPN1				90.32	3	3						
Q08209	Serine/threonine-protein phosphatase 2B catalytic subunit alpha isoform GN=PPP3CA				93.96	3	3						
Q9UNQ2	Probable dimethyladenosine transferase GN=DIMT1				64.95	3	3						
P78316	Nucleolar protein 14 GN=NOP14				76	3	3						
Q9NVP1	ATP-dependent RNA helicase DDX18 GN=DDX18				68.59	3	3						
Q12788	Transducin beta-like protein 3 GN=TBL3				109.36	3	3						
Q06587	E3 ubiquitin-protein ligase RING1 GN=RING1				206.93	5	3						
P55317	Hepatocyte nuclear factor 3-alpha GN=FOXA1				102.69	3	3						
Q8NI36	WD repeat-containing protein 36 GN=WDR36				82.71	3	3						
P37268	Squalene synthase GN=FDFT1				125.59	2	2						
P53621	Coatomer subunit alpha GN=COPA				61.68	2	2						
Q9UH99	SUN domain-containing protein 2 GN=SUN2				67.79	2	2						
Q9H6R4	Nucleolar protein 6 GN=NOL6				89.65	2	2						
Q9Y2U8	Inner nuclear membrane protein Man1 GN=LEMD3				85.63	2	2						
P40938	Replication factor C subunit 3 GN=RFC3				78.1	2	2						
P60468	Protein transport protein Sec61 subunit beta GN=SEC61B				55.28	2	2						
P36776	Lon protease homolog mitochondrial GN=LONP1				57.42	2	2						
Q8NI60	Atypical kinase COQ8A mitochondrial GN=COQ8A				45.78	2	2						

		WT 1			WT 2			Null 1			Null 2		
Acc Number	Description	Prot score (-10logP)	Peptide No.	Unique Peptide No.	Prot score (-10logP)	Peptide No.	Unique Peptide No.	Prot score (-10logP)	Peptide No.	Unique Peptide No.	Prot score (-10logP)	Peptide No.	Unique Peptide No.
Q9HC52	Chromobox protein homolog 8 GN=CBX8				90.67	2	2						
Q1ED39	Lysine-rich nucleolar protein 1 GN=KNOP1				65.6	2	2						
Q99417	c-Myc-binding protein GN=MYCBP				69.26	2	2						
P46781	40S ribosomal protein S9 GN=RPS9				46.73	2	2						
P22415	Upstream stimulatory factor 1 GN=USF1				67.51	2	2						
P40227	T-complex protein 1 subunit zeta GN=CCT6A				61.44	2	2						
Q14119	Vascular endothelial zinc finger 1 GN=VEZF1				60.68	2	2						
Q9UMY1	Nucleolar protein 7 GN=NOL7				59.8	2	2						
P0DOX5	Immunoglobulin gamma-1 heavy chain				30.26	1	1						
Q86VP6	Cullin-associated NEDD8-dissociated protein 1 GN=CAND1				51.97	1	1						
Q86W42	THO complex subunit 6 homolog GN=THOC6				29.41	1	1						
P20929	Nebulin GN=NEB				28.65	1	1						
Q9Y3A4	Ribosomal RNA-processing protein 7 homolog A GN=RRP7A				37.95	1	1						
P0C0S5	Histone H2A.Z GN=H2AZ1				35	1	1						
Q9BTM1	Histone H2A.J GN=H2AFJ				33.74	1	1						
P0C0S8	Histone H2A type 1 GN=H2AC11				33.74	1	1						
O75533	Splicing factor 3B subunit 1 GN=SF3B1				29.51	1	1						
Q7L7L0	Histone H2A type 3 GN=HIST3H2A				33.74	1	1						
Q8WY22	BRI3-binding protein GN=BRI3BP				57.94	1	1						
P51148	Ras-related protein Rab-5C GN=RAB5C				33.34	1	1						
P51587	Breast cancer type 2 susceptibility protein GN=BRCA2				35.09	1	1						
P53618	Coatomer subunit beta GN=COPB1				33.29	1	1						
P54886	Delta-1-pyrroline-5-carboxylate synthase GN=ALDH18A1				43.81	1	1						
Q9Y5Q9	General transcription factor 3C polypeptide 3 GN=GTF3C3				57.32	1	1						
O14556	Glyceraldehyde-3-phosphate dehydrogenase testis specific GN=GAPDHS				42.9	1	1						
Q13268	Dehydrogenase/reductase SDR family member 2 mitochondrial GN=DHRS2				51.85	1	1						

		WT 1			WT 2			Null 1			Null 2		
Acc Number	Description	Prot score (-10logP)	Peptide No.	Unique Peptide No.	Prot score (-10logP)	Peptide No.	Unique Peptide No.	Prot score (-10logP)	Peptide No.	Unique Peptide No.	Prot score (-10logP)	Peptide No.	Unique Peptide No.
Q99878	Histone H2A type 1-J GN=H2AC14				33.74	1	1						
Q12931	Heat shock protein 75 kDa mitochondrial GN=TRAP1				29.99	1	1						
Q8IYT2	Cap-specific mRNA (nucleoside-2'-O-)-methyltransferase 2 GN=CMTR2				31.26	1	1						
O43615	Mitochondrial import inner membrane translocase subunit TIM44 GN=TIMM44				48.08	1	1						
P62826	GTP-binding nuclear protein Ran GN=RAN				44.74	1	1						
Q9NVH2	Integrator complex subunit 7 GN=INTS7				31.09	1	1						
P62979	Ubiquitin-40S ribosomal protein S27a GN=RPS27A				33.65	1	1						
Q86X55	Histone-arginine methyltransferase CARM1 GN=CARM1				37.36	1	1						
Q96DT7	Zinc finger and BTB domain-containing protein 10 GN=ZBTB10				63.41	1	1						
O96019	Actin-like protein 6A GN=ACTL6A				31.01	1	1						
P61803	Dolichyl-diphospho oligosaccharide protein glycosyltransferase subunit DAD1 GN=DAD1				51.83	1	1						
Q8NAF0	Zinc finger protein 579 GN=ZNF579				46.57	1	1						
P84077	ADP-ribosylation factor 1 GN=ARF1				55.09	1	1						
Q99988	Growth/differentiation factor 15 GN=GDF15				55.04	1	1						
Q9NRL2	Bromodomain adjacent to zinc finger domain protein 1A GN=BAZ1A				48.09	1	1						
Q8N3C7	CAP-Gly domain-containing linker protein 4 GN=CLIP4				37.61	1	1						
P62820	Ras-related protein Rab-1A GN=RAB1A				67.75	2	1						
P20671	Histone H2A type 1-D GN=H2AC7				33.74	1	1						
P62987	Ubiquitin-60S ribosomal protein L40 GN=UBA52				33.65	1	1						
P84085	ADP-ribosylation factor 5 GN=ARF5				55.09	1	1						
Q76N89	E3 ubiquitin-protein ligase HECW1 GN=HECW1				28.94	1	1						
P0CG48	Polyubiquitin-C GN=UBC				33.65	1	1						
Q9NYU1	UDP-glucose glycoprotein glucosyltransferase 2 GN=UGGT2				29.8	1	1						
Q9BZF1	Oxysterol-binding protein-related protein 8 GN=OSBPL8				44.69	1	1						
P20226	TATA-box-binding protein GN=TBP				64.95	1	1						
Q49A26	Putative oxidoreductase GLYR1 GN=GLYR1				31.78	1	1						

		WT 1			WT 2			Null 1			Null 2		
Acc Number	Description	Prot score (-10logP)	Peptide No.	Unique Peptide No.	Prot score (-10logP)	Peptide No.	Unique Peptide No.	Prot score (-10logP)	Peptide No.	Unique Peptide No.	Prot score (-10logP)	Peptide No.	Unique Peptide No.
P20339	Ras-related protein Rab-5A GN=RAB5A				33.34	1	1						
Q9H0U4	Ras-related protein Rab-1B GN=RAB1B				67.75	2	1						
Q16777	Histone H2A type 2-C GN=HIST2H2AC				33.74	1	1						
Q16718	NADH dehydrogenase [ubiquinone] 1 alpha subcomplex subunit 5 GN=NDUFA5				32.19	1	1						
P61204	ADP-ribosylation factor 3 GN=ARF3				55.09	1	1						
Q5SRE5	Nucleoporin NUP188 homolog GN=NUP188				32.63	1	1						
P35251	Replication factor C subunit 1 GN=RFC1				46.74	1	1						
Q8TF72	Protein Shroom3 GN=SHROOM3				28.27	1	1						
Q86WA8	Lon protease homolog 2 peroxisomal GN=LONP2				34.67	1	1						
Q8N1F7	Nuclear pore complex protein Nup93 GN=NUP93				36.96	1	1						
P0CG47	Polyubiquitin-B GN=UBB				33.65	1	1						
Q9H0M5	Zinc finger protein 700 GN=ZNF700				31.24	1	1						
P01860	Immunoglobulin heavy constant gamma 3 GN=IGHG3				30.26	1	1						
Q8N1G0	Zinc finger protein 687 GN=ZNF687				30.26	1	1						
P50991	T-complex protein 1 subunit delta GN=CCT4				69.03	1	1						
A6NKH3	Putative 60S ribosomal protein L37a-like protein GN=RPL37AP8				28.48	1	1						
P62316	Small nuclear ribonucleoprotein Sm D2 GN=SNRPD2				31.81	1	1						
P61020	Ras-related protein Rab-5B GN=RAB5B				33.34	1	1						
P35249	Replication factor C subunit 4 GN=RFC4				59.14	1	1						
Q15269	Periodic tryptophan protein 2 homolog GN=PWP2				42.48	1	1						
Q93077	Histone H2A type 1-C GN=HIST1H2AC				33.74	1	1						
Q92928	Putative Ras-related protein Rab-1C GN=RAB1C				67.75	2	1						
Q71UI9	Histone H2A.V GN=H2AFV				35	1	1						
P61026	Ras-related protein Rab-10 GN=RAB10				60.96	2	1						
Q13823	Nucleolar GTP-binding protein 2 GN=GNL2				57.67	1	1						
Q9BVP2	Guanine nucleotide-binding protein-like 3 GN=GNL3				38.6	1	1						
Q13185	Chromobox protein homolog 3 GN=CBX3				54.15	1	1						

		WT 1			WT 2			Null 1			Null 2		
Acc Number	Description	Prot score (-10logP)	Peptide No.	Unique Peptide No.	Prot score (-10logP)	Peptide No.	Unique Peptide No.	Prot score (-10logP)	Peptide No.	Unique Peptide No.	Prot score (-10logP)	Peptide No.	Unique Peptide No.
Q92552	28S ribosomal protein S27 mitochondrial GN=MRPS27				32.79	1	1						
Q9Y383	Putative RNA-binding protein Luc7-like 2 GN=LUC7L2				52.96	1	1						
P15954	Cytochrome c oxidase subunit 7C mitochondrial GN=COX7C				37.67	1	1						
Q01344	Interleukin-5 receptor subunit alpha GN=IL5RA				28.96	1	1						
P01857	Immunoglobulin heavy constant gamma 1 GN=IGHG1				30.26	1	1						
Q14692	Ribosome biogenesis protein BMS1 homolog GN=BMS1				29.2	1	1						
P49792	E3 SUMO-protein ligase RanBP2 GN=RANBP2				28.36	1	1						
Q03701	CCAAT/enhancer-binding protein zeta GN=CEBPZ				34.2	1	1						
Q9NZM5	Ribosome biogenesis protein NOP53 GN=NOP53				67.59	1	1						
Q9Y5M8	Signal recognition particle receptor subunit beta GN=SRPRB				39.13	1	1						
Q8N8A6	ATP-dependent RNA helicase DDX51 GN=DDX51				54.22	1	1						
Q96EL3	39S ribosomal protein L53 mitochondrial GN=MRPL53				48.43	1	1						
Q8N183	NADH dehydrogenase [ubiquinone] 1 alpha subcomplex assembly factor 2 GN=NDUFAF2				29.27	1	1						
Q5CZC0	Fibrous sheath-interacting protein 2 GN=FSIP2				30.4	1	1						
Q7Z7H8	39S ribosomal protein L10 mitochondrial GN=MRPL10				31.17	1	1						
Q96KK5	Histone H2A type 1-H GN=HIST1H2AH				33.74	1	1						
Q9H0U9	Testis-specific Y-encoded-like protein 1 GN=TSPYL1				31.04	1	1						
O43929	Origin recognition complex subunit 4 GN=ORC4				30.81	1	1						
A8MTT3	Protein CEBPZOS GN=CEBPZOS				37.83	1	1						
O43913	Origin recognition complex subunit 5 GN=ORC5				39.75	1	1						
Q6FI13	Histone H2A type 2-A GN=HIST2H2AA3				33.74	1	1						
P04908	Histone H2A type 1-B/E GN=H2AC4				33.74	1	1						
Q14669	E3 ubiquitin-protein ligase TRIP12 GN=TRIP12				45.78	1	1						
P42166	Lamina-associated polypeptide 2 isoform alpha GN=TMPO				172.68	7	1						
Q9C005	Protein dpy-30 homolog GN=DPY30				67.66	1	1						
Q8TED0	U3 small nucleolar RNA-associated protein 15 homolog GN=UTP15				45.15	1	1						

		WT 1			WT 2			Null 1			Null 2		
Acc Number	Description	Prot score (-10logP)	Peptide No.	Unique Peptide No.	Prot score (-10logP)	Peptide No.	Unique Peptide No.	Prot score (-10logP)	Peptide No.	Unique Peptide No.	Prot score (-10logP)	Peptide No.	Unique Peptide No.
Q92797	Symplekin GN=SYMPK				34.57	1	1						
Q6DKI1	60S ribosomal protein L7-like 1 GN=RPL7L1				35.96	1	1						
Q14244	Ensconsin GN=MAP7				28.69	1	1						
Q96DB2	Histone deacetylase 11 GN=HDAC11				30.52	1	1						
Q9UNX3	60S ribosomal protein L26-like 1 GN=RPL26L1				29.13	1	1						
Q93009	Ubiquitin carboxyl-terminal hydrolase 7 GN=USP7				67.26	1	1						
Q92621	Nuclear pore complex protein Nup205 GN=NUP205				32.98	1	1						
P49368	T-complex protein 1 subunit gamma GN=CCT3				71.76	1	1						
P07900	Heat shock protein HSP 90-alpha GN=HSP90AA1				29.99	1	1						
P57721	Poly(rC)-binding protein 3 GN=PCBP3							32.97	1	0			
P39023	60S ribosomal protein L3 GN=RPL3							46.84	1	1			
Q14525	Keratin type I cuticular Ha3-II GN=KRT33B							35.74	1	1			
Q16740	ATP-dependent Clp protease proteolytic subunit mitochondrial GN=CLPP							33.49	1	1			
Q02447	Transcription factor Sp3 GN=SP3							33.05	1	1			
P14923	Junction plakoglobin GN=JUP							31.78	1	1			
Q9BQ39	ATP-dependent RNA helicase DDX50 GN=DDX50							46.85	1	1			
Q2M1P5	Kinesin-like protein KIF7 GN=KIF7							34.63	1	1			
P20674	Cytochrome c oxidase subunit 5A mitochondrial GN=COX5A							40.36	1	1			
Q8IX03	Protein KIBRA GN=WWC1							31.14	1	1			
P12235	ADP/ATP translocase 1 GN=SLC25A4							48.96	1	1			
Q3ZCT1	Zinc finger protein 260 GN=ZNF260							52.02	1	1			
Q96FJ2	Dynein light chain 2 cytoplasmic GN=DYNLL2							31.44	1	1			
P81605	Dermcidin GN=DCD							47.19	1	1			
Q00536	Cyclin-dependent kinase 16 GN=CDK16							34.25	1	1			
Q9NQ39	Putative 40S ribosomal protein S10-like GN=RPS10P5							72.29	2	2			
P31930	Cytochrome b-c1 complex subunit 1 mitochondrial GN=UQCRC1										105.29	3	3
Q9BSJ8	Extended synaptotagmin-1 GN=ESYT1										62.63	2	2

		WT 1			WT 2			Null 1			Null 2		
Acc Number	Description	Prot score (-10logP)	Peptide No.	Unique Peptide No.	Prot score (-10logP)	Peptide No.	Unique Peptide No.	Prot score (-10logP)	Peptide No.	Unique Peptide No.	Prot score (-10logP)	Peptide No.	Unique Peptide No.
P21912	Succinate dehydrogenase [ubiquinone] iron-sulphur subunit mitochondrial GN=SDHB										68.28	2	2
Q8N3Y7	Epidermal retinol dehydrogenase 2 GN=SDR16C5										76.02	2	2
P14625	Endoplasmin GN=HSP90B1										72.67	2	2
P02656	Apolipoprotein C-III GN=APOC3										53.75	1	1
Q9Y3D7	Mitochondrial import inner membrane translocase subunit TIM16 GN=PAM16										48.96	1	1
P15336	Cyclic AMP-dependent transcription factor ATF-2 GN=ATF2										49.29	1	1
P13073	Cytochrome c oxidase subunit 4 isoform 1 mitochondrial GN=COX4I1										38.83	1	1
Q71U36	Tubulin alpha-1A chain GN=TUBA1A										45.07	1	1
P35232	Prohibitin GN=PHB										36.41	1	1
O14979	Heterogeneous nuclear ribonucleoprotein D-like GN=HNRNPDL										41.47	1	1
Q9NY65	Tubulin alpha-8 chain GN=TUBA8										45.07	1	1
P05023	Sodium/potassium-transporting ATPase subunit alpha-1 GN=ATP1A1										40.14	1	1
Q9UL25	Ras-related protein Rab-21 GN=RAB21										50.83	1	1
O95202	Mitochondrial proton/calcium exchanger protein GN=LETM1										47.82	1	1
A6NIZ1	Ras-related protein Rap-1b-like protein										41.45	1	1
P47985	Cytochrome b-c1 complex subunit Rieske mitochondrial GN=UQCRFS1										38.18	1	1
P68366	Tubulin alpha-4A chain GN=TUBA4A										45.07	1	1
Q96DA6	Mitochondrial import inner membrane translocase subunit TIM14 GN=DNAJC19										40.9	1	1
Q15286	Ras-related protein Rab-35 GN=RAB35										39.91	1	1
P50993	Sodium/potassium-transporting ATPase subunit alpha-2 GN=ATP1A2										40.14	1	1
P0DPH8	Tubulin alpha-3D chain GN=TUBA3D										45.07	1	1
O75915	PRA1 family protein 3 GN=ARL6IP5										39.36	1	1
Q6PEY2	Tubulin alpha-3E chain GN=TUBA3E										45.07	1	1
Q04695	Keratin type I cytoskeletal 17 GN=KRT17										53.25	1	1
A6NHL2	Tubulin alpha chain-like 3 GN=TUBAL3										45.07	1	1
Q9UDW1	Cytochrome b-c1 complex subunit 9 GN=UQCR10										35.64	1	1

		WT 1			WT 2			Null 1			Null 2		
Acc Number	**Description**	**Prot score (-10logP)**	**Peptide No.**	**Unique Peptide No.**	**Prot score (-10logP)**	**Peptide No.**	**Unique Peptide No.**	**Prot score (-10logP)**	**Peptide No.**	**Unique Peptide No.**	**Prot score (-10logP)**	**Peptide No.**	**Unique Peptide No.**
P61019	Ras-related protein Rab-2A GN=RAB2A										36.94	1	1
Q9BYE2	Transmembrane protease serine 13 GN=TMPRSS13 PE=2 SV=5										51.31	1	1
P62834	Ras-related protein Rap-1A GN=RAP1A										41.45	1	1
P29590	Protein PML GN=PML										42.71	1	1
O00217	NADH dehydrogenase [ubiquinone] iron-sulphur protein 8 mitochondrial GN=NDUFS8										37.61	1	1
Q05639	Elongation factor 1-alpha 2 GN=EEF1A2										38.43	1	1
P0DPH7	Tubulin alpha-3C chain GN=TUBA3C										45.07	1	1
Q02413	Desmoglein-1 GN=DSG1										41.87	1	1
P14927	Cytochrome b-c1 complex subunit 7 GN=UQCRB										51.81	1	1
P13637	Sodium/potassium-transporting ATPase subunit alpha-3 GN=ATP1A3										40.14	1	1

8.4 Antibody List

Antibody	Company	Cat. No	Applications
AKT	Cell Signalling Technology	CST-9272	WB
Androgen Receptor	Cell Signalling Technology	CST-5153	WB
Anti-His-Tag	Cell Signalling Technology	CST-2365	IF, WB
Anti-Histone H3 (mono methyl K4) antibody (H3K4me1)	Abcam	ab8895	ChIP
DNA-PKcs	Sigma Aldrich	D4060	WB
DNA-PKcs (18-2)	ThermoFisher Scientific	MA5-13238	IP
EGFR	Cell Signalling Technology	CST-4267	WB
H2AX	Abcam	ab124781	WB
IGF-1Rα (N-20)	Santa Cruz Biotechnology	sc-712	IF, WB
IGF-1Rα (24-60)	ThermoFisher Scientific	MA5-13817	ChIP, IF, IP
IGF-1Rα (αIR-3)	Abcam	ab16890	IF
IGF-1Rβ	Cell Signalling Technology	CST-3027	ChIP, IP, WB
IGF-1Rβ (D23H3)	Cell Signalling Technology	CST-9750	IF, IHC
Ku70/80	MyBioSource	MBS9601641	WB
Ku80	Neomarkers	MS-285-P1	WB
Lamin A/C	BD Transduction Labs	612162	WB
Normal Rabbit IgG	Cell Signalling Technology	CST-2729	IP
PARP-1	Abcam	ab227244	WB
Phospho-AKT	Cell Signalling Technology	CST-4060	WB
Phospho-DNA-PK S2056	ThermoFisher Scientific	PA5-78130	WB
Phospho-DNA-PK S3025	(Neal *et al.*, 2011)	N/A	WB
Phospho-DNA-PK T2609	Abcam	ab18356	WB
Phospho-IGF-1Rβ (Tyr1135/1136)	Cell Signalling Technology	CST-3024	WB
Phospho-RPA (S4/8)	Abcam	ab243866	WB
RNA Polymerase II (CTD repeat YSPTSPS (phospho S2)	Abcam	ab5095	ChIP
RPA	GeneTex	GTX15783	WB
β-tubulin	Cell Signalling Technology	CST-86298	WB
γH2AX	Abcam	ab11174	WB

ChIP – Chromatin immunoprecipitation, IF – Immunofluorescence, IHC – Immunohistochemistry, IP – Immunoprecipitation, WB – Western blot

9 Bibliography

Abou-Alfa, G.K. *et al.* (2014) "A phase II study of cixutumumab (IMC-A12, NSC742460) in advanced hepatocellular carcinoma," *Journal of Hepatology*, 60(2), pp. 319–324.

Adams, T.E. *et al.* (2000) "Structure and function of the type 1 insulin-like growth factor receptor," *Cellular and Molecular Life Sciences*, 57, pp. 1050–1093.

Ahnesorg, P., Smith, P. and Jackson, S.P. (2006) "XLF interacts with the XRCC4-DNA Ligase IV complex to promote DNA nonhomologous end-joining," *Cell*, 124(2), pp. 301–313.

Aleksic, T. *et al.* (2010) "Type 1 Insulin-like Growth Factor Receptor Translocates to the Nucleus of Human Tumor Cells," *Cancer Research*, 70(16), pp. 6412–6420.

Aleksic, T., Browning, L., *et al.* (2016) "Durable Response of Spinal Chordoma to Combined Inhibition of IGF-1R and EGFR," *Frontiers in Oncology*, 6(98), pp. 1–6.

Aleksic, T., Ross Worrall, A., *et al.* (2016) "Improved Immunohistochemical Detection of Type 1 Insulin-Like Growth Factor Receptor in Human Tumors," *Immunochemistry & Immunopathology*, 2(1), pp. 1–5.

Aleksic, T. *et al.* (2017) "IGF-1R associates with adverse outcomes after radical radiotherapy for prostate cancer," *BJC*, (117), pp. 1600–1606.

Aleksic, T. *et al.* (2018) "Nuclear IGF1R Interacts with Regulatory Regions of Chromatin to Promote RNA Polymerase II Recruitment and Gene Expression Associated with Advanced Tumor Stage," *Cancer Research*, 78(13), pp. 3497–3509.

Alexandrov, A., Colognori, D. and Steitz, J.A. (2011) "Human eIF4AIII interacts with an eIF4G-like partner, NOM1, revealing an evolutionarily conserved function outside the exon junction complex," *Genes and Development*, 25(10), pp. 1078–1090.

Allalunis-Turner, M.J. *et al.* (1995) "Radiation-induced DNA damage and repair in cells of a radiosensitive human malignant glioma cell line," *Radiation Research*, 144(3), pp. 288–293.

Andersen, P.L., Xu, F. and Xiao, W. (2008) "Eukaryotic DNA damage tolerance and translesion synthesis through covalent modifications of PCNA," *Cell Research*, 18(1), pp. 162–173.

Anderson, P.M. *et al.* (2016) "A phase II study of clinical activity of SCH 717454 (robatumumab) in patients with relapsed osteosarcoma and Ewing sarcoma," *Pediatric Blood and Cancer*, 63(10), pp. 1761–1770.

Angel, P. *et al.* (1988) "The jun proto-oncogene is positively autoregulated by its product, Jun/AP-1," *Cell*, 55(5), pp. 875–885.

de Angelis Campos, A.C. *et al.* (2011) "Epidermal growth factor receptors destined for the nucleus are internalized via a clathrin-dependent pathway," *Biochemical and Biophysical Research Communications*, 412(2), pp. 341–346.

Angelloz-Nicoud, P. and Binoux, M. (1995) "Autocrine regulation of cell proliferation by the insulin-like growth factor (IGF) and IGF binding protein-3 protease system in a human prostate carcinoma cell line (PC-3)," *Endocrinology*, 136(12), pp. 5485–5492.

Van Antwerp, D.J. *et al.* (1996) "Suppression of TNF-α-induced apoptosis by NF-κB," *Science*, 274(5288), pp. 787–789.

Arora, V.K. *et al.* (2013) "Glucocorticoid receptor confers resistance to antiandrogens by bypassing androgen receptor blockade," *Cell*, 155(6), pp. 1309–1322.

Ashley, A.K. *et al.* (2014) "DNA-PK Phosphorylation of RPA32 Ser4/Ser8 Regulates Replication Stress Checkpoint Activation, Fork Restart, Homologous Recombination and Mitotic Catastrophe," *DNA Repair (Amst)*, (21), pp. 131–139.

Asmane, I. *et al.* (2012) "Insulin-like growth factor type 1 receptor (IGF-1R) exclusive nuclear staining: A predictive biomarker for IGF-1R monoclonal antibody (Ab) therapy in sarcomas," *European Journal of Cancer*, 48(16), pp. 3027–3035.

Aubrey, B.J. *et al.* (2018) "How does p53 induce apoptosis and how does this relate to p53-mediated tumour suppression?," *Cell Death and Differentiation*, 25(1), pp. 104–113.

Bachelder, R.E. *et al.* (2005) "Glycogen synthase kinase-3 is an endogenous inhibitor of Snail transcription: Implications for the epithelial - Mesenchymal transition," *Journal of Cell Biology*, 168(1), pp. 29–33.

Bae, S. and Lesch, B.J. (2020) “H3K4me1 Distribution Predicts Transcription State and Poising at Promoters,” *Frontiers in Cell and Developmental Biology*, 8.

Baron, O. *et al.* (2012) “Cooperation of nuclear fibroblast growth factor receptor 1 and Nurr1 offers new interactive mechanism in postmitotic development of mesencephalic dopaminergic neurons,” *Journal of Biological Chemistry*, 287(24), pp. 19827–19840.

Barrallo-Gimeno, A. and Nieto, M.A. (2005) “The Snail genes as inducers of cell movement and survival: Implications in development and cancer,” *Development*, 132(14), pp. 3151–3161.

Barrie, S.E. *et al.* (1994) “Pharmacology of novel steroidal inhibitors of cytochrome P45017α (17α-hydroxylase/C17-20 lyase),” *Journal of Steroid Biochemistry and Molecular Biology*, 50(5–6), pp. 267–273.

Barysch, S. V. *et al.* (2009) “Sorting in early endosomes reveals connections to docking- and fusion-associated factors,” *Proceedings of the National Academy of Sciences of the United States of America*, 106(24), pp. 9697–9702.

Baserga, R. *et al.* (1997) “The IGF-I receptor in cell growth, transformation and apoptosis,” *Biochimica et Biophysica Acta - Reviews on Cancer*, 1332(3), pp. F105–F126.

Baserga, R., Peruzzi, F. and Reiss, K. (2003) “The IGF-1 receptor in cancer biology,” *Int J Cancer*, 107(6), pp. 873–877.

Baxter, R.C. (2015) “Nuclear actions of insulin-like growth factor binding protein-3,” *Gene*, 569(1), pp. 7–13.

Becerra, C.R. *et al.* (2014) “Figitumumab in patients with refractory metastatic colorectal cancer previously treated with standard therapies: A nonrandomized, open-label, phase II trial,” *Cancer Chemotherapy and Pharmacology*, 73(4), pp. 695–702.

Beer, T.M. *et al.* (2014) “Enzalutamide in metastatic prostate cancer before chemotherapy,” *New England Journal of Medicine*, 371(5), pp. 424–433.

Belani, C.P., Goss, G. and Blumenschein, G. (2012) “Recent clinical developments and rationale for combining targeted agents in non-small cell lung cancer (NSCLC),” *Cancer Treatment Reviews*, 38(3), pp. 173–184.

Belfiore, A. and Frasca, F. (2008) “IGF and insulin receptor signaling in breast cancer,” *Journal of Mammary Gland Biology and Neoplasia*, 13(4), pp. 381–406.

Bellanger, J.-M. *et al.* (2000) “The Rac1- and RhoG-specific GEF domain of Trio targets filamin to remodel cytoskeletal actin,” *Nature Cell Biology*, 2(12).

Beltran, P.J. *et al.* (2009) “AMG 479, a fully human anti-insulin-like growth factor receptor type I monoclonal antibody, inhibits the growth and survival of pancreatic carcinoma cells,” *Molecular Cancer Therapeutics*, 8(5), pp. 1095–1105.

Benayoun, B.A. *et al.* (2014) “H3K4me3 breadth is linked to cell identity and transcriptional consistency,” *Cell*, 158(3), pp. 673–688.

Bergman, D. *et al.* (2013) “Insulin-like growth factor 2 in development and disease: A mini-review,” *Gerontology*, 59(3), pp. 240–249.

Bernier-Villamor, V. *et al.* (2002) “Structural basis for E2-mediated SUMO conjugation revealed by a complex between ubiquitin-conjugating enzyme Ubc9 and RanGAP1,” *Cell*, 108(3), pp. 345–356.

Blackford, A.N. and Jackson, S.P. (2017) “ATM, ATR, and DNA-PK: The Trinity at the Heart of the DNA Damage Response,” *Molecular Cell*, 66(6), pp. 801–817.

Blazquez, C. *et al.* (2006) “Phosphorylated KDR can be located in the nucleus of neoplastic cells,” *Cell Research*, 16(1), pp. 93–98.

Bode, A.M. and Dong, Z. (2007) “The functional contrariety of JNK,” *Molecular Carcinogenesis*, 46(8), pp. 591–598.

Bodzin, A.S. *et al.* (2012) “Gefitinib resistance in HCC mahlavu cells: Upregulation of CD133 expression, activation of IGF-1R signaling pathway, and enhancement of IGF-1R nuclear translocation,” *Journal of Cellular Physiology*, 227(7), pp. 2947–2952.

Boehm, E.M., Gildenberg, M.S. and Washington, M.T. (2016) “The many roles of PCNA,” *Enzymes*, 39, pp. 231–254.

Böhm, M. *et al.* (2009) "A role for GATA-2 in transition to an aggressive phenotype in prostate cancer through modulation of key androgen-regulated genes," *Oncogene*, 28(43), pp. 3847–3856.

De Bono, J.S. *et al.* (2011) "Abiraterone and increased survival in metastatic prostate cancer," *New England Journal of Medicine*, 364(21), pp. 1995–2005.

De Bono, J.S. *et al.* (2014) "Phase II randomized study of figitumumab plus docetaxel and docetaxel alone with crossover for metastatic castration-resistant prostate cancer," *Clinical Cancer Research*, 20(7), pp. 1925–1934.

Brand, T.M. *et al.* (2013) "Nuclear EGFR as a Molecular Target in Cancer," *Radiotherapy and Oncology*, 108(3), pp. 1–18.

Brandon Parker, J. *et al.* (2014) "Host cell factor-1 recruitment to E2F-bound and cell-cycle-control genes is mediated by THAP11 and ZNF143," *Cell Reports*, 9(3), pp. 967–982.

Braulke, T. (1999) "Type-2 IGF Receptor : A Multi-Ligand Binding Protein," *Horm Metab Res*, (31), pp. 242–246.

Breuhahn, K. and Schirmacher, P. (2008) "Reactivation of the insulin-like growth factor-II signaling pathway in human hepatocellular carcinoma," *World Journal of Gastroenterology*, 14(11), pp. 1690–1698.

Britton, S., Coates, J. and Jackson, S.P. (2013) "A new method for high-resolution imaging of Ku foci to decipher mechanisms of DNA double-strand break repair," *Journal of Cell Biology*, 202(3), pp. 579–595.

Brodt, P. *et al.* (2001) "Cooperative Regulation of the Invasive and Metastatic Phenotypes by Different Domains of the Type I Insulin-like Growth Factor Receptor β Subunit," *Journal of Biological Chemistry*, 276(36), pp. 33608–33615.

Brown, J. *et al.* (2008) "Structure and functional analysis of the IGF-II/IGF2R interaction," *EMBO Journal*, 27(1), pp. 265–276.

Browne, B.C. *et al.* (2011) "Inhibition of IGF1R activity enhances response to trastuzumab in HER-2-positive breast cancer cells," *Annals of Oncology*, 22(1), pp. 68–73.

Brunet, A. *et al.* (2004) “Stress-Dependent Regulation of FOXO Transcription Factors by the SIRT1 Deacetylase,” *Science*, 303(5666), pp. 2011–2015.

Bryant, D.M. and Stow, J.L. (2005) “Nuclear translocation of cell-surface receptors: Lessons from fibroblast growth factor,” *Traffic*, 6(10), pp. 947–953.

Brzozowski, A.M. *et al.* (2002) “Structural origins of the functional divergence of human insulin-like growth factor-I and insulin,” *Biochemistry*, 41(30), pp. 9389–9397.

Buck, D. *et al.* (2006) “Cernunnos, a novel nonhomologous end-joining factor, is mutated in human immunodeficiency with microcephaly,” *Cell*, 124(2), pp. 287–299.

Buck, E. *et al.* (2010) “Compensatory insulin receptor (IR) activation on inhibition of insulin-like growth factor-1 receptor (IGF-1R): Rationale for cotargeting IGF-1R and IR in cancer,” *Molecular Cancer Therapeutics*, 9(10), pp. 2652–2664.

Burgering, B.M.T. and Kops, G.J.P.L. (2002) “Cell cycle and death control: Long live Forkheads,” *Trends in Biochemical Sciences*, 27(7), pp. 352–360.

Butler, A.A. *et al.* (1998) “Insulin-like growth factor-I receptor signal transduction: At the interface between physiology and cell biology,” *Comparative Biochemistry and Physiology - B Biochemistry and Molecular Biology*, 121(1), pp. 19–26.

Cai, C. *et al.* (2009) “Reactivation of androgen receptor-regulated TMPRSS2:ERG gene expression in castration-resistant prostate cancer,” *Cancer Research*, 69(15), pp. 6027–6032.

Cai, J. *et al.* (2011) “Y-Secretase and Presenilin Mediate Cleavage and Phosphorylation of Vascular Endothelial Growth Factor Receptor-1,” *Journal of Biological Chemistry*, 286(49), pp. 42514–42523.

Cai, W. *et al.* (2017) “Domain-dependent effects of insulin and IGF-1 receptors on signalling and gene expression,” *Nature Communications*, 8(14892), pp. 1–14.

Calo, E. and Wysocka, J. (2013) “Modification of Enhancer Chromatin: What, How, and Why?,” *Molecular Cell*, 49(5), pp. 825–837.

Canonici, A. *et al.* (2008) “Insulin-like growth factor-I receptor, E-cadherin and αv integrin form a dynamic complex under the control of α-catenin,” *International Journal of Cancer*, 122(3), pp. 572–582.

Carboni, J.M. *et al.* (2009) “BMS-754807, a small molecule inhibitor of insulin-like growth factor-1R/IR,” *Molecular Cancer Therapeutics*, 8(12), pp. 3341–3349.

Carceles-Cordon, M. *et al.* (2020) “Cellular rewiring in lethal prostate cancer: the architect of drug resistance,” *Nature Reviews Urology*, 17(May), pp. 292–307.

Cardone, M.H. *et al.* (1998) “Regulation of cell death protease caspase-9 by phosphorylation,” *Science*, 282(5392), pp. 1318–1321.

Cargnello, M. and Roux, P.P. (2011) “Activation and Function of the MAPKs and Their Substrates, the MAPK-Activated Protein Kinases,” *Microbiology and Molecular Biology Reviews*, 75(1), pp. 50–83.

Carpenter, G. and Liao, H. (2009) “Trafficking of Receptor Tyrosine Kinases to the Nucleus,” *Experimental Cell Research*, 315(9), pp. 1556–1566.

Carpenter, G. and Liao, H. (2013) “Receptor Tyrosine Kinases in the Nucleus,” *Cold Spring Harb Perspect Biol*, 5(10), pp. 1–17.

Carpentier, J.L. (1994) “Insulin receptor internalization: molecular mechanisms and physiopathological implications,” *Diabetologia*, 37(2), pp. 117–124.

Carter, H.B. *et al.* (2006) “Detection of life-threatening prostate cancer with prostate-specific antigen velocity during a window of curability,” *Journal of the National Cancer Institute*, 98(21), pp. 1521–1527.

Carver, B.S. *et al.* (2009) “Aberrant ERG expression cooperates with loss of PTEN to promote cancer progression in the prostate,” *Nature Genetics*, 41(5), pp. 619–624.

Chakravarti, A., Loeffler, J.S. and Dyson, N.J. (2002) “Insulin-like growth factor receptor I mediates resistance to anti-epidermal growth factor receptor therapy in primary human glioblastoma cells through continued activation of phosphoinositide 3-kinase signaling,” *Cancer Research*, 62(1), pp. 200–207.

Chan, D.W. *et al.* (2002) "Autophosphorylation of the DNA-dependent protein kinase catalytic subunit is required for rejoining of DNA double-strand breaks," *Genes and Development*, 16(18), pp. 2333–2338.

Chang, F. *et al.* (2003) "Involvement of PI3K/Akt pathway in cell cycle progression, apoptosis, and neoplastic transformation: A target for cancer chemotherapy," *Leukemia*, 17(3), pp. 590–603.

Chang, W.H. *et al.* (2017) "Smek1/2 is a nuclear chaperone and cofactor for cleaved Wnt receptor Ryk, regulating cortical neurogenesis," *Proceedings of the National Academy of Sciences of the United States of America*, 114(50), pp. E10717–E10725.

Charvet, C. and Maurer, U. (2011) "GSK-3 turns p53 deadly," *Cell Cycle*, 10(21), pp. 3621–3622.

Chen, B.P.C. *et al.* (2005) "Cell cycle dependence of DNA-dependent protein kinase phosphorylation in response to DNA double strand breaks," *Journal of Biological Chemistry*, 280(15), pp. 14709–14715.

Chen, B.P.C. *et al.* (2007) "Ataxia telangiectasia mutated (ATM) is essential for DNA-PKcs phosphorylations at the Thr-2609 cluster upon DNA double strand break," *Journal of Biological Chemistry*, 282(9), pp. 6582–6587.

Chen, C., Edelstein, L.C. and Gelinas, C. (2000) "The Rel/NF-kappa B Family Directly Activates Expression of the Apoptosis Inhibitor Bcl-xL," *Molecular and Cellular Biology*, 20(8), pp. 2687–2695.

Chen, D. *et al.* (2011) "Insulin-like growth factor-binding protein-7 functions as a potential tumor suppressor in hepatocellular carcinoma," *Clinical Cancer Research*, 17(21), pp. 6693–6701.

Chen, H. *et al.* (1999) "A testis-specific gene, TPTE, encodes a putative transmembrane tyrosine phosphatase and maps to the pericentromeric region of human chromosomes 21 and 13, and to chromosomes 15, 22, and Y.," *Human genetics*, 105(5).

Chen, H.X. and Sharon, E. (2013) "IGF-1R as an anti-cancer target-trials and tribulation," *Chinese Journal of Cancer*, 32(5), pp. 242–252.

Chen, L. *et al.* (2012) “Dynamic regulation of platelet-derived growth factor receptor α expression in alveolar fibroblasts during realveolarization,” *American Journal of Respiratory Cell and Molecular Biology*, 47(4), pp. 517–527.

Chen, M.K. and Hung, M.C. (2015) “Proteolytic cleavage, trafficking, and functions of nuclear receptor tyrosine kinases,” *FEBS Journal*, 282(19), pp. 3693–3721.

Chen, X., Zaro, J.L. and Shen, W.C. (2013) “Fusion protein linkers: Property, design and functionality,” *Advanced Drug Delivery Reviews*, 65(10), pp. 1357–1369.

Chen, Z. *et al.* (2001) “MAP kinases,” *Chemical Reviews*, 101(8), pp. 2449–2476.

Cheng, Q.C. *et al.* (2003) “Ectodomain cleavage of ErbB-4. Characterization of the cleavage site and m80 fragment,” *Journal of Biological Chemistry*, 278(40), pp. 38421–38427.

Chitnis, M.M. *et al.* (2008) “The Type 1 Insulin-Like Growth Factor Receptor Pathway,” *Molecular Pathways*, 14(20), pp. 6364–6371.

Chitnis, M.M. *et al.* (2014) “IGF-1R inhibition enhances radiosensitivity and delays double-strand break repair by both non-homologous end-joining and homologous recombination,” *Oncogene*, 33(45), pp. 5262–5273.

Chu, I.M., Hengst, L. and Slingerland, J.M. (2008) “The Cdk inhibitor p27 in human cancer: Prognostic potential and relevance to anticancer therapy,” *Nature Reviews Cancer*, 8(4), pp. 253–267.

Clegg, N.J. *et al.* (2012) “ARN-509: A novel antiandrogen for prostate cancer treatment,” *Cancer Research*, 72(6), pp. 1494–1503.

Codony-servat, J. *et al.* (2017) “Nuclear IGF-1R predicts chemotherapy and targeted therapy resistance in metastatic colorectal cancer,” *BJC*, (July), pp. 1777–1786.

Cohen, P. *et al.* (1992) “Prostate-Specific Antigen (PSA) is an Insulin-Like Growth Factor Binding Protein-3 Protease Found in Seminal Plasma,” *Journal of Clinical Endocrinology and Metabolism*, 75(4), pp. 1046–1053.

Constantino Rosa Santos, S. *et al.* (2007) "VEGF and VEGFR-2 (KDR) internalization is required for endothelial recovery during wound healing," *Experimental Cell Research*, 313(8), pp. 1561–1574.

Cornell, L. *et al.* (2015) "DNA-PK- A candidate driver of hepatocarcinogenesis and tissue biomarker that predicts response to treatment and survival," *Clinical Cancer Research*, 21(4), pp. 925–933.

Cortes, J. *et al.* (2008) "Preliminary Clinical Activity in a Phase I Trial of the BCR-ABL/IGF- 1R/Aurora Kinase Inhibitor XL228 in Patients with Ph++ Leukemias with Either Failure to Multiple TKI Therapies or with T315I Mutation," *Blood*, 112(11), p. 3232.

Cortot, A.B. *et al.* (2013) "Resistance to irreversible EGF receptor tyrosine kinase inhibitors through a multistep mechanism involving the IGF1R pathway," *Cancer Research*, 73(2), pp. 834–843.

Cosaceanu, D. *et al.* (2007) "Ionizing radiation activates IGF-1R triggering a cytoprotective signaling by interfering with Ku-DNA binding and by modulating Ku86 expression via a p38 kinase-dependent mechanism," *Oncogene*, 26(17), pp. 2423–2434.

Cox, M.E. *et al.* (2009) "Insulin receptor expression by human prostate cancers," *Prostate*, 69(1), pp. 33–40.

Cox, O.T. *et al.* (2015) "IGF-1 receptor and adhesion signaling: An important axis in determining cancer cell phenotype and therapy resistance," *Frontiers in Endocrinology*, 6(JUL).

Critchlow, S.E., Bowater, R.P. and Jackson, S.P. (1997) "Mammalian DNA double-strand break repair protein XRCC4 interacts with DNA ligase IV," *Current Biology*, 7(8), pp. 588–598.

Cross, D.A.E. *et al.* (1995) "Inhibition of glycogen synthase kinase-3 by insulin mediated by protein kinase B," *Nature*, 378(6559), pp. 785–789.

Crown, J. *et al.* (2019) "Xentuzumab (BI 836845), an insulin-like growth factor (IGF)-neutralizing antibody (Ab), combined with exemestane and everolimus in hormone receptor-positive (HR+) locally advanced/metastatic breast cancer (LA/mBC): Randomized phase 2 results," *Cancer Research*, 79(4 Supplement), pp. P6-21-01 LP-P6-21–01.

Cui, H. *et al.* (2003) "Loss of IGF2 imprinting: A potential marker of colorectal cancer risk," *Science*, 299(5613), pp. 1753–1755.

Currie, R.A. *et al.* (1999) "Role of phosphatidylinositol 3,4,5-trisphosphate in regulating the activity and localization of 3-phosphoinositide-dependent protein kinase-1," *Biochemical Journal*, 337(2–3), pp. 575–583.

Dale, O.T. *et al.* (2015) "IGF-1R expression is associated with HPV-negative status and adverse survival in head and neck squamous cell cancer," *Carcinogenesis*, 36(6), pp. 648–655.

Datta, S.R. *et al.* (1997) "Akt phosphorylation of BAD couples survival signals to the cell-intrinsic death machinery," *Cell*, 91(2), pp. 231–241.

Daughaday, W.H. and Rotwein, P. (1989) "Insulin-like growth factors I and II. Peptide, messenger ribonucleic acid and gene structures, serum, and tissue concentrations," *Endocrine Reviews*, 10(1), pp. 68–91.

Davey, R.A. and Grossmann, M. (2016) "Androgen Receptor Structure, Function and Biology: From Bench to Bedside," *The Clinical Biochemist Reviews*, 37(1), pp. 3–15.

Deacon, S.W. *et al.* (2003) "Dynactin is required for bidirectional organelle transport," *Journal of Cell Biology*, 160(3), pp. 297–301.

Dehm, S.M. *et al.* (2008) "Splicing of a novel androgen receptor exon generates a constitutively active androgen receptor that mediates prostate cancer therapy resistance," *Cancer Research*, 68(13), pp. 5469–5477.

Dejosez, M. *et al.* (2010) "Ronin/Hcf-1 binds to a hyperconserved enhancer element and regulates genes involved in the growth of embryonic stem cells," *Genes and Development*, 24(14), pp. 1479–1484.

Deng, Z.H. *et al.* (2015) "Nuclear FAM21 participates in NF-κB-dependent gene regulation in pancreatic cancer cells," *Journal of Cell Science*, 128(2), pp. 373–384.

Diehl, J.A. *et al.* (1998) "Glycogen synthase kinase-3B regulates cyclin D1 proteolysis and subcellular localization," *Genes and Development*, 12(22), pp. 3499–3511.

Ding, Q. *et al.* (2005) “Erk associates with and primes GSK-3β for its inactivation resulting in upregulation of β-catenin,” *Molecular Cell*, 19(2), pp. 159–170.

Dittmann, K. *et al.* (2005) “Radiation-induced epidermal growth factor receptor nuclear import is linked to activation of DNA-dependent protein kinase,” *Journal of Biological Chemistry*, 280(35), pp. 31182–31189.

Domingues, I. *et al.* (2011) “VEGFR2 translocates to the nucleus to regulate its own transcription,” *PLoS ONE*, 6(9), p. e25668.

Dong, X.Y. *et al.* (2003) “Identification of two novel CT antigens and their capacity to elicit antibody response in hepatocellular carcinoma patients,” *British Journal of Cancer*, 89(2), pp. 291–297.

Douglas, P. *et al.* (2002) “Identification of in vitro and in vivo phosphorylation sites in the catalytic subunit of the DNA-dependent protein kinase,” *Biochemical Journal*, 368(1), pp. 243–251.

Douglas, P. *et al.* (2014) “Polo-like kinase 1 (PLK1) and protein phosphatase 6 (PP6) regulate DNA-dependent protein kinase catalytic subunit (DNA-PKcs) phosphorylation in mitosis,” *Bioscience Reports*, 34(3), pp. 257–271.

Draisma, G. *et al.* (2003) “Lead times and overdetection due to prostate-specific antigen screening: Estimates from the European randomized study of screening for prostate cancer,” *Journal of the National Cancer Institute*, 95(12), pp. 868–878.

Dumas, J.J. *et al.* (2001) “Multivalent endosome targeting by homodimeric EEA1,” *Molecular Cell*, 8(5), pp. 947–958.

Dunham-Ems, S.M. *et al.* (2009) “Fibroblast Growth Factor Receptor-1 (FGFR1) Nuclear Dynamics Reveal a Novel Mechanism in Transcription Control,” *Molecular Biology of the Cell*, 20(9), pp. 2401–2412.

Dunn, S.E. *et al.* (1998) *A Dominant Negative Mutant of the Insulin-like Growth Factor-I Receptor Inhibits the Adhesion, Invasion, and Metastasis of Breast Cancer1*, *CANCER RESEARCH*.

Dvir, A. *et al.* (1992) "Ku autoantigen is the regulatory component of a template-associated protein kinase that phosphorylates RNA polymerase II," *Proceedings of the National Academy of Sciences of the United States of America*, 89(24), pp. 11920–11924.

Eder, I.E. *et al.* (2001) "Molecular biology of the androgen receptor: From molecular understanding to the clinic," *European Urology*, 40(3), pp. 241–251.

Eferl, R. and Wagner, E.F. (2003) "AP-1: A double-edged sword in tumorigenesis," *Nature Reviews Cancer*, 3(11), pp. 859–868.

Enguita-Germán, M. and Fortes, P. (2014) "Targeting the insulin-like growth factor pathway in hepatocellular carcinoma," *World Journal of Hepatology*, 6(10), pp. 716–737.

Epstein, J.I. *et al.* (2016) "The 2014 international society of urological pathology (ISUP) consensus conference on gleason grading of prostatic carcinoma. Definition of grading patterns and proposal for a new grading system," *American Journal of Surgical Pathology*, 40(2), pp. 244–252.

Etzioni, R. *et al.* (2002) "Overdiagnosis Due to Prostate-Specific Antigen Screening: Lessons From U.S. Prostate Cancer Incidence Trends," *Journal of the National Cancer Institute*, 94(13), pp. 981–990.

Evert, M. *et al.* (2013) "Deregulation of DNA-dependent protein kinase catalytic subunit contributes to human hepatocarcinogenesis development and has a putative prognostic value," *British Journal of Cancer*, 109(10), pp. 2654–2664.

Fanayan, S. *et al.* (2000) "Growth inhibition by insulin-like growth factor-binding protein-3 in T47D breast cancer cells requires transforming growth factor-β (TGF-β) and the type II TGF-β receptor," *Journal of Biological Chemistry*, 275(50), pp. 39146–39151.

Fassnacht, M. *et al.* (2015) "Linsitinib (OSI-906) versus placebo for patients with locally advanced or metastatic adrenocortical carcinoma: A double-blind, randomised, phase 3 study," *The Lancet Oncology*, 16(4), pp. 426–435.

Federici, M., Porzio, O., Zucaro, L., Fusco, A., *et al.* (1997) "Distribution of insulin/insulin-like growth factor-I hybrid receptors in human tissues," *Molecular and Cellular Endocrinology*, 129(2), pp. 121–126.

Federici, M., Porzio, O., Zucaro, L., Giovannone, B., *et al.* (1997) "Increased abundance of insulin/IGF-I hybrid receptors in adipose tissue from NIDDM patients," *Molecular and Cellular Endocrinology*, 135(1), pp. 41–47.

Firth, S. and Baxter, R. (2002) "Cellular Actions of the Insulin-Like Growth Factor Binding Proteins," *Endocrine Reviews*, 23(6), pp. 824–854.

Fishman, J.B. and Berg, E.A. (2019) "Protein A and protein G purification of antibodies," *Cold Spring Harbor Protocols*, 2019(1), pp. 82–84.

Flores-Rodriguez, N. *et al.* (2011) "Roles of dynein and dynactin in early endosome dynamics revealed using automated tracking and global analysis," *PLoS ONE*, 6(9), pp. 1–11.

Florkiewicz, R.Z., Baird, A. and Gonzalez, A.M. (1991) "Multiple forms of bFGF: Differential nuclear and cell surface localization," *Growth Factors*, 4(4), pp. 265–275.

Forest, A. *et al.* (2015) "Intrinsic resistance to cixutumumab is conferred by distinct isoforms of the insulin receptor," *Molecular Cancer Research*, 13(12), pp. 1615–1626.

Fox, S.B. *et al.* (2004) "Phosphorylated KDR is expressed in the neoplastic and stromal elements of human renal tumours and shuttles from cell membrane to nucleus," *Journal of Pathology*, 202(3), pp. 313–320.

Frasca, F. *et al.* (1999) "Insulin Receptor Isoform A, a Newly Recognized, High-Affinity Insulin-Like Growth Factor II Receptor in Fetal and Cancer Cells," *Molecular and Cellular Biology*, 19(5), pp. 3278–3288.

Friedbichler, K. *et al.* (2014) "Pharmacodynamic and Antineoplastic Activity of BI 836845, a Fully Human IGF Ligand-Neutralizing Antibody, and Mechanistic Rationale for Combination with Rapamycin," *Molecular Cancer Therapeutics*, 13(2), pp. 399–409.

Fu, Z. and Tindall, D.J. (2008) "FOXOs, cancer and regulation of apoptosis," *Oncogene*, 27(16), pp. 2312–2319.

Fuchs, C.S. *et al.* (2015) "A phase 3 randomized, double-blind, placebo-controlled trial of ganitumab or placebo in combination with gemcitabine as first-line therapy for metastatic adenocarcinoma of the pancreas: The GAMMA trial," *Annals of Oncology*, 26(5), pp. 921–927.

van Gaal, J.C. *et al.* (2013) "Simultaneous targeting of insulin-like growth factor-1 receptor and anaplastic lymphoma kinase in embryonal and alveolar rhabdomyosarcoma: A rational choice," *European Journal of Cancer*, 49(16), pp. 3462–3470.

G-Amlak, M. *et al.* (2002) "Regulation of myeloma cell growth through Akt/Gsk3/forkhead signaling pathway," *Biochemical and Biophysical Research Communications*, 297(4), pp. 760–764.

Gao, J. *et al.* (2011) "Dual IGF-I/II-neutralizing antibody MEDI-573 potently inhibits IGF signaling and tumor growth," *Cancer Research*, 71(3), pp. 1029–1040.

García-Alai, M.M. *et al.* (2006) "Molecular basis for phosphorylation-dependent, PEST-mediated protein turnover," *Structure*, 14(2), pp. 309–319.

Gell, D. and Jackson, S.P. (1999) "Mapping of protein-protein interactions within the DNA-dependent protein kinase complex," *Nucleic Acids Research*, 27(17), pp. 3494–3502.

Ghosh, P., Dahms, N.M. and Kornfeld, S. (2003) "Mannose 6-phosphate receptors: New twists in the tale," *Nature Reviews Molecular Cell Biology*, 4(3), pp. 202–212.

Giese, K. *et al.* (1995) "Assembly and function of a TCRα enhancer complex is dependent on LEF-1-induced DNA bending and multiple protein-protein interactions," *Genes and Development*, 9(8), pp. 995–1008.

Giri, D.K. *et al.* (2005) "Endosomal Transport of ErbB-2: Mechanism for Nuclear Entry of the Cell Surface Receptor," *Molecular and Cellular Biology*, 25(24), pp. 11005–11018.

Gleason, D.F. and Mellinger, G.T. (1974) "Prediction of prognosis for prostatic adenocarcinoma by combined histological grading and clinical staging," *Journal of Urology*, 111(1), pp. 58–64.

Goldfine, I.D. *et al.* (1977) *Cellular uptake and nuclear binding of insulin in human cultured lymphocytes: Evidence for potential intracellular sites of insulin action (insulin receptors/hormone action/hormone binding/autoradiography/plasma membrane)*.

Goldfine, I.R.A.D. and Smith, G.J. (1976) "Binding of insulin to," *Proceedings of the National Academy of Sciences USA*, 73(5), pp. 1427–1431.

Van Golen, C.M. *et al.* (2006) “Insulin-like growth factor-I receptor expression regulates neuroblastoma metastasis to bone,” *Cancer Research*, 66(13), pp. 6570–6578.

Goodwin, J.F. and Knudsen, K.E. (2014) “Beyond DNA repair: DNA-PK function in cancer,” *Cancer Discovery*, 4(10), pp. 1126–1139.

Gradishar, W.J. *et al.* (2016) “Clinical and Translational Results of a Phase II, Randomized Trial of an AntiIGF-1R (Cixutumumab) in Women with Breast Cancer That Progressed on Endocrine Therapy,” *Clinical Cancer Research*, 22(2), pp. 301–309.

Graff, J.R. *et al.* (2000) “Increased AKT activity contributes to prostate cancer progression by dramatically accelerating prostate tumor growth and diminishing p27(Kip1) expression,” *Journal of Biological Chemistry*, 275(32), pp. 24500–24505.

Graham, T.G.W., Walter, J.C. and Loparo, J.J. (2016) “Two-Stage Synapsis of DNA Ends during Non-homologous End Joining,” *Molecular Cell*, 61(6), pp. 850–858.

Graham, T.R. *et al.* (2008) “Insulin-like growth factor-I - Dependent up-regulation of ZEB1 drives epithelial-to-mesenchymal transition in human prostate cancer cells,” *Cancer Research*, 68(7), pp. 2479–2488.

Grasl-Kraupp, B. *et al.* (2002) “A novel mechanism for mitogenic signaling via pro-transforming growth factor α within hepatocyte nuclei,” *Hepatology*, 35(6), pp. 1372–1380.

Grawunder, U. *et al.* (1997) “Activity of DNA ligase IV stimulated by complex formation with XRCC4 protein in mammalian cells,” *Nature*, 388(6641), pp. 492–495.

Grzmil, M. *et al.* (2004) “Blockade of the type I IGF receptor expression in human prostate cancer cells inhibits proliferation and invasion, up-regulates IGF binding protein-3 and suppresses MMP-2 expression,” *Journal of Pathology*, 202(1), pp. 50–59.

Guevara-Aguirre, J. *et al.* (2011) “Growth Hormone Receptor Deficiency Is Associated with a Major Reduction in Pro-Aging Signaling, Cancer, and Diabetes in Humans,” *Science Translational Medicine*, 3(70), pp. 20–23.

Guix, M. *et al.* (2008) “Acquired resistance to EGFR tyrosine kinase inhibitors in cancer cells is mediated by loss of IGF-binding proteins Find the latest version : Acquired

resistance to EGFR tyrosine kinase inhibitors in cancer cells is mediated by loss of IGF-binding proteins," *Journal of Clinical Investigation*, 118(7), pp. 2609–2619.

Gunawardena, S.R. *et al.* (2008) "NOM1 targets protein phosphatase I to the nucleolus," *Journal of Biological Chemistry*, 283(1), pp. 398–404.

Halford, M.M. and Stacker, S.A. (2001) "Revelations of the RYK receptor," *BioEssays*, 23(1), pp. 34–45.

Haluska, P. *et al.* (2011) "Phase II trial of the dual IGF-1R/IR inhibitor BMS-754807 with or without letrozole in aromatase inhibitor-resistant breast cancer.," *Journal of Clinical Oncology*, 29(15_suppl), pp. TPS111–TPS111.

Haluska, P. *et al.* (2014) "Phase I dose-escalation study of MEDI-573, a bispecific, antiligand monoclonal antibody against IGFI and IGFII, in patients with advanced solid tumors," *Clinical Cancer Research*, 20(18), pp. 4747–4757.

Hamada, M. *et al.* (2011) "Ran-dependent docking of importin β- to RanBP2/Nup358 filaments is essential for protein import and cell viability," *Journal of Cell Biology*, 194(4), pp. 597–612.

Hamilton, T.G. *et al.* (2003) "Evolutionary Divergence of Platelet-Derived Growth Factor Alpha Receptor Signaling Mechanisms," *Molecular and Cellular Biology*, 23(11), pp. 4013–4025.

Hanahan, D. and Weinberg, R.A. (2000) "The Hallmarks of Cancer," *Cell*, 100(1), pp. 57–70.

Hanahan, D. and Weinberg, R.A. (2011) "Hallmarks of Cancer: The Next Generation," *Cell*, 144(5), pp. 646–674.

Hancock, M.L. *et al.* (2019) "Insulin Receptor Associates with Promoters Genome-wide and Regulates Gene Expression," *Cell*, 177(3), pp. 722–736.

Haupt, Y. *et al.* (1997) "Mdm2 promotes the rapid degradation of p53," *Nature*, 387(6630), pp. 296–299.

Hay, N. and Sonenberg, N. (2004) “Upstream and downstream of mTOR,” *Genes and Development*, 18, pp. 1926–1945.

He, G. *et al.* (2010) “Gamma-secretase activating protein, a therapeutic target for Alzheimer’s disease,” *Nature*, 467(7311), pp. 95–98.

Hellawell, G.O. *et al.* (2002) “Expression of the type 1 insulin-like growth factor receptor is up-regulated in primary prostate cancer and commonly persists in metastatic disease,” *Cancer Research*, 62(10), pp. 2942–2950.

Hentges, L.D. *et al.* (2021) “LanceOtron: a deep learning peak caller for ATAC-seq, ChIP-seq, and DNase-seq,” *bioRxiv* [Preprint].

Heskamp, S. *et al.* (2015) “Upregulation of IGF-1R expression during neoadjuvant therapy predicts poor outcome in breast cancer patients,” *PLoS ONE*, 10(2), pp. 1–13.

Hiraga, T. *et al.* (2012) “Bone-derived IGF mediates crosstalk between bone and breast cancer cells in bony metastases,” *Cancer Research*, 72(16), pp. 4238–4249.

Hocking, T.D. *et al.* (2017) “Optimizing ChIP-seq peak detectors using visual labels and supervised machine learning,” *Bioinformatics*, 33(4), pp. 491–499.

Hoeflich, K.P. *et al.* (2000) “Requirement for glycogen synthase kinase-3β in cell survival and NF-κB activation,” *Nature*, 406(6791), pp. 86–90.

Hoeing, K. *et al.* (2011) “Presenilin-1 processing of ErbB4 in fetal type II cells is necessary for control of fetal lung maturation,” *Biochimica et Biophysica Acta - Molecular Cell Research*, 1813(3), pp. 480–491.

Holmes, K. *et al.* (2007) “Vascular endothelial growth factor receptor-2: Structure, function, intracellular signalling and therapeutic inhibition,” *Cellular Signalling*, 19(10), pp. 2003–2012.

Hong, S.Y. *et al.* (2000) “Involvement of two NF-κB binding elements in tumor necrosis factor α-, CD40-, and Epstein-Barr virus latent membrane protein 1-mediated induction of the cellular inhibitor of apoptosis protein 2 gene,” *Journal of Biological Chemistry*, 275(24), pp. 18022–18028.

Hsu, S.C. and Hung, M.C. (2007) “Characterization of a novel tripartite nuclear localization sequence in the EGFR family,” *Journal of Biological Chemistry*, 282(14), pp. 10432–10440.

Hu, C.K. *et al.* (2006) “Loss of heterozygosity of M6P/IGF2R gene is an early event in the development of prostate cancer,” *Prostate Cancer and Prostatic Diseases*, 9(1), pp. 62–67.

Huang, J. and Manning, B.D. (2008) “The TSC1–TSC2 complex: a molecular switchboard controlling cell growth,” *Biochemical Journal*, 412(2), pp. 179–190.

Huggins, C. and Hodges, C. V (1941) “The Effect of Castration, Of Estrogen and of Androgen Injection on Serum Phosphatases in Metastatic Carcinoma of the Prostate,” *Cancer Research*, 1, pp. 293–297.

Huo, L., Hsu, J.L. and Hung, M.-C. (2014) “Receptor Tyrosine Kinases in the Nucleus: Nuclear Functions and Therapeutic Implications in Cancers,” in Kumar, R. (ed.) *Nuclear Signaling Pathways and Targeting Transcription in Cancer*. New York, NY: Springer New York, pp. 189–229.

Huss, M. and Wieczorek, H. (2009) “Inhibitors of V-ATPases: Old and new players,” *Journal of Experimental Biology*, 212(3), pp. 341–346.

Hussain, S.A. *et al.* (2019) “Targeting IGF-1/2 with xentuzumab (Xe) plus enzalutamide (En) in metastatic castration-resistant prostate cancer (mCRPC) after progression on docetaxel chemotherapy (DCt) and abiraterone (Abi): Randomized phase II trial results.,” *Journal of Clinical Oncology*, 37(15_suppl), p. 5030.

Hutten, S. *et al.* (2008) “The Nup358-RanGAP Complex Is Required for Efficient Importin α/β-dependent Nuclear Import,” *Molecular Biology of the Cell*, 19, pp. 2300–2310.

Hwa, V., Oh, Y. and Rosenfeld, R.G. (1999) “The Insulin-Like Growth Factor-Binding Protein (IGFBP) Superfamily,” 20(6), pp. 761–787.

Idelman, G. *et al.* (2003) “WT1-p53 interactions in insulin-like growth factor-I receptor gene regulation,” *Journal of Biological Chemistry*, 278(5), pp. 3474–3482.

Iida, M. *et al.* (2019) “Compensatory role of insulin-like growth factor 1 receptor in estrogen receptor signaling pathway and possible therapeutic target for hormone therapy-resistant breast cancer,” *Breast Cancer*, 26(3), pp. 272–281.

Iida, Y. *et al.* (2018) “Predominance of triple wild-type and IGF-2R mutations in mucosal melanomas,” *BMC Cancer*, 18(1), pp. 1–10.

Inoki, K. *et al.* (2002) “TSC2 is phosphorylated and inhibited by Akt and suppresses mTOR signalling,” *Nature Cell Biology*, 4(9), pp. 648–657.

Ireland, L. *et al.* (2016) “Chemoresistance in pancreatic cancer is driven by stroma-derived insulin-like growth factors,” *Cancer Research*, 76(23), pp. 6851–6863.

Jamwal, G. *et al.* (2018) “Identification of a unique loss-of-function mutation in IGF1R and a crosstalk between IGF1R and Wnt/β-catenin signaling pathways,” *Biochimica et Biophysica Acta - Molecular Cell Research*, 1865(6), pp. 920–931.

Jassem, J. *et al.* (2010) “Randomized, open label, phase III trial of figitumumab in combination with paclitaxel and carboplatin versus paclitaxel and carboplatin in patients with non-small cell lung cancer (NSCLC).,” *Journal of Clinical Oncology*, 28(15_suppl), p. 7500.

Javerzat, S., Auguste, P. and Bikfalvi, A. (2002) “The role of fibroblast growth factors in vascular development,” *Trends in Molecular Medicine*, 8(10), pp. 483–489.

Jette, N. and Lees-Miller, S.P. (2015) “The DNA-dependent protein kinase: a multifunctional protein kinase with roles in DNA double strand break repair and mitosis,” *Prog Biophys Mol Biol.*, 117(0), pp. 194–205.

Jiang, Y.G. *et al.* (2007) “Role of Wnt/β-catenin signaling pathway in epithelial-mesenchymal transition of human prostate cancer induced by hypoxia-inducible factor-1α,” *International Journal of Urology*, 14(11), pp. 1034–1039.

Jones, R.L. *et al.* (2015) “Phase I Study of Intermittent Oral Dosing of the Insulin-like Growth Factor-1 and Insulin Receptors Inhibitor OSI-906 in Patients With Advanced Solid Tumors,” *Clinical Cancer Research*, 21(4), pp. 693–700.

Joy, A. *et al.* (1997) “Nuclear accumulation of FGF-2 is associated with proliferation of human astrocytes and glioma cells,” *Oncogene*, 14(2), pp. 171–183.

Kajanne, R. *et al.* (2009) “Transcription factor AP-1 promotes growth and radioresistance in prostate cancer cells,” *International Journal of Oncology*, 35(5), pp. 1175–1182.

Karp, D.D. *et al.* (2009) “Phase II Study of the Anti–Insulin-Like Growth Factor Type 1 Receptor Antibody CP-751,871 in Combination With Paclitaxel and Carboplatin in Previously Untreated, Locally Advanced, or Metastatic Non–Small-Cell Lung Cancer,” *Journal of Clinical Oncology*, 27(15), pp. 2516–2522.

Katso, R.M., Russell, R.B. and Ganesan, T.S. (1999) “Functional Analysis of H-Ryk, an Atypical Member of the Receptor Tyrosine Kinase Family,” *Molecular and Cellular Biology*, 19(9), pp. 6427–6440.

Kelman, Z. (1997) “PCNA: structure, functions and interactions.,” *Oncogene*, 14(6), pp. 629-640.

Key, T.J. *et al.* (2010) “Insulin-like growth factor 1 (IGF1), IGF binding protein 3 (IGFBP3), and breast cancer risk: Pooled individual data analysis of 17 prospective studies,” *The Lancet Oncology*, 11(6), pp. 530–542.

Kiely, P.A. *et al.* (2005) “RACK1-mediated integration of adhesion and insulin-like growth factor I (IGF-I) signaling and cell migration are defective in cells expressing an IGF-I receptor mutated at tyrosines 1250 and 1251,” *Journal of Biological Chemistry*, 280(9), pp. 7624–7633.

Kim, D.H. *et al.* (2002) “mTOR interacts with raptor to form a nutrient-sensitive complex that signals to the cell growth machinery,” *Cell*, 110(2), pp. 163–175.

Kim, H.-J. *et al.* (2007) “Constitutively Active Type I Insulin-Like Growth Factor Receptor Causes Transformation and Xenograft Growth of Immortalized Mammary Epithelial Cells and Is Accompanied by an Epithelial-to-Mesenchymal Transition Mediated by NF-κB and Snail,” *Molecular and Cellular Biology*, 27(8), pp. 3165–3175.

Kindler, H.L. *et al.* (2010) “A placebo-controlled, randomized phase II study of conatumumab (C) or AMG 479 (A) or placebo (P) plus gemcitabine (G) in patients (pts) with metastatic pancreatic cancer (mPC).,” *Journal of Clinical Oncology*, 28(15_suppl), p. 4035.

King, H. *et al.* (2014) “Can we unlock the potential of IGF-1R inhibition in cancer therapy?,” *Cancer Treatment Reviews*, 40(9), pp. 1096–1105.

King, J.C. *et al.* (2009) "Cooperativity of TMPRSS2-ERG with PI3-kinase pathway activation in prostate oncogenesis," *Nature Genetics*, 41(5), pp. 524–526.

Koumakpayi, I.H. *et al.* (2006) "Expression and nuclear localization of ErbB3 in prostate cancer," *Clinical Cancer Research*, 12(9), pp. 2730–2737.

Koumakpayi, I.H. *et al.* (2011) "Macropinocytosis inhibitors and Arf6 regulate ErbB3 nuclear localization in prostate cancer cells," *Molecular Carcinogenesis*, 50(11), pp. 901–912.

Kreuz, S. *et al.* (2001) "NF- B Inducers Upregulate cFLIP, a Cycloheximide-Sensitive Inhibitor of Death Receptor Signaling," *Molecular and Cellular Biology*, 21(12), pp. 3964–3973.

Krueckl, S.L. *et al.* (2004) "Increased insulin-like growth factor I receptor expression and signaling are components of androgen-independent progression in a lineage-derived prostate cancer progression model," *Cancer Research*, 64(23), pp. 8620–8629.

Kucab, J.E. and Dunn, S.E. (2003) "Role of IGF-1R in mediating breast cancer invasion and metastasis," *Breast Disease*, 17, pp. 41–47.

Kurzrock, R. *et al.* (2010) "A phase I study of weekly R1507, a human monoclonal antibody insulin-like growth factor-I receptor antagonist, in patients with advanced solid tumors," *Clinical Cancer Research*, 16(8), pp. 2458–2465.

Kyriakis, J.M. and Avruch, J. (2001) "Mammalian mitogen-activated protein kinase signal transduction pathways activated by stress and inflammation," *Physiological Reviews*, 81(2), pp. 807–869.

Lacy, E.R. *et al.* (2005) "Molecular basis for the specificity of p27 toward cyclin-dependent kinases that regulate cell division," *Journal of Molecular Biology*, 349(4), pp. 764–773.

Lai, Y.-T. *et al.* (2015) "Rapid labeling of intracellular His-tagged proteins in living cells," *Proceedings of the National Academy of Sciences*, 112(10), pp. 2948–2953.

Langmead, B. and Salzberg, S.L. (2012) "Fast gapped-read alignment with Bowtie 2," *Nature Methods*, 9(4), pp. 357–359.

Laron, Z. (2001) “Insulin-like growth factor 1 (IGF-1): a growth hormone,” *Molecular Pathology*, 54(5), pp. 311–316.

Law, J.H. *et al.* (2008) “Phosphorylated insulin-like growth factor-I/insulin receptor is present in all breast cancer subtypes and is related to poor survival,” *Cancer Research*, 68(24), pp. 10238–10246.

Lawrence, J.B. *et al.* (1999) “The insulin-like growth factor (IGF)-dependent IGF binding protein-4 protease secreted by human fibroblasts is pregnancy-associated plasma protein-A,” *Proceedings of the National Academy of Sciences of the United States of America*, 96(6), pp. 3149–3153.

Lee, J. and Pilch, P.F. (1994) “The insulin receptor: structure, function, and signaling,” *American Journal of Physiology*, 266(2), pp. 319–334.

Lee, J.S. *et al.* (2015) “STAT3-mediated IGF-2 secretion in the tumour microenvironment elicits innate resistance to anti-IGF-1R antibody,” *Nature Communications*, 6.

Leighl, N.B. *et al.* (2017) “Phase 2 Study of Erlotinib in Combination With Linsitinib (OSI-906) or Placebo in Chemotherapy-Naive Patients With Non–Small-Cell Lung Cancer and Activating Epidermal Growth Factor Receptor Mutations,” *Clinical Lung Cancer*, 18(1), pp. 34-42.e2.

Leimbacher, P.A. *et al.* (2019) “MDC1 Interacts with TOPBP1 to Maintain Chromosomal Stability during Mitosis,” *Molecular Cell*, 74(3), pp. 571-583.e8.

Li, H. *et al.* (2014) “Ubiquitin ligase Cbl-b represses IGF-I-induced epithelial mesenchymal transition via ZEB2 and microRNA-200c regulation in gastric cancer cells,” *Molecular Cancer*, 13(1), pp. 1–13.

Li, H. *et al.* (2015) “Insulin-like growth factor-i induces epithelial to mesenchymal transition via GSK-3β and ZEB2 in the BGC-823 gastric cancer cell line,” *Oncology Letters*, 9(1), pp. 143–148.

Li, H. *et al.* (2017) “IGF-1R signaling in epithelial to mesenchymal transition and targeting IGF- IR therapy : overview and new insights,” *Molecular Cancer*, 16(6), pp. 1–15.

Li, J. *et al.* (2017) “Aberrant corticosteroid metabolism in tumor cells enables GR takeover in enzalutamide resistant prostate cancer,” *eLife*, 6, pp. 1–17.

Li, J. *et al.* (2019) “Structural basis of the activation of type 1 insulin-like growth factor receptor,” *Nature Communications*, 10(1), pp. 1–11.

Li, L.Y. *et al.* (2011) “Nuclear ErbB2 enhances translation and cell growth by activating transcription of ribosomal RNA genes,” *Cancer Research*, 71(12), pp. 4269–4279.

Li, Z. *et al.* (1995) “The XRCC4 gene encodes a novel protein involved in DNA double-strand break repair and V(D)J recombination,” *Cell*, 83(7), pp. 1079–1089.

Liang, J. *et al.* (2002) “PKB/Akt phosphorylates p27, impairs nuclear import of p27 and opposes p27-mediated G1 arrest,” *Nature Medicine*, 8(10), pp. 1153–1160.

Liao, H.-J. and Carpenter, G. (2007) “Role of the Sec61 Translocon in EGF Receptor Trafficking to the Nucleus and Gene Expression,” *Molecular Biology of the Cell*, 18(3), pp. 1064–1072.

Liccardi, G., Hartley, J.A. and Hochhauser, D. (2011) “EGFR nuclear translocation modulates DNA repair following cisplatin and ionizing radiation treatment,” *Cancer Research*, 71(3), pp. 1103–1114.

Lieber, M.R. (2010) “The mechanism of double-strand DNA break repair by the nonhomologous DNA end-joining pathway,” *Annual Review of Biochemistry*, 79(D), pp. 181–211.

Lin, H.K. *et al.* (2001) “Akt suppresses androgen-induced apoptosis by phosphorylating and inhibiting androgen receptor,” *Proceedings of the National Academy of Sciences of the United States of America*, 98(13), pp. 7200–7205.

Lin, M.Z. *et al.* (2014) “The role of insulin-like growth factor binding protein-3 in the breast cancer cell response to DNA-damaging agents,” *Oncogene*, 33(1), pp. 85–96.

Lin, S. *et al.* (2001) “Nuclear localization of EGF receptor and its potential new role as a transcription factor,” *Nature Cell Biology*, 3(9), pp. 802–808.

Lin, Y. *et al.* (2017) "SUMO-modified insulin-like growth factor 1 receptor (IGF-1R) increases cell cycle progression and cell proliferation," *Journal of Cellular Physiology*, 232(10), pp. 2722–2730.

Liu, B. *et al.* (2000) "Direct functional interactions between insulin-like growth factor-binding protein-3 and retinoid X receptor-α regulate transcriptional signaling and apoptosis," *Journal of Biological Chemistry*, 275(43), pp. 33607–33613.

Livingstone, C. (2013) "IGF2 and cancer," *Endocrine-Related Cancer*, 20(6), pp. 321–339.

Lloret, M. *et al.* (2007) "IGF-1R expression in localized cervical carcinoma patients treated by radiochemotherapy," *Gynecologic Oncology*, 106(1), pp. 8–11.

Lo, H. *et al.* (2006) "Nuclear-cytoplasmic transport of EGFR involves receptor endocytosis, importin β1 and CRM1," *J Cell. Biochem.*, 98(6), pp. 1570–1583.

Lo, H.W. *et al.* (2005) "Nuclear interaction of EGFR and STAT3 in the activation of the iNOS/NO pathway," *Cancer Cell*, 7(6), pp. 575–589.

Lyu, J., Wesselschmidt, R.L. and Lu, W. (2009) "Cdc37 regulates ryk signaling by stabilizing the cleaved ryk intracellular domain," *Journal of Biological Chemistry*, 284(19), pp. 12940–12948.

Lyu, J., Yamamoto, V. and Lu, W. (2008) "Cleavage of the Wnt Receptor Ryk Regulates Neuronal Differentiation during Cortical Neurogenesis," *Developmental Cell*, 15(5), pp. 773–780.

Ma, J. *et al.* (1999) "Prospective study of colorectal cancer risk in men and plasma levels of insulin-like growth factor (IGF)-I and IGF-binding protein-3," *Journal of the National Cancer Institute*, 91(7), pp. 620–625.

Ma, L. *et al.* (2005) "Phosphorylation and functional inactivation of TSC2 by Erk: Implications for tuberous sclerosis and cancer pathogenesis," *Cell*, 121(2), pp. 179–193.

Ma, Y. *et al.* (2012) "Induction of IGF-1R expression by EGR-1 facilitates the growth of prostate cancer cells," *Cancer Letters*, 317(2), pp. 150–156.

Ma, Y. *et al.* (2016) "InsR/IGF1R pathway mediates resistance to EGFR inhibitors in glioblastoma," *Clinical Cancer Research*, 22(7), pp. 1767–1776.

Macaulay, V.M. *et al.* (2016) "Phase I dose-escalation study of linsitinib (OSI-906) and erlotinib in patients with advanced solid tumors," *Clinical Cancer Research*, 22(12), pp. 2897–2907.

Machanick, P. and Bailey, T.L. (2011) "MEME-ChIP: Motif analysis of large DNA datasets," *Bioinformatics*, 27(12), pp. 1696–1697.

Maeda, H. *et al.* (2009) "Prostate-specific antigen enhances bioavailability of insulin-like growth factor by degrading insulin-like growth factor binding protein 5," *Biochemical and Biophysical Research Communications*, 381(3), pp. 311–316.

Maher, P.A. (1996) "Nuclear translocation of fibroblast growth factor (FGF) receptors in response to FGF-2," *Journal of Cell Biology*, 134(2), pp. 529–536.

Majumder, P.K. and Sellers, W.R. (2005) "Akt-regulated pathways in prostate cancer," *Oncogene*, 24(50), pp. 7465–7474.

Van Maldegem, A.M. *et al.* (2016) "Ewing sarcoma: The clinical relevance of the insulin-like growth factor 1 and the poly-ADP-ribose-polymerase pathway," *European Journal of Cancer*, 53, pp. 171–180.

Maldonado, E. *et al.* (1996) "A human RNA polymerase II complex associated with SRB and DNA-repair proteins," *Nature*, 381, pp. 86–89.

Malempati, S. *et al.* (2012) "Phase I/II trial and pharmacokinetic study of cixutumumab in pediatric patients with refractory solid tumors and Ewing sarcoma: A report from the Children's Oncology Group," *Journal of Clinical Oncology*, 30(3), pp. 256–262.

Mancarella, C. *et al.* (2017) "ERG deregulation induces IGF-1R expression in prostate cancer cells and affects sensitivity to anti-IGF-1R agents," *Oncotarget*, 6(18), pp. 16611–16622.

Manin, M. *et al.* (2002) "Androgen receptor expression is regulated by the phosphoinositide 3-kinase/Akt pathway in normal and tumoral epithelial cells," *Biochemical Journal*, 366(3), pp. 729–736.

Manstein, V. *et al.* (2014) “Resistance of Cancer Cells to Targeted Therapies Through the Activation of Compensating Signaling Loops,” *Current Signal Transduction Therapy*, 8(3), pp. 193–202.

Maor, S. *et al.* (2007) “Elevated insulin-like growth factor-I receptor (IGF-IR) levels in primary breast tumors associated with BRCA1 mutations,” *Cancer Letters*, 257(2), pp. 236–243.

Maor, S.B. *et al.* (2000) “BRCA1 suppresses insulin-like growth factor-I receptor promoter activity: Potential interaction between BRCA1 and Sp1,” *Molecular Genetics and Metabolism*, 69(2), pp. 130–136.

Massie, C. and Mills, I.G. (2006) “The developing role of receptors and adaptors,” *Nature Reviews CancerCancer*, 6(May), pp. 403–409.

Mccubrey, J.A. *et al.* (2014) “GSK-3 as potential target for therapeutic intervention in cancer,” *Oncotarget*, 5(10), pp. 2881–2911.

McLeay, R.C. and Bailey, T.L. (2010) “Motif Enrichment Analysis: A unified framework and an evaluation on ChIP data,” *BMC Bioinformatics*, 11.

Medema, R.H. *et al.* (2000) “AFX-like Forkhead transcription factors mediate cell-cycle regulation by Ras and PKB through p27(kip1),” *Nature*, 404, pp. 782–787.

De Meyts, P. *et al.* (1994) “The Insulin-Like Growth Factor-I Receptor. Structure, Ligand-Binding Mechanism and Signal Transduction,” *Hormone research*, 42, pp. 152–169.

De Meyts, P. and Whittaker, J. (2002) “Structural biology of insulin and IGF1 receptors: Implications for drug design,” *Nature Reviews Drug Discovery*, 1(10), pp. 769–783.

Michael, D. and Oren, M. (2003) “The p53-Mdm2 module and the ubiquitin system,” *Seminars in Cancer Biology*, 13(1), pp. 49–58.

Mills, J. v. *et al.* (2021) “IGF-1R nuclear import and recruitment to chromatin involves both alpha and beta subunits,” *Discover Oncology*, 12(1).

Mireuta, M. *et al.* (2014) “Quantification of binding of IGF-1 to BI 836845, a candidate therapeutic antibody against IGF-1 and IGF-2, and effects of this antibody on IGF-

1:IGFBP-3 complexes in vitro and in male C57BL/6 mice," *Endocrinology*, 155(3), pp. 703–715.

Mitchell, T. and Neal, D.E. (2015) "The genomic evolution of human prostate cancer," *British Journal of Cancer*, 113(2), pp. 193–198.

Modur, V. *et al.* (2002) "FOXO proteins regulate tumor necrosis factor-related apoptosis inducing ligand expression: Implications for PTEN mutation in prostate cancer," *Journal of Biological Chemistry*, 277(49), pp. 47928–47937.

Moldovan, G.L., Pfander, B. and Jentsch, S. (2007) "PCNA, the Maestro of the Replication Fork," *Cell*, 129(4), pp. 665–679.

Morcavallo, A. *et al.* (2014) "Ligand-mediated endocytosis and trafficking of the insulin-like growth factor receptor I and insulin receptor modulate receptor function," *Frontiers in Endocrinology*, 5(220), pp. 1–7.

Mulvihill, M.J. *et al.* (2009) "Discovery of OSI-906: A selective and orally efficacious dual inhibitor of the IGF-1 receptor and insulin receptor," *Future Medicinal Chemistry*, 1(6), pp. 1153–1171.

Myers, J.M. *et al.* (2003) "Nuclear trafficking of FGFR1: A role for the transmembrane domain," *Journal of Cellular Biochemistry*, 88(6), pp. 1273–1291.

Nagle, A.M. *et al.* (2018) "Loss of E-cadherin enhances IGF1-IGF1R pathway activation and sensitizes breast cancers to anti-IGF1R/InsR inhibitors," *Clinical Cancer Research*, 24(20), pp. 5165–5177.

Nakajima, N. *et al.* (2005) "The expresssion of Mdm2 on Helicobacter pylori infected intestinal metaplasia and gastric cancer," *Journal of Clinical Biochemistry and Nutrition*, 128(4), pp. A401–A402.

Neal, J.A. *et al.* (2011) "Inhibition of Homologous Recombination by DNA-Dependent Protein Kinase Requires Kinase Activity, Is Titratable, and Is Modulated by Autophosphorylation," *Molecular and Cellular Biology*, 31(8), pp. 1719–1733.

Nelson, E.A. *et al.* (2008) "Nifuroxazide inhibits survival of multiple myeloma cells by directly inhibiting STAT3," *Blood*, 112(13), pp. 5095–5102.

Nelson, J.D., LeBoeuf, R.C. and Bomsztyk, K. (2011) “Direct recruitment of insulin receptor and ERK signaling cascade to insulin-inducible gene loci,” *Diabetes*, 60(1), pp. 127–137.

Ni, C.Y. *et al.* (2001) “γ-secretase cleavage and nuclear locatization of ErbB-4 receptor tyrosine kinase,” *Science*, 294(5549), pp. 2179–2181.

Nithianandarajah-Jones, G.N. *et al.* (2014) “The role of ERK5 in endothelial cell function,” *Biochemical Society Transactions*, 42(6), pp. 1584–1589.

Nusse, R. (2005) “Wnt signaling in development and disease,” *Cell Research*, 15(1), pp. 28–32.

Ochi, T. *et al.* (2015) “PAXX, a paralog of XRCC4 and XLF, interacts with Ku to promote DNA double-strand break repair,” *Science*, 347(6218), pp. 185–188.

Oda, K. *et al.* (2005) “A comprehensive pathway map of epidermal growth factor receptor signaling,” *Molecular Systems Biology*, 1(1), pp. 1–17.

Offterdinger, M. *et al.* (2002) “C-erbB-3: A nuclear protein in mammary epithelial cells,” *Journal of Cell Biology*, 157(6), pp. 929–939.

Ogawara, Y. *et al.* (2002) “Akt enhances Mdm2-mediated ubiquitination and degradation of p53,” *Journal of Biological Chemistry*, 277(24), pp. 21843–21850.

Oliner, J.D. *et al.* (1993) “Oncoprotein MDM2 conceals the activation domain of tumour suppressor p53,” *Nature*, 362(6423), pp. 857–860.

Olmos, D. *et al.* (2010) “Safety, pharmacokinetics, and preliminary activity of the anti-IGF-1R antibody figitumumab (CP-751,871) in patients with sarcoma and Ewing’s sarcoma: a phase 1 expansion cohort study,” *The Lancet Oncology*, 11(2), pp. 129–135.

Ono, K. and Han, J. (2000) “The p38 signal transduction pathway Activation and function,” *Cellular Signalling*, 12(1), pp. 1–13.

Orkin, S.H. (1992) “GATA-Binding Transcription Factors in Hematopoietic Cells,” *Blood*, 80(3), pp. 575–581.

Osher, E. and Macaulay, V.M. (2019) “Therapeutic Targeting of the IGF Axis,” *Cells*, 8(895), pp. 1–25.

Oshiro, N. *et al.* (2007) “The Proline-rich Akt Substrate of 40 kDa (PRAS40) Is a Physiological Substrate of Mammalian Target of Rapamycin Complex,” *Journal of Biological Chemistry*, 282(28), pp. 20329–20339.

Oxvig, C. (2015) “The role of PAPP-A in the IGF system: location, location, location,” *Journal of Cell Communication and Signaling*, 9(2), pp. 177–187.

Oza, A. *et al.* (2018) “Phase 2 study evaluating intermittent and continuous linsitinib and weekly paclitaxel in patients with recurrent platinum resistant ovarian epithelial cancer,” *Gynecologic Oncology*, 149(2), pp. 275–282.

Paatero, I. *et al.* (2012) “Interaction with ErbB4 promotes hypoxia-inducible factor-1α signaling,” *Journal of Biological Chemistry*, 287(13), pp. 9659–9671.

Packham, S. *et al.* (2014) “Nuclear translocation of IGF-1R via p150 Glued and an importin-β/RanBP2-dependent pathway in cancer cells,” *Oncogene*, 34(17), pp. 2227–2238.

Pandini, G. *et al.* (2002) “Insulin/insulin-like growth factor I hybrid receptors have different biological characteristics depending on the insulin receptor isoform involved,” *Journal of Biological Chemistry*, 277(42), pp. 39684–39695.

Pandini, G. *et al.* (2005) “Androgens Up-regulate the Insulin-like Growth Factor-I Receptor in Prostate Cancer Cells,” *Cancer Research*, 65(5), pp. 1849–1858.

Pandini, G. *et al.* (2007) “Functional responses and in vivo anti-tumour activity of h7C10: A humanised monoclonal antibody with neutralising activity against the insulin-like growth factor-1 (IGF-1) receptor and insulin/IGF-1 hybrid receptors,” *European Journal of Cancer*, 43(8), pp. 1318–1327.

Papadopoulos, N., Lennartsson, J. and Heldin, C.H. (2018) “PDGFRβ translocates to the nucleus and regulates chromatin remodeling via TATA element-modifying factor 1,” *Journal of Cell Biology*, 217(5), pp. 1701–1717.

Park, J.H. *et al.* (2016) “Activation of the IGF1R pathway potentially mediates acquired resistance to mutant-selective 3rd-generation EGF receptor tyrosine kinase inhibitors in advanced non-small cell lung cancer,” *Oncotarget*, 7(16), pp. 22005–22015.

Paull, T.T. *et al.* (2000) “A critical role for histone H2AX in recruitment of repair factors to nuclear foci after DNA damage,” *Current Biology*, 10(15), pp. 886–895.

Perks, C.M. (1999) “Effect of insulin-like growth factor binding protein-1 on integrin signalling and the induction of apoptosis in human breast cancer cells,” *Journal of Molecular Endocrinology*, 22(3), pp. 141–150.

Petrylak, D.P. *et al.* (2004) “Docetaxel and estramustine compared with mitoxantrone and prednisone for advanced refractory prostate cancer,” *New England Journal of Medicine*, 351(15), pp. 1513–1520.

Pettersson, A. *et al.* (2013) “Modification of the association between obesity and lethal prostate cancer by TMPRSS2:ERG,” *Journal of the National Cancer Institute*, 105(24), pp. 1881–1890.

Phillips, P.D. *et al.* (1991) “The Protooncogene c-myb Increases the Expression of Insulin-like Growth Factor 1 and Insulin-like Growth Factor 1 Receptor Messenger RNAs by a Transcriptional Mechanism,” *Cancer Research*, 51(21), pp. 5997–6000.

Pichler, A. *et al.* (2002) “The nucleoporin RanBP2 has SUMO1 E3 ligase activity,” *Cell*, 108(1), pp. 109–120.

Pierce Cell Surface Protein Biotinylation and Isolation Kit User Guide (2020) *ThermoScientific*.

Playford, M.P. *et al.* (2000) “Insulin-like growth factor 1 regulates the location, stability, and transcriptional activity of β-catenin,” *Proceedings of the National Academy of Sciences of the United States of America*, 97(22), pp. 12103–12108.

pNLCoI2 [luc2-P2A-NlucP/minP/Hygro] Vector: Promega Certificate of Analysis (2012).

Podlecki, D.A. *et al.* (1987) “Nuclear translocation of the insulin receptor. A possible mediator of insulin’s long term effects,” *Journal of Biological Chemistry*, 262(7), pp. 3362–3368.

Podust, V.N. *et al.* (1995) “Mechanism of Inhibition of Proliferating Cell Nuclear Antigen-Dependent DNA Synthesis by the Cyclin-Dependent Kinase Inhibitor p21,” *Biochemistry*, 34(27), pp. 8869–8875.

Pollak, M. (2012) “The insulin and insulin-like growth factor receptor family in neoplasia: An update,” *Nature Reviews Cancer*, 12(3), pp. 159–169.

Prager, D. *et al.* (1992) “Human insulin-like growth factor I receptor function in pituitary cells is suppressed by a dominant negative mutant,” *Journal of Clinical Investigation*, 90(5), pp. 2117–2122.

Presta, M. *et al.* (2005) “Fibroblast growth factor/fibroblast growth factor receptor system in angiogenesis,” *Cytokine and Growth Factor Reviews*, 16(2), pp. 159–178.

Price, A.J. *et al.* (2012) “Insulin-like growth factor-I concentration and risk of prostate cancer: Results from the European prospective investigation into cancer and nutrition,” *Cancer Epidemiology Biomarkers and Prevention*, 21(9), pp. 1531–1541.

Prisco, M. *et al.* (2002) “Nuclear translocation of insulin receptor substrate-1 by the simian virus 40 T antigen and the activated type 1 insulin-like growth factor receptor,” *Journal of Biological Chemistry*, 277(35), pp. 32078–32085.

Rajah, R., Valentinis, B. and Cohen, P. (1997) “Insulin-like growth factor (IGF)-binding protein-3 induces apoptosis and mediates the effects of transforming growth factor-β1 on programmed cell death through a p53- and IGF-independent mechanism,” *Journal of Biological Chemistry*, 272(18), pp. 12181–12188.

Rakowicz-Szulczynska, E.M. *et al.* (1986) *Chromatin binding of epidermal growth factor, nerve growth factor, and platelet-derived growth factor in cells bearing the appropriate surface receptors (intracellular distribution/DNase IU-sensitive sites)*, *Biochemistry*.

Ramcharan, R. *et al.* (2015) “IGF-1R inhibition induces schedule-dependent sensitization of human melanoma to temozolomide,” *Oncotarget*, 6(37), pp. 39877–39890.

Rechsteiner, M. and Rogers, S.W. (1996) “PEST sequences and regulation by proteolysis,” *Trends in Biochemical Sciences*, 21(7), pp. 267–271.

Reilly, J.F. and Maher, P.A. (2001) "Importin β-mediated nuclear import of fibroblast growth factor receptor: Role in cell proliferation," *Journal of Cell Biology*, 152(6), pp. 1307–1312.

Reiss, K. *et al.* (1998) *Inhibition of Tumor Growth by a Dominant Negative Mutant of the Insulin-like Growth Factor I Receptor with a Bystander Effect1*.

Renehan, A.G. *et al.* (2004) "Insulin-like growth factor (IGF)-I, IGF binding protein-3, and cancer risk: Systematic review and meta-regression analysis," *Lancet*, 363(9418), pp. 1346–1353.

Resnicoff, M. *et al.* (1995) "The Insulin-like Growth Factor I Receptor Protects Tumor Cells from Apoptosis in Vivo," *Cancer Research*, 55(11), pp. 2463–2469.

Reusch, H.P. *et al.* (2001) "Regulation of Raf by Akt Controls Growth and Differentiation in Vascular Smooth Muscle Cells," *Journal of Biological Chemistry*, 276(36), pp. 33630–33637.

Reverter, D. and Lima, C.D. (2005) "Insights into E3 ligase activity revealed by a SUMO-RanGAP1-Ubc9-Nup358 complex," *Nature*, 435(7042), pp. 687–692.

Reverter, D. and Lima, C.D. (2006) "Structural basis for SENP2 protease interactions with SUMO precursors and conjugated substrates," *Nature Structural and Molecular Biology*, 13(12), pp. 1060–1068.

Riccio, A. *et al.* (2009) "Inherited and sporadic epimutations at the IGF2-H19 locus in beckwith-wiedemann syndrome and wilms' tumor," *Endocrine Development*, 14, pp. 1–9.

Richter, J.D. and Sonenberg, N. (2005) "Regulation of cap-dependent translation by eIF4E inhibitory proteins," *Nature*, 433(7025), pp. 477–480.

Rieunier, G. *et al.* (2019) "Bad to the bone: The role of the insulin-like growth factor axis in osseous metastasis," *Clinical Cancer Research*, 25(12), pp. 3479–3485.

Rieunier, G. *et al.* (2021) "Targeting IGF Perturbs Global Replication through Ribonucleotide Reductase Dysfunction," *Cancer Research*, 81(8), pp. 2128–2141.

Rio, C. *et al.* (2000) “Tumor necrosis factor-α-converting enzyme is required for cleavage of ErbB4/HER4,” *Journal of Biological Chemistry*, 275(14), pp. 10379–10387.

Robertson, J.F.R. *et al.* (2009) “Activity of fulvestrant in HER2-overexpressing advanced breast cancer,” *Annals of Oncology*, 21(6), pp. 1246–1253.

Rochester, M.A. *et al.* (2005) “Silencing of the IGF1R gene enhances sensitivity to DNA-damaging agents in both PTEN wild-type and mutant human prostate cancer,” *Cancer Gene Therapy*, 12(1), pp. 90–100.

Rodriguez-Bravo, V. *et al.* (2017) “The role of GATA2 in lethal prostate cancer aggressiveness,” *Nature Reviews Urology*, 14(1), pp. 38–48.

Le Roith, D. *et al.* (1991) “Insulin-like growth factors and their receptors as growth regulators in normal physiology and pathologic states,” *Trends in Endocrinology and Metabolism*, 2(4), pp. 134–139.

Le Roith, D. *et al.* (1995) “Molecular and Cellular Aspects of the Insulin-Like Growth Factor I Receptor,” *Endocrine Reviews*, 16(2), pp. 143–163.

Le Roith, D. (2003) “The insulin-like growth factor system,” *Experimental Diabesity Research*, 4(4), pp. 205–212.

Rommel, C. *et al.* (1999) “Differentiation stage-specific inhibition of the Raf-MEK-ERK pathway by Akt,” *Science*, 286(5445), pp. 1738–1741.

Le Roy, C. and Wrana, J.L. (2005a) “Clathrin- and non-clathrin-mediated endocytic regulation of cell signalling,” *Nature Reviews Molecular Cell Biology*, 6(2), pp. 112–126.

Le Roy, C. and Wrana, J.L. (2005b) “Signaling and endocytosis: A team effort for cell migration,” *Developmental Cell*, 9(2), pp. 167–168.

Ryan, A.J. *et al.* (2009) “Expression of a protease-resistant insulin-like growth factor-binding protein-4 inhibits tumour growth in a murine model of breast cancer,” *British Journal of Cancer*, 101(2), pp. 278–286.

Sabatel, C. (2017) *Best Workflow Practices for ChIP-seq Analysis with Small Samples*.

Sachdev, D. *et al.* (2003) "A chimeric humanized single-chain antibody against the type I insulin-like growth factor (IGF) receptor renders breast cancer cells refractory to the mitogenic effects of IGF-I," *Cancer Research*, 63(3), pp. 627–635.

Sachdev, D. *et al.* (2006) "Down-regulation of insulin receptor by antibodies against the type I insulin-like growth factor receptor: Implications for anti-insulin-like growth factor therapy in breast cancer," *Cancer Research*, 66(4), pp. 2391–2402.

Saha, M. *et al.* (2012) "RSK phosphorylates SOS1 creating 14-3-3-docking sites and negatively regulating MAPK activation," *Biochemical Journal*, 447(1), pp. 159–166.

Saikali, Z. *et al.* (2008) "Role of IGF-1/IGF-1R in regulation of invasion in DU145 prostate cancer cells," *Cancer Cell International*, 8, pp. 1–8.

Salahifar, H., Baxter, R.C. and Martin, J.L. (1997) "Insulin-like growth factor binding protein (IGFBP)-3 protease activity secreted by MCF-7 breast cancer cells: Inhibition by IGFs does not require IGF-IGFBP interaction," *Endocrinology*, 138(4), pp. 1683–1690.

Samani, A.A. *et al.* (2004) "Loss of tumorigenicity and metastatic potential in carcinoma cells expressing the extracellular domain of the type 1 insulin-like growth factor receptor," *Cancer Research*, 64(10), pp. 3380–3385.

Samani, A.A. *et al.* (2007) "The role of the IGF system in cancer growth and metastasis: Overview and recent insights," *Endocrine Reviews*, 28(1), pp. 20–47.

Sancak, Y. *et al.* (2007) "PRAS40 Is an Insulin-Regulated Inhibitor of the mTORC1 Protein Kinase," *Molecular Cell*, 25(6), pp. 903–915.

Sancak, Y. *et al.* (2008) "The Rag GTPases bind raptor and mediate amino acid signaling to mTORC1," *Science*, 320(5882), pp. 1496–1501.

Sanderson, M.P. *et al.* (2017) "The IGF1R/INSR inhibitor BI 885578 selectively inhibits growth of IGF2-overexpressing colorectal cancer tumors and potentiates the efficacy of anti-VEGF therapy," *Molecular Cancer Therapeutics*, 16(10), pp. 2223–2233.

Sarfstein, R. *et al.* (2012) "Insulin-like Growth Factor-I Receptor (IGF-IR) translocates to nucleus and autoregulates IGF-IR gene expression in breast cancer cells," *Journal of Biological Chemistry*, 287(4), pp. 2766–2776.

Sayeed, A. *et al.* (2013) “IGF-IR Promotes Prostate Cancer Growth by Stabilizing α5β1 Integrin Protein Levels,” *PLoS ONE*, 8(10), pp. 1–9.

Schayek, H. *et al.* (2010) “Differential regulation of insulin-like growth factor-I receptor gene expression by wild type and mutant androgen receptor in prostate cancer cells,” *Molecular and Cellular Endocrinology*, 323(2), pp. 239–245.

Schedlich, L.J. *et al.* (2007) “Molecular basis of the interaction between IGFBP-3 and retinoid X receptor: Role in modulation of RAR-signaling,” *Archives of Biochemistry and Biophysics*, 465(2), pp. 359–369.

Scher, H.I. *et al.* (2012) “Increased survival with enzalutamide in prostate cancer after chemotherapy,” *New England Journal of Medicine*, 367(13), pp. 1187–1197.

Schlessinger, J. (2002) “Ligand-induced, receptor-mediated dimerization and activation of EGF receptor,” *Cell*, 110(6), pp. 669–672.

Schneewind, O., Model, P. and Fischetti, V.A. (1992) “Sorting of Protein A to the staphylococcal cell wall,” *Cell*, 70(2), pp. 267–281.

Schwartz, G.K. *et al.* (2016) “Preclinical and first-in-human phase I studies of KW-2450, An oral tyrosine kinase inhibitor with insulin-like growth factor receptor-1/insulin receptor selectivity,” *Cancer Science*, 107(4), pp. 499–506.

Sehat, B. *et al.* (2010) “SUMOylation Mediates the Nuclear Translocation and Signaling of the IGF-1 Receptor,” *Sci. Signal.*, 3(108), pp. 1–12.

Selkoe, D.J. and Wolfe, M.S. (2007) “Presenilin: Running with Scissors in the Membrane,” *Cell*, 131(2), pp. 215–221.

Sell, C. *et al.* (1994) “Effect of a Null Mutation of the Insulin-Like Growth Factor I Receptor Gene on Growth and Transformation of Mouse Embryo Fibroblasts,” *Molecular and Cellular Biology*, 14(6), pp. 3604–3612.

Seluanov, A., Mao, Z. and Gorbunova, V. (2010) “Analysis of DNA double-strand break (DSB) repair in mammalian cells,” *Journal of Visualized Experiments*, (43), pp. 1–6.

Sevier, C.S. and Kaiser, C.A. (2002) “Formation and transfer of disulphide bonds in living cells,” *Nature Reviews Molecular Cell Biology*, 3(11), pp. 836–847.

Shariat, S.F. *et al.* (2002) “Association of preoperative plasma levels of insulin-like growth factor I and insulin-like growth factor binding proteins-2 and -3 with prostate cancer invasion, progression, and metastasis,” *Journal of Clinical Oncology*, 20(3), pp. 833–841.

Sharma, N.L. *et al.* (2013) “The Androgen Receptor Induces a Distinct Transcriptional Program in Castration-Resistant Prostate Cancer in Man,” *Cancer Cell*, 23(1), pp. 35–47.

Sharma, S. V. *et al.* (2010) “A Chromatin-Mediated Reversible Drug-Tolerant State in Cancer Cell Subpopulations,” *Cell*, 141(1), pp. 69–80.

Sharon, S.M. *et al.* (2016) “TMPRSS2-ERG fusion protein regulates insulin-like growth factor-1 receptor (IGF1R) gene expression in prostate cancer: Involvement of transcription factor Sp1,” *Oncotarget*, 7(32), pp. 51375–51392.

Sharp, A., De Bono, J.S. and Plymate, S.R. (2019) “Androgen receptor splice variant-7 expression emerges with castration resistance in prostate cancer,” *J Clin Invest*, 129(1), pp. 192–208.

Shen, K. *et al.* (2012) “Inhibition of IGF-IR increases chemosensitivity in human colorectal cancer cells through MRP-2 promoter suppression,” *Journal of Cellular Biochemistry*, 113(6), pp. 2086–2097.

Shen, L. *et al.* (2006) “SUMO protease SENP1 induces isomerization of the scissile peptide bond,” *Nature Structural and Molecular Biology*, 13(12), pp. 1069–1077.

Shen, M. and Abate-Shen, C. (2010) “Molecular genetics of prostate cancer: new prospects for old challenges,” *Genes & Development*, 24(212), pp. 1967–2000.

Shen, M.R. *et al.* (2006) “Insulin-like growth factor 1 is a potent stimulator of cervical cancer cell invasiveness and proliferation that is modulated by αvβ3 integrin signaling,” *Carcinogenesis*, 27(5), pp. 962–971.

Shibuya, M. (2011) “Vascular Endothelial Growth Factor (VEGF) and Its Receptor (VEGFR) Signaling in Angiogenesis: A Crucial Target for Anti- and Pro-Angiogenic Therapies,” *Genes and Cancer*, 2(12), pp. 1097–1105.

Shih, I.M. and Wang, T.L. (2007) “Notch signaling, γ-secretase inhibitors, and cancer therapy,” *Cancer Research*, 67(5), pp. 1879–1882.

Shin, I. *et al.* (2002) “PKB/Akt mediates cell-cycle progression by phosphorylation of p27Kip1 at threonine 157 and modulation of its cellular localization,” *Nat Med*, 8(10), pp. 1145–1152.

Sibanda, B.L. *et al.* (2017) “DNA-PKcs structure suggests an allosteric mechanism modulating DNA double-strand break repair,” *Science*, 355(6324), pp. 520–524.

Simpson, A. *et al.* (2017) “Insulin-Like Growth Factor (IGF) Pathway Targeting in Cancer : Role of the IGF Axis and Opportunities for Future Combination Studies,” *Targ Oncol*, 12(5), pp. 571–597.

Singh, A.A. *et al.* (2019) “Optimized ChIP-seq method facilitates transcription factor profiling in human tumors,” *Life Science Alliance*, 2(1), pp. 1–12.

Singh, A.P. *et al.* (2008) “Genome-wide expression profiling reveals transcriptomic variation and perturbed gene networks in androgen-dependent and androgen-independent prostate cancer cells,” *Cancer Letters*, 259(1), pp. 28–38.

Smith, M.R. *et al.* (2018) “Apalutamide treatment and metastasis-free survival in prostate cancer,” *New England Journal of Medicine*, 378(15), pp. 1408–1418.

Solomon-Zemler, R. *et al.* (2019) “Identification of nucleolar protein NOM1 as a novel nuclear IGF1R-interacting protein,” *Molecular Genetics and Metabolism*, 126(3), pp. 259–265.

Sonenberg, N. and Hinnebusch, A.G. (2009) “Regulation of translation initiation in eukaryotes: Mechanisms and Biological Targets,” *Cell*, 136(4), pp. 731–745.

Song, S., Rosen, K.M. and Corfas, G. (2013) “Biological function of nuclear receptor tyrosine kinase action,” *Cold Spring Harbor Perspectives in Biology*, 5(7), pp. 1–10.

Sorkin, A. and Von Zastrow, M. (2002) “Signal transduction and endocytosis: Close encounters of many kinds,” *Nature Reviews Molecular Cell Biology*, 3(8), pp. 600–614.

Soung, Y.H., Clifford, J.L. and Chung, J. (2010) "Crosstalk between integrin and receptor tyrosine kinase signaling in breast carcinoma progression," *BMB Reports*, 43(5), pp. 311–318.

Stachowiak, E.K. *et al.* (2003) "cAMP-induced differentiation of human neuronal progenitor cells is mediated by nuclear fibroblast growth factor receptor-1 (FGFR1)," *Journal of Neurochemistry*, 84(6), pp. 1296–1312.

Stachowiak, M.K. *et al.* (1996a) "Nuclear accumulation of fibroblast growth factor receptors is regulated by multiple signals in adrenal medullary cells," *Molecular Biology of the Cell*, 7(8), pp. 1299–1317.

Stachowiak, M.K. *et al.* (1996b) "Nuclear localization of functional FGF receptor 1 in human astrocytes suggests a novel mechanism for growth factor action," *Molecular Brain Research*, 38(1), pp. 161–165.

Steuerman, R., Shevah, O. and Laron, Z. (2011) "Congenital IGF1 deficiency tends to confer protection against post-natal development of malignancies," *European Journal of Endocrinology*, 164(4), pp. 485–489.

Steurer, S. *et al.* (2014) "TMPRSS2-ERG fusions are strongly linked to young patient age in low-grade prostate cancer," *European Urology*, 66(6), pp. 978–981.

Suda, K. *et al.* (2014) "The insulin-like growth factor 1 receptor causes acquired resistance to erlotinib in lung cancer cells with the wild-type epidermal growth factor receptor," *International Journal of Cancer*, 135(4), pp. 1002–1006.

Sumanasuriya, S. and De Bono, J. (2018) "Treatment of advanced prostate cancer—A review of current therapies and future promise," *Cold Spring Harbor Perspectives in Medicine*, 8(6), pp. 1–14.

Sun, W.-Y. *et al.* (2015) "Insulin-like growth factor 1 receptor expression in breast cancer tissue and mammographic density," *Molecular and Clinical Oncology*, 3(3), pp. 572–580.

Takada, Y., Takada, Y.K. and Fujita, M. (2017) "Crosstalk between insulin-like growth factor (IGF) receptor and integrins through direct integrin binding to IGF1," 34, pp. 67–72.

Takahashi, T. *et al.* (2001) "A single autophosphorylation site on KDR/Flk-1 is essential for VEGF-A-dependent activation of PLC-γ and DNA synthesis in vascular endothelial cells," *EMBO Journal*, 20(11), pp. 2768–2778.

Taliaferro-Smith, L.T. *et al.* (2015) "FAK activation is required for IGF1R-mediated regulation of EMT, migration, and invasion in mesenchymal triple negative breast cancer cells," *Oncotarget*, 6(7), pp. 4757–4772.

Taniguchi, C.M., Emanuelli, B. and Kahn, R.C. (2006) "Critical nodes in signalling pathways: Insights into insulin action," *Nature Reviews Molecular Cell Biology*, 7(2), pp. 85–96.

Tannock, I.F. *et al.* (2004) "Docetaxel plus prednisone or mitoxantrone plus prednisone for advanced prostate cancer," *New England Journal of Medicine*, 351(15), pp. 1502–1512.

Tarassishin, L. *et al.* (2004) "Processing of Notch and amyloid precursor protein by γ-secretase is spatially distinct," *Proceedings of the National Academy of Sciences of the United States of America*, 101(49), pp. 17050–17055.

Tartare-Deckert, S. *et al.* (1995) "Evidence for a differential interaction of SHC and the insulin receptor substrate-1 (IRS-1) with the insulin-like growth factor-I (IGF-I) receptor in the yeast two-hybrid system," *Journal of Biological Chemistry*, 270(40), pp. 23456–23460.

Teh, H.F. *et al.* (2007) "Characterization of protein-DNA interactions using surface plasmon resonance spectroscopy with various assay schemes," *Biochemistry*, 46(8), pp. 2127–2135.

Tetsu, O. and McCormick, F. (1999) "β-catenin regulates expression of cyclin D1 in colon carcinoma cells," *Nature*, 398(6726), pp. 422–426.

Tognon, C.E. (2012) "Targeting the insulin-like growth factor 1 receptor (IGF1R) signaling pathway for cancer therapy," *Expert Opin. Ther. Targets*, 16, pp. 33–48.

Tolcher, A.W. *et al.* (2009) "Phase I, pharmacokinetic, and pharmacodynamic study of AMG 479, a fully human monoclonal antibody to insulin-like growth factor receptor 1," *Journal of Clinical Oncology*, 27(34), pp. 5800–5807.

Tomlins, S. a *et al.* (2005) "Recurrent Fusion of TMPRSS2 and ETS Transcription Factor Genes in Prostate Cancer," *Science*, 310(October), pp. 644–648.

Tomlins, S.A. *et al.* (2008) "Role of the TMPRSS2-ERG gene fusion in prostate cancer," *Neoplasia*, 10(2), pp. 177–188.

Tomlins, S.A. *et al.* (2009) "ETS Gene Fusions in Prostate Cancer: From Discovery to Daily Clinical Practice," *European Urology*, 56(2), pp. 275–286.

Toulany, M. *et al.* (2012) "Akt promotes post-irradiation survival of human tumor cells through initiation, progression, and termination of DNA-PKcs-dependent DNA double-strand break repair," *Molecular Cancer Research*, 10(7), pp. 945–957.

Towatari, M. *et al.* (1995) "Regulation of GATA-2 Phosphorylation by Mitogen-activated Protein Kinase and Interleukin-3," *The Journal of Biological Chemistry*, 270, pp. 4101–4107.

Tran, C. *et al.* (2009) "Development of a Second-Generation Antiandrogen for Treatment of Advanced Prostate Cancer," *Science*, 324(5928), pp. 787–790.

Travis, R.C. *et al.* (2016) "A Meta-analysis of Individual Participant Data Reveals an Association between Circulating Levels of IGF-I and Prostate Cancer Risk," *Cancer Research*, 76(8), pp. 2288–2301.

Triezenberg, S.J. (1995) *Structure and function of transcriptional activation domains*, *Current Opinion in Genetics and Development*.

Trojan, J. *et al.* (2007) "Insulin-like growth factor type I biology and targeting in malignant gliomas," *Neuroscience*, 145(3), pp. 795–811.

Tsai, F.Y. *et al.* (1994) "An early haematopoietic defect in mice lacking the transcription factor GATA-2," *Nature*, 371(6494), pp. 221–226.

Turney, B.W. *et al.* (2011) "Serial analysis of resected prostate cancer suggests up-regulation of type 1 IGF receptor with disease progression," *BJU International*, 107(9), pp. 1488–1499.

Turney, B.W. *et al.* (2012) “Depletion of the type 1 IGF receptor delays repair of radiation-induced DNA double strand breaks,” *Radiotherapy and Oncology*, 103(3), pp. 402–409.

Ullrich, A. *et al.* (1986) “Insulin-like growth factor I receptor primary structure: comparison with insulin receptor suggests structural determinants that define functional specificity,” *The EMBO Journal*, 5(10), pp. 2503–2512.

Unger, C. *et al.* (2017) “Stromal-derived IGF2 promotes colon cancer progression via paracrine and autocrine mechanisms,” *Oncogene*, 36(38), pp. 5341–5355.

Ungricht, R. *et al.* (2015) “Diffusion and retention are major determinants of protein targeting to the inner nuclear membrane,” *Journal of Cell Biology*, 209(5), pp. 687–704.

Valenciano, A. *et al.* (2012) “Role of IGF-1 receptor in radiation response,” *Translational Oncology*, 5(1), pp. 1–9.

Veeken, J. *et al.* (2009) “Crosstalk Between Epidermal Growth Factor Receptor- and Insulin-Like Growth Factor-1 Receptor Signaling: Implications for Cancer Therapy,” *Current Cancer Drug Targets*, 9(6), pp. 748–760.

Vidal, G.A. *et al.* (2005) “Presenilin-dependent γ-secretase processing regulates multiple ERBB4/HER4 activities,” *Journal of Biological Chemistry*, 280(20), pp. 19777–19783.

Vidal, S.J. *et al.* (2015) “A Targetable GATA2-IGF2 Axis Confers Aggressiveness in Lethal Prostate Cancer,” *Cancer Cell*, 27(2), pp. 223–239.

Viglietto, G. *et al.* (2002) “Cytoplasmic relocalization and inhibition of the cyclindependent kinase inhibitor p27Kip1 by PKB/Akt-mediated phosphorylation in breast cancer,” *Nat Med*, 8, pp. 1136–1144.

Wade Harper, J. *et al.* (1993) “The p21 Cdk-interacting protein Cip1 is a potent inhibitor of G1 cyclin-dependent kinases,” *Cell*, 75(4), pp. 805–816.

Waga, S., Hannon, G.J. and Beach, D. (1994) “The p21 inhibitor of cyclin-dependent kinases controls DNA replication by interaction with PCNA,” *Nature*, 369, pp. 730–734.

Wang, G. *et al.* (2018) “Genetics and biology of prostate cancer,” *Genes and Development*, 32(17–18), pp. 1105–1140.

Wang, S.C. *et al.* (2004) “Binding at and transactivation of the COX-2 promoter by nuclear tyrosine kinase receptor ErbB-2,” *Cancer Cell*, 6(3), pp. 251–261.

Wang, S.C. *et al.* (2006) “Tyrosine phosphorylation controls PCNA function through protein stability,” *Nature Cell Biology*, 8(12), pp. 1359–1368.

Wang, S.C. and Hung, M.C. (2009) “Nuclear translocation of the epidermal growth factor receptor family membrane tyrosine kinase receptors,” *Clinical Cancer Research*, 15(21), pp. 6484–6489.

Wang, Y. and Dasso, M. (2009) “SUMOylation and deSUMOylation at a glance,” *Journal of Cell Science*, 122(23), pp. 4249–4252.

Wang, Yan *et al.* (2005) “Inhibition of insulin-like growth factor-I receptor (IGF-IR) signaling and tumor cell growth by a fully human neutralizing anti-IGF-IR antibody,” *Molecular Cancer Therapeutics*, 4(8), pp. 1214–1221.

Wang, Y.-N. *et al.* (2010) “COPI-mediated retrograde trafficking from the Golgi to the ER regulates EGFR nuclear transport,” *Biochemical and Biophysical Research Communications*, 399(4), pp. 498–504.

Wang, Y.N. *et al.* (2012) “Membrane-bound trafficking regulates nuclear transport of integral epidermal growth factor receptor (EGFR) and ErbB-2,” *Journal of Biological Chemistry*, 287(20), pp. 16869–16879.

Wang, Z. *et al.* (2008) “Glycogen synthase kinase 3 in MLL leukaemia maintenance and targeted therapy,” *Nature*, 455(7217), pp. 1205–1209.

Waraky, A. *et al.* (2017) “Nuclear insulin-like growth factor 1 receptor phosphorylates proliferating cell nuclear antigen and rescues stalled replication forks after DNA damage,” *JBC*, 292(44), pp. 18227–18239.

Warsito, D. *et al.* (2012) “Nuclear IGF1R is a transcriptional co-activator of LEF1/TCF,” *EMBO Reports*, 13(3), pp. 244–250.

Warsito, D. *et al.* (2016) "Nuclearly translocated insulin-like growth factor 1 receptor phosphorylates histone H3 at tyrosine 41 and induces SNAI2 expression via Brg1 chromatin remodeling protein," *Oncotarget*, 7(27), pp. 42288–42302.

Waterman-Storer, C.M., Karki, S. and Holzbaur, E.L.F. (1995) "The p150(Glued) component of the dynactin complex binds to both microtubules and the actin-related protein centractin (Arp-1)," *Proceedings of the National Academy of Sciences of the United States of America*, 92(5), pp. 1634–1638.

Watkins, D.J. *et al.* (2011) "A randomized phase II/III study of the anti-IGF-1R antibody MK-0646 (dalotuzumab) in combination with cetuximab (Cx) and irinotecan (Ir) in the treatment of chemorefractory metastatic colorectal cancer (mCRC) with wild-type (wt) KRAS status.," *Journal of Clinical Oncology*, 29(15_suppl), p. 3501.

Van Weeren, P.C. *et al.* (1998) "Essential role for protein kinase B (PKB) in insulin-induced glycogen synthase kinase 3 inactivation. Characterization of dominant-negative mutant of PKB," *Journal of Biological Chemistry*, 273(21), pp. 13150–13156.

Welcker, M. *et al.* (2003) "Multisite phosphorylation by Cdk2 and GSK3 controls cyclin E degradation," *Molecular Cell*, 12(2), pp. 381–392.

Wen, Y. *et al.* (2000) "HER-2/neu promotes androgen-independent survival and growth of prostate cancer cells through the Akt pathway," *Cancer Research*, 60(24), pp. 6841–6845.

Werner, A., Flotho, A. and Melchior, F. (2012) "The RanBP2/RanGAP1 *SUMO1/Ubc9 Complex Is a Multisubunit SUMO E3 Ligase," *Molecular Cell*, 46(3), pp. 287–298.

Werner, H. *et al.* (1995) "Inhibition of cellular proliferation by the Wilms' tumor suppressor WT1 is associated with suppression of insulin-like growth factor I receptor gene expression.," *Molecular and Cellular Biology*, 15(7), pp. 3516–3522.

Werner, H. *et al.* (1996) "Wild-type and mutant p53 differentially regulate transcription of the insulin-like growth factor I receptor gene," *Proceedings of the National Academy of Sciences of the United States of America*, 93(16), pp. 8318–8323.

Williams, C.C. *et al.* (2004) "The ERBB4/HER4 receptor tyrosine kinase regulates gene expression by functioning as a STAT5A nuclear chaperone," *Journal of Cell Biology*, 167(3), pp. 469–478.

Willmore, E. *et al.* (2008) "DNA-dependent protein kinase is a therapeutic target and an indicator of poor prognosis in B-cell chronic lymphocytic leukemia," *Clinical Cancer Research*, 14(12), pp. 3984–3992.

Wilson, T.R. *et al.* (2012) "Widespread potential for growth-factor-driven resistance to anticancer kinase inhibitors," *Nature*, 487(7408), pp. 505–509.

Wiseman, L.R. *et al.* (1993) "Type I IGF receptor and acquired tamoxifen resistance in oestrogen-responsive human breast cancer cells," *European Journal of Cancer*, 29(16), pp. 2256–2264.

Wiza, C., Nascimento, E.B.M. and Ouwens, D.M. (2012) "Role of PRAS40 in Akt and mTOR signaling in health and disease," *American Journal of Physiology - Endocrinology and Metabolism*, 302(12), pp. 1453–1460.

Wong, V.C.L. (2018) "Nuclear EGFR and Integrator/Super Elongation Complex concurrently binds to Immediate Early Genes for gene transactivation," *Journal of Cancer*, 9(1), pp. 108–116.

Wu, D. *et al.* (2014) "Three-tiered role of the pioneer factor GATA2 in promoting androgen-dependent gene expression in prostate cancer," *Nucleic Acids Research*, 42(6), pp. 3607–3622.

Wu, J.D. *et al.* (2006) "Interaction of IGF signaling and the androgen receptor in prostate cancer progression," *Journal of Cellular Biochemistry*, 99(2), pp. 392–401.

Wu, Y. *et al.* (2002) "Circulating insulin-like growth factor-I levels regulate colon cancer growth and metastasis," *Cancer Research*, 62(4), pp. 1030–1035.

Wu, Y.C., Zhu, M. and Robertson, D.M. (2012) "Novel nuclear localization and potential function of insulin-like growth factor-1 receptor/insulin receptor hybrid in corneal epithelial cells," *PLoS ONE*, 7(8), pp. 1–11.

Xing, J. *et al.* (2008) "Prognostic significance of ataxia-telangiectasia mutated, DNA-dependent protein kinase catalytic subunit, and Ku heterodimeric regulatory complex 86-kD subunit expression in patients with nonsmall cell lung cancer," *Cancer*, 112(12), pp. 2756–2764.

Xiong, Y. *et al.* (1993) "p21 is a universal inhibitor of cyclin kinases," *Nature*, 366(6456), pp. 701–704.

Xu, N. *et al.* (2012) "Akt: A double-edged sword in cell proliferation and genome stability," *Journal of Oncology*, 2012(951724), pp. 1–15.

Xu, Y. *et al.* (2018) "How ligand binds to the type 1 insulin-like growth factor receptor," *Nature Communications*, 9(821).

Yada, M. *et al.* (2004) "Phosphorylation-dependent degradation of c-Myc is mediated by the F-box protein Fbw7," *EMBO Journal*, 23(10), pp. 2116–2125.

Yajima, H., Lee, K.-J. and Chen, B.P.C. (2006) "ATR-Dependent Phosphorylation of DNA-Dependent Protein Kinase Catalytic Subunit in Response to UV-Induced Replication Stress," *Molecular and Cellular Biology*, 26(20), pp. 7520–7528.

Yang, C. *et al.* (2020) "Nuclear IGF1R interacts with PCNA to preserve DNA replication after DNA-damage in a variety of human cancers," *PLoS ONE*, 15(7 July).

Yang, C. *et al.* (2021) "Nuclear IGF1R interacts with NuMA and regulates 53BP1-dependent DNA double-strand break repair in colorectal cancer," *Oncology Reports*, 46(2), pp. 1–11.

Yang, G. *et al.* (2019) "Structural basis of Notch recognition by human γ-secretase," *Nature*, 565(7738), pp. 192–197.

Yang, H. *et al.* (2011) "Insulin-like growth factor 1 activates methionine adenosyltransferase 2A transcription by multiple pathways in human colon cancer cells," *Biochemical Journal*, 436(2), pp. 507–516.

Yang, Y. *et al.* (2014) "Functional roles of p38 mitogen-activated protein kinase in macrophage-mediated inflammatory responses," *Mediators of Inflammation*, 2014, pp. 352–371.

Yeo, C.D. *et al.* (2015) "Expression of insulin-like growth factor 1 receptor (IGF-1R) predicts poor responses to epidermal growth factor receptor (EGFR) tyrosine kinase inhibitors in non-small cell lung cancer patients harboring activating EGFR mutations," *Lung Cancer*, 87(3), pp. 311–317.

Yin, L. and Hu, Q. (2014) “CYP17 inhibitors - Abiraterone, C17,20-lyase inhibitors and multi-targeting agents,” *Nature Reviews Urology*, 11(1), pp. 32–42.

Yip, C.K. *et al.* (2010) “Structure of the human mTOR Complex I and its implications for rapamycin inhibition,” *Molecular Cell*, 38(5), pp. 768–774.

Youngren, J.F. *et al.* (2005) “Nordihydroguaiaretic acid (NDGA) inhibits the IGF-1 and c-erbB2/HER2/neu receptors and suppresses growth in breast cancer cells,” *Breast Cancer Research and Treatment*, 94(1), pp. 37–46.

Yu, E.Y. *et al.* (2015) “SWOG S0925: A randomized phase II study of androgen deprivation combined with cixutumumab versus androgen deprivation alone in patients with new metastatic hormone-sensitive prostate cancer,” *Journal of Clinical Oncology*, 33(14), pp. 1601–1608.

Yu, Jindan *et al.* (2010) “An Integrated Network of Androgen Receptor, Polycomb, and TMPRSS2-ERG Gene Fusions in Prostate Cancer Progression,” *Cancer Cell*, 17(5), pp. 443–454.

Yuen, J.S.P. *et al.* (2007) “The VHL tumor suppressor inhibits expression of the IGF1R and its loss induces IGF1R upregulation in human clear cell renal carcinoma,” *Oncogene*, 26(45), pp. 6499–6508.

Yun, Y.R. *et al.* (2010) “Fibroblast growth factors: Biology, function, and application for tissue regeneration,” *Journal of Tissue Engineering*, 1(1), pp. 1–18.

Yunus, A.A. and Lima, C.D. (2006) “Lysine activation and functional analysis of E2-mediated conjugation in the SUMO pathway,” *Nature Structural and Molecular Biology*, 13(6), pp. 491–499.

Zargar, Z.U. and Tyagi, S. (2012) “Role of host cell factor-1 in cell cycle regulation,” *Transcription*, 3(4), pp. 187–192.

Zhang, D., Samani, A.A. and Brodt, P. (2003) “The Role of the IGF-I Receptor in the Regulation of Matrix Metalloproteinases, Tumor Invasion and Metastasis,” *Hormone and Metabolic Research*, 35(11–12), pp. 802–808.

Zhang, J. *et al.* (2015) “SUMOylation of insulin-like growth factor 1 receptor, promotes proliferation in acute myeloid leukemia,” *Cancer Letters*, 357(1), pp. 297–306.

Zhang, T. *et al.* (2014) "Antitumor effects and molecular mechanisms of figitumumab, a humanized monoclonal antibody to IGF-1 receptor, in esophageal carcinoma," *Scientific Reports*, 4, pp. 1–11.

Zhang, T. *et al.* (2020) "Androgen Receptor Splice Variant, AR-V7, as a Biomarker of Resistance to Androgen Axis-Targeted Therapies in Advanced Prostate Cancer," *Clinical Genitourinary Cancer*, 18(1), pp. 1–10.

Zhang, X.H.F. *et al.* (2013) "Selection of bone metastasis seeds by mesenchymal signals in the primary tumor stroma," *Cell*, 154(5), pp. 1060–1073.

Zhang, Y. *et al.* (2008) "Model-based analysis of ChIP-Seq (MACS)," *Genome Biology*, 9(9).

Zhao, L. *et al.* (2012) "Nimotuzumab promotes radiosensitivity of EGFR-overexpression esophageal squamous cell carcinoma cells by upregulating IGFBP-3," *Journal of Translational Medicine*, 10(1), pp. 1–9.

Zhou, B.P. *et al.* (2004) "Dual regulation of Snail by GSK-3β-mediated phosphorylation in control of epithelial-mesenchymal transition," *Nature Cell Biology*, 6(10), pp. 931–940.

Zhu, S., Zhang, H. and Matunis, M.J. (2006) "SUMO modification through rapamycin-mediated heterodimerization reveals a dual role for Ubc9 in targeting RanGAP1 to nuclear pore complexes," *Experimental Cell Research*, 312(7), pp. 1042–1049.

Zscheppang, K. *et al.* (2011) "Neuregulin receptor ErbB4 functions as a transcriptional cofactor for the expression of surfactant protein B in the fetal lung," *American Journal of Respiratory Cell and Molecular Biology*, 45(4), pp. 761–767.